ALBERTA INNOVATES

CLEAN RESOURCES FINAL REPORT PACKAGE

Project proponents are required to submit a Final Report Package, consisting of a Final Public Report and a Final Financial Report. These reports are to be provided under separate cover at the conclusion of projects for review and approval by Alberta Innovates (AI) Clean Resources Division. Proponents will use the two templates that follow to report key results and outcomes achieved during the project and financial details. The information requested in the templates should be considered the minimum necessary to meet AI reporting requirements; proponents are highly encouraged to include other information that may provide additional value, including more detailed appendices. Proponents must work with the AI Project Advisor during preparation of the Final Report Package to ensure submissions are of the highest possible quality and thus reduce the time and effort necessary to address issues that may emerge through the review and approval process.

Final Public Report

The Final Public Report shall outline what the project achieved and provide conclusions and recommendations for further research inquiry or technology development, together with an overview of the performance of the project in terms of process, output, outcomes and impact measures. The report must delineate all project knowledge and/or technology developed and must be in sufficient detail to permit readers to use or adapt the results for research and analysis purposes and to understand how conclusions were arrived at. It is incumbent upon the proponent to ensure that the Final Public Report **is free of any confidential information or intellectual property requiring protection**. The Final Public Report will be released by Alberta Innovates after the confidentiality period has expired as described in the Investment Agreement.

Final Financial Report

The Final Financial Report shall provide complete and accurate accounting of all project expenditures and contributions over the life of the project pertaining to Alberta Innovates, the proponent, and any project partners. The Final Financial Report will not be publicly released.

Alberta Innovates is governed by FOIP. This means Alberta Innovates can be compelled to disclose the information received under this Application, or other information delivered to Alberta Innovates in relation to a Project, when an access request is made by anyone in the general public.

In the event an access request is received by Alberta Innovates, exceptions to disclosure within FOIP may apply. If an exception to disclosure applies, certain information may be withheld from disclosure. Applicants are encouraged to familiarize themselves with FOIP. Information regarding FOIP can be found at http://www.servicealberta.ca/foip/. Should you have any questions about the collection of this information, you may contact the Manager, Grants Administration Services at 780-450-5551.

ALBERTA INNOVATES

CLEAN RESOURCES FINAL PUBLIC REPORT TEMPLATE

1. PROJECT INFORMATION:

Project Title:	**Value-Added Opportunities for Alberta Asphalt Binder in Road Construction**
Alberta Innovates Project Number:	212201460
Submission Date:	April 30, 2024
Total Project Cost:	$1,234,230.70
Alberta Innovates Funding:	$650,000
AI Project Advisor:	Dr. Paolo Bomben

2. APPLICANT INFORMATION:

Applicant (Organization):	**Department of Chemistry, Queen's University**
Address:	90 Bader Lane, Kingston, Ontario, K7L 3N6
Applicant Representative Name:	Simon A.M. Hesp
Title:	Full Professor
Phone Number:	613-876-1742
Email:	Simon.Hesp@chem.queensu.ca

3. PROJECT PARTNERS

Please provide an acknowledgement statement for project partners, if appropriate.

RESPOND BELOW

We hereby wish to gratefully acknowledge the major financial support for this research from the Bitumen Beyond Combustion program of Alberta Innovates, the Regional Municipality of Durham, the Discovery Grant program of the Natural Sciences and Engineering Research Council of Canada, as well as contributions from additional government, industrial and non-profit sector partners.

Our sincere thanks go out to the many government agencies in North America and Asia for their active participation, support and for providing asphalt samples which have proven essential for advancing the progress of our research program on the development of enhanced asphalt acceptance specifications. Special recognition is due to the Durham Region team involved in the commissioning of the Newtonville Road pavement trial using Cold Lake asphalt binder and recycled plastics, an innovative project that was awarded with the Project of the Year Award under $2M by the Ontario Public Works Association.

We wish to thank Professors Haibo Ding (Chengdu), Yiming Li (Harbin), and Yihua Nie (Hunan) for their expertise in supporting the research with Chinese asphalt samples.

Finally, additional thanks are extended to the Alberta and Federal Governments for their consideration of future funding, which will enable the construction of a further 10-15 demonstration pavement sections and associated important research activities.

EXECUTIVE SUMMARY

This project focused on promoting the utilization of asphalt binders derived from Alberta oil sands, highlighting how these can be leveraged in road construction to enhance durability and performance of road pavement. The research has emerged against a backdrop where the road construction industry, a major consumer of asphalt, frequently relies on simplified procurement policies that often overlook the intrinsic quality of the materials. This practice places high-quality products, such as those from Alberta, at a disadvantage due to prevailing specifications that are neither precise nor holistic. Historically, Alberta binders have demonstrated superior performance, but they have not been widely adopted due to existing market dynamics and specification frameworks that fail to acknowledge their distinct advantages.

This research aimed to validate and promote the superior characteristics of Alberta oil sands-derived asphalt binders through rigorous scientific evaluation and comparative analysis against other commercial binders. Objectives were set to: (1) Develop and optimize new, environmentally friendly methodologies for the extraction, recovery, aging, and testing of asphalt binders that are not only more accurate but also reduce potential health risks associated with conventional solvents; (2) Engage with user agencies across North America and China to educate them about the benefits of adopting advanced specification methods that can more accurately assess the quality of asphalt binders; (3) Demonstrate through real-world application and scholarly dissemination that Alberta's asphalt binders provide enhanced performance and durability, thereby influencing specification standards and market acceptance.

This research project yielded several critical findings that substantiate the high performance of Alberta asphalt binders and propose methodological advancements in binder testing: (1) The research introduced innovative methodologies for the extraction, recovery, and testing of asphalt binders that offer significant improvements over traditional techniques. Key advancements include the adoption of sieve filtration and plate heating evaporation, which replace the conventional centrifuge and rotary evaporation processes. This method, characterized by reduced time and material requirements, is poised to set a new standard in asphalt acceptance; (2) A pivotal aspect of the research was the introduction of a greener solvent, HDPRO, which significantly reduces potential health risks compared to traditionally used solvents. This solvent does not adversely affect the rheological properties of the asphalt, ensuring that the environmental footprint of asphalt production is minimized. Additionally, the optimized methods ensure that residual solvents can be effectively removed, thus preventing any negative impact on the performance of the recovered asphalt; (3) The study provided new insights into the aging processes of asphalt, particularly how these processes affect asphalt's long-term performance. It was found that the current oven aging conditions do not adequately simulate long-term aging effects observed in field

conditions. Adjustments to the temperature and duration of aging could bring laboratory simulations closer to replicating actual aging effects, providing more accurate predictions of the asphalt's lifespan and performance; (4) The introduction of more accurate and less resource-intensive testing methods, such as those involving the Dynamic Shear Rheometer (DSR), can enhance the grading of asphalt binders, ensuring asphalt meets performance standards more efficiently. This research supports the implementation of specification tests like the Double Edge Notched Tension (DENT) and Extended Bending Beam Rheometer (EBBR), which have already demonstrated their ability to improve lifecycles of pavements significantly.

The project surpassed its dissemination goals, producing numerous scientific publications and presentations that have helped to elevate the profile of Alberta asphalt binders within the academic community and industry circles. Engagements at conferences and seminars have facilitated wider exposure and discussions around the adoption of the new testing standards proposed by the research.

Continuous efforts to educate user agencies about the benefits of Alberta binders and the new testing protocols have begun to shift perceptions and pave the way for the adoption of these standards. As agencies recognize the long-term economic and performance benefits of using high-quality binders, a shift in market dynamics is anticipated. By demonstrating the economic benefits of using superior asphalt materials—such as reduced road maintenance costs and longer lifecycles—the project supports a more sustainable approach to road construction. Additionally, the environmental impact of the research is noted in the reduced greenhouse gas emissions associated with the production and application of Alberta binders.

The findings from this project suggest substantial potential for future research, particularly in expanding the application of the new binder specifications internationally. The development of 10-15 demonstration projects as part of the research’s next phase will provide empirical data that can further solidify the case for Alberta asphalt binders and support widespread implementation in new markets.

Table of Contents

LIST OF FIGURES

LIST OF TABLES

1. INTRODUCTION

1.1 Sector Introduction

In the pursuit of providing current asphalt roads with improved durability with the help of Alberta oil sands-based asphalt binder, this project introduces improved grading methods which could recognize the superior performance of Alberta asphalt binder and downgrades inferior binders tainted with harmful modifiers or additives. Unlike conventional methods, which predominantly rely on simple purchase agreements and inadequate performance specifications, this project advocates for a shift towards more rigorous, performance-based specifications that leverage the superior properties of Alberta's bitumen.

Historically, the road construction industry has used approximately 100 million tonnes of asphalt binder annually. However, the quality and durability of these binders have been variable, often leaving user agencies reliant on the assurance of suppliers. Alberta's asphalt binders, characterized by their low wax content and superior performance at both high and low temperatures, are expected to revolutionize the road asphalt industry. These binders not only offer enhanced durability and reduced maintenance costs but also align with environmental sustainability goals by potentially reducing greenhouse gas emissions by 50 % or more.

This project involved a comprehensive research program based on materials from user agencies in Canada, China and the USA. It engaged user agencies across North America and in China. A major pavement trial was commissioned to showcase the benefits of using high-quality Alberta asphalt, especially in regions that experience severe weather variations, thus ensuring road longevity and safety. Additional Alberta binder demonstration projects are planned for 2024 and 2025. By increasing market share through informed and data-driven specification adjustments, Alberta binder could set a new benchmark in the asphalt industry.

In conclusion, this proposal is not merely about enhancing the material quality used in road construction; it is about setting a new standard that could potentially lead to a paradigm shift in how asphalt binders are selected and utilized on a global scale. The anticipated outcomes of this project include not only economic benefits but also advancements in technological and environmental fronts, paving the way for a more sustainable future in road construction.

1.2 Knowledge and Technology Gaps

Despite advances in asphalt technology, significant gaps remain in the formulation and application of asphalt binders, particularly those derived from Alberta oil sands. These gaps hinder the optimal utilization of high-quality Alberta asphalt in road construction, limiting its competitive edge in the market.

1.2.1 Lack of Advanced Performance-Based Specifications

Traditional specifications for asphalt selection are primarily based on simple purchase agreements and empirical testing methods that do not accurately predict long-term pavement performance. This practice disadvantages high-quality asphalt binders from Alberta, which exhibit superior performance in durability tests but are not differentiated under current specifications. There is a need for a deeper understanding of how advanced performance-based specifications can be formulated and implemented to accurately reflect the superior properties of Alberta-derived asphalt binders.

1.2.2 Inadequate Testing and Grading Systems

The existing grading systems, such as Superpave™, often fail to capture the true performance characteristics of different asphalt binders, especially under extreme climatic conditions. These systems also do not consider the effects of modern additives and recycled materials (e.g., RAP, RAS) on asphalt properties. It is crucial to develop more sophisticated, rheological testing methods that can provide a more accurate assessment of an asphalt binder's performance, particularly how these materials behave over time under varying environmental conditions.

1.2.3 Limited Understanding of the Impact of Climate Change

Climate change introduces new challenges on road materials, including higher temperatures and more variable weather patterns, which can degrade asphalt quicker than expected. Research is needed to understand how Alberta asphalt binders perform under these changing conditions and how formulations might need to be adjusted for enhanced resilience.

1.2.4 Educational and Awareness Deficiencies

There is a lack of awareness among user agencies about the benefits of high-quality asphalt binders. This results in continued reliance on inferior products that do not deliver the best value or performance. Strategies are needed to educate stakeholders, including transport departments and construction companies, about the advantages of using superior asphalt binders and the long-term economic and environmental benefits they offer.

1.2.5 Scalability and Implementation of New Technologies

While laboratory results show promising benefits of using advanced asphalt binders, scaling these solutions to real-world applications remains challenging. Practical, cost-effective methods for producing and testing these binders in large volumes are needed.

2. PROJECT DESCRIPTION

2.1 Knowledge and Technology Description

The Superpave system, established in the late 1980s with funding from the U.S. government, is the standard methodology for grading asphalt binders across much of North America. This system classifies asphalt binders based on their rheological properties at high, intermediate, and low temperatures, denoted by Performance Grades (PG) such as PG XX-II-YY. Despite its widespread adoption, the Superpave system exhibits limitations in accurately predicting long-term pavement performance, particularly concerning fatigue and thermal cracking. For instance, the intermediate temperature grade (ITPG) often fails to accurately predict fatigue cracking as it does not effectively differentiate energy lost through viscous or damage. Similarly, the low-temperature grade (LTPG) correlates poorly with thermal cracking performance due to insufficient conditioning time and non-representative testing temperatures.

Alberta oil sands-derived asphalt binders inherently possess superior qualities due to their optimal balance of asphaltenes and low wax content, which confer enhanced durability and thermal stability. However, the full potential of these high-quality binders has not been fully realized in the market due to the limitations of current grading systems and the global nature of oil companies that often prioritize more readily available local crudes. This project aims to refine the understanding and application of Alberta asphalt binders through advanced rheological and chemical analyses, going beyond the conventional Superpave specifications.

Building on the shortcomings of the Superpave system, this project proposes the development of enhanced testing methodologies that more accurately reflect the real-world performance of asphalt binders. This includes extended conditioning periods and more precise measurements of the asphalt's behavior at critical temperatures, ensuring a better correlation with field performance. The goal is to establish a new set of specifications that can distinguish the superior qualities of Alberta-derived asphalt, promoting its use on a broader scale.

This project also emphasizes the environmental benefits of utilizing Alberta asphalt, such as reduced greenhouse gas emissions and enhanced recyclability. These aspects are critical as the industry moves

towards sustainable construction practices. Through lifecycle analyses and recycling studies, the project will document the environmental advantages of Alberta asphalt, providing a strong case for its adoption.

To overcome the market inertia and established practices favoring local crudes, this project includes a comprehensive outreach and education component. By engaging directly with user agencies and presenting findings at conferences and in scientific journals, the project aims to shift industry perceptions and practices towards a preference for high-quality Alberta asphalt. Demonstrations of the material's superior performance in various climatic conditions and mixture tests will be crucial in persuading stakeholders of its benefits.

This project represents a significant step forward in asphalt technology, challenging existing standards and introducing a new paradigm for asphalt binder evaluation and use. By providing a deeper understanding of Alberta oil sands-derived asphalt binders and advocating for their adoption through robust scientific evidence and strategic outreach, the project aims to influence industry standards and practices, leading to more durable and sustainable road infrastructure globally.

2.2 Performance Metrics

The success of this research project is characterized by the achievements in advancing asphalt binder technology, dissemination of knowledge through peer review publications, and educational impacts via theses and webinars. Below, the key performance metrics that demonstrate the project's progress and impact are summarized:

2.2.1 Academic Contributions

Seven peer-reviewed articles published in high-impact journals such as *Construction and Building Materials* and *Transportation Research Record*, covering topics from oil exudation tests to the effects of aging on asphalt mixtures. These publications reflect the project's commitment to advancing the scientific understanding of asphalt binder properties and performance. Two additional articles submitted, focusing on sustainable use of recycled plastics in pavement and the performance grading of asphalt binders. Several additional manuscripts in preparation and soon to be submitted. Presented findings at major industry conferences, including the Transportation Research Board (TRB) Annual Meeting and the European Asphalt Technology Association (EATA), facilitating the exchange of knowledge with professionals and researchers in the field. Several additional conference presentations scheduled.

2.2.2 Educational Impact

Three theses completed, significantly contributing to the education and training of new experts in the field of asphalt technology. These theses focused on practical aspects of specification grading and

performance grading of asphalt binders. Twelve webinars and lectern presentations delivered by Professor Hesp, reaching a broad audience to disseminate findings and promote the use of advanced asphalt technologies. These webinars also served to educate industry and government practitioners on new specification grading and the use of recycled materials in pavement.

2.2.3 Technical Innovations and Findings

Developed and validated a new, greener extraction, recovery, aging, and testing protocol for asphalt binders, significantly reducing the time and material required for traditional tests. Introduced the use of modulated differential scanning calorimetry (MDSC) as a novel method to understand the field performance of asphalt binders, specifically focusing on thermo-reversible aging and phase compatibility. Demonstrated the application of the DSR as an efficient alternative to traditional EBBR and DENT tests, reducing both the material requirements and the duration of testing.

2.2.4 Impact on Industry Standards and Practices

This research project has led to empirical changes in asphalt specifications based on phase angle and relaxation properties, validated through extensive field trials. These changes are expected to improve the accuracy and reliability of performance grading systems. The findings from this project have influenced the development of enhanced aging techniques and testing protocols, which are essential for improving the durability and performance of pavements, particularly in challenging climates.

The project has successfully achieved its objectives, as evidenced by the scholarly output, educational advancements, and technical innovations. The performance metrics demonstrate significant progress toward enhancing the understanding and application of asphalt technology, thereby supporting more durable and sustainable pavement solutions. This comprehensive approach ensures that the project's impacts extend beyond academia into practical, real-world applications in pavement engineering.

2.3 Status of Research Task Completion

This project progressed through a structured sequence of tasks, starting with the procurement of essential equipment and engaging with project partners to ensure collaborative efforts. Following these initial stages, the research team has focussed on collecting the necessary samples for analysis. The technical phase included a series of specialized grading and testing tasks: AASHTO M 320 grading for material specification compliance, DENT and EBBR grading to assess material performance, and MDSC and DSR grading for evaluating viscoelastic properties. Additionally, Hamburg Wheel Tracking Test (HWTT) and Semicircular Bend Tests (SCB) were conducted to determine the resistance of asphalt mixture to rutting and cracking at various service temperatures. These efforts culminated in a comprehensive reporting phase, where data from various tests were compiled, analyzed, and synthesized into actionable insights

and recommendations. This structured approach ensured a thorough evaluation of materials and methodologies, guiding the project towards its objectives with precision and depth.

The following provides a concise overview of each task's core content and the work completed. Detailed accomplishments for each task are outlined as follows:

Task 1 – Equipment Procurement

To acquire critical laboratory equipment that was either unavailable, inoperable, or obsolete within the current lab setup, including an asphalt extractor, a rheometer, and a system controller. The procurement finished, with orders placed based on the specified needs essential for conducting advanced testing and analysis of asphalt materials. Details of equipment procured under this project are given in Table 1.

Table 1. List of equipment procured under this project.

Name of equipment	Function
HDR-10 Rheometer	Rheological tests of asphalt binder.
FlexTest 40 Digital Controller	Cracking tests of asphalt mixture.
PerkinElmer FTIR spectrometer	Wax crystallization, thermal oxidative aging.

Task 2 – Partner Engagement

This task mainly aimed to engage a wide range of user agencies in North America and China through targeted presentations that discussed the advantages of Alberta asphalt binders and propose new testing methodologies. This task was finished by outreach efforts led by Professor Hesp at (1) the Annual Meeting of the Ontario Municipal Engineers Association (MEA, 2022), (2) the Northeastern State Materials Engineers Association (NESMEA, 2023) and at a webinar for (3) the Ontario Public Works Association (OPWA, 2024), as well as numerous online meetings with user agencies in Canada, China and the USA.

A pavement trial with Cold Lake asphalt binder and recycled plastics was constructed in Durham Region and won a Project of the Year Award in the category under $2M from the Ontario Public Works Association. The award was presented at an OPWA Award Luncheon on May 16, 2023. Presentations were tailored to both technical staff and asset managers, emphasizing lifecycle cost benefits. As a result, more than 300 asphalt samples, based on which extensive experimental research was performed, were provided by user agencies. More than 15 demonstration pavement trials have been committed to by Durham Region (6 sections total in 2 locations), the City of Toronto (6 sections total in two locations), Kansas DOT (2 sections in separate locations), Nebraska DOT (2 sections) and New Hampshire DOT (2 sections). The testing of asphalt samples from these pavement trials will be conducted under a subsequent research project, the proposal for which has been submitted to Alberta Innovates for review and approval.

Task 3 – Sample Collection

The objective of this task was to collect between 150-200 samples of asphalt binder and mixtures from ongoing road construction projects across targeted regions. Professor Hesp and his team actively engaged with various transportation departments and agencies to gather necessary samples. This includes high-profile projects and remote locations such as national parks. As a result, a total of 332 asphalt samples, which is far above expectation, were provided by user agencies from Canada, China and the USA. A detailed overview is provided in Table 2.

Table 2. List of asphalt samples collected from user agencies in Canada, China and the USA.

Region Name	Number of Tank Samples	Number of Recovered Samples
USA		
California	9	11
Connecticut	2	8
Massachusetts	8	9
New Hampshire	N/A	9
Nebraska	2	4
Kansas	2	2
Colorado	4	8
Ohio	N/A	8
Minnesota	6	6
Alaska	2	2
Illinois	5	6
Western Federal Lands	N/A	13
Maine	5	5
Michigan	2	N/A
Canada		
Durham	3	80
Kingston	N/A	1
Toronto	4	39
Peel	7	12
York	2	18

Ontario	N/A	7
Edmonton	N/A	3
Quebec	1	N/A
China		
China (2)	16	2
Total	80	252

Task 4 – AASHTO M 320 Grading

This task aimed to grade collected asphalt binders according to the AASHTO M 320 standard test methods to determine their performance grades. All the asphalt binders, either tank sample or extracted and recovered, were aged and tested according to AASHTO M320 grading methods via DSR and Bending Beam Rheometer (BBR) tests to determine High, Intermediate, and Low-Temperature Performance Grades (HTPG, ITPG, LTPG) of the binders. Among them, the results of 9 samples were incomplete due to various reasons including operational difficulties encountered with highly modified asphalt and anomalies in the results for asphalt binders tainted by substandard modifiers. Figure 1 below shows plots for tank samples and extracted and recovered asphalt binder samples in terms of their regular AASHTO M 320 specification grades XX-YY. It shows grades originating from different nominal PG XX-34, XX-28 and XX-22 zones and from wide geographical areas.

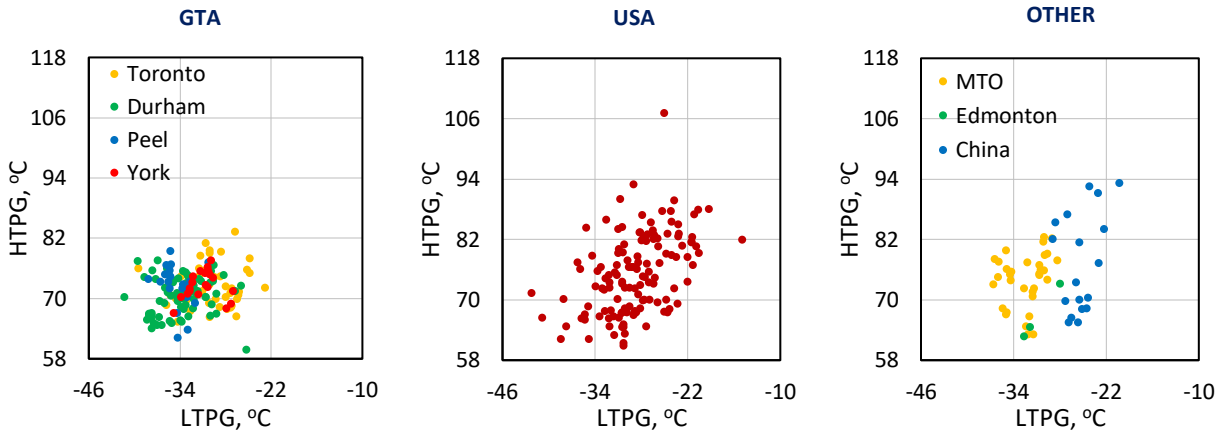

Figure 1. AASHTO M 320 XX versus YY box plots.

Samples were extracted and recovered from loose mix and sampled from the storage tank at the asphalt plant. Note that Durham and Peel implemented improved specifications as reflected in softer grades. MTO data include some obtained before 2022.

The results are summarized in Table A-1 in Appendix for reference. It is important to highlight that the HTPG results for asphalt binders from asphalt mixtures were exclusively derived from the recovered asphalt. In the case of tank asphalt binder, assessments were conducted on both unaged and RTFO-aged samples to ascertain the HTPG, with the lower of the two values being documented. The analysis and outcomes can be found in Section 4.4.1.

Task 5 – DENT and EBBR Grading

This task aimed to use DENT and EBBR test protocols to further assess and enhance the grading of Alberta binders, focusing on ductile strain tolerance and durability. The results of Crack Tip Opening Displacement (CTOD) measurements obtained from the DENT test were plotted against limiting low temperature grades (LLTPG) from the EBBR test, as shown in Figure 2. The corresponding results for the DENT test include the CTOD, specific essential work, and specific plastic work and are listed in Table A-2 in the Appendix.

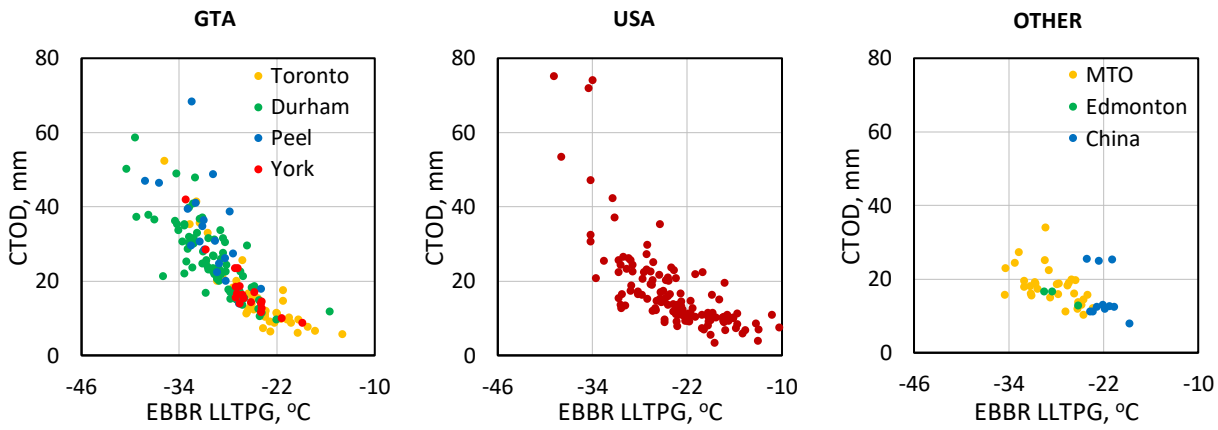

Figure 2. CTOD versus EBBR LLTPG plots.

Samples were extracted and recovered from loose mix and sampled from the storage tank at the asphalt plant. Note that Durham and Peel implemented improved binder specifications as reflected in softer grades and higher CTOD values.

The DENT testing has shown that there are wide ranges of ductile strain tolerance as reflected in the CTOD for binders of ostensibly the same Superpave grade. It is noteworthy that some binders (especially those from China), suffered from brittle failure in tension and therefore their CTOD value is not available.

The EBBR test provides information on how stable asphalt binder composition and properties are when conditioned at low winter temperatures. Samples are typically cooled at 10°C and 20°C above the pavement design temperature YY. For instance, for Toronto the low design is -28°C, so the samples collected from the city are typically conditioned at -18°C and -8°C, for 1, 24 and 72 hours prior to pass/fail testing. Due to time and funding limitations the bulk of recent samples were tested after conditioning of only 1 and 72 hours, at T_{design} + 10 for pass/fail performance, i.e. -18°C for GTA binders. Hence, data presented here represent simplified AASHTO TP 122 results, however they are considered good approximations for those that would have been obtained under the full protocol. Figure 3 below shows the grade loss versus the LLTPG from EBBR for all samples, the raw data of EBBR test can be found in Table A-2 in the Appendix.

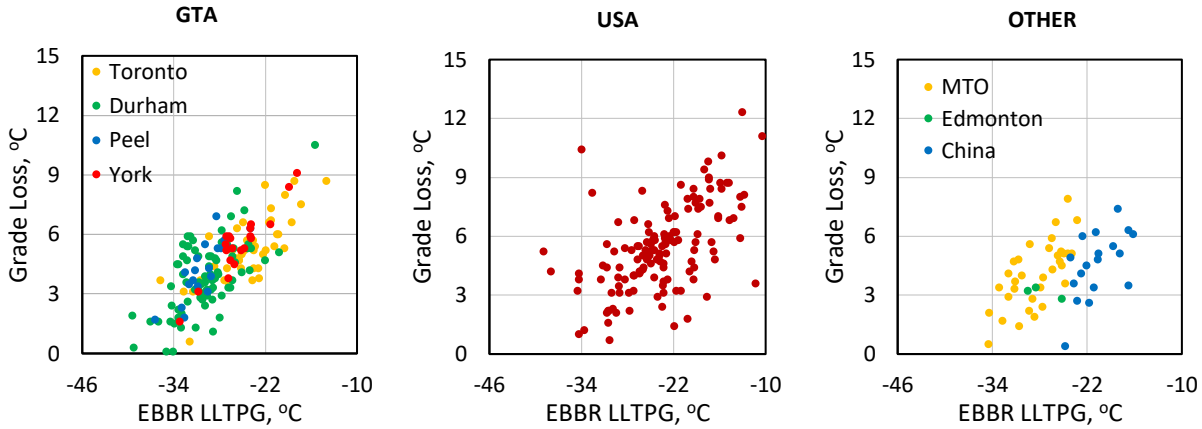

Figure 3. EBBR LLTPG versus grade loss plots.

Samples were extracted and recovered from loose mix and sampled from the storage tank at the asphalt plant. Note that both Durham and Peel implemented improved asphalt binder specifications as reflected in lower grades and grade losses.

The data in Figure 3 shows that results are good for Durham and Peel where superior quality asphalt binders from Alberta are being used. Results are not so good for Toronto and York, where a switch to improved specifications will happen soon. The USA samples show a wide range of attributes from good to acceptable to unacceptable. Grade losses of 6°C typically reduce the confidence that a pavement is not exposed to damaging temperatures in any given year from the intended 98 % to around 50 %. Findings are reasonable for MTO, where the tank sample is well controlled through regular inspections at the production facility. The grade loss for the Edmonton sample remains at a reasonably low level as those from MTO. However, it is important to note that only three samples were collected from Edmonton, which

indicates that this conclusion requires further validation with a larger dataset of asphalt samples. Regarding the asphalt binders from China, the grade loss is moderate. The correlation between DENT/EBBR results of different asphalt binders and other properties of asphalt binder and mixture was explored and the results and discussion can be found in Section 4.4.1.

EBBR and DENT results of selected asphalt binders from contract roads in Durham Region of Ontario, Canada further validated the effectiveness of EBBR and DENT in differentiating asphalt binders with extraordinarily different durability. The service life of asphalt pavement can be significantly increased by limiting the minimum CTOD from the DENT test and maximum grade loss from the EBBR test. The related findings are summarized in Section 4.7 and submitted for presentation and publication at the Transportation Association of Canada (TAC) Conference in Vancouver from September 22-24, 2024.

Task 6 – MDSC and DSR Grading

This task was to investigate the potential of MDSC and DSR tests for grading asphalt binders, aiming for a method that is accurate, precise, and more practical than current approaches. Progress on this task has been informed significantly by the insights gained from MDSC analysis. A total of 53 samples including Timmins pavement trial binders and contract binders were tested in the modulated differential scanning calorimeter at 100, 30 and 10°C/hour cooling rates. Asphalt samples from a Timmins pavement trial were aged to various degrees before performing MDSC testing. Both reversible and non-reversible analysis were performed, and insights were derived from these results to better understand the difference in field performance among different asphalt binders. The corresponding results were published in *Construction and Building Materials* (Sandrasagra et al., 2023) and a detailed discussion is provided in Section 4.3.1.

By investigating the relationship between phase separation and thermo-reversible aging in asphalt binders, it was found that there is no direct correlation. Analysis revealed that faster cooling rates resulted in more pronounced phase separation in asphalt, yet this did not correlate with LTPG or thermo-reversible aging as measured by grade loss. While phase separation occurs under specific conditions, it merely precedes the critical oil exudation process, which contributes to thermo-reversible aging. This insight challenges the traditional understanding of asphalt thermo-reversible aging and underscores the importance of re-evaluating how asphalt binders are tested and predicted to perform in field conditions. The results were summarized in a conference paper accepted as a poster at the 20th International Conference on Cold Regions Engineering (ICCRE) in Anchorage, Alaska, USA, from May 13-16, 2024. The detailed results and discussion can be found in Section 4.3.2.

In terms of DSR, significant findings were obtained for the potential of replacing traditional EBBR and DENT protocols with DSR testing. First, the relationship among limiting phase angle temperature, ITPG, rheological indicators derived from master curve, CTOD, LLTPG, grade loss were systematically analyzed. Results indicate that the rheological indicators derived from master curves have no obvious correlation with limiting phase angle temperature. However, there exists a strong correlation between limiting phase angle temperature with LLTPG from EBBR and CTOD from DENT test. This means that limiting phase angle temperature can be used to predict the cracking resistance of asphalt binder at intermediate and low temperature. Furthermore, limiting phase angle temperature can be used to replace EBBR and DENT tests as a performance acceptance test method. Moreover, the effect of cooling rate on the response of rheological properties of asphalt binder was investigated, the corresponding results are summarized in Section 4.4.1. Secondly, an attempt was made to explore the link between the rheological properties of asphalt binder and the corresponding lifespan of asphalt pavement. It was found that there was a good correlation between limiting phase angle temperature and projected lifespan of asphalt pavement. In contrast, rheological master curve and Black space diagram are not capable of predicting the lifespan of asphalt pavement. The related findings were published in *Construction and Building Materials* (Ma et al., 2023), and the details can be found in Section 4.4.2.

Task 7 – Hamburg Testing

Hamburg testing was conducted on a total of 31 samples at 30°C, 40°C, and 50°C until failure at a rut depth of 20 mm. The results were compared with the high temperature Superpave grade (XX, HTPG) as well as the Multiple Stress Creep Recovery (MSCR) results (J_{nr} and ER). The findings are provided in Figure 4 below and show that, as expected, there is no correlation between high temperature binder properties and rut resistance. Hence, it is important to work towards the implementation of the Hamburg test for acceptance of the mixture at an early opportunity.

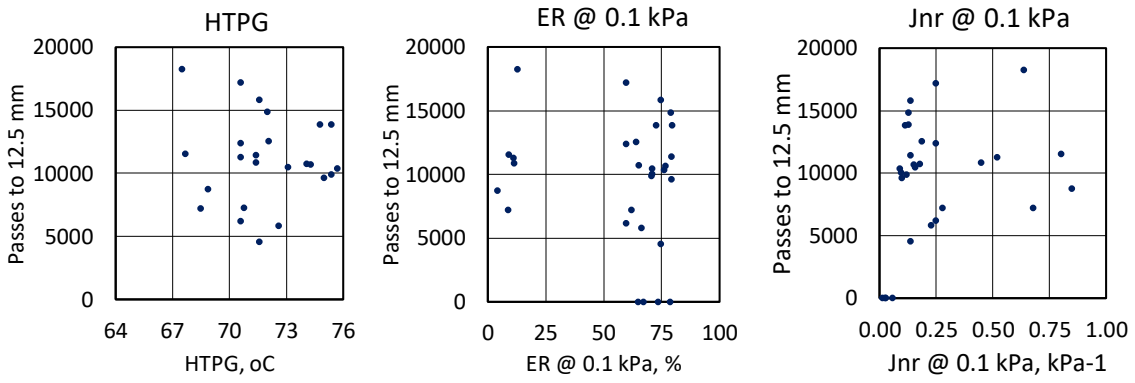

Figure 4. Hamburg passes to 12.5 mm rut depth at 50°C versus DSR HTPG, MSCR ER and J_{nr}.

Another lesson learned from the HWTT results is that testing temperature is critical in ranking the rutting resistance of different asphalt mixtures, especially when fiber and plastic modifier are added. The effect of adding fiber and plastic on the rutting resistance of asphalt mixture can be better manifested at an optimum temperature of 40°C. The related results are summarized in Section 4.6 and were submitted to *Science of the Total Environment* for review and publication.

Task 8 – Semicircular Bend Testing

This task aimed to grade asphalt binders in terms of cracking resistance at the mixture level based on the Semi-Circular Bend (SCB) test. Initially, laboratory prepared asphalt mixtures were evaluated to analyze the effect of mixture aging method, testing conditions including loading rate and temperature on the cracking resistance results. Based on these results, the current testing method was optimized towards improved repeatability and sensitivity. The related results were summarized in Section 4.5.1 and published in *Construction and Building Materials* (Ren et al., 2023). Then, core samples from a Durham Region pavement trial were tested to investigate the effect of recycled plastics/fibers on the cracking resistance of asphalt mixture. The results show that Alberta binder combined with PET fiber provided asphalt mixture with significantly improved cracking resistance. The related results were summarized in Section 4.5.2 and submitted to *Science of the Total Environment* for review and publication.

Finally, the cracking resistance test based on SCB was optimized to include thermo-reversible aging. The related results were detailed in Section Section 4.5.3, and the results were published in the *Transportation Research Record* journal (Elliott et al., 2024).

Task 9 – Reporting

Task 9 aimed to ensure thorough documentation and dissemination of the research findings through presentations at industry conferences and publications in scholarly journals. Extensive efforts have been devoted to presenting results at conferences and peer-reviewed journals, aiming for broad dissemination of the research outcomes. To summarize, seven papers have been published in prestigious journals, including one in *Road Materials and Pavement Design*, five in *Construction and Building Materials*, and one in *Transportation Research Record*. Two additional manuscripts have been submitted for review. A paper was presented at the 103rd Transportation Research Board (TRB) Annual Meeting in Washington, D.C., USA, in January 2024. Another paper was featured at the 10th International Conference of the European Asphalt Technology Association (EATA) in Gdańsk, Poland, in June 2023. At the 60th Petersen Asphalt Research Conference (PARC) held in Laramie, WY, USA, in July 2023, two papers were presented—one in a speaking session and the other as a poster. Moreover, four papers have been approved for

upcoming conference presentations. Two are slated for oral presentations at the 8th International Conference on Bituminous Mixtures and Pavements (ICONFBMP) in Thessaloniki, Greece, from June 12-14, 2024, and two for poster presentations at the 20th International Conference on Cold Regions Engineering (ICCRE) in Anchorage, Alaska, USA, from May 13-16, 2024. Additionally, one paper is submitted to the Transportation Association of Canada Conference (TACC) in Vancouver in September 2024. Details of all submissions are provided below under the section on project communications.

3. METHODOLOGY

The research activities for this project took place in the asphalt laboratories at the Department of Chemistry of Queen's University at Kingston, Ontario. Both asphalt binder tests and mixture tests were conducted. A detailed description of experimental methods is introduced hereinafter. Asphalt binder samples include both tank samples and samples extracted and recovered from asphalt mixtures. Asphalt mixture samples included contract samples taken from the paving equipment and those prepared in lab.

3.1 Optimized Extraction & Recovery Process

3.1.1 Simplified Extraction & Recovery Process

In this research project, the initial phase is dedicated to improving the existing extraction and recovery method. A streamlined protocol for extraction, recovery, and aging was proposed. Despite this, the traditional extraction and recovery method was also applied across all asphalt mixtures to obtain asphalt binder samples for analytical purposes. To begin with, we provide a concise overview of the conventional extraction and recovery process for comparative analysis. Traditional extraction and recovery method, as depicted in Figure 5, encompasses the following steps: (i) First, the asphalt mixture is immersed in dichloromethylene (DCM) solvent overnight to ensure the complete dissolution of the asphalt binder; (ii) Second, the sample is sieved to remove coarse and fine aggregates. Aggregates are washed with fresh DCM to remove remaining asphalt; (iii) Third, the asphalt solution is fed through a high-speed centrifuge to remove most of the fines; (iv) Fourth, the solution is transferred into a round bottom flask which is heated in an oil bath at temperatures increasing from 90℃ to 160℃, while rotating under an applied vacuum maintained at 550 mbar initially and slowly reduced to below 50 mbar. This process, which takes approximately 2 hours, is conducted under a dry nitrogen gas atmosphere to prevent the aging of the binder. After evaporating most of the solvent, the temperature is gradually increased in steps to ensure the complete recovery of the pure binder; (v) Then, the recovered binder is aged using the PAV according to standard procedures (AASHTO R 28, 2009). The aging conditions involve exposing the asphalt film of 3.2 mm thickness to 100℃ for 20 hours under a compressed air pressure of 2.08 MPa. Following the PAV aging process, the PAV-aged residue is subjected to performance evaluation tests, including the DENT and EBBR tests.

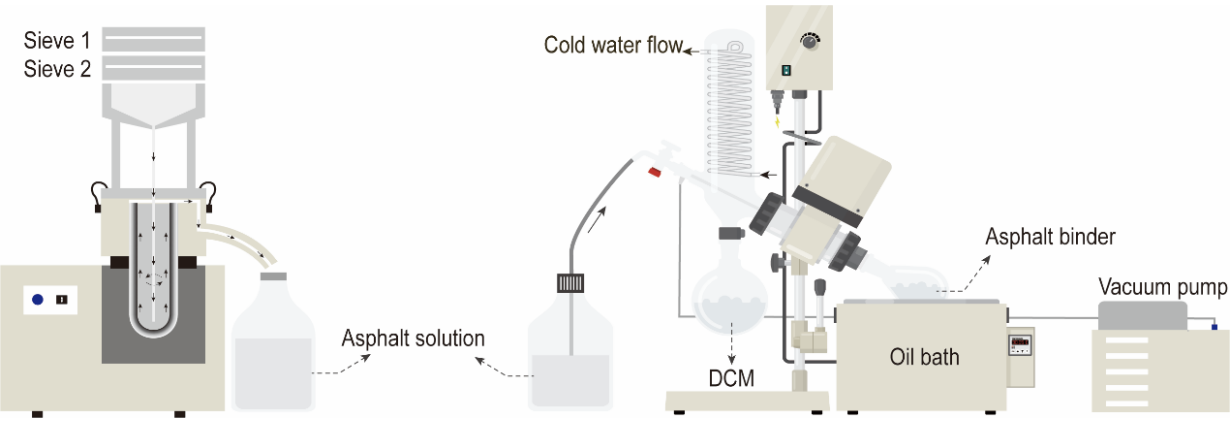

Figure 5. Schematic diagram of the extraction and recovery process of asphalt binder from mix.

To save time and efforts in extraction and recovery process, the simplified extraction and recovery process was proposed potentially as an alternative of traditional extraction and recovery method. As shown in Figure 6, this protocol consists of the following steps: (1) soak around 200 g HMA in a paint can in 140–160 mL of solvent; (2) put the sealed can in an ultrasonic cleaner for about 10 min; (3) remove coarse and fine aggregates with sieves of different sizes (75 µm and 25 µm); (4) heat the extracted asphalt solution on a hot plate in the fume hood to evaporate the bulk of the solvent; (5) place the recovered binder in the oven at 140 °C for 16 h to simulate PAV aging (Wright et al., 2011). The asphalt film thickness is the same as that for the PAV test (3.2 mm). To standardize the method proposed the following key issues are addressed. First, a new, less toxic solvent is used to reduce potential health risks. The proposed green solvent, HD PRO, together with two commonly used solvents are listed in Table 3. HD PRO is a new precision cleaning solvent mixture of 1,2-trans-dichloroethylene and proprietary fluorinated compounds, which are designed with hydrofluorocarbons (HFCs) that will not induce any serious health problems (Charlesworth and Swinton, 2017; Tsai, 2005). DCM and TCE are commonly used solvents for asphalt binder. Although HD PRO is less volatile than DCM, it still has a high hydrocarbon solubility and low boiling point of around 48 °C. Four mixes, A-1, A-2, B-1 and/C, were used to analyze the effect of solvent type in the simplified extraction, recovery and aging protocol on the properties of the recovered asphalt binder. The standard protocol as specified in the AASHTO standard was also used to recover the four mixes using DCM solvent, which is designated as the control (AASHTO T 319-15, 2008). Properties of the recovered asphalt binders were evaluated via DSR and Fourier transform infrared (FTIR) spectroscopy which will be introduced later.

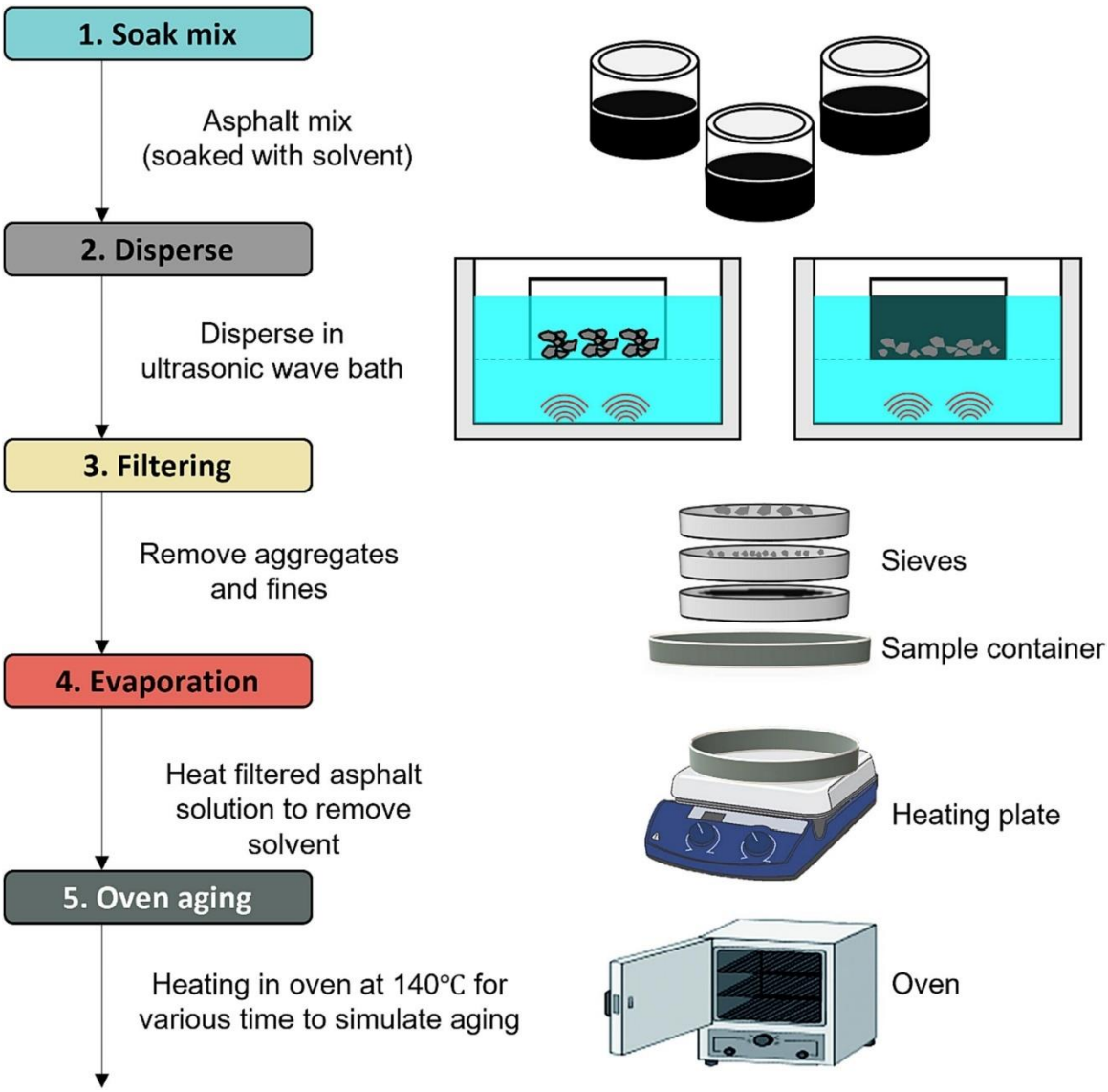

Figure 6. Schematic diagram of simplified extraction and recovery.

Table 3. Solvents investigated.

Label	Boiling point, °C	Composition	TWA, ppm
HD PRO	48.0	1,2-trans-dichloroethylene	200
		1,1,2,2-tetrafluoroethyl-2,2,2-trifluoroethyl ether	75
DCM	39.6	Dichloromethane	25
TCE	87.2	Trichloroethylene	50

3.1.2 Ethanol Ultrasonication

As part of the optimized extraction & recovery process task, the simplified extraction and recovery was further optimized to address the oil exudation issue which was ignored in the current standard. In light of this challenge, an innovative exudation test protocol, referred to as “Ethanol Ultrasonication Test”, was proposed in this research project. The methodology of the simplified five-step exudation test protocol as depicted in Figure 7 is as follows: (1) Approximately 3.5 g of pressure aging vessel (PAV)-aged binder is divided into small pieces by rolling it into a long string and cutting it with a single edge razor; (2) Binder pieces are placed into a 250 mL metal can and immersed in 200 mL of anhydrous ethanol before closing the lid; (3) The sample is ultrasonicated for 20 minutes, starting at an initial temperature of approximately 35°C, ensuring the internal temperature does not exceed 50°C; (4) Ethanol is decanted and the binder is transferred into a 50 mm diameter tin, allowing it to air dry for at least 30 minutes; (5) Recovered binder is heated in an oven at 160°C for 20 minutes to remove residual ethanol. The dry binder is poured for dynamic shear rheometer (DSR) testing of complex modulus and phase angle to determine the changes in rheology both after exudation.

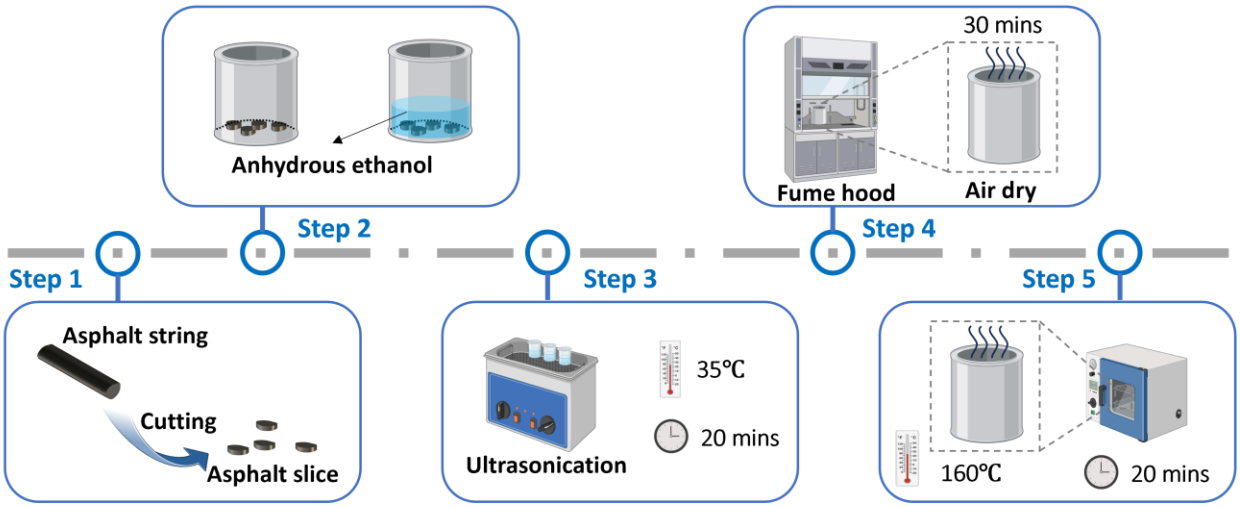

Figure 7. Schematic of five step exudation test protocol.

3.2 Binder Tests

3.2.1 Laboratory Accelerated Aging

The asphalt binders analyzed in this study are classified into two primary groups. The first group consists of tank asphalt samples in their unaged state, while the second are those extracted and recovered from asphalt mixtures. For all these samples, laboratory-accelerated aging was conducted to simulate the field aging experienced by asphalt pavements over years before assessing properties such as cracking

resistance and fatigue resistance which are critical when the aging degree of asphalt binder is high. Specifically, tank asphalt binders were subjected to short-term aging using rolling thin film oven (RTFO) method alongside their unaged counterparts before being evaluated for their resistance to high-temperature rutting. Following this, the residue from short-term aging is subjected to long-term aging using standard pressure aging vessel (PAV) method before the assessment of cracking resistance at intermediate and low temperatures is performed.

In contrast, recovered asphalt binders are only required to undergo long-term aging before their evaluation for cracking resistance at intermediate and low temperatures. Additionally, these recovered binders can directly be assessed for high-temperature rutting resistance, as it is assumed that an equivalent short-term aging process has already occurred during the extraction and recovery process. In this project, RTFO and PAV method were used to perform short-term and long-term aging simulation, respectively. The standard protocols for RTFO and PAV are detailed in the specifications (AASHTO R 28, 2009; AASHTO T240, 2013).

3.2.2 Dynamic Shear Rheometer (DSR) Test

The rheological characteristics of asphalt samples were examined using a Dynamic Shear Rheometer (DSR), as depicted in Figure 8. The assessment via DSR includes three principal testing methodologies: (1) frequency sweeping, which is predominantly utilized for evaluating asphalt's performance at high and intermediate temperatures; (2) Temperature sweeping, aimed at identifying the limiting phase angle temperatures; (3) Master curve, which aims to capture the rheological properties of asphalt binder over a broader frequency range. In the evaluation of asphalt's high-temperature performance, parallel plates of 25 mm diameter were utilized, setting the gap between them to 1 mm. Oscillatory shear tests were conducted across temperatures ranging from 46 ℃ to 82 ℃, at 6 ℃ intervals, with a shear frequency of 10 rad/s, in accordance with AASHTO R29 and AASHTO M320 standards (AASHTO M320, 2016; AASHTO R29, 2015). At each temperature, the rutting factor, denoted as G*/sin δ, was recorded. For the intermediate temperature performance assessment of asphalt, parallel plates of 8 mm diameter were employed, with the inter-plate gap fixed at 2 mm. Oscillatory shear tests were carried out at temperatures from 7 ℃ to 22 ℃, with 3 ℃ intervals between each temperature, maintaining a loading frequency of 10 rad/s, as per AASHTO R29 and AASHTO M320 guidelines (AASHTO M320, 2016; AASHTO R29, 2015). At each temperature point, the fatigue factor, G*·sin δ, was recorded.

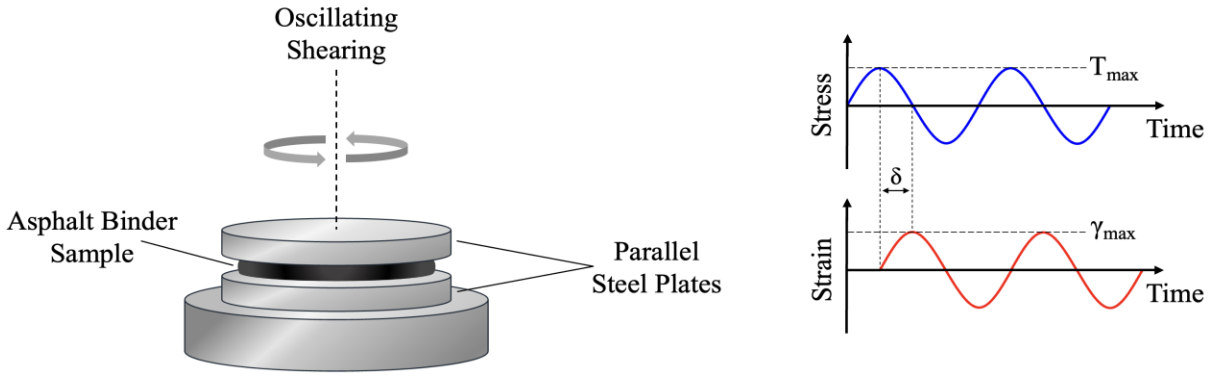

Figure 8. Schematic diagram of dynamic shear rheometer (DSR) setup.

To determine limiting phase angle temperature, parallel plates with an 8 mm diameter and a 2 mm gap were employed. Temperature sweep was performed over a range from -6 ℃ to 60 ℃ at a constant frequency of 10 rad/s. The change of phase angle over temperature is depicted in Figure 9 from which the limiting temperatures corresponding to phase angles 30° and 45° can be determined, which were referred to as limiting phase angle temperature $T_{30°}$ and $T_{45°}$. The difference of the two was referred to as $\Delta T_{C\delta}$ (Ma et al., 2023). $\Delta T_{C\delta}$ primarily reflects the slope of phase angle master curve over temperatures, providing insights into the asphalt's stress relaxation capabilities.

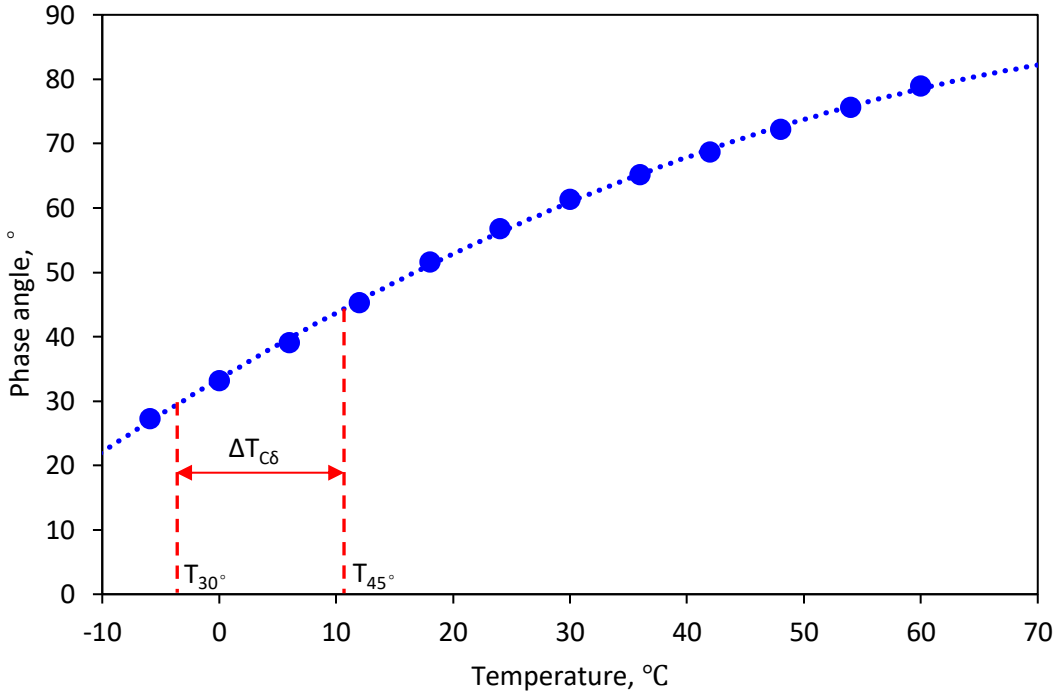

Figure 9. Determination of limiting phase angle temperature.

To obtain complex modulus and phase angle master curve, frequency sweep was performed from 0.1 rad/s to 10 rad/s, at temperatures from 60°C to -6°C at 6°C intervals. During the frequency sweep at each temperature, complex modulus and phase angle data were collected for the construction of master curve. To compare the effect of cooling rate, both slow and rapid cooling were employed during the frequency sweep test. The slow cooling was achieved by conditioning asphalt sample at each testing temperature for 1 hour prior to frequency sweep testing. In contrast, rapid cooling was achieved by conditioning asphalt sample for 10 minutes prior to testing. To ensure that the rheological properties obtained were within the linear viscoelastic (LVE) range, the strain was adjusted to 0.1 % for temperatures below 30°C and to 1 % for temperatures above 30°C (Bahia et al., 2001). Finally, Time-Temperature Superposition Principle (TTSP) was used to shift complex modulus at each temperature to the reference temperature 0°C, as shown in Figure 10. The determination of shifting factor at each temperature was introduced hereinafter. The obtained shift factors at each temperature were then applied to phase angle data each temperature to determine phase angle master curve as shown in Figure 11.

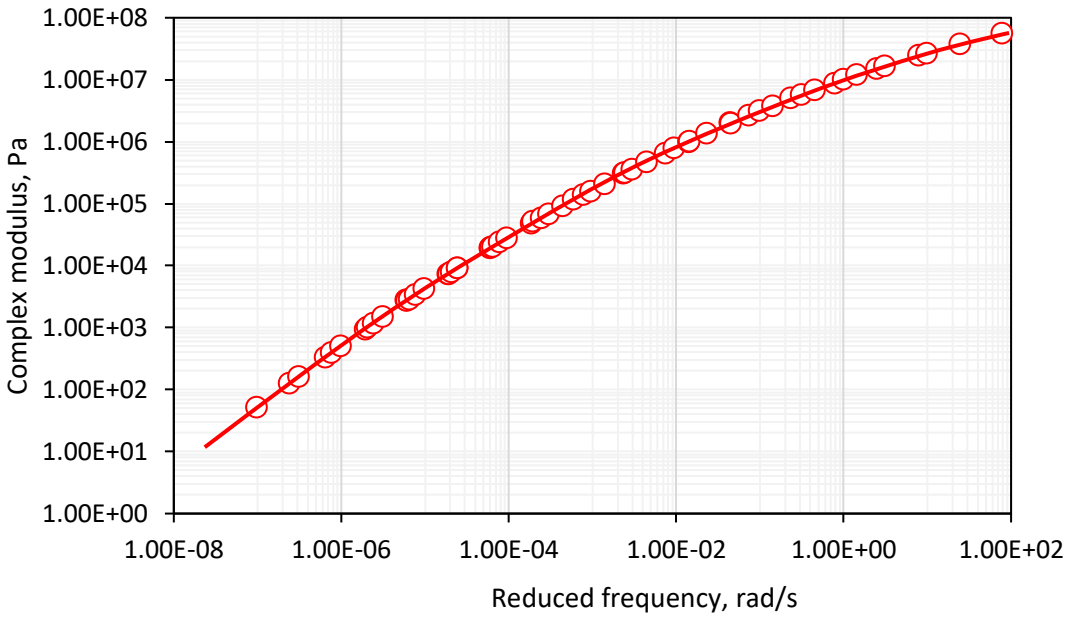

Figure 10. Example of complex modulus master curve.

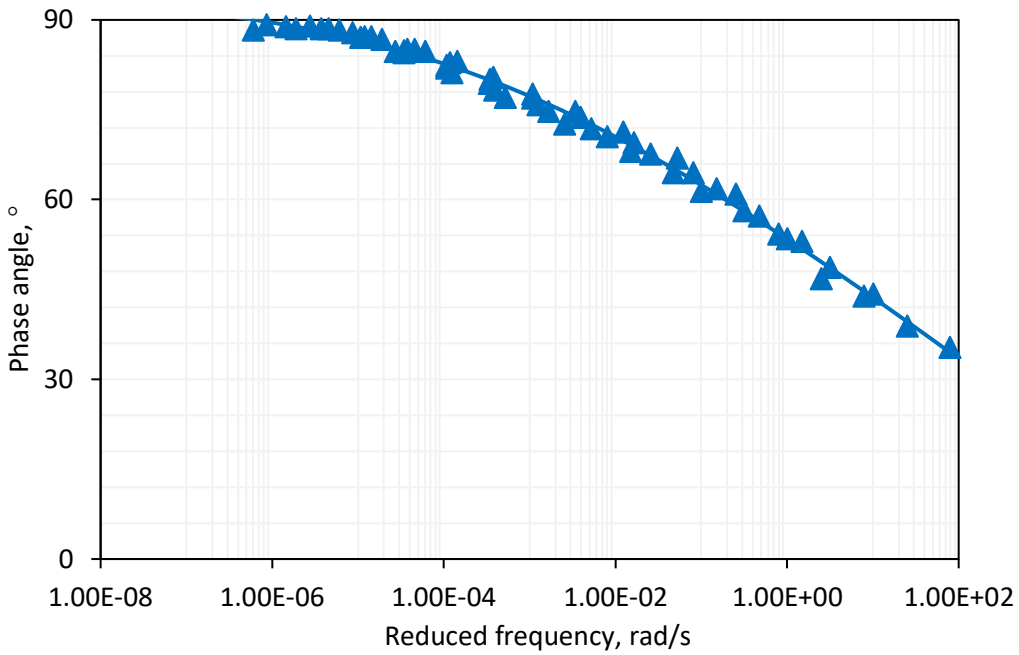

Figure 11. Example of phase angle master curve.

The determined complex modulus and phase angle master curve were fitted using Eqs. (1) and (2).

$$G^*(f,T) = \frac{G_\infty}{[1+(f_c/a_T f)^k]^{m_e/k}} \quad (1)$$

$$\delta = \frac{90 m_e}{1+(f_c/f)^k} \quad (2)$$

Where f is the frequency, in rad/s; f_c is a positional parameter; a_T is the horizontal shift factor at temperature T; G_∞ is the complex modulus of asphalt binder at glassy state; k and m_e are shape parameters which are dimensionless. The shift factor a_T is automatically calculated by the built-in TA Trios Software in DSR based on the WLF (Williams, Landel and Ferry) equation as shown in Eq. (3) (Bahia et al., 2001).

$$\log a_T = \frac{-c_1(T-T_0)}{c_2} + (T-T_0) \quad (3)$$

Where T_0 is the reference temperature, and c_1 and c_2 are the curve fitting constants.

Aside from rheological evaluation of aspahlt binder, stress relaxation was also performed via DSR. The stress relaxation test employed 8 mm parallel plates set at a 0.5 mm gap where the asphalt sample was sandwiched, as shown in Figure 12. A constant shear strain of 0.5 % was applied within 0.1 seconds, and the attenuation of the modulus was recorded over 7,046 seconds. Prior to testing, the asphalt sample is

heated to 75°C to eliminate potential residual thermal stress. The sample is then cooled to 0°C for the stress relaxation test. To examine the effect of cooling rates on the stress relaxation behavior of asphalt, two different cooling methods were employed: rapid cooling and slow cooling. For rapid cooling, the temperature was swiftly reduced from 75°C to 0°C within approximately 5 minutes. Conversely, the slow cooling approach involved conditioning asphalt for 1 hour for every 5°C decrement, ranging from 75°C down to 0°C, before conducting tests. Hereinafter, the sample ended with "R" indicates rapid cooling while that ended with "S" indicates slow cooling. This study focuses exclusively on the shear stress relaxation process. Although a normal force is present during testing, its impact on shear stress relaxation is considered minimal, thus the relaxation processes of normal and shear stress are assumed to be independent.

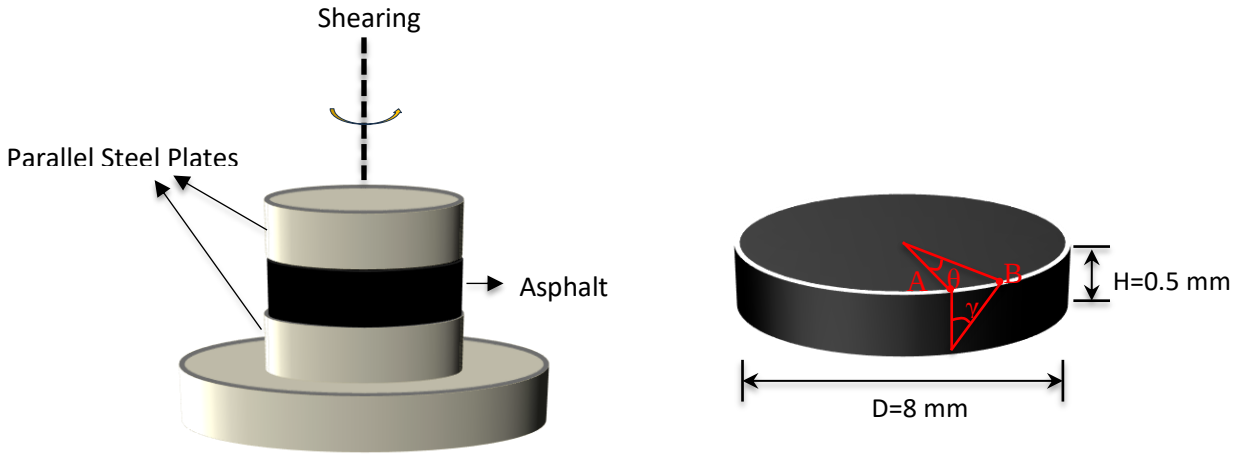

Figure 12. Schematic diagram of stress relaxation test using DSR.

When a constant shear strain, γ_0, is applied to an asphalt sample, the shear stress is recorded over a specified time interval ($0 < t < \tau$) as $\sigma(t)$. The relaxation modulus at time t is defined as $G(t) = \sigma(t)/\gamma_0$. G(t) can be expressed in an integral form as shown in Eq. (4), where G(t) is the relaxation modulus at time t and $H(\tau)$ represents the relaxation spectra.

$$G(t) = \int_{-\infty}^{\infty} H(\tau) e^{-\frac{t}{\tau}} d \ln \tau \quad (4)$$

In this study, the ReSpect code is utilized to calculate the relaxation spectrum curve (Shanbhag, 2019). Research indicates that relaxation spectra more accurately reflect the stress relaxation behavior of polymer materials, considering their chemical composition and molecular chain structure, and highlighting the contribution ratios of different components to stress relaxation (Shanbhag, 2019).

The process for deriving the relaxation spectrum curve involves first determining the parameter range using Eqs. (5) ~ (7), where t_{min} and t_{max} denote the minimum and maximum times in the stress relaxation test. As this study relies solely on measured data, the method indicated in Eq. (7) is adopted. Subsequently, the cost function estimates the total computational error of the relaxation spectrum curve, calculated for a specific frequency as per Eq. (8). $\hat{G}(t)i$ is the predicted relaxation modulus, while G(t)i is the measured relaxation modulus, as depicted in Figure 13 (a).

$$S_{\min} = e^{-\frac{\pi}{2}} \times t_{\min}; S_{\max} = e^{-\frac{\pi}{2}} \times t_{\max} \tag{5}$$

$$S_{\min} = t_{\min}; S_{\max} = t_{\max} \tag{6}$$

$$S_{\min} = e^{(+\frac{\pi}{2})} \times t_{\min}; S_{\max} = e^{(+\frac{\pi}{2})} \times t_{\max} \tag{7}$$

$$V(\lambda) = \frac{1}{N}\sum_{i=1}^{N}\left(\frac{\hat{G}(t)_i - G(t)_i}{G_i}\right)^2 + \frac{\lambda}{\eta_\tau}\int_{-\infty}^{\infty}\left(\frac{d^2}{d\tau^2}H(\tau)\right)^2 d\ln\tau \tag{8}$$

The total error comprises two parts: $\rho(\lambda)$ and $\eta(\lambda)$, with a calculation range of λ=10^{-10} to 10^2, facilitating the determination of λ's optimal value. Thus, Eq. (8) can be simplified to Eq. (9).

$$V(\lambda) = \rho^2 + \lambda\eta^2 \tag{9}$$

Where ρ^2 signifies the relative mean square error between calculated and measured relaxation moduli, and η^2 is the mean square curvature of the relaxation modulus curve. The relaxation spectrum $H(\lambda)$ corresponding to each λ's minimum cost equation $V(\lambda)$ is calculated. λ serves as a regularization parameter, balancing the equation's two terms in Eq. (9). A higher λ value yields a smoother relaxation modulus curve but at the expense of increased error, and vice versa. Therefore, the optimal λ value is identified using the L-curve method illustrated in Figure 13 (b), resulting in the final relaxation spectrum curve. Figure 13 (c) displays the typical results of the relaxation spectrum curve, which is characterized by multiple overlapping peaks. This pattern arises from the diverse stress relaxation characteristics of the different components within the asphalt. To enable a clearer comparative analysis, Origin software is employed for deconvolution processing. This process segments the relaxation spectrum curve into distinct Gaussian distribution peaks, allowing for the precise determination of each peak's position and area. Subsequently, the deconvoluted data is normalized to provide a more coherent interpretation. The final, normalized results are presented in Figure 13 (d), offering a detailed insight into the stress relaxation dynamics of the asphalt components.

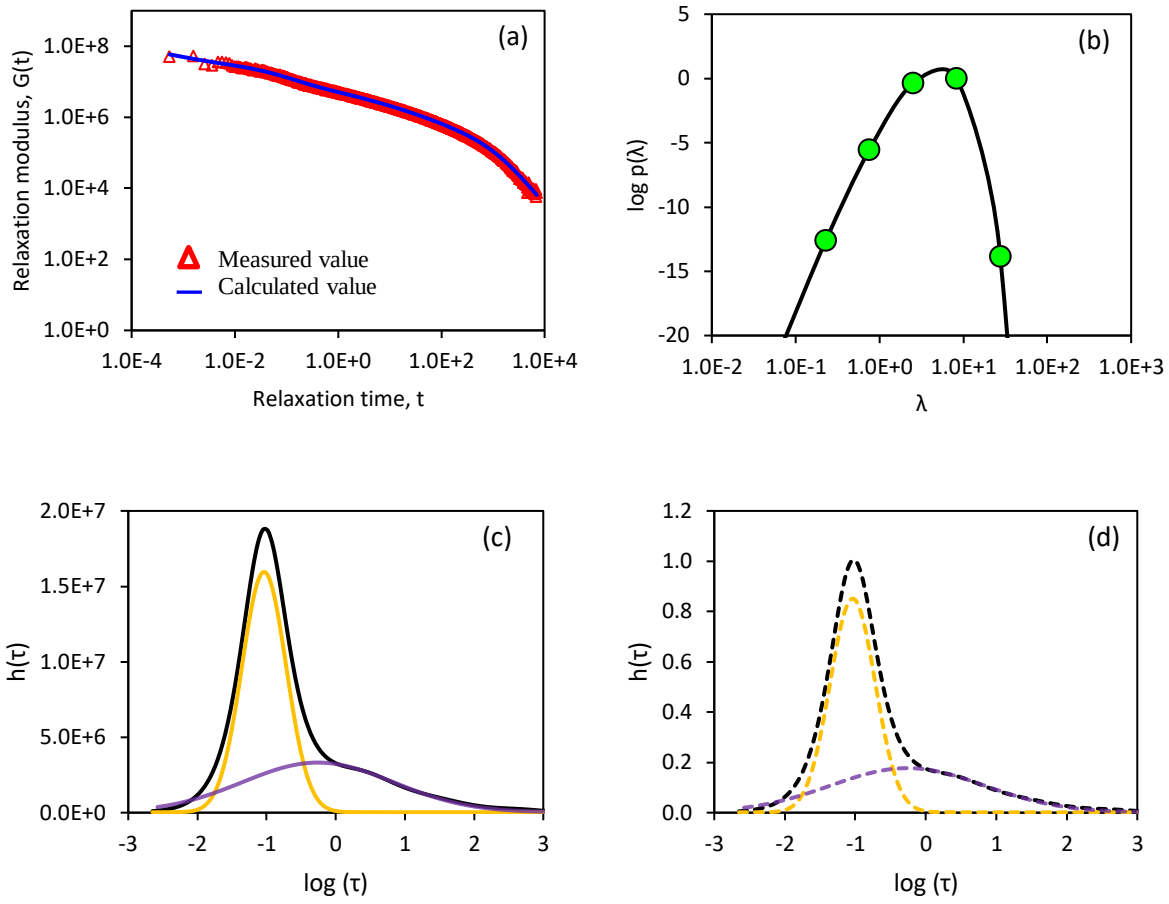

Figure 13. Example of results in each step of calculating stress relaxation spectra.

3.2.3 Extended Bending Beam Rheometer (EBBR) Test

The EBBR test was performed using the BBR apparatus as shown in Figure 14 (a), adhering to established protocols (AASHTO T 406, 2023; Hesp et al., 2009). Twelve beams were subjected to conditioning in ethanol baths maintained at temperatures of T_d + 10 and T_d + 20, where T_d represents the designated low temperature for the pavement design as determined by the LTPPBind™ software. Each bath accommodated six beams for conditioning. Three beams from each bath were tested at intervals following 1 h, 24 h, and 72 h of conditioning. After conditioning, the asphalt beam is positioned on the two support points. A vertical force of 980 ± 50 mN was applied to the center of the beam and maintained for 240 s. The deflection versus time curve is shown in Figure 14 (b). After the test, the creep stiffness S(t) was calculated according to Eq. (10) shown below.

$$S(t) = \frac{PL^3}{4bh^3\Delta(t)} \tag{10}$$

Where S(t) is the creep stiffness at time t, MPa; P is the vertical load, mN; L is the distance between the two supporting points at the bottom of the asphalt small beam, 102 mm; B and h represent the width and thickness of the small beam, which are 12.5 mm and 6.25 mm, respectively; Δ (t) The mid span deflection of the asphalt small beam at time t, mm.

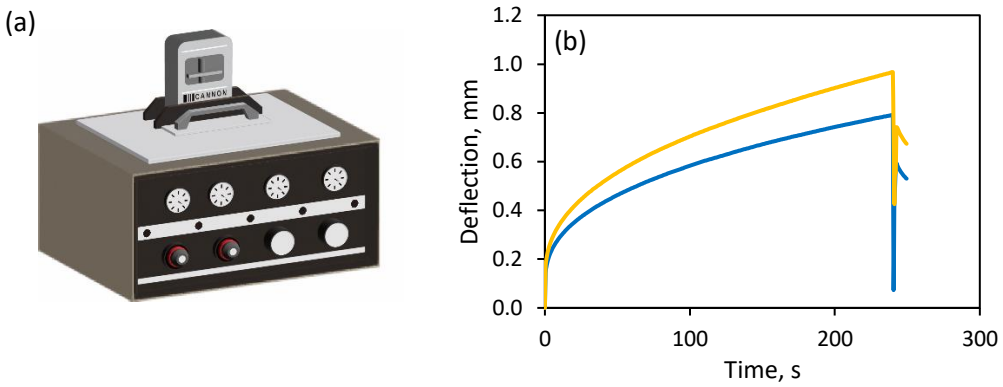

Figure 14. Schematic diagram of EBBR test.

(a) BBR equipment; (b) typical deflection-time curves after 1 h (gold) and 72 h (blue) conditioning.

The creep stiffness S(t) at 60 s is determined and the corresponding tangent slope m value at that point in logarithmic coordinates is also determined. Among them, S(t) reflects the hardness of the binder while the m value represents the creep rate, both of which are closely related to cracking resistance at low temperatures. After obtaining S(t) and m values at two temperatures, the continuous grading temperatures based on the two indicators, namely, $T_{C,S}$ and $T_{C,m}$, are calculated where the S(t) = 300 MPa and m value = 0.3, respectively, according to Eqs. (11) and (12).

$$T_{C,S} = T_i + \left[\frac{(T_i - T_{i+1}) \cdot (\log(300) - \log(S_i))}{\log(S_i) - \log(S_{i+1})} \right] \quad (11)$$

$$T_{C,m} = T_i + \left[\frac{(T_i - T_{i+1}) \cdot (0.3 - m_i)}{(m_i - m_{i+1})} \right] \quad (12)$$

Where T_i is the i-th test temperature, °C; S_i is the creep stiffness at the i-th temperature, MPa; m_i is the m value at the i-th temperature. The grade loss for the continuous low-temperature grade after 72 hours of conditioning is finally determined to evaluate the thermo-reversible aging tendency and durability of the asphalt binder. In the meantime, the LLTPG after 72 hours were calculated.

3.2.4 Double Edge Notched Tension (DENT) Test

The DENT test was conducted according to standard protocols (AASHTO T 405, 2023). In the test, six specimens with three notch depths (ligament lengths: 5 mm, 10 mm and 15 mm) were prepared for each binder. Each notch depth was tested in duplicates. Samples were subjected to tensile testing at a controlled rate of 50 ± 2.5 mm/min inside a 15 ℃ water bath until failure. A typical force-displacement curve is shown in Figure 15 (b). The facture energy determined, based on the area under the force-displacement curve, was used to calculate the specific total work of failure W_t as shown in Eq. (13). The W_t is defined as the sum of the total essential work of failure, W_e, and the total plastic work, W_p, as expressed in Eq. (14). Eq. (14) can be rewritten by assuming that the essential work is proportional to the cross-sectional area of the ligament (calculated as specimen thickness multiplied by ligament length), and the plastic work corresponds to a volume around the ligament, as depicted in Eq. (15).

$$W_t = \int_0^{t_f} P \times d \tag{13}$$

$$W_t = W_e + W_p \tag{14}$$

$$W_t = L \times B \times w_e + \beta \times L^2 \times B \times w_p \tag{15}$$

Where W_t is the specific total work of fracture, MPa; W_e is the total essential work of fracture, MPa; W_p is the plastic fracture work, MPa; w_e is the initial fracture work, MPa; β_{wp} is the plastic fracture work, MPa; t_f is the time to reach ductile fracture, s; P is the tensile force, N; d is the displacement, mm; L is the width of the ligament, mm; B is the height of the ligament, mm.

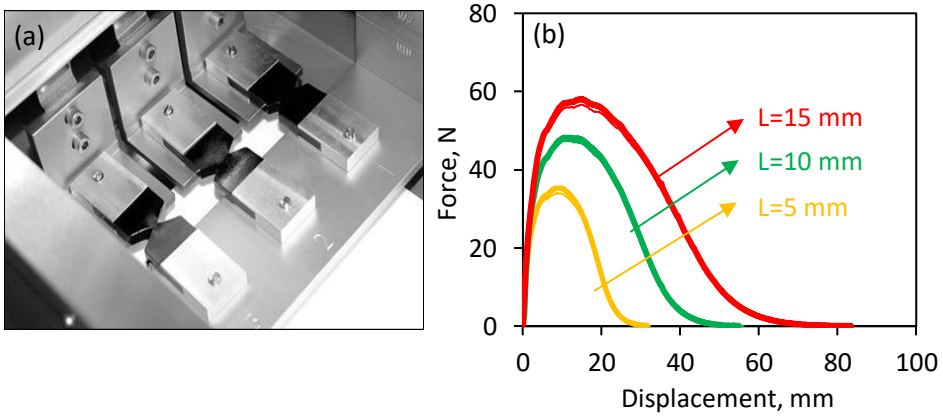

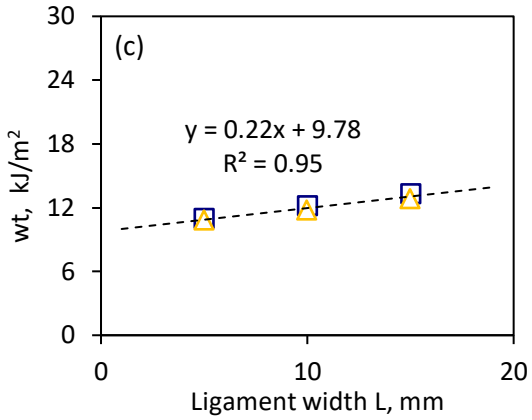

Figure 15. Schematic of the DENT test.

(a) Asphalt samples in water bath; (b) Representative load-displacement curves for DENT samples with different ligament lengths, L; (c) Determination of essential failure and plastic works from intercept and slope, respectively. Duplicate measurements provide representative repeatability.

After obtaining the force-displacement curve shown in Figure 15 (b), the total specific fracture work W_t is fitted with the ligament length L to obtain w_e and w_p as shown in Figure 15 (c). The intercept and slope of the fitting line represent the initial fracture work w_e and the plastic work βw_p, respectively. Therefore, the total specific fracture work w_t can be calculated using Eq. (16). The CTOD value was determined using data from the specimen with the smallest ligament width (5 mm), as per Eqs. (17) and (18).

$$w_t = \frac{W_t}{L \times B} = w_e + \beta w_p \times L \tag{16}$$

$$\sigma_{n=5mm} = \frac{P_{peak}}{B \times L} \tag{17}$$

$$CTOD_{L=5mm} = \frac{w_e}{\sigma_{L=5mm}} \tag{18}$$

Where σ represents the net section stress, N/mm²; P_{peak} represents the average maximum load, N; L represents the ligament length, mm; B represents the thickness of the ligament, mm.

3.2.5 Fourier Transform Infrared Spectroscopy (FTIR) Test.

FTIR spectra provide qualitative or semi-quantitative assessment of chemical changes occurring in the asphalt binder. In this study, a Perkin Elmer Spectrum 400 was used to evaluate the potential aging occurring in the extraction and recovery process. As shown in Figure 16, dissolved asphalt binder was coated on the surface of a KBr plate to form a thin film. The absorption information was collected in the

wavenumber domain from 4000 cm^{-1} to 600 cm^{-1}. The absorption peaks for CH_2 and CH_3 within wavenumber from 3150 cm^{-1} to 2700 cm^{-1} remain constant and can be used as an internal standard. The absorption peaks C=O (carbonyl group) and S=O (sulfoxide group) as shown in Figure 16 are sensitive to oxidative aging of asphalt binder and can be used to quantify the aging degree of asphalt binde. The aging index based on C=O and S=O can be calculated according to Eqs. (19) and (20).

$$I_{C=O} = A_C / A_R \tag{19}$$

$$I_{S=O} = A_S / A_R \tag{20}$$

Where $I_{C=O}$ and $I_{S=O}$ are aging indices, A_C represents the area of carbonyl peak, A_S represents the area of sulfoxide peak, A_R represents the sum of the areas for the CH_2 and CH_3 peaks.

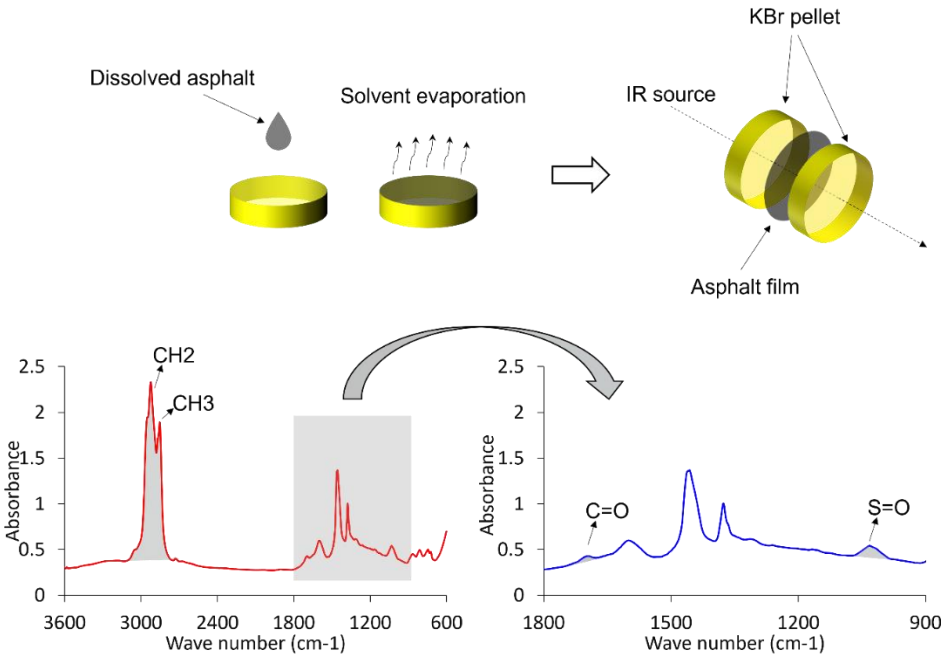

Figure 16. Schematic diagram of FTIR test and typical absorbance peaks

3.2.6 Gas Chromatography Mass Spectrometry (GC-MS) Test

Ethanol extracts obtained from the ultrasonication of samples were blown down to roughly 20 % of their original volume. The gas chromatography-mass spectroscopy (GC-MS) protocol was conducted by running the samples on an Agilent DB-17HT column in a GC-MS via quick infusion (flow injection). The schematic diagram of the GC-MS test is shown in Figure 17. Samples were tested on the following temperature gradient: starting at T_i = 60°C, hold for 1 minute before ramping up to 180°C at a rate of 12°C/min, hold

for another minute before ramping up to 340°C at a rate of 5°C/min, and proceeding to hold for a final 5 minutes.

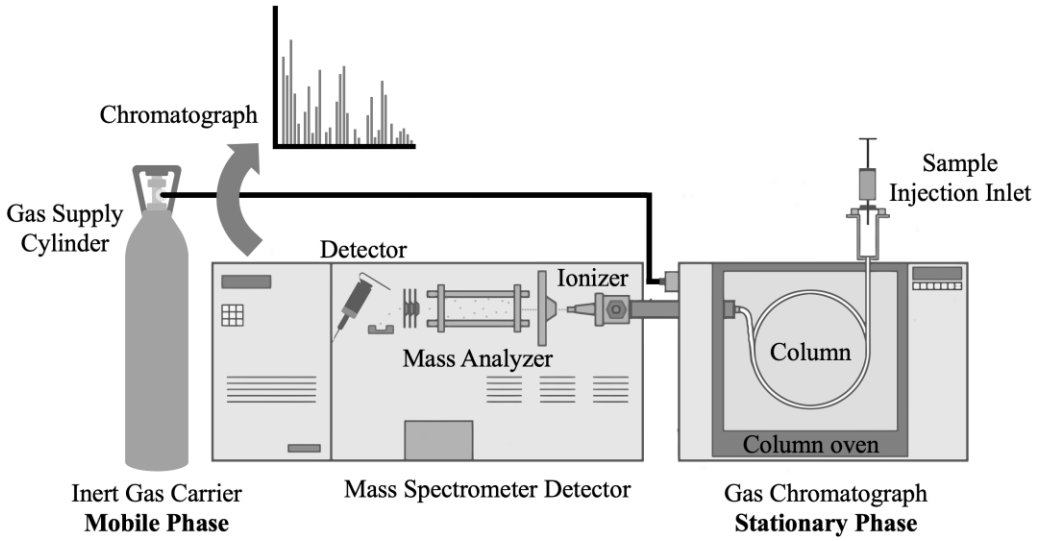

Figure 17. Schematic diagram of the GC-MS test.

3.2.7 Modulated Differential Scanning Calorimetry (MDSC) Test

A TA Instruments Q2000 DSC was used in this study. For each test, a sample between 10 and 15 mg was sealed in a hermetic aluminum pan. Samples of high mass give high sensitivity while samples of low mass increase resolution, the choice of 10-15 mg is seen as a good compromise between sensitivity and resolution (Verdonck et al., 1999). Throughout the experiment, the sample chamber was purged with extra-dry nitrogen gas at a rate of 50 mL/min to prevent oxidation and condensation. As shown in Figure 1, a non-isothermal testing program was used to enable analysis following the Ozawa framework for crystallization (Ozawa, 1971). At the beginning of a run, the sample was isothermally held at 140 ℃ for 10 min to erase the thermal history. Then, the sample was cooled until −90 ℃ at the first cooling rate (10 ℃/h) with an applied modulation every minute of amplitude 0.08 ℃. Once the sample reached -90 ℃, it was isothermally held for 10 min. Finally, the sample was heated until 140 ℃ at a rate of 10 ℃/min with an applied modulation every minute of amplitude 1.59 ℃. Once the first run was completed at 10 ℃/h, the second and the third run commenced at 30 ℃/h and 100 ℃/h. The data during heating process as highlighted in green in Figure 18 were collected for analysis. The non-reversible heat flow data were used to perform crystallization kinetic analysis based on Ozawa's framework. The reversible heat flow and reversible heat capacity data were used to determine glass transition temperature and evaluate the phase compatibility of asphalt binder.

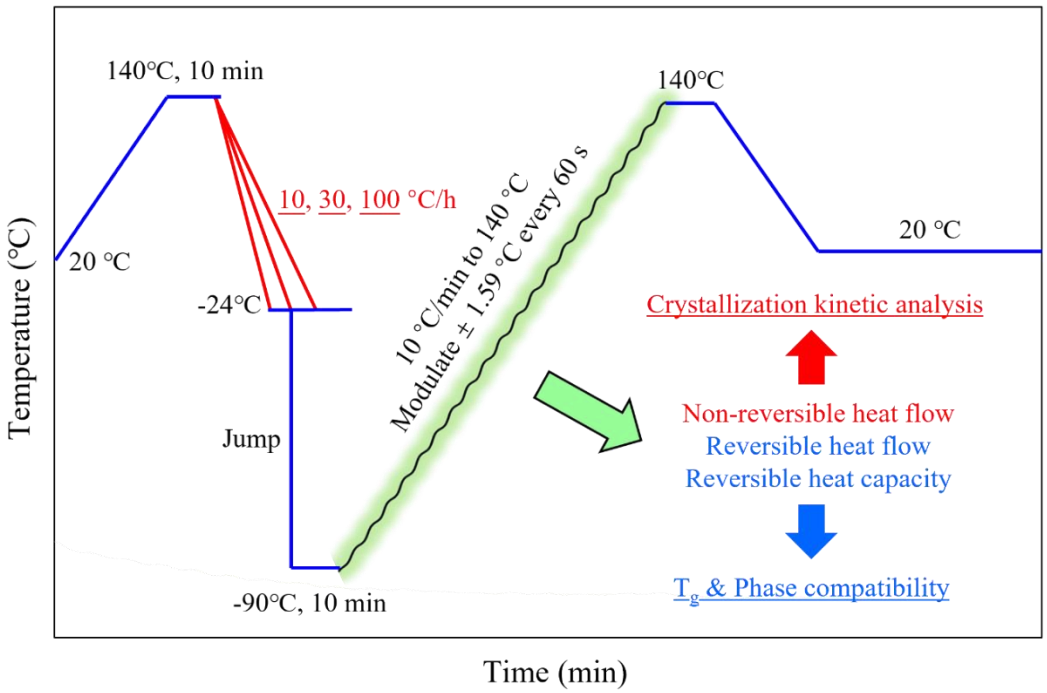

Figure 18. Temperature program of non-isothermal analysis based on Ozawa's framework.

Thermal events including structural relaxation, crystallization, and melting of crystals appear on the non-reversible heat flow signal. Linear hydrocarbons in asphalt binder are prone to crystallize upon cooling and will melt upon heating. To investigate the crystallization of the binder, thermal analysis was conducted using TA Instruments Universal Analysis software. The onset and end of the endotherm were determined as the points where the non-reversible heat flow signal deviated and returned to the baseline, respectively. The change in enthalpy is taken as the area bounded by the endotherm and the baseline. Under the framework of the Ozawa theory (Frolov et al., 2020), the non-isothermal kinetics of crystallization from an amorphous melt can be modelled. The crystalline fraction is proportional to the change in enthalpy as shown in Eq. (21):

$$CF(T) = \frac{\Delta H}{\Delta H_\infty} \tag{21}$$

Where $CF(T)$ is the crystalline fraction of the binder at a given cooling rate, ΔH is the calculated enthalpy of dissolution taken as the area enclosed by the endotherm, J/g; ΔH_∞ is the enthalpy of dissolution of wax, J/g. For this study, ΔH_∞ was taken as 200 J/g, informed by the early work of Claudy and coworkers (Claudy et al., 1988). Ozawa's (Ozawa, 1971) derivation for the model of crystallization can be found elsewhere and is presented in Eq. (22):

$$1 - CF(T) = \exp\left(-\frac{K(T)}{\beta^m}\right) \quad (22)$$

Where $K(T)$ is the temperature-dependent crystallization rate constant, β is the cooling rate, and m is the Ozawa exponent. To determine the crystallization rate constant and the Ozawa exponent, Eq. (22) is log-transformed to yield Eq. (23):

$$\log(-\ln[1 - CF(T)]) = \log(K(T)) - m\log(\beta) \quad (23)$$

Plotting $\log(-\ln[1 - CF(T)])$ against $\log(\beta)$ yields the Ozawa exponent as the negative of the slope and the crystallization rate constant as the antilog of the intercept. The Ozawa exponent implies the rate at which the system equilibrates upon crystallization. Thus, a high Ozawa exponent implies rapid crystallization and is thought to exacerbate thermo-reversible aging (Rigg et al., 2017).

Heat capacity-related events, namely the glass transition, appear on the reversible heat flow signal. The glass transition temperature serves as a representative value for the glass transition and is without an absolute definition. Two methods of determination are commonly used: the inflection point T_g(I) method and the half-height T_g(H) method. As shown in Figure 19, the former determines the glass transition temperature as the maximum rate of change of the reversible heat flow and is a rate-based parameter, namely, the temperature corresponding to the peak position of the derivative reversible heat flow curve in yellow line. The latter offers an average value of the glass transition as it takes the temperature at which half the material is vitrified or devitrified. TA Instruments Universal Analysis software was used to determine the glass transition temperature. Firstly, the onset and end temperatures of the glass transition are found through extrapolation by fitting linear tangents above and below the glass transition. Then, within these bounds, the glass transition temperature as measured by each method is obtained. The derivative of the reversible heat capacity with respect to temperature is used to characterize the phase compatibility of asphalt binder. For a completely compatible amorphous system, the derivative of the reversible heat capacity plotted against temperature will yield a uniform Gaussian with a single peak (Song et al., 1998).

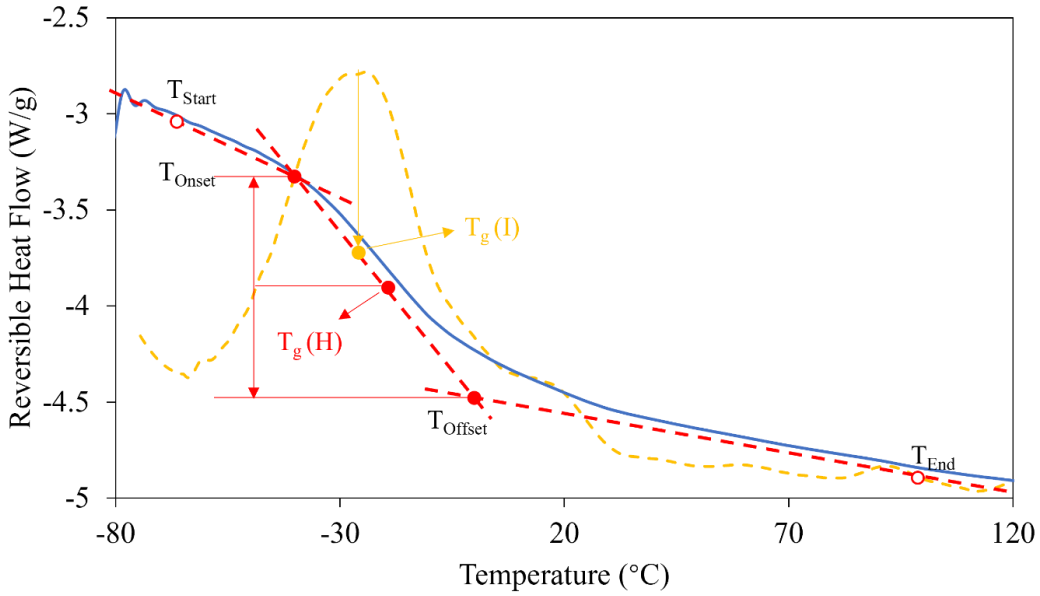

Figure 19. Schematic diagram of the methods of determining glass transition temperature.

Apart from the crystallization kinetic analysis and glass transition analysis, the reversible heat capacity data were also obtained from the heating process for analysis with the aim of providing more insights into wax crystallization, melting and recrystallization events. The derivative of reversible heat capacity versus temperature was obtained as shown in Figure 20. Based on the previous study by Kriz and coworkers (Kriz et al., 2008), it was hypothesized that the appearance of additional peaks in the derivative reversible heat capacity dCp/dT data indicates phase separation. Three indicators were obtained to quantify the degree of phase separation. The first indicator is the Main Peak (%) which is defined as the area ratio of the main peak to the entire peak. A smaller value of which indicates a higher degree of phase separation. The second indicator is the peak range which is defined as the distance between the center of the two separate peaks. The third indicator is the number of peaks.

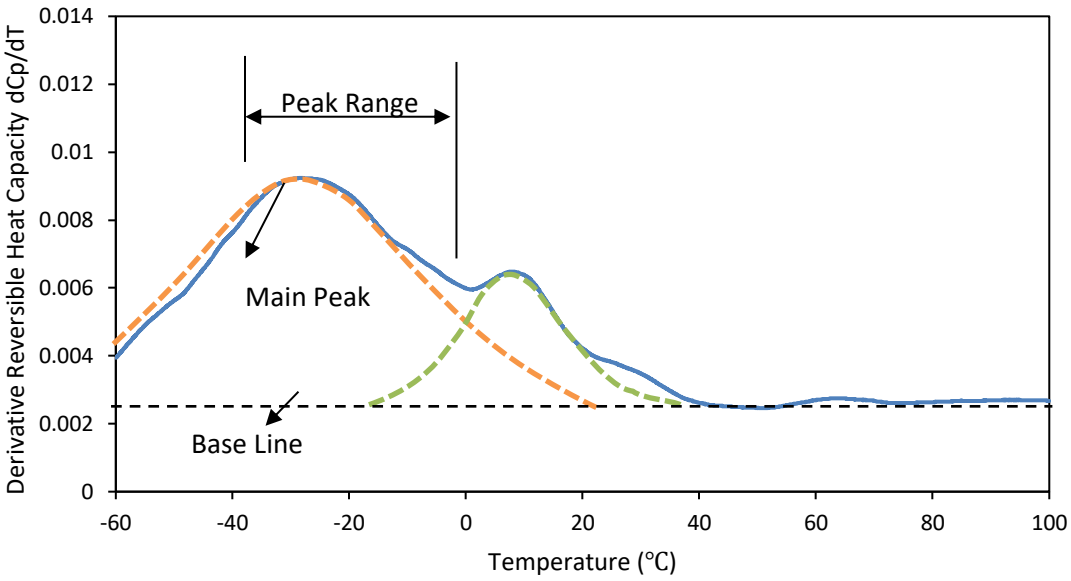

Figure 20. Phase separation indicators derived from derivative reversible heat capacity dCp/dT.

3.3 Mixture Tests

3.3.1 Semi-Circular Bend (SCB) Test

Prior to SCB test, semi-circular specimens need be prepared. For core samples collected from pavement trial, only cutting was conducted to cut asphalt specimen into designated dimension. For loose mixture, compaction was performed first to obtain a cylinder specimen with the air void of 4 % before cutting. As shown in Figure 21, mixtures were heated for 30 min until loose enough to be transferred to paint cans. After sealing the cans, these were placed in an oven at 140°C for 16 hours to produce material with an equivalent aging level of approximately 8-10 years of service (Bird et al., 2020). Specimens were compacted using a Superpave gyratory compactor to a height of 50 mm and radius of 75 mm. The air void content for all specimens in this study was set to a constant 4 %. Artificial aging of mix prior to SCB testing is used to better predict field performance in terms of cracking. In this study, a commonly used oven protocol at 140°C for 16 hours was used for chemical aging. The same oven protocol together with a cold conditioning protocol at −20°C for 3 days was used to simulate thermo-reversible aging (also known as physical aging, physical hardening, steric hardening). Finally, unaged mixes were tested for comparison. Samples were conditioned at the test temperature for 2.5 hours prior to failure in the SCB test. The temperature inside the broken SCB specimens was measured to make sure that all tests were conducted at the same temperature. Ten mixes were included at 4 replicates for each aging condition.

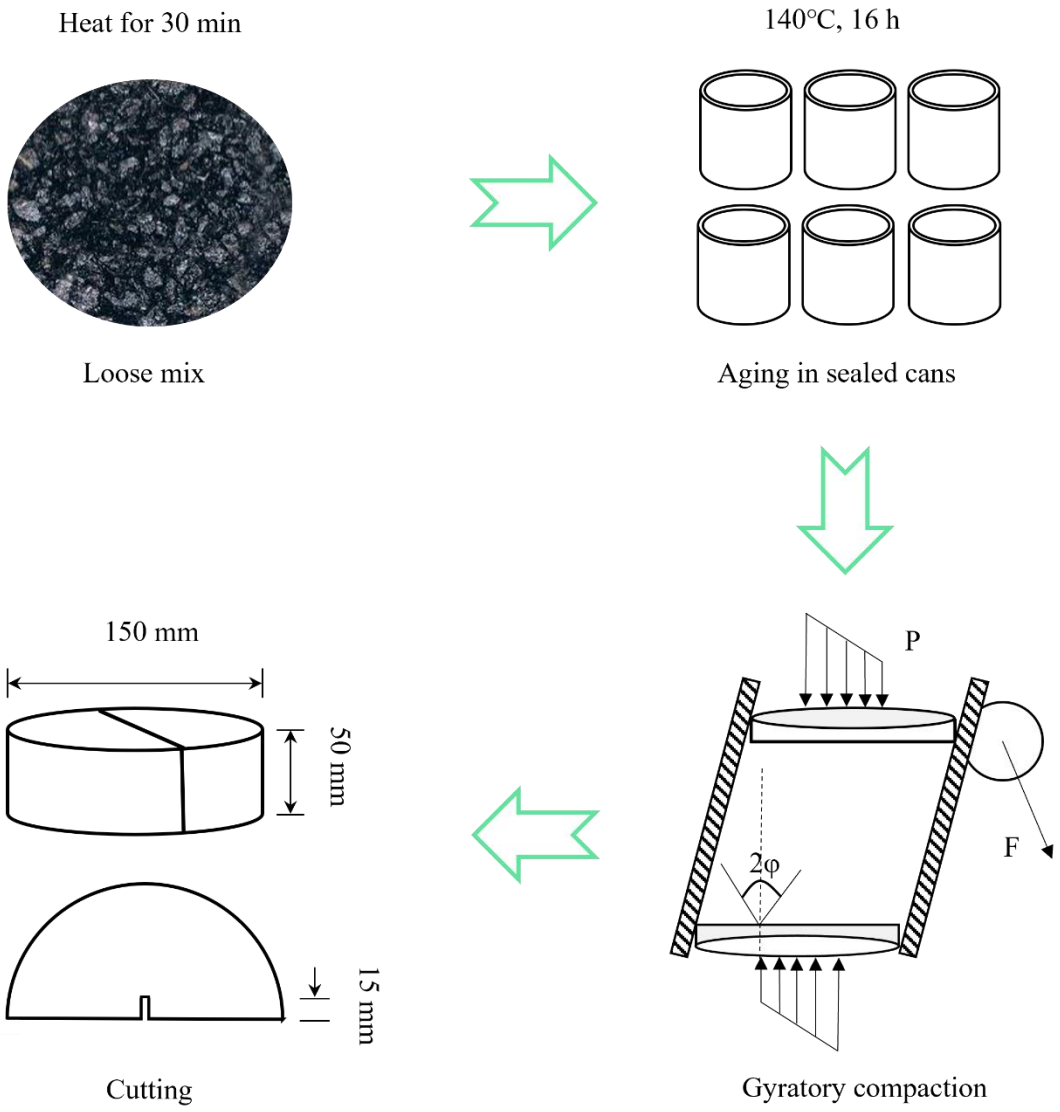

Figure 21. Schematic diagram of sample preparation for SCB testing.

In addition to room temperature experiments, the effect of test temperature was investigated for a limited number of mixtures. For the room temperature tests, SCB samples were tested at constant loading rates of both 50 mm/min and 0.05 mm/min. At low temperature, SCB samples were conditioned at −10°C for 2 hours prior to testing to ensure a homogenous temperature.

In this study, a servo-hydraulic materials test system (MTS 810, MTS Corporation, Minneapolis, Minnesota) was used and the support rollers at the bottom were placed symmetrically at a span of 100 mm. Based on the force-displacement diagram of each sample, a series of commonly used indicators listed in Table 4 were calculated. The SCB test, as per the IL-SCB standard (Al-Qadi et al., 2015a), is conducted under a

single load application. Before testing, each sample was separated into two groups, each consisting of four replicates. The first group, hereinafter referred to as “2 h”, underwent a conditioning process at 0℃ for 2 hours before being tested at the same temperature. In contrast, the second group, hereinafter referred to as “72 h”, was conditioned at −20℃ for 72 hours, followed by a subsequent 2-hour conditioning period at 0℃, prior to testing at 0℃. The primary objective of this study is to evaluate the build-up of thermal shrinkage following low temperature conditioning and its subsequent effect on the SCB test results. The test setup, shown in Figure 22, places rollers 100 mm apart to ensure the span is 80 % of the specimen length. A servo-hydraulic materials testing system (MTS 810, MTS Corporation, Minneapolis, Minnesota) applies a monotonic compressive force, recording data every 0.1 seconds. The Force- LLD (Load Line Displacement) curve and the Force-CMOD (Crack Mouth Opening Displacement) curve, used for calculating various indicators, are depicted in Figure 22 (b) and (c). The SCB test is carried out in a LLD controlled mode, maintaining a vertical load rate of 50 mm/min, following the IL-SCB standard protocol (Al-Qadi et al., 2015a). The LLD is measured as the vertical movement of the upper rod from its initial contact with the top of the SCB sample, a reading obtainable via the MTS control software. Table 4 provides a comprehensive summary of each indicator, including their formulas and units. Historically in asphalt mixture research, both the Force-LLD and Force-CMOD curves have been used to determine cracking resistance indicators. The Fracture Energy (FE), a key parameter, is calculated as the total work done in creating two separate surfaces in a specimen, divided by the fractured area. Work, from a physics perspective, is the force component in the direction of displacement times the distance. Thus, using the Force-CMOD curve to calculate FE is theoretically incorrect, as the CMOD is perpendicular to the force direction. Consequently, the Force-LLD curve is predominantly used for determining indicators like FE, adhering to RILEM Technical Committee TC 50-FMC guidelines (Pérez-Jiménez et al., 2013; R.T.C. 50-FCM, 1985). Asphalt mixture FE assessment standards are documented in AASHTO TP 124 and AASHTO TP 105-13. While the Force-LLD curve is widely utilized, the Force-CMOD curve has gained acceptance in SCB testing. Research by Son and coworkers (Son et al., 2019) indicated that FE values for asphalt mixtures derived from the Force-CMOD curve were 29~66 % higher than those from the Force-LLD curve. Notably, Force-CMOD curves offer a more detailed observation of crack initiation and propagation in samples compared to Force-LLD curves (Roy and Hesp, 2001a; Togunde and Hesp, 2012).

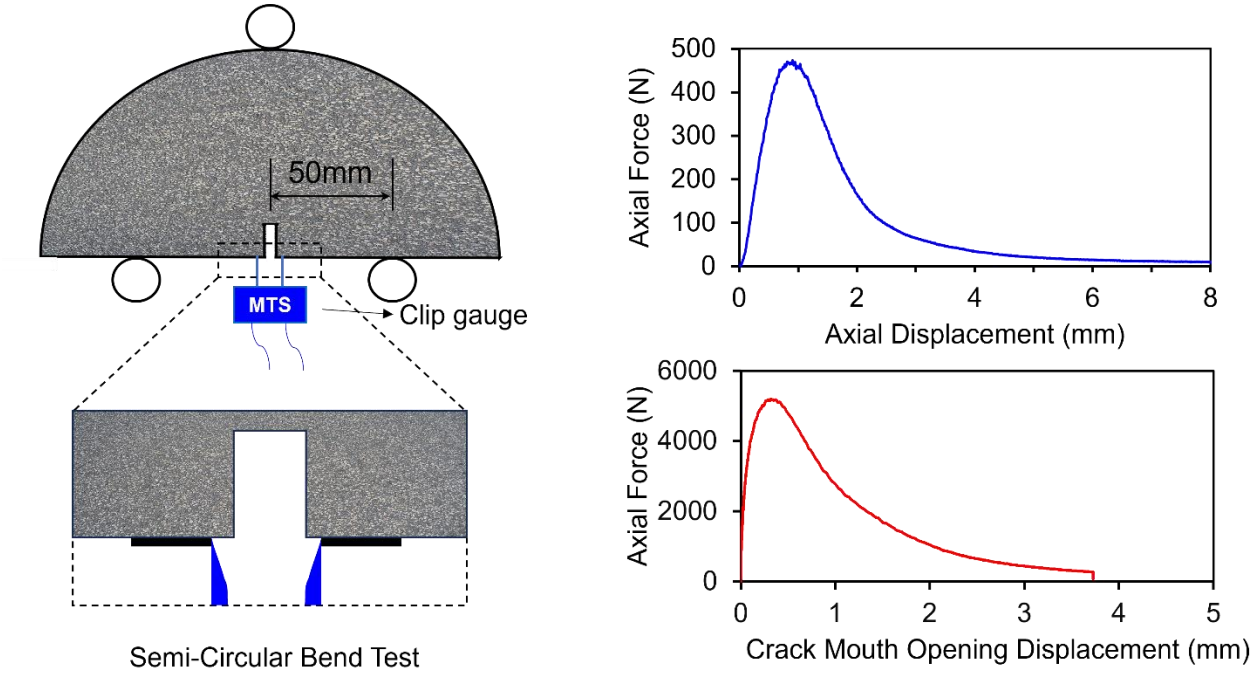

Figure 22. Schematic diagram of the SCB test.

(a) sample and CMOD gauge setup; (b) load-LLD curve; (c) load-CMOD curve.

Table 4. Cracking Resistance Indices

Indicator	Name	Equation	Units
FE	Fracture Energy	$G_f = \frac{W_f}{A_{lig}}$	J/m^2
FI	Flexibility Index	$FI = \frac{G_f}{\lvert m \rvert} * 0.01$	-
CRI	Cracking Resistance Index	$CRI = \frac{G_f}{P_{max}}$	m^{-1}
BCI	Balanced Cracking Index	$BCI = L_{75} * G_f * 0.01$	N
CII	Crack Initiation Index	$CII = \frac{E_{peak}}{P_{max}}$	mm^{-1}

Note: G_f = fracture energy, W_f = work fracture/area under L-D curve, A_{lig} = area of the ligament, m = post-peak slope of L-D curve, P_{max} = peak force, L_{75} = displacement at 75 % of the peak load, E_{peak} = pre-peak fracture energy.

Fracture energy (FE) and flexibility index (FI), which were proposed by University of Illinois researchers, are commonly used to predict fracture resistance. They were calculated as per the semi-circular bending Illinois flexibility index (SCB-IFIT) test standard (Al-Qadi et al., 2015b). As FE alone was not enough to rank performance properties of asphalt mixture at room temperature. The post peak slope at the inflection

point was added to formulate an empirical flexibility index, FI, defined as the ratio of the normalized fracture energy and the post peak slope. It was shown to be able to capture the effects caused by various changes in the materials and volumetric design of asphalt concrete. The FE and FI indices are calculated according to Eqs. (24) and (25):

$$G_f = \frac{w_f}{A_{lig}} \tag{24}$$

$$FI = \frac{G_f}{|m|} \times 0.01 \tag{25}$$

Where G_f is fracture energy, $J \cdot m^{-2}$; W_f is work of fracture which is defined as the area under the load versus displacement curve, J; A_{lig} is the ligament area which is defined as ligament length multiplied by the thickness of the specimen, m^2; m is the post peak slope at the inflection point.

The cracking resistance index (CRI) is an alternative index proposed by researchers at Texas A&M University (Kaseer et al., 2018). Compared with FI, it has a higher repeatability and is more easy to calculate. Importantly, the CRI is also able to capture brittle properties of mixtures. The index is defined as the total fracture energy divided by the peak load, which is easy to acquire from the force-displacement plot. The CRI index can be determined according to Eq. (26):

$$CRI = \frac{G_f}{P_{max}} \tag{26}$$

Where G_f is fracture energy, $J \cdot m^{-2}$; P_{max} is peak load, N.

The balanced cracking index (BCI) was proposed by Majidifard and coworkers (Majidifard et al., 2021) to better characterize brittle and aged mixtures. It is the product of the total fracture energy and a parameter L_{75}, which is the displacement corresponding to the time when 75 % of peak load is reached in the post-peak section. The first use of L_{75} was in the indirect tensile asphalt cracking test (IDEAL-CT) proposed by researchers at the Texas Transportation Institute (Zhou et al., 2017), who reasoned that the inflection point occurs at approximately the 75 % of peak load point in the post-peak force-displacement curve. The BCI index is calculated following Eq. (27):

$$BCI = 0.01 \times L_{75} \times G_f \tag{27}$$

Where L_{75} is the displacement corresponding to 75 % of peak load. As an alternative to FE, FI and CRI, the BCI gives equal weight to both the fracture energy and the L_{75} parameter (a type of ductility measure for mixtures). Consequently, it provides different trends as produced by FI and CRI indices, which according

to the authors gives a more rational ranking of cracking resistance for polymer modified mixtures (Majidifard et al., 2021).

Roy and Hesp (Roy and Hesp, 2001b, 2001a) suggested that the plane strain fracture energy (G_{Ic}) and CTOD or crack mouth opening displacement (CMOD) at cold temperatures are very sensitive to asphalt source and grade as well as modifier type and content (Roy and Hesp, 2001a). Based on those early studies, a new index called cracking initiation index or CII is proposed and investigated in this study. Instead of calculating the overall fracture energy, it focuses on the energy to peak load. This index is approximately equal to the displacement of the crack mouth at the initiation of cracking. The CII is characterized by remarkably low coefficients of variation (COV) compared to the FI index. One possible reason for why the FI has a high COV is the inhomogeneity along the crack path in the post-peak domain. When cracks propagate, the energy required is rather different for every specimen at each point in time and the slope at the inflection point varies accordingly. So for the CII calculation, only the initiation energy is used and as such it is expected to be a more repeatable index, especially at low rates of loading that are more realistic for cracking in service. CII is calculated according to Eq. (28):

$$CII = \frac{E_{peak}}{P_{max}} \tag{28}$$

Where P_{max} is peak load, N; E_{peak} is prepeak fracture energy, $J \cdot m^{-2}$.

To perform the analysis of the variability for each index, the pooled standard deviation (SD_p) for each sample group was calculated using Eq. (29) below (Edwards and Hesp, 2006). The SD_p is defined as a weighted average of the standard deviation from two or more groups of data that are assumed to possess a nearly identical standard deviation (Killeen, 2005). It is a common method to estimate a single standard deviation from the sum of a set of independent groups. In this study, mixtures came from different agencies and were independent of each other. A single coefficient of variance for all independent groups under the same test setup was calculated using the pooled standard deviation and the weighted average to have a general idea of the repeatability of different indices and parameters. From dynamic range analysis it was found that the FI varies widely. However, this is not sufficient to show that FI is good at distinguishing different mixtures because it also has a higher variability. Thus, to compare the repeatability against dynamic range, the *R* value as shown in Eq. (30), which is the ratio of difference between the maximum and the minimum value in a group and pooled standard deviation of the group, was proposed and investigated in this study.

$$SD_P = \sqrt{\frac{\sum_{i=1}^{j}(n_i - 1) \cdot SD_i^2}{\sum_{i=1}^{j}(n_i - 1)}} \quad (29)$$

$$R = \frac{\max - \min}{SD_P} \quad (30)$$

Where SD_i is the standard deviation of population i; n_i represents the size of population i; j represents the total number of populations analyzed.

3.3.2 Hamburg Wheel Tracking (HWT) Test

The HWTT was performed to assess rutting resistance of cores from the pavement trial. As shown in Figure 23 (a), a vertical load of 72 kg was applied to the samples with a wheel reciprocating at a speed of 52 passes per minute. Testing temperatures selected are 30℃, 40℃, and 50℃, which were maintained using a circulating water bath. The test was terminated upon reaching either a final rut depth of 12.5 mm or a maximum of 20,000 passes, whichever occurred first. Figure 23 (b) illustrates the relationship between rut depth and the number of wheel passes. For evaluating asphalt rutting resistance, two empirical indicators were employed: the rut depth at a predetermined number of passes, and the number of passes required to reach a predetermined rut depth. Furthermore, a novel methodology was introduced to measure the impact of modifiers on rutting resistance. The method involves calculating the percentage change in the area under the rutting curve, when comparing modified mixtures unmodified ones. This innovative approach aimed to more precisely quantify effects of modifiers on rutting resistance.

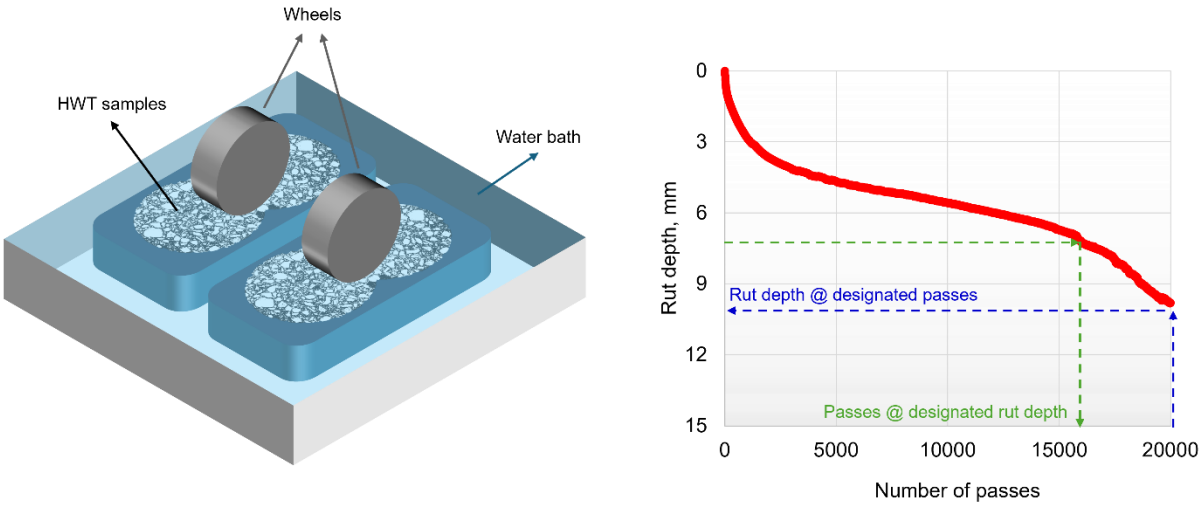

Figure 23.Schematic diagram of HWTT and definition of rutting resistance indicator.

(a) setup of HWTT; (b) definition of rutting resistance indicators.

4. PROJECT RESULTS

4.1 Simplified Extraction and Recovery Method

With the ever-increasing use of recycled asphalt pavement (RAP) in road construction, extraction and recovery of binders from mixtures as placed becomes a critical aspect of quality assurance testing. However, current extraction and recovery methods are associated with shortcomings, as they are often time consuming, costly, inaccurate and involve toxic solvents. The objective of this section was to develop a practical and more environmentally friendly protocol for the accurate and precise acceptance testing of recovered binder. The process uses a low toxicity solvent for extraction, followed by simple filtration, evaporation and thin film oven aging. Residual solvent is removed from the binder during initial thin film oven aging and fines are found to have an insignificant effect on the rheological properties of importance. Results of this study provide guidance for further optimization of a simplified extraction, recovery, and aging protocol for the acceptance testing of asphalt binder and mixture.

4.1.1 Materials Tested

In this section, a set of 19 asphalt mixtures were collected from different regions of North America. The general origin for each mixture and their laboratory codes are shown in Table 5. Three solvents that were investigated are listed in Table 3. Among these, DCM and TCE are most widely used in the asphalt industry. The HD PRO is a new, commercially available solvent with reduced toxicity produced by Enviro Tech International of Melrose Park, Illinois. The DCM and TCE were both obtained from Sigma-Aldrich Canada of Oakville, Ontario. Table 6 shows five different fillers obtained from local asphalt producers that were added to base asphalt to assess the impact of residual fines in the recovered binder on relevant rheological properties.

Table 5. Samples as collected from around North America.

Source	Label
Ontario City	A-1
	A-2
	A-3
	A-4
	A-5

New England State DOT	B-1
	B-2
New England State DOT	C-1
Midwestern State DOT	D-1
	D-2
New England State DOT	E-1
	E-2
	E-3
	E-4
Ontario Regional Municipality	F-1
	F-2
Midwestern State DOT	G-1
	G-2
Western State DOT	H-1

Table 6. Compositional information of fillers.

Name of filler	Compositions
FA	Limestone Filler, Source A
FB	Limestone Filler, Source B
FC	Baghouse Fines (Limestone + Sand Mix)
FD	Baghouse Fines (Acidic Granite Mix)
FE	Portland Cement Filler
FF	Limestone Filler, Source C

4.1.2 Validation Analysis

4.1.2.1 Effect of operational parameters on the performance of recovered asphalt.

To2standardize the simplified extraction and recovery method, the operational parameters during the filtering and oven evaporation steps were investigated. Repeating filtration using two sieves of 75 µm and 25 µm, and the duration of plate heating for evaporation at 140 °C were explored with a set of trials to obtain the optimum combination of operational parameters. The results of HTPG, ITPG, T_{30° and T_{45° of asphalts recovered with the simplified method under different combination of operational parameters

are plotted against those obtained through the traditional extraction, recovery and PAV aging method as shown in Figure 24 below.

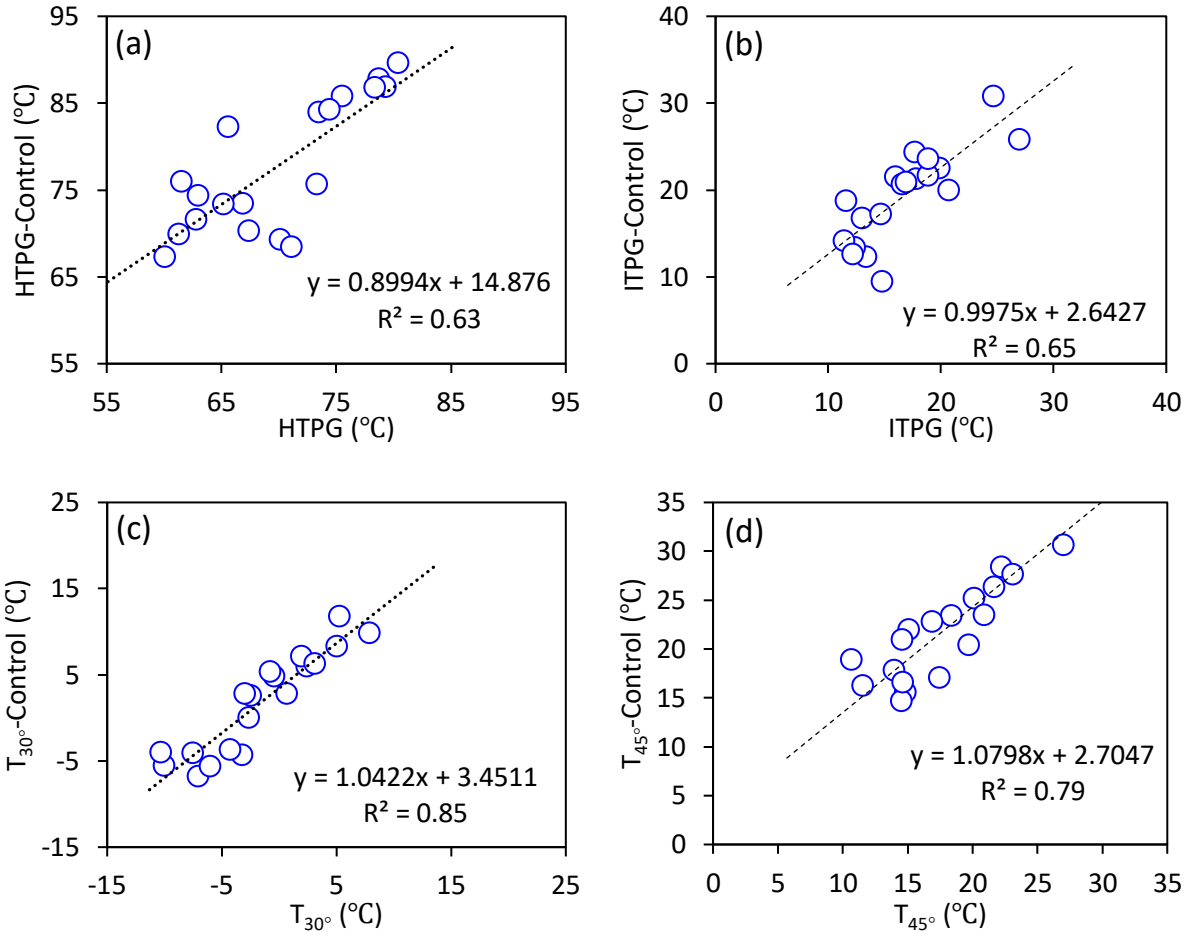

Figure 24. Correlation between traditional and simplified recovery and aging method.

(a) HTPG, (b) ITPG, (c) $T_{30°}$ and (d) $T_{45°}$.

It can be found from Figure 24 that the rheological results of asphalt binders recovered via the two methods are highly correlated with each other in terms of continuous grading temperatures and limiting phase angle temperatures. The correlation between the simplified method and the conventional one is more significant in terms of the limiting phase angle temperature compared with the continuous grading temperature. This indicates that the limiting phase angle temperature is more sensitive to changes in operational parameters than the continuous grading temperature.

Table 7 summarized the detailed information of operational parameters in terms of sieve size and oven heating time. Besides, the ash content results were also included to show the effectiveness of sieves with different sizes. Moreover, the rheological results in terms of continuous grading temperature and limiting

phase angle temperature as depicted in Figure 24 were listed against the corresponding data from the traditional method to show the effect of different operational parameters. It can be found that the ash content can be reduced significantly by repeating the filtration of fines or by using sieves with smaller sizes. In terms of heating evaporation time, it can be found that increasing the heating evaporation time tends to increase the age hardening effect, as indicated by the increase of continuous grading and limiting phase angle temperatures. Based on this preliminary examination, it is suggested to repeat the filtration process to reduce ash content to more acceptable levels. On the other hand, the heating evaporation time can be extended to fully remove solvent and avoid over heating of the asphalt binder. It is noteworthy that most recovered asphalts using the simplified extraction and recovery method did not reach an equivalent aging degree to the PAV under the designated 140 ℃ and 16 hours.

While it is anticipated that the stiffness of asphalt binder can be reached to the levels achieved through the standard PAV protocol by fine-tuning experimental parameters such as temperature and time, it is important to note that the thermal oxidative aging process and resulting aging products may differ from those of PAV-aged samples. Extensive research supporting the PAV test indicates that temperature is a critical factor in determining both the rate of thermal oxidative aging and the nature of the compounds formed during this process (Branthaver et al., 1993). Temperatures exceeding 140 ℃ may cause over-aging of the asphalt binder by disrupting polar molecular associations, thus allowing more molecules to react with oxygen in ways they would not at lower temperatures (Branthaver et al., 1993). Therefore, the aging method proposed in this study offers a way to produce an asphalt binder with a stiffness similar to that obtained through the PAV protocol and in-service aging. However, further research is needed to fully understand the extent to which this proposed method can accurately simulate in-service aging of asphalt binder, particularly from the perspective of chemical composition and molecular structure.

Table 7. Results of rheological properties of binders with simplified method.

Label	75 µm	25 µm	Heating evaporation time at 140 ℃, min	Ash content,%	HTPG, ℃	HTPG-Control, ℃	ITPG, ℃	ITPG-Control, ℃	T_{30°, ℃	T_{30°-Control, ℃	T_{45°, ℃	T_{45°-Control, ℃
A-1	2	0	245	12.4	70.1	69.3	14.8	9.5	-3.1	-4.36	17.4	17.0
A-2	2	0	255	8.7	67.4	70.3	20.7	20.0	2.4	5.92	20.1	25.1
A-3	1	1	265	1.4	62.8	71.6	19.9	22.5	1.9	7.10	18.3	23.3
A-4	1	2	265	1.3	66.9	73.5	16.0	21.5	-0.4	4.80	16.9	22.7
A-5	1	2	250	0.7	65.2	73.4	17.8	21.3	-0.7	5.34	15.0	21.9
B-1	2	0	260	11.9	78.7	87.8	27.0	25.8	7.8	9.80	27.0	30.5
B-2	2	1	350	0.9	79.3	86.9	24.7	30.8	5.0	8.30	21.6	26.3
C-1	2	0	350	0.6	60.1	67.3	16.6	20.7	-2.6	-0.02	14.8	15.5
D-1	1	1	320	5.2	65.6	82.3	17.7	24.4	-2.4	2.57	14.5	20.9
D-2	2	1	350	1.0	75.5	85.8	13.0	16.8	-10.0	-5.60	11.5	16.2
E-1	1	1	320	2.6	73.5	84.0	11.6	18.8	-3.0	2.79	22.2	28.3
E-2	2	1	360	2.0	78.4	86.8	16.9	20.9	0.6	2.75	20.9	23.4
E-3	2	1	360	1.2	61.3	69.9	18.9	21.7	3.1	6.25	23.1	27.6
E-4	1	1	360	0.7	74.4	84.3	13.4	12.3	-4.2	-3.72	19.7	20.3
F-1	2	1	360	0.8	63.0	74.4	12.4	13.4	-7.5	-4.12	13.9	17.8
F-2	2	1	360	0.7	61.5	76.0	11.4	14.2	-10.3	-4.01	10.6	18.8
G-1	1	1	350	7.4	71.1	68.5	12.2	12.6	-7.0	-6.82	14.5	14.6
G-2	1	1	360	1.1	73.3	75.7	14.7	17.2	-5.9	-5.62	14.6	16.5
H-1	2	1	360	1.2	80.4	89.7	18.9	23.6	5.3	11.77	28.1	37.2

4.1.2.2 Effect of solvent type on the properties of the recovered asphalt binder.

(1) Rheological results

The effect of solvent type as well as extraction and recovery methods on the properties of recovered asphalt binder in terms of continuous grading high and intermediate temperature are shown in Figure 25. The value on the top of the bar represents the continuous high temperature grade while that on the bottom of the bar represents the continuous intermediate temperature grade. The continuous high temperature grade was determined on recovered binder while the continuous intermediate grade temperature was determined on recovered binder after long term aging (PAV aging or thin film oven aging). It can be found from Figure 25 that traditional extraction and recovery processes may lead to excessive hardening of the asphalt binder, which can be observed from the relatively high continuous high temperature grade for the control group, for which the traditional extraction and recovery method was used, in comparison with the DCM group, for which the simplified extraction and recovery method was used. It is noteworthy that both groups used DCM as the solvent. Therefore, it can be speculated that traditional extraction and recovery processes could possibly age the asphalt binder too much during the long recovery process. It can be found that the type of solvent on the rheological performance of recovered asphalts is mix type dependent. The continuous grading intermediate temperature is almost consistent with each other for the recovered binders using different solvents. For the continuous grading high temperature results, three out of four mixes are close to each other. Overall, the incorporation of the new solvent HD PRO in the simplified extraction, recovery and aging method has only minor effects on the rheological performance of the recovered asphalt binder.

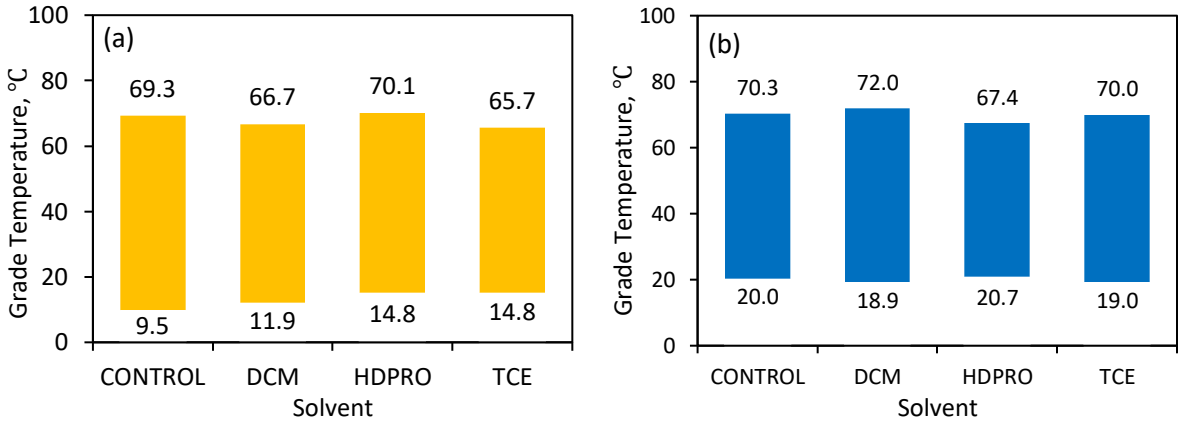

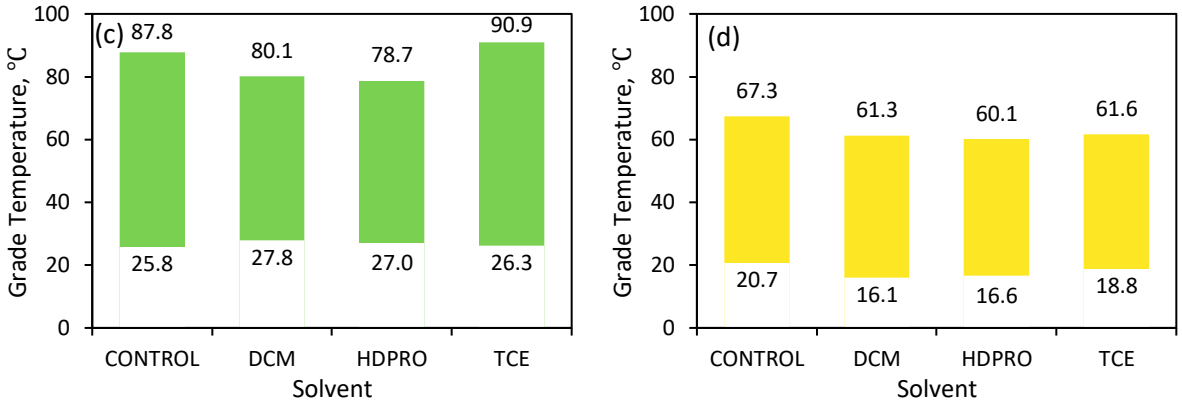

Figure 25. Effect of solvent on the performance grade of recovered asphalt binder.

(a) OC-8, (b) OC-3, (c) NESC-1, and (d) NESM-1.

Apart from continuous grading temperatures, limiting phase angle temperatures $T_{30°}$ and $T_{45°}$ were also used to further understand the effect of extraction, recovery and aging methods and the type of solvent on the rheological performance of recovered asphalt binder. The limiting phase angle temperature results of the recovered asphalts using traditional and simplified extraction, recovery and aging method and various solvents are shown in Figure 26. The value above the bar represents $T_{45°}$ while that below the bar represents $T_{30°}$. First, it can be found that $T_{30°}$ and $T_{45°}$ of recovered binders using the traditional method are all higher than that using the simplified method. This is consistent with the finding from continuous grading temperature results that over aging may be occurring in the traditional extraction and recovery method. With respect to the type of solvent on the limiting phase angle temperature, it is found that asphalt binder recovered via TCE shows the highest limiting phase angle temperatures, followed by that via HD PRO and DCM.

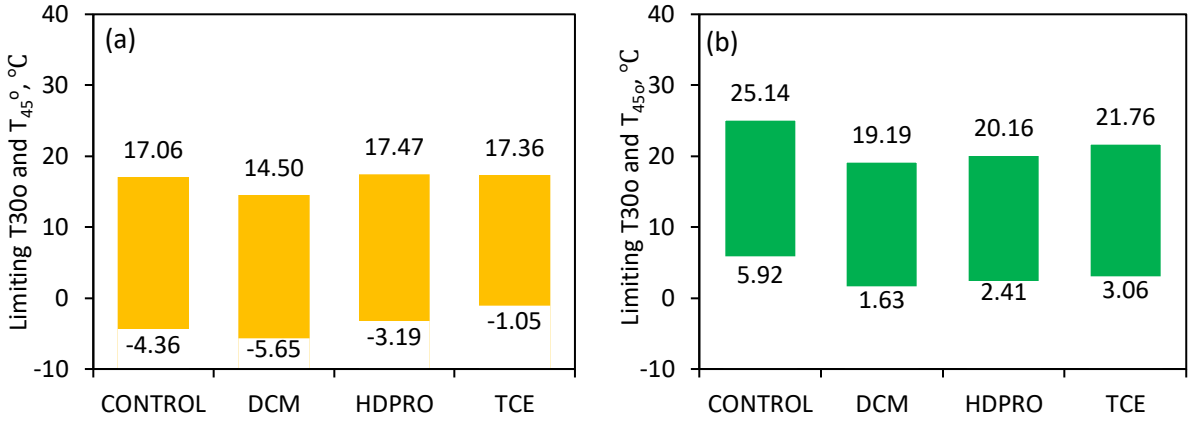

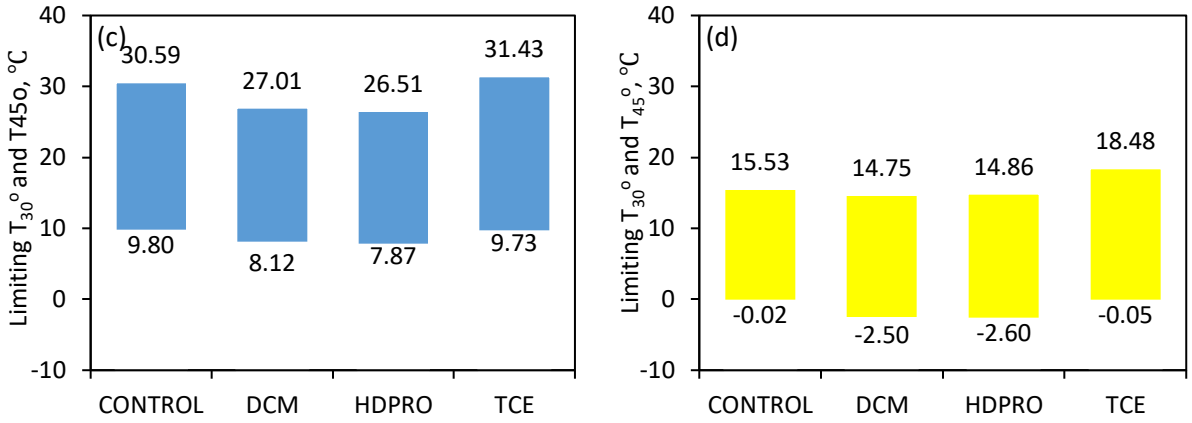

Figure 26. Effect of solvent on the limiting phase angle temperature of recovered asphalt binder. (a) A-1, (b) A-2, (c) B-1, and (d) C-1.

(2) FTIR results

A significant concern for the extraction and recovery method is whether the solvent can be removed to a sufficiently low level so that the rheological performance of recovered asphalt will not be affected to any significant degree. Farrar and coworkers (Farrar et al., 2015) proposed a limit of detection (LOD) method to qualitatively evaluate solvent remaining in asphalt after extraction via FTIR. The existence of TCE solvent can be detected with the absorbance peak of the =C-H functional group in TCE. It is also found that the content of TCE can be predicted by the area of the peak between 918^{-1} and 938 cm^{-1}, which positively correlated with the complex modulus for the recovered binder (Ge et al., 2019). To ensure that the rheological performance of recovered binder is consistent, the residual solvent is supposed to be low enough. Figure 27 shows the FTIR spectra of three solvents and the unrecovered asphalt and solvent recovered asphalt using simplified extraction and recovery method proposed in this study. The unrecovered asphalt is taken from asphalt mixture and coated to KBr at high temperature. Figure 27 (a)-(c) show the whole spectra for solvent and asphalt. Figure 27 (d)-(f) show the fingerprint regions of the full spectra to detect residual solvents. It can be found that there is no detectable change in the spectra in solvent recovered asphalts where characteristic peaks of solvent exist. It can therefore be concluded that solvent is largely removed using the simplified extraction and recovery method.

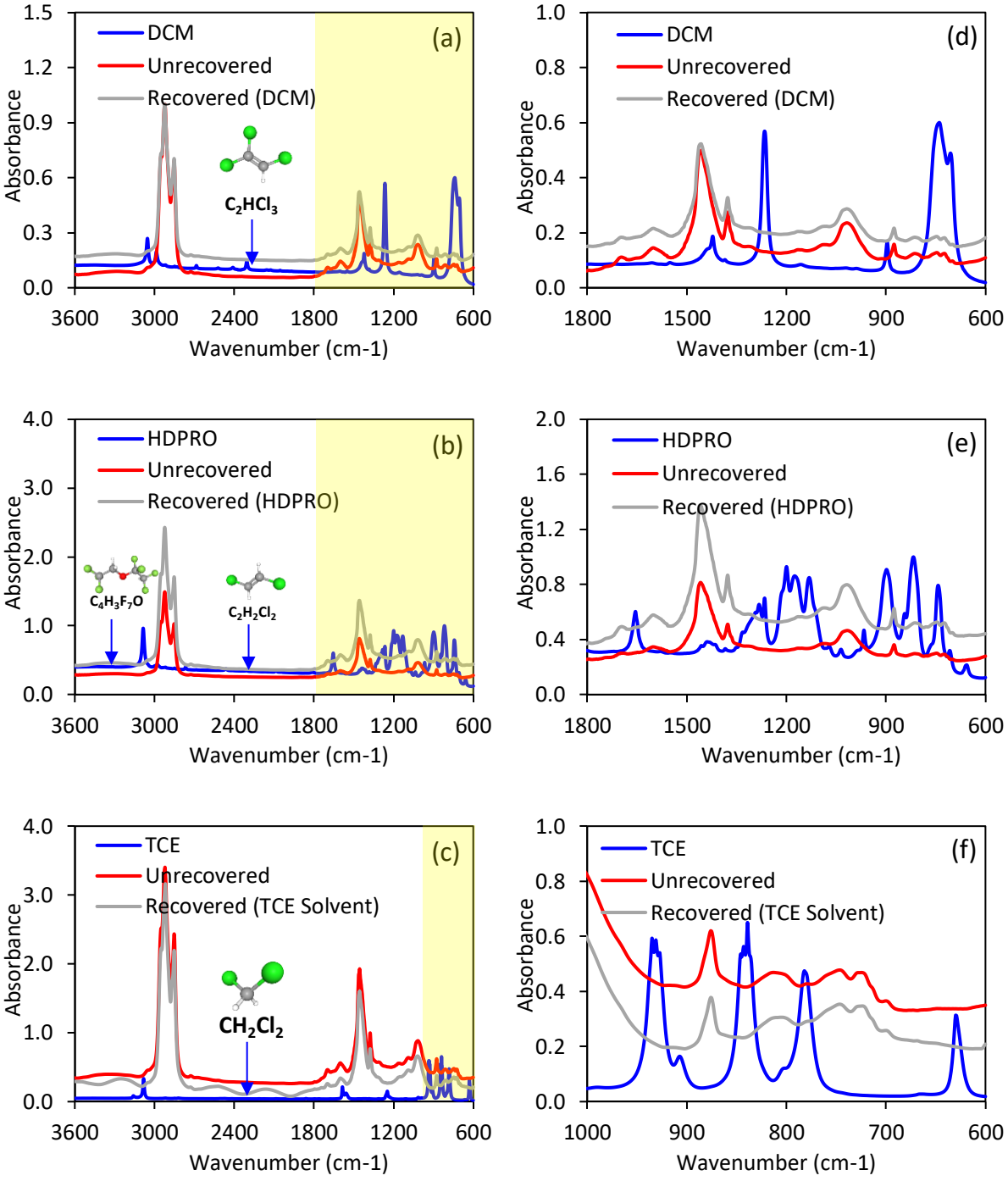

Figure 27. FTIR spectra of pure solvents and asphalts.

(a)-(c) full scale spectra, (d)-(f) fingerprint regions.

Another concern of the simplified extraction and recovery method is the quantification of the degree of aging of reclaimed asphalt from RAP or RAS. For a given mixture, the aging degree of the asphalt binder

in mix should be consistent with that of solvent recovered binder. It is necessary to investigate the effect of solvents on the aging degree of recovered asphalt. The aging indices from FTIR spectra of recovered asphalts with different solvents are shown in Figure 28 and Figure 29. The binders labeled as “unaged” refer to the recovered asphalts from the simplified extraction and recovery method. While those labeled as “aged” refer to the recovered asphalts through simplified extraction and recovery followed by oven aging at 140 ℃ for 16 hours. It is noteworthy that the control group was recovered via traditional extraction, recovery and aging, namely, centrifuge, rotary evaporation and PAV aging. It can be found that carbonyl indices increased dramatically after aging, which is caused by thermal oxidative aging of asphalt binder during the laboratory accelerated aging process. It can also be found from the control and DCM group that the simplified extraction and recovery process did not cause obvious age hardening effects compared with traditional extraction and recovery processes. It is noteworthy that this conclusion should be further validated by expanding the number of mixture samples. For the effect of solvent type, it can be found that the aging degree of recovered asphalts depends on the type of solvent selected. However, the aging degree rankings for asphalts recovered using different solvents is not consistent among different mixtures. The aging degree of asphalt binders using different solvents from the same mixture fluctuates within a small range.

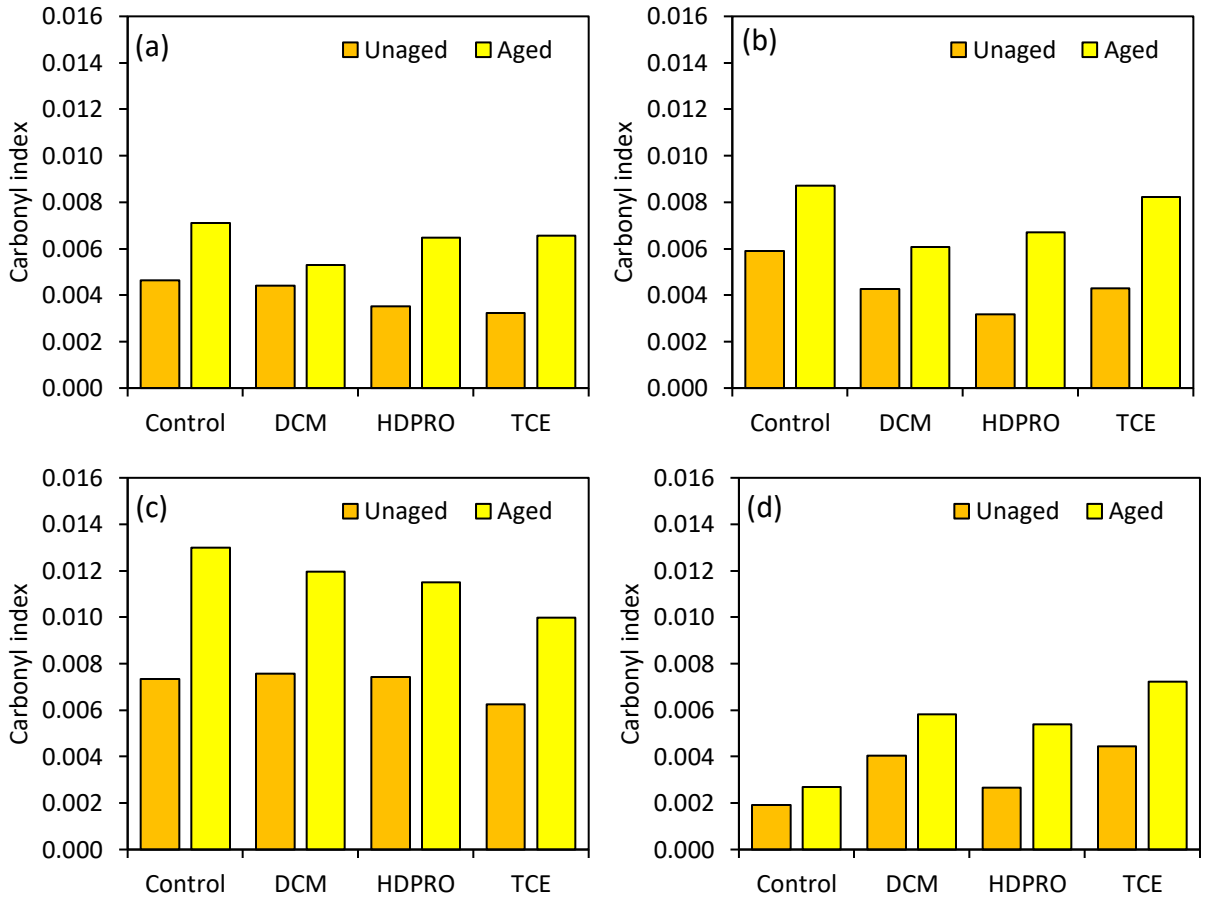

Figure 28. Carbonyl indices of recovered asphalts with different methods and solvents.

(a) A-1, (b) A-2, (c) C-1, and (d) D-1.

With respect to sulfoxide index results, no obvious trend can be found to explain the effect of extraction and recovery method and solvent type. The sulfoxide index results are mainly mixture type dependent. In this regard, the application of sulfoxide index to evaluate the effect of solvent and extraction and recovery methods should be further analyzed.

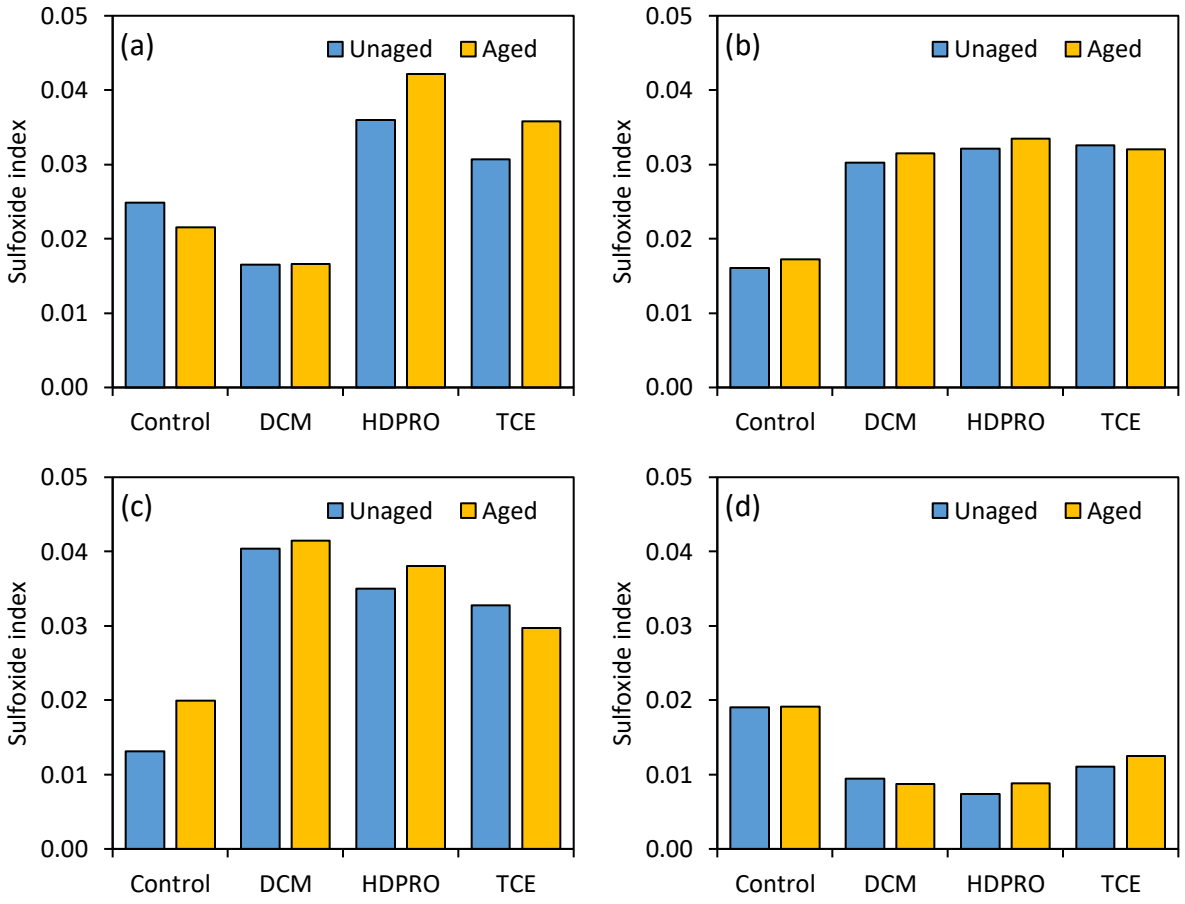

Figure 29. Sulfoxide index results of recovered asphalts with different methods and solvents.

(a) A-1; (b) A-2; (c) C-1; (d) D-1.

(3) Effect of residual ash content

As discussed earlier, the ash content can be reduced by repeating the sieve filtration process. However, the effect of ash composition and content on the rheological performance of recovered asphalt binder remains largely unknown. Therefore, six different fillers were added to two asphalt binders at two different contents of 3 % and 6 %, to simulate recovered asphalt with high residual ash. The rheological results in terms of continuous grading temperature and limiting phase angle temperature are shown in Figure 30. Sample 1 and sample 2 are two different base asphalts with different performance grade. For sample 1, the control binder represents the base asphalt without filler, while FA, FC, FD, FE, FF, and FG represent the ones with different type of ash and their content is constant at 3 %. In comparison, the

content of the six types of ashes is 6 % in sample 2. The HTPG is the high temperature performance grading that was determined on unaged binder while the ITPG, intermediate temperature performance grade, is determined on standard RTFO and PAV aging residue. It can be found from Figure 30 (a) that the HTPG and ITPG of asphalt binders remain nearly constant with the incorporation of filler. Besides, the increase of filler content did not lead to significant increases in either HTPG or ITPG of asphalt binder. Consistent results can be found from Figure 30 (b) that the limiting phase angle temperature of asphalt binder is insensitive to the incorporation of filler. It can therefore be concluded that the effect of type and dosage of filler on the rheological performance of asphalt binders is negligible within the range investigated. It should be noted that the fillers used in this study are fines passing the 0.075 mm sieve. It means that there is supposed to be a threshold of size of fines below which the residual fines will not lead to significant change in the rheological performance of recovered asphalt.

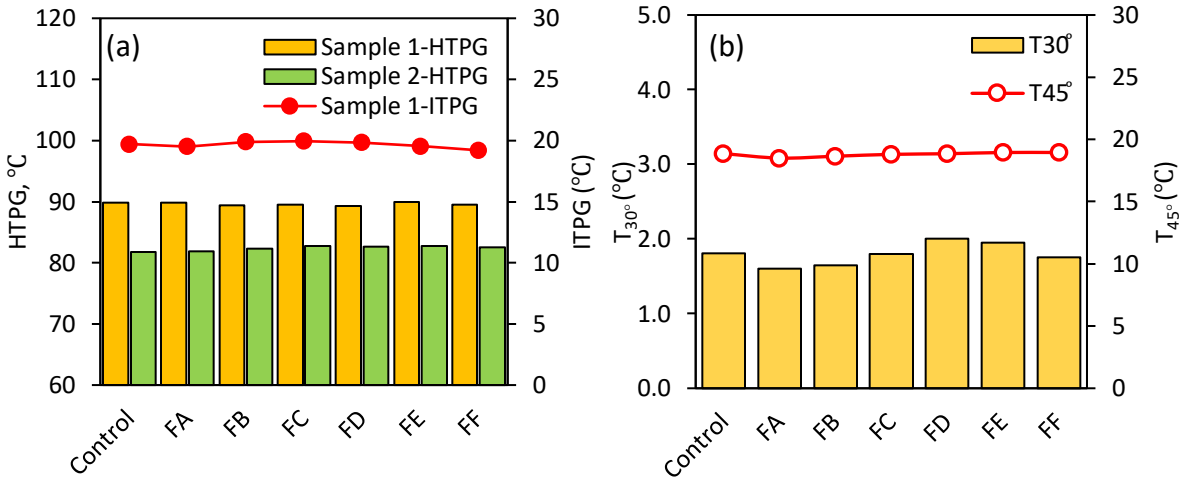

Figure 30. Effect of filler type and dosage on the rheological performance of asphalt binders.

(a) HTPG and ITPG, (b) limiting phase angle temperature.

4.1.3 Summary and Conclusions

This section aims to propose an efficient, accurate and greener extraction, recovery, aging and testing protocol for accepting recovered asphalt binders. The proposed method was optimized with 19 mixtures collected from different regions around North America. Key issues in terms of operational parameters and the effect of solvents and residual filler were analyzed. The main findings are summarized below.

(1) The sieve filtration and plate heating evaporation can be used to replace traditional centrifuge and rotary evaporation procedures. The ash content can be reduced to acceptable levels by the repeating sieve filtration process. Residual fines have only minor effects on the rheological performance of recovered asphalt. The evaporation of solvent upon heating is time and temperature dependent. The residual solvent can be fully reduced by simply extending the heating time.

(2) The use of a greener solvent HD PRO reduced the potential health risk. Compared with other commonly used solvents, HD PRO has no significant effects on the rheological properties of recovered asphalt binder.

Solvent can be effectively removed during the simplified extraction and recovery process to avoid negative effect on the rheological performance of recovered asphalt.

(3) The heating evaporation method did not produce obvious hardening of the recovered asphalt. The current oven aging condition of 140 ℃ for 16 hours is not enough to generate an equivalent aging degree in the asphalt binder subjected to PAV conditioning for 20 hours. It is expected that equivalent long-term aging effect in terms of stiffness can be achieved by fine-tuning temperature, extending the aging time or film thickness.

(4) The proposed simplified extraction, recovery, aging and testing protocol is characterized by the need for less time and material. This method is being further optimized in ongoing research in our laboratory. Additional mixture types will be included to determine the optimum oven aging conditions that can reproduce aging levels even closer to those obtained through the PAV protocol.

(5) The limitation of this study lies in the fact that the proposed aging method provides only an accelerated thermal oxidative aging approach to produce asphalt binder with a stiffness comparable to that of field-aged material. However, the thermal oxidative aging kinetics of asphalt in this accelerated method may differ from those experienced in field conditions. Additional analysis is therefore essential to clarify the differences in aging mechanisms and products, particularly at the atomic and molecular levels.

4.2 Exudation Evaluation Prior to Performance Acceptance Testing

Asphalt binders harden over time through both thermo-reversible and irreversible processes which, in turn, promotes cracking and moisture damage in service. Oil exudation plays a significant role in accelerating both pavement distresses. Given the increasing use of oils to facilitate polymer modification and soften or rejuvenate reclaimed asphalt, a test for exudation is key to safeguarding binder quality and durability. The objective of this study was to develop a simplified, precise and accurate test protocol to evaluate the degree of oil exudation and further optimize the simplified extraction and recovery method.

4.2.1 Materials

The binders used in this study were from 14 test sections along Highway 655 located just north of Timmins in northeastern Ontario. A map of the trial locations is provided in Figure 31. Binder samples were sourced onsite during the construction of the trials in 2003 and 2007 and were subsequently delivered to Queen's University, where they have remained stored in airtight 5-gallon buckets in an air-conditioned building. Binders were subjected to RTFO and PAV aging as specified in AASHTO R 28 specification. Table 7 offers a general summary of the collected samples with their associated modifier compositions and AASHTO M 320 performance grades.

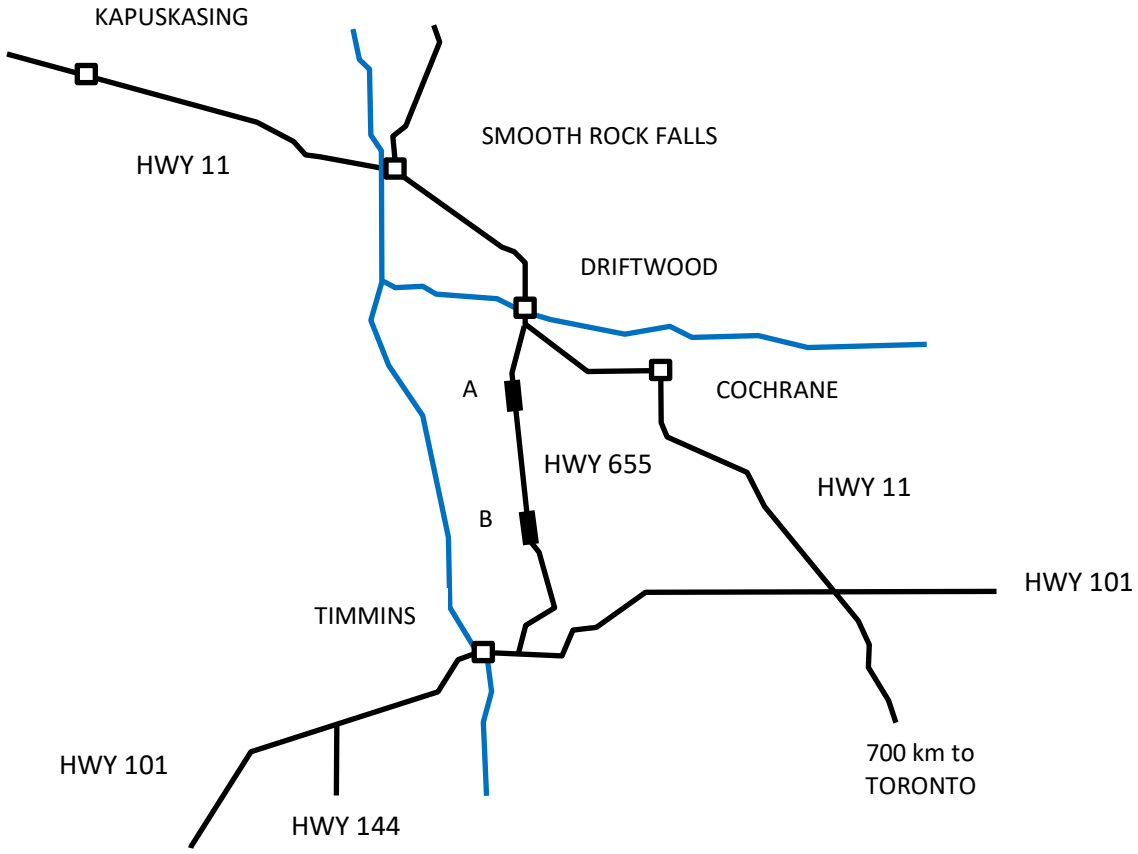

Figure 31.Locations of the two pavement trials on Highway 655.

Trial A from 2003 with sections 1-7 and Trial B from 2007 with sections 9-15.

Table 8. Summary of test section binders and their performance.

Sample Code	Modification	Performance Grade, °C	Lifecycle, Years
665-1	RET/PPA	PG 65-36	25
665-2	SBS	PG 65-36	18
665-3	SBS and REOB	PG 65-36	17
665-4	SBS + REOB	PG 67-35	14
665-5	4 % SBS	PG 66-35	21
665-6	Air Blown + PPA	PG 59-35	17
665-7	REOB	PG 54-35	17
665-9	Cold Lake 300/400A + 0.3 % PET	PG 52-37	38
665-10	1 % PPA + 2 % SBS	PG 67-34	25
665-11	7 % SB	PG 76-37	29

665-12	RET/PPA	PG 67-37	28
665-13	7 % SBS	PG 82-40	23
665-14	3.5 % SBS	PG 64-37	36
665-15	REOB	PG 55-34	22

Note: RET = reactive elastomeric terpolymers, PPA = polyphosphoric acid, SB and SBS = styrene butadiene type elastomeric modifiers, REOB = recycled engine oil bottoms, PET = polyethylene terephthalate fiber. Note that the mix for section 655-8 was overheated so it is therefore not considered in this study.

Eight reference samples from the Strategic Highway Research Program Materials Reference Library and purposely distilled from superior quality Alberta crude bitumen were used for contrast with respect to the effects of exudation on binder properties. The origins and grades for the reference binders are provided in Table 9. It should be noted that samples BC, F3 and F4 are in no way reflective of current asphalt grades but were rather used as three soft asphalt materials. The proposed oil exudation protocol makes use of anhydrous ethanol (USP/NF grade from Commercial Alcohols by Greenfield Global Inc.) as the ultrasonication medium.

Table 9. Summary of reference binder sources and AASHTO M 320 grades.

Sample Code	Source	Performance Grade, °C
EAC	Toronto, Ontario	58-28
AAA-2	Lloydminster, Alberta	46-34
AAL	Cold Lake, Alberta	58-28
AAN	Bow River, Alberta	58-16
ABG	Laguna, Venezuela	64-28
BC	Cold Lake, Alberta	51-30
F3	Athabasca, Alberta	54-25
F4	Athabasca, Alberta	47-37

4.2.2 DSR Results

4.2.2.1 Limiting phase angle temperature determination.

The $T_{30°}$ and $T_{45°}$ values before and after ultrasonication in ethanol (EtOH) were plotted against each other as shown in Figure 6. The dashed line of equivalency illustrates the ideal scenario under which there exists no difference in the rheological performance of binders before and after ethanol ultrasonication. Since this study proposed the primary reason for any deviations to be the exudation of low molecular paraffin oils, data points grouped closely along the reference line can be interpreted as binders containing little to no exudable oil content. From Figure 32, it is evident that the reference binders are tightly clustered along the dashed line for both $T_{30°}$ and $T_{45°}$ plots, suggesting the presence of only minute quantities of low

molecular weight paraffinic oils and hence very little expression of exudation. Average changes due to ultrasonication for 20 minutes at 35°C to 50°C are 0.0°C for $T_{30°}$ and -1.1°C for $T_{45°}$, both of which can be considered within the repeatability for the DSR limiting phase angle temperature measurement. This agrees with what is known about the reference binders, that they are high quality straight unmodified materials that contain very low paraffin contents (Jones, 1993). Those working in the industry know that straight Alberta and Venezuelan binders are of superior performance (Hesp et al., 2007a).

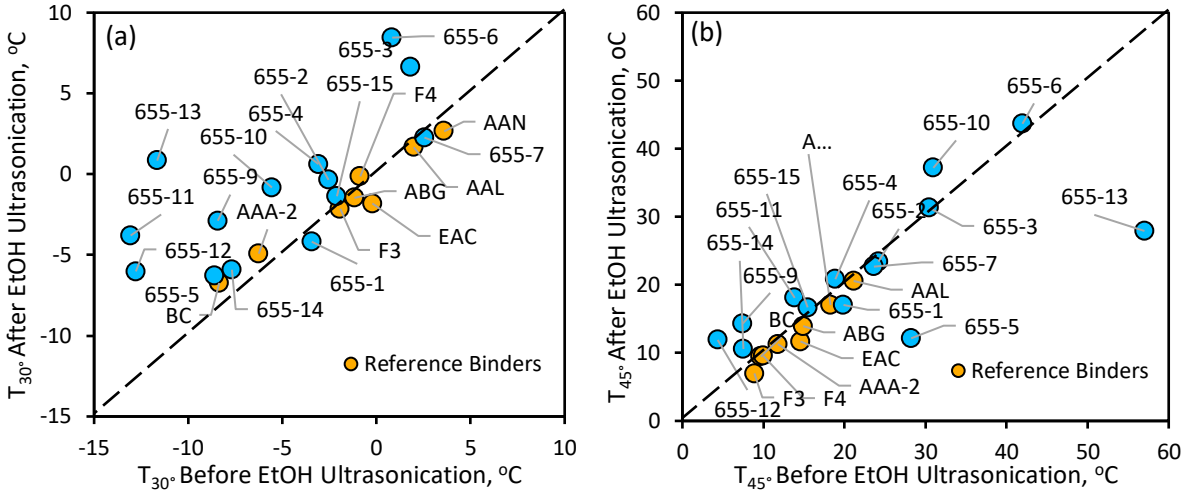

Figure 32. Comparison of rheological properties before and after ethanol (EtOH) ultrasonication. (a) limiting $T_{30°}$ temperatures and (b) limiting $T_{45°}$ temperatures.

In contrast, the test section binders show much greater dispersion from the line of equivalence, which is especially notable for the $T_{30°}$ parameter as it became warmer by an average of 4.3°C. Many test section binders exhibit a drastically higher $T_{30°}$ value after being ultrasonicated in ethanol. The significance of this lies in the fact that greater $T_{30°}$ values represent a decrease in relaxation ability and an associated increase in stiffness which could be attributed to a loss in the softer components of asphalt binder, those being the lower molecular weight and incompatible paraffins (saturates fraction). These binders are expected to perform poorly in mixtures with absorptive aggregates that are amenable to exudative hardening. A 6°C loss in grade typically reduces the confidence that a pavement is not exposed to damaging temperatures in any given winter from the intended 98 % to around 50 %. Furthermore, the loss also causes the thermal stress to be about double from the design which then leads to excessive cracking at cold temperatures (Hesp et al., 2000a). Since 665-9 was a straight unmodified Cold Lake binder, it was expected to change very little in T30° values as it possessed the best lifespan at 38 years (Ma et al., 2023). However, the results proved otherwise with a moderate 5.5°C loss in grade. This, however, is likely because a particularly soft binder with higher-than-expected solubility in ethanol was used, prompting it to favorably undergo dissolution instead of exudation. The worst exuding binders from a limiting $T_{30°}$ perspective are 655-13, 655-11, 655-6 and 655-12, which lost 12.5°C, 9.3°C, 7.6°C and 6.8°C, respectively. All of these performed rather poorly in service with lifespans of 23, 29, 17 and 28 years, respectively (Ma et al., 2023).

The worst lifespan for these two trials was obtained for section 655-4, which reached a pavement condition index of 50 % after only 14 years (Ma et al., 2023). It lost a modest 3.7°C due to exudation suggesting that other factors are likely equally if not more important. In the case of 655-4 the binder was heavily modified with REOB that is high in heavy metals and oxidized residues and hence causes premature oxidative aging that is not necessarily captured by a single PAV round of 20 hours at 100°C (Erskine et al., 2012; Rubab et al., 2011; Wright et al., 2011).

It should be noted that the ultrasonication in ethanol provides a worst-case scenario from an exudation point of view as the binder in service only sees the aggregate and is not necessarily affected to the same degree when non-absorptive aggregates are used in good mixture designs. Finally, the test developed here does not measure any loss in adhesion as the aggregates are not included in the assessment. Hence, it is possible that a small change in limiting phase angle temperature can still lead to significant degradation of the asphalt binder-aggregate interface and resultant poor pavement performance.

4.2.2.2 Limiting complex shear modulus temperatures.

To investigate the stiffening effect induced by the loss of low molecular weight oils, the limiting temperatures where the complex shear modulus G* reached 30 MPa were calculated for each binder. The limit was set at 30 MPa as it is close to the average G* of 29.1 MPa for all test section binders at their 30° phase angle temperatures. Crack initiation and propagation in asphalt pavements occurs in the stiffness range between a few tens of megapascals to a few hundreds of megapascals (Erskine et al., 2012). Figure 33 provides the results for this analysis.

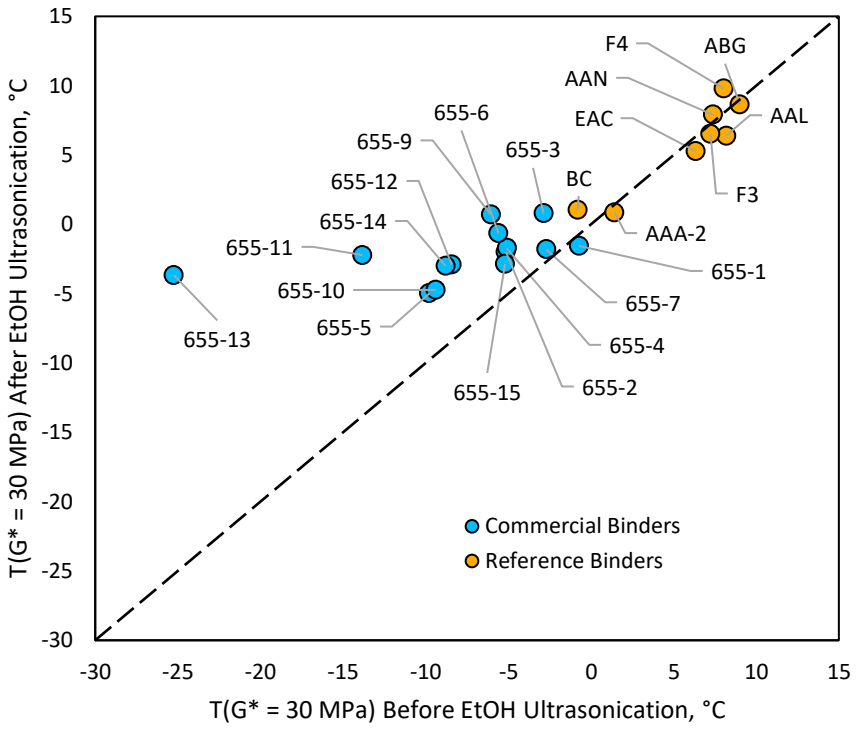

Figure 33. Comparison of limiting G* = 30 MPa temperatures before and after ultrasonication.

The graph shows that there are insignificant changes in modulus for the straight reference binders but again significant changes for modified binders because of oil exudation. The biggest change was seen for the binder used in section 655-13 as it lost 21.6°C in the limiting 30 MPa stiffness temperature. Other big losers included 655-10 which lost 10.6°C and 655-9 which lost 6.8°C. The average change for all 14 modified binders was 5.6°C, representing about a doubling in stiffness which is significant in terms of thermal and fatigue stress cracking. The 655-9 binder loses a significant amount, yet it performed best with an expected lifespan of 38 years (Table 8). Hence, this once more suggests that the exudation phenomenon is just one of several factors that contributes to low temperature and fatigue cracking distress. It should be emphasized that these results present worst-case scenarios from an exudation perspective that might only materialize in exudation amenable mixture designs with porous aggregates and in old age pavements.

The main observation from these experiments is that straight binders from Alberta and Venezuela lose little to no performance due to exudation and that this contrasts with the results for nearly all trial section binders. It requires only a small amount of saturates to break the bond with the aggregate so this effect can have negative consequences in the real world and may well be a root cause for the precipitous decline in pavement lifecycles as depicted in Figure 34.

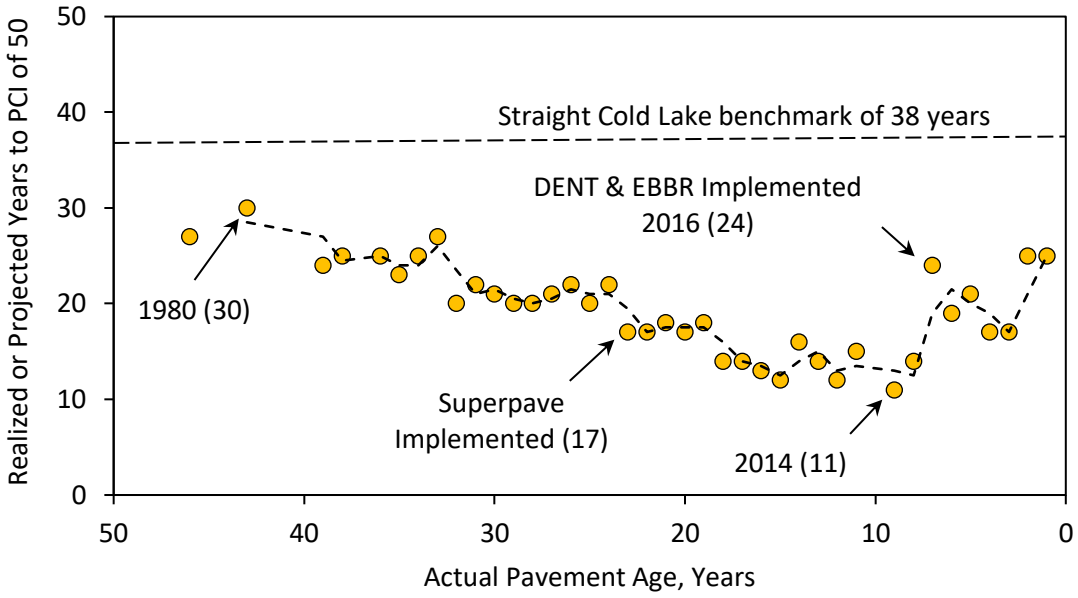

Figure 34. Lifespans of asphalt pavements in an Ontario municipality over the last 50 years.

Note: DENT = double-edge-notched tension test and EBBR = extended bending beam rheometer test.

4.2.3 GC-MS Results

The GC-MS results were obtained to provide further insights into the type of molecules that are exuding from the asphalt binders. Figure 35 provides an example of a gas chromatogram for one of the binders while Figure 36 provides an example of a mass spectrum for one of the compounds eluted as a distinct peak in Figure 35. Table 10 provides a listing of the saturates that were identified through a library search for all mass spectra produced by the GC-MS instrument.

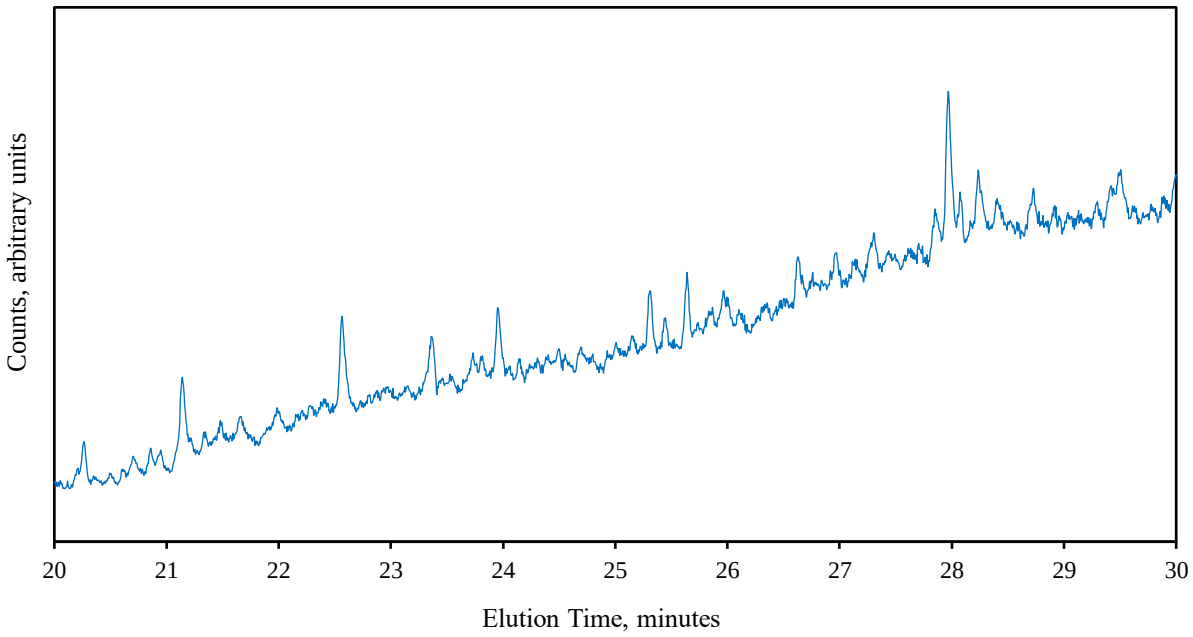

Figure 35. Gas chromatogram for ethanol solution of exuded saturates showing distinct peaks.

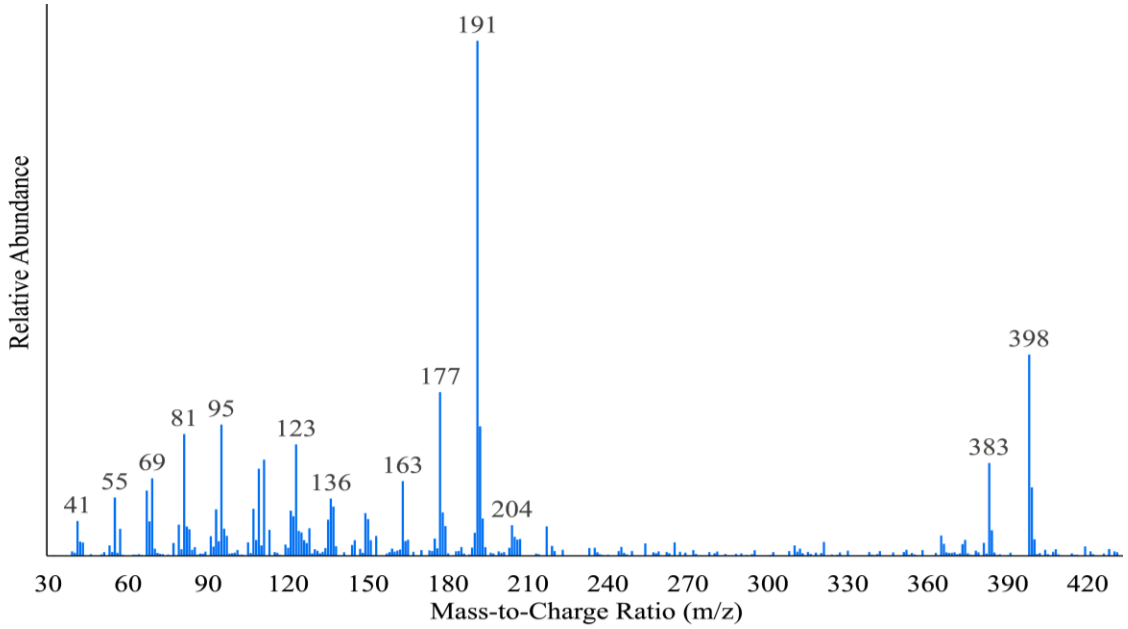

Figure 36. Mass spectrum for one of the peaks eluted from the GC column.

It is obvious from the findings that there are a reasonable number of distinct peaks that can be separated and that many of these relate to the presence of long chain saturates with boiling points in the 170°C to 400°C range. Normal asphalt binders are produced with cut points typically above 370°C, suggesting that

the peaks identified here might well be residual traces from normal asphalt binder or originate from oils added to the binders as part of the modification process.

The results for all 14 test section samples were similar to the ones shown in Figure 35 and Figure 36. Assuming that primarily organic compounds are leaching out of the binder samples into the ethanol, these graphs suggest the particularly strong presence of molecules of lower molecular weight and a paraffinic structure (long chain saturates). This agrees with the findings from the seminal work by Romberg, Nesmith and Traxler in the late 1950s (Romberg et al., 1959) who found the exudate to be of a primarily paraffinic nature.

Table 10. Selection of long chain saturates exuded into ethanol from binder.

Compound Name	Molecular Formula	Molar Mass (g/mol)	Boiling Point (°C)
2,4,6-trimethyloctane	$C_{11}H_{24}$	156.35	172.2
3,7-dimethylnonane	$C_{11}H_{24}$	156.35	183.3
cyclododecane	$C_{12}H_{24}$	168.36	244.0
9-methyl-1-undecene	$C_{12}H_{24}$	168.36	207.3
3,7-dimethyldecane	$C_{12}H_{26}$	170.38	203.0
6-tridecene	$C_{13}H_{26}$	182.39	235.3
2-methyldodecane	$C_{13}H_{28}$	184.41	229.5
6-ethyl-2-methyldecane	$C_{13}H_{28}$	184.41	217.0
7-tetradecene	$C_{14}H_{28}$	196.42	250.0
tetradecane	$C_{14}H_{30}$	198.44	253.6
pentadecane	$C_{15}H_{32}$	212.47	270.6
5,8-diethyldodecane	$C_{16}H_{34}$	226.50	275.0
hexadecane	$C_{16}H_{34}$	226.50	286.9
2,6,10-trimethyltetradecane	$C_{17}H_{36}$	240.53	282.5
octadecane	$C_{18}H_{38}$	254.56	317.0
eicosane	$C_{20}H_{42}$	282.62	343.0
2-methylnonadecane	$C_{20}H_{42}$	282.62	329.7
heneicosane	$C_{21}H_{44}$	296.65	356.1
docosane	$C_{22}H_{46}$	310.68	368.6
9-hexylheptadecane	$C_{23}H_{48}$	324.71	397.5
9-octylheptadecane	$C_{25}H_{52}$	352.77	384.7

Table 10 offers a compilation of specific saturates identified to have come out of the binders into the ethanol solution through the GC-MS analysis. This confirms our suspicions of low molecular weight organics exuding out. This exudation may be due to the insertion of oils at the wholesale and contractor level, or possibly the result of binder modification influencing the colloidal structure of the binder, making it more susceptible to let go of its inherent saturate fraction. The chief reasoning behind this is the fact that practically no oils exuded from the straight refined binders used as the controls.

Given the widespread presence of exuding oils in current asphalt binders sold for road construction, the question that needs an answer is whether the precipitous decline in lifecycles as shown in Figure 34 can

be explained in part by the decrease in adhesion that results from the exudation phenomenon. The recent change in trend shows that the implementation of both the DENT and EBBR specification tests have been able to reverse the decline to a significant degree. Whether a return to lifecycles in the 40-year range is possible by using straight Alberta binders with improved mixture designs remains to be investigated with carefully controlled pavement trials. In this context it is interesting to note that for the four Ontario pavement trials constructed since 2003, the least modified binders have performed best (Ma et al., 2023).

4.2.4 Summary and Conclusions

Given the results presented, the following summary and conclusions are offered: Lifecycles for Ontario pavements have shrunk by 50 % or more since the early 1980s, likely due to the increasing use of modified asphalt binders and/or the improper use of recycled materials (RAP, RAS, REOB, etc.). Straight asphalt binders made from superior Alberta and Venezuelan crude sources show little to no tendency for exudation of low molecular weight saturated oils. Modified asphalt binders from trial sections on Highway 655 in northeastern Ontario show varying degrees of exudation. A simplified ultrasonication protocol in ethanol, combined with the measurement of changes in limiting phase angle temperatures, can provide an indication of vulnerability to exudative hardening. Implementation of the DENT and EBBR specification tests have had a major positive effect on lifecycles by limiting the use of improper modifiers, RAP and/or softening oils. Given the significance of the findings regarding the changes in pavement lifecycles as indicated in Figure 34, this is an issue that deserves further attention.

4.3 Grading Asphalt Binder using MDSC

4.3.1 Asphalt Binder from 655 Phase 2 Pavement Trial

In this section, asphalt binders including straight and modified asphalts from a pavement trial from northern Ontario, Canada were employed to build link between thermal properties from MDSC results and their field performance. In this test road, eight sections were constructed with asphalts which varied in modification type and dose. After 13 years of monitoring, modification is found to significantly influence pavement performance with differences in expected lifespan exceeding 15 years. MDSC test was performed on the trial binders and their aged residues to shed light on the inherent mechanisms that govern field performance. Paved with recycled engine oil bottom (REOB) tainted asphalt, test section 655-15 has the shortest lifespan. Results showed this section suffered from accelerated aging and had the lowest degree of phase compatibility. Paved with 7 % styrene-butane-styrene (SBS) modified asphalt, section 655-13 is expected to last for only 23 years, in contrast to section 655-14, paved with 3.5 % SBS modified asphalt, which is expected to last for 36 years. Glass transition results show that SBS modification suppresses the glass transition temperature but high SBS content increases phase incompatibility. A test section paved with straight Cold Lake binder from Alberta oil sand, modified with 0.3 % PET fiber on the mixture, is expected to outperform all others with an expected lifespan of 38 years.

The asphalt binders used in this study were sampled during the construction of the test sections in 2007. These asphalt samples had been collected in their original state, sealed in paint cans and been stored in a fridge at low temperature. These eight binders as listed in Table 11 cover a broad range of polymer and fiber modified asphalts that are widely used in Canada and the USA [36]. The base asphalt for these

sections was produced from Cold Lake, Alberta bitumen to a penetration grade of 300/400. Fibers of polypropylene (PP) and polyethylene terephthalate (PET) were used in sections 8 and 9 and blended into hot mix asphalt (HMA) during construction. Accordingly, the fiber-modified 655-8 and 655-9 binders were not adopted for thermal analysis. Further, the 655-8 section is not the subject of further study as its HMA was overheated during construction. Along with the binders from section 655-10 through 655-15, a sample of the unmodified 655-9 binder was used for analysis as a control. To simulate oxidative aging experienced in the field, each binder was conditioned according to a standard pressure aging vessel (PAV) protocol for 20, 40, and 100 hours at 2.1 MPa and 100 ℃. Materials with different aging degree were labeled as Unaged, PAV20, PAV40 and PAV100, respectively.

Table 11. Information of asphalt binders in each test section and their expected lifespan.

Section	Modification	Superpave Grade, ℃	Expected Lifespan, Years
655-8	0.3 % PP fiber	PG 52-37	-
655-9	0.3 % PET fiber	PG 52-37	38
655-10	1 % PPA + 2 % SBS	PG 67-34	25
655-11	7 % SB	PG 76-37	29
655-12	2.5 % RET	PG 67-37	28
655-13	7 % SBS	PG 82-40	23
655-14	3.5 % SBS	PG 64-37	36
655-15	REOB	PG 55-34	22

Note: The binder in each test section is referred to as the same name as its corresponding section. As the HMA for 655-8 was overheated during production this section is omitted from the analysis. The percentages given are by weight.

The trial sections were surveyed annually by the Ministry of Transportation of Ontario (MTO) using an Automatic Road Analyzer (ARAN) vehicle to measure distresses and a corresponding pavement condition index (PCI) (Ma et al., 2021). The PCI reflects the amount of distress, including but not limited to transverse cracking, rutting, and raveling. A new road will have a PCI of 100 which will decay as it ages. The end of service life is reached when the PCI decays to 50 for a secondary highway. By fitting a linear model to the yearly PCI index, the year at which all sections are expected to reach their end-of-life was calculated (Ma et al., 2023).

4.3.1.1 Field performance.

The linear model of the expected lifespans gave excellent correlations (R^2 ranging from 0.90 to 0.99), an example of fitting for section 655-9 (best) and 655-15 (worst) is shown in Figure 37. The expected lifespan of each section, as calculated by extrapolating the linear model to the year at which the PCI reaches 50, is presented in Table 11.

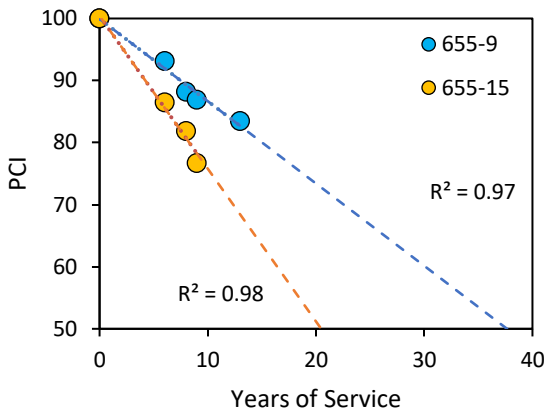

Figure 37. Linear fitting of PCI for the best-performing and worst-performing sections.

Expected lifespans vary as much as 16 years across the test sections, illustrating the sensitivity of pavement performance to modification. Section 655-9 (unmodified) is the best performing section, with an expected lifespan of 38 years, while section 655-15 (REOB) is the worst performing section, with an expected lifespan of 22 years. Of the two sections modified exclusively with SBS, the highly modified section 655-13 (7 % SBS) was the second worst performer while the lower modified section 655-14 (3.5 % SBS) was the second-best performer. Section 655-11 and 655-13 are modified at equivalent 7 % doses, yet section 655-11, modified with SB, is expected to last 6 years longer than section 655-13, modified with SBS. Thus, both modification dose and modification type cause differences in pavement performance.

4.3.1.2 Non-isothermal crystallization kinetic analysis.

The non-reversible heat flow curves vary with the cooling rate, the age of the binder, and modification. Take the unaged sample of the unmodified binder for example, there is a large primary endotherm centered at −25 ℃ followed by a smaller secondary endotherm centered at 30℃, as shown in Figure 38 (a). The origin of double endotherms is debated, but a plausible explanation is a cold crystallization mechanism outlined by Frolov and coworkers (Frolov et al., 2020). This is consistent with the observation that the area enclosed by the primary endotherm increases at low cooling rates. The corresponding fitting analysis based on the Ozawa framework is shown in Figure 38 (b).

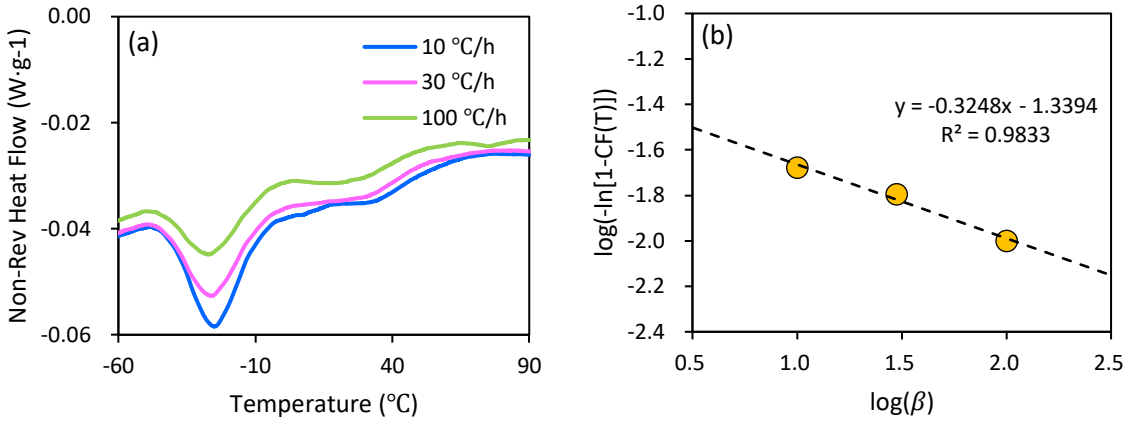

Figure 38. Unaged sample of the unmodified binder.

(a) effect of cooling rate on the non-reversible heat flow curves; (b) corresponding Ozawa plot.

Aside from two outliers, fitting the thermal analysis results yielded high correlations (R^2 ranging from 0.84 to 0.99), indicating the applicability of the Ozawa theory for asphalt binders. The Ozawa exponent and the maximum crystalline fraction for each sample are shown in Figure 39 (a) and (b), respectively. Since crystallinity is in part responsible for thermo-reversible aging, it was expected that these parameters would differentiate poor-performing sections from well-performing sections. However, no such trend was observed in either the Ozawa exponents or the crystalline fraction. For example, section 655-11 had higher Ozawa exponents for all samples in comparison to section 655-15, suggesting that it more readily crystallizes, yet 655-11 is expected to last 7 years longer. Most samples fell within a narrow 2-4 % range for crystalline fraction, consequently, the crystalline fraction is also unable to explain field performance. It can be concluded that in the case of the 2007 Timmins trial, crystallization was not the main factor leading to differences in lifespan. There are other more important factors controlling the lifespan of the sections in this trial such as rheology and/or phase separation (Ma et al., 2023).

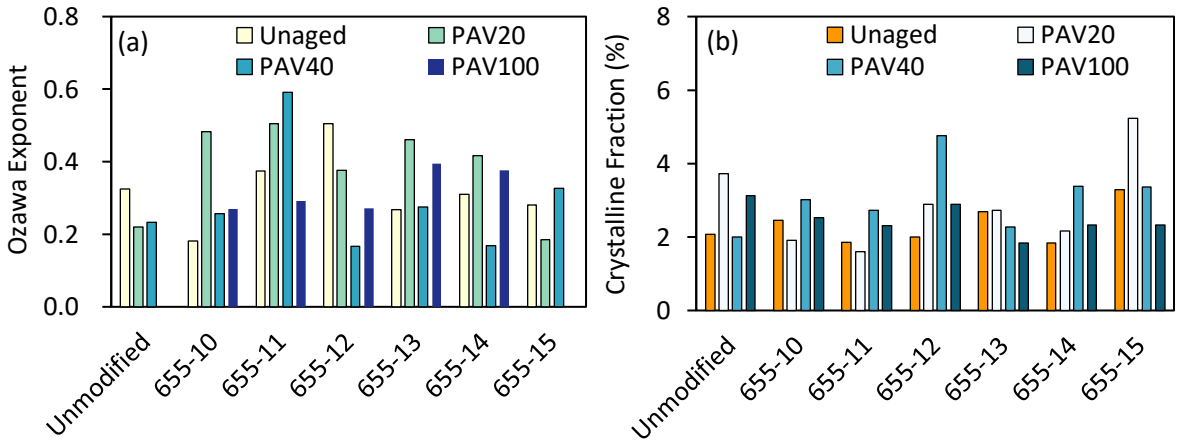

Figure 39. Crystallization kinetics parameters for the samples of each section.

(a) Ozawa exponent; (b) crystalline fraction formed at the slowest cooling rate (10 °C/h).

4.3.1.3 Reversible heat flow analysis.

The glass transition temperatures for each sample are shown in Table A-3 in Appendix . T_g(I) and T_g(H) are tabulated and the difference between these estimates is presented as DT_g. Previous study shows that the reversible heat flow curve of a compatible asphalt binder exhibits a Gaussian distribution (Bricker and Hesp, 2013). As a Gaussian is symmetrical about its peak, the area beneath the curve on either side of the peak is equivalent. According to the definition of T_g(I) and T_g(H), if a system is fully compatible, T_g(I) and T_g(H) are equivalent. Thus, it is expected that the difference between T_g(I) and T_g(H) can be used to quantitatively evaluate the compatibility of asphalt binder, the larger the difference, the less compatible the asphalt binder (Masson et al., 2005).

A general trend can be found from Table A-3 in Appendix. Forming the continuous phase in the unmodified binder, the maltenes exhibit the most intense transition and consequently T_g(I) always occurs around the temperature of the maltene transition. As such, T_g(I) only provides information regarding the transition of the maltenes, not the entire system. Conversely, T_g(H) considers the temperature at which half the material vitrifies and is representative of the entire system. This is why upon aging, T_g(I) stays relatively constant with age, while DT_g and T_g(H) increases, reflecting an increase in high molecular weight fractions. In terms of the evolution of glass transition temperature with aging, it can be found that the evolution of T_g(H) of modified asphalt with age is complex and follows no continuous trend while T_g(I) tends to decrease with age.

There is no obvious link between glass transition parameters of asphalt binders and expected life span of test sections. However, the glass transition temperature results potentially provide new insights into the effect of polymer dosage on the durability of asphalt binder in field. The glass transition temperature for binders from sections 655-13 (7 % SBS) and 655-14 (3.5 % SBS) exhibit lower T_g(I) compared to the unmodified binder in section 655-9. Hence, SBS modification suppresses the glass transition of the continuous phase which delays the vitrification and stiffening of the binder. Vitrification and stiffening are detrimental as it inhibits stress relaxation and induces thermal cracking. Thus, the addition of SBS and its consequent suppression of the glass transition is favorable. From T_g(I) and T_g(H) alone, it is difficult to detect the onset of network degradation. Over time, the rigid SBS network degrades which increases the system's flexibility and consequently decreases its glass transition temperature. However, this may be offset by an increase in the glass transition from the formation of oxidized components such as asphaltenes. The vast difference in performance, the expected lifespan of section 655-14 (3.5 % SBS) exceeding that of section 655-13 (7 % SBS) by 13 years, is a function of multiple factors. Tg(I) and Tg(H) only fail to capture the complexity of incompatible systems which necessitates plotting the derivative of the reversible heat capacity against temperature hereinarivative reversible heat capacity of unaged sample from section 655-9 (unmodified) is shown in Figure B-1 (a_1) to (a_4) in Appendix. It can be found that a Gaussian distribution ranges from −45°C to 0°C and peaks between −26°C and −22°C, depending on the cooling rate. A smaller Gaussian distribution arises at a lower temperature, centered at −55°C. Beyond 0°C, there are small Gaussian distributions of relatively small intensity. Amorphous regions of low molecular weight and high flexibility transition occur normally at low temperatures, given this, previous researchers have attributed the transition at −55°C to a paraffinic phase (Masson et al., 2005). The peak

appearing between −50°C and 0°C results from the transition of the continuous maltene phase, hence this Gaussian distribution has the largest area enclosed beneath it (Masson et al., 2005). The transitions beyond 0°C are attributable to higher stiffness and higher molecular weight fractions, including precipitated asphaltenes (Masson et al., 2005). Firstly, for the unaged sample, the peak of the maltene transition shifts to higher temperatures as the cooling rate decreases. Thus, the flexibility of the maltene phase decreases at low cooling rates. Crystalline content was found to increase upon lowering cooling rates, which may further increase the fraction of the rigid amorphous phase. An increase in the rigid amorphous phase in turn reduces flexibility, which is consistent with the observed increase in glass transition temperature. Secondly, the intensity of the maltene transition decreases with the increase of cooling rate, suggesting that a smaller fraction acts as maltenes at high cooling rates. One explanation is that at high cooling rates, there is insufficient time for the entire maltene phase to take transition. Notably, upon cooling the PAV20 and PAV40 samples at 10°C/h, the maltene peak at −29°C and −26°C is accompanied by a peak of similar intensity centered at −20 °C and −16 °C. Masson and coworkers (Masson et al., 2005) also observed peak splitting and attributed the new peak to an interphase at the asphaltene-maltene interface. The peak splitting occurs only at the lowest cooling rate, suggesting that the development of this interphase is time dependent. Lastly, at PAV100, the binder exhibits poor phase compatibility as peaks of strong intensity develop after the maltene peak. As the binder ages, the maltene peak shifts to lower temperatures. Thus, phase compatibility decreases with oxidation as incompatible fractions of high weight form at the expense of low weight fractions. As shown in Figure B-1 (b_1) to (b_4), for the derivative reversible heat capacity curves of section 655-10 binder (1 % PPA + 2 % SBS), an intense, single Gaussian curve from the maltene transition broadens at PAV40 and PAV100. Though PPA is known to increase asphaltene content at the expense of maltenes, this effect is not obvious through qualitative analysis of the curves since no extra peaks appear. Overall, the 655-10 binder remains compatible upon aging. Shown in Figure B-1 (c_1) to (c_4) are the derivative reversible heat capacity curves of section 655-11 binder (7 % SB). The transition of the continuous phase is broader than that of section 655-14 (3.5 % SBS) shown in Figure B-1 (f_1) to (f_4), and seems to be composed of multiple transitions. Specifically, a transition centered at 7°C develops with age and becomes prominent at the highest cooling rate. Overall, asphalt binder from this section exhibits higher phase incompatibility than the second-best performing section, 655-14 (3.5 % SBS). That said, it exhibits higher phase incompatibility than section 655-10 (1 % PPA + 2% SBS), despite being expected to last four more years.

The derivative reversible heat capacity curves of section 655-12 binders (2.5 % RET) are shown in Figure B-1 (d_1) to (d_4). The unaged sample shows an intense transition of the maltenes centered at −24°C that broadens with age. For both the unaged and PAV20 sample, a Gaussian distribution is centered at 30°C which arises from the transition of an insoluble gel formed upon modification with RET. Upon further aging, the binder becomes more phase incompatible with peak splitting observed at the slowest cooling rate of the PAV40 sample. The unaged and PAV20 samples from sections 655-10 (1 % PPA + 2 % SBS) and 655-12 (2.5 % RET) appear to be more compatible than that from section 655-11 (7 % SB), despite both sections 655-10 (1 % PPA + 2 % SBS) and 655-12 (2.5 % RET) having shorter expected lifespans. That said, all three sections show higher phase compatibility than the worst performing section, 655-15 (REOB), and lower phase compatibility than the best performing section, 655-14 (3.5 % SBS). It is to be expected that

the differences in performance of these sections are more difficult to explain from a phase separation perspective. After all, these sections contain different modifiers and fall within a relatively narrow range for expected lifespan. In contrast, the effect of phase separation is clear when considering the best performing and worst performing sections, or when comparing sections of equivalent modifier that vary in dosage. To precisely rank the trail sections from best to worst, rheological indicators are required. A rheological study of the binders from this pavement trial found that the expected lifespan correlated with the width of the temperature range in which the phase angle increased from 30° to 45°(Ma et al., 2023). This index characterizes the degree of solid-like behavior and the ability of the binder to relax stress when exposed to the freeze-thaw temperature region (Ma et al., 2023).

The derivative reversible heat capacity curves of sections 655-13 (7 % SBS) and 655-14 (3.5 % SBS) are shown in Figure B-1 (e_1) to (e_4) and Figure B-1 (f_1) to (f_4), respectively. In the range of −60 ℃ to 0 ℃ for the unaged samples, 655-14 (3.5 % SBS) exhibits a higher degree of phase compatibility than 655-13 (7 % SBS). For the 655-14 binder (3.5 % SBS), there is a single, intense Gaussian from the transition of the maltenes. In contrast, the 655-13 (7 % SBS) binder exhibits two Gaussian distributions, one of small intensity centered at −49°C to −47°C, and one of larger intensity centered at −31°C to −24°C, depending on the cooling rate. Thus, high dosages of SBS induce exudative aging, expelling low-weight fractions, and causing them to transition at a lower temperature. For the 655-13 samples (7 % SBS), the exclusion of low-weight fractions is notable on all but the PAV100 sample. At PAV100, the low-weight fractions are likely oxidized, hence the disappearance of the low-temperature Gaussian. Aside from the repositioning of small transitions that occur at high temperatures, the 655-14 (3.5 % SBS) unaged and PAV20 samples show high phase compatibility as indicated by an intense Gaussian at low temperatures. Like the unmodified binder, both the 655-13 (7 % SBS) and 655-14 (3.5 % SBS) samples experience a shift in their glass transition towards higher temperatures with oxidation. This is indicated by the broadening of the Gaussian of the continuous phase upon PAV40 and PAV100. Additionally, qualitative analysis of the derivative reversible heat capacity curves shows that section 655-13 suffered a higher degree of phase incompatibility. Particularly, the binder of 655-13 showed a strong Gaussian at low temperatures which indicates exudative aging and phase separation. In contrast, the low dosage of SBS in section 655-14 gave a high degree of phase compatibility, similar to that of the unmodified binder. Thus, highly SBS-modified binders suffer phase incompatibility and exudative aging, both factors explain the difference in expected lifespans.

In comparison to the unmodified samples, the 655-15 (REOB) samples exhibit peak splitting at low degrees of aging. As such, section 655-15 likely experienced phase incompatibility and separation early in its lifespan. This would have produced high-energy interfaces for crack propagation and decay in rheological properties including fatigue endurance. Moreover, the existence of multiple Gaussians of similar intensity implies that regions within the binder will transition at different temperatures. At a given temperature, one region of the binder will be viscous while another region will be glassy. Therefore, there will be a discontinuity in mechanical and rheological properties. Finally, the existence of an intense low-temperature Gaussian confirms that section 655-15 suffered exudative aging. The light oils would have been expelled from the asphalt matrix and migrated to the aggregate. This reduces the adhesive force

between the binder and the aggregate, consequently increasing susceptibility to moisture cracking (López-Montero and Miró, 2016). These effects explain why section 655-15 had the shortest expected lifespan, 16 years shorter than the best performing section.

4.3.2 Contract Asphalt Binders

The phase compatibility of asphalt binder plays a significant role in controlling the durability of an asphalt pavement. With the ever-increasing use of recycled asphalt, polymer modifiers, waste oils and other additives, current acceptance testing methods may pass binders with poor phase compatibility, potentially causing unexpected cracking because of exudation or thermo-reversible aging. However, the relationship between phase separation and thermo-reversible aging remains largely unclear. This section aims to explore the link between phase compatibility based on MDSC and thermo-reversible aging degree based on the EBBR test. Tank and recovered asphalt binders were used for analysis.

Quantifying the extent of phase separation in asphalt binders at low temperatures is crucial for controlling both oil exudation and thermo-reversible aging. Kriz and coworkers (Kriz et al., 2008) developed a method that employs reversible heat capacity data from MDSC tests to assess the degree of phase separation. Typically, the derivative of heat capacity data with respect to temperature (dCp/dT) displays a single peak, indicating that the asphalt binder is compatible under the tested conditions and no phase separation occurs. It was generally accepted that phase separation is closely related to thermo-reversible aging of asphalt. However, the relationship between phase separation and thermo-reversible aging in asphalt binders remains unclear.

In this section, asphalt binders from across North America were collected for analysis. The degree of phase separation was quantified using derivative heat capacity data from MDSC tests, while the extent of thermo-reversible aging was assessed through grade loss data from EBBR tests. The correlation between these phenomena is investigated and the potential underlying mechanisms are discussed.

A total of 21 types of asphalt binders were used. Out of these, five were tank samples that were aged using RTFO and PAV techniques, as specified by ASTM D 2872 and AASHTO R 28 standards, respectively. The remaining binders were extracted from asphalt mixtures collected from various construction projects across different regions in North America. The extraction process followed ASTM D 2172 guidelines. The basic properties of these asphalt binders are summarized in Table 12 below.

Table 12. Basic properties of asphalt binders from tank or asphalt mixture.

Sample	HTPG (℃)	ITPG (℃)	LTPG (℃)	Sample	HTPG (℃)	ITPG (℃)	LTPG (℃)
1	71.3	5.5	-42.2	22	74.7	10.8	-36.0
2	75.1	4.5	-44.1	23	76.6	12.4	-35.8
3	80.3	5.4	-44.4	24	76.8	13.7	-35.2
4	81.6	20.8	-27.4	25	73.3	11.2	-36.6
5	65.0	18.7	-30.3	26	74.4	14.5	-35.3

6	64.7	10.2	-37.0	27	75.6	14.7	-35.4
7	74.3	23.4	-26.2	28	67.1	13.3	-34.4
8	73.5	23.6	-22.0	29	72.1	18.2	-33.1
9	67.4	24.9	-24.6	30	71.9	11.7	-35.4
10	68.1	26.1	-24.3	31	71.9	13.5	-33.7
11	69.2	20.4	-23.3	32	72.7	15.4	-33.6
12	80.6	28.2	-20.9	33	73.3	13.2	-35.5
13	83.1	24.9	-23.1	34	70.3	14.4	-33.1
14	79.2	27.5	-20.5	35	74.8	16.3	-30.1
15	69.0	14.2	-32.0	36	73.1	16.8	-32.4
16	77.1	18.4	-30.3	37	71.4	24.3	-27.0
17	79.4	16.3	-35.3	38	75.0	17.6	-30.7
18	63.7	16.3	-33.0	39	76.2	19.8	-30.4
19	62.1	15.1	-34.3	40	74.3	16.4	-32.3
20	73.3	15.0	-32.7	41	71.4	15.9	-32.7
21	73.8	9.6	-38.2	42	74.1	17.8	-29.7

4.3.2.1 Correlation analysis.

It was found in our previous study that the phase separation degree of asphalt binder depends on the cooling rate. The separated peak in the derivative heat capacity curve is more obvious at higher cooling rates . For this reason, only the data at 100℃/h was used for analysis. The relationship between the degree of phase separation and LTPG is shown in Figure 40. It can be found that there is no obvious correlation between the three phase separation indicators and LTPG. This failed to confirm our hypothesis that phase separation affects thermo-reversible aging. However, the LTPG data were determined with BBR beams after 1 hour of conditioning before thermo-reversible aging. The relationship between phase separation and thermo-reversible aging degree of different asphalt binders will be discussed next.

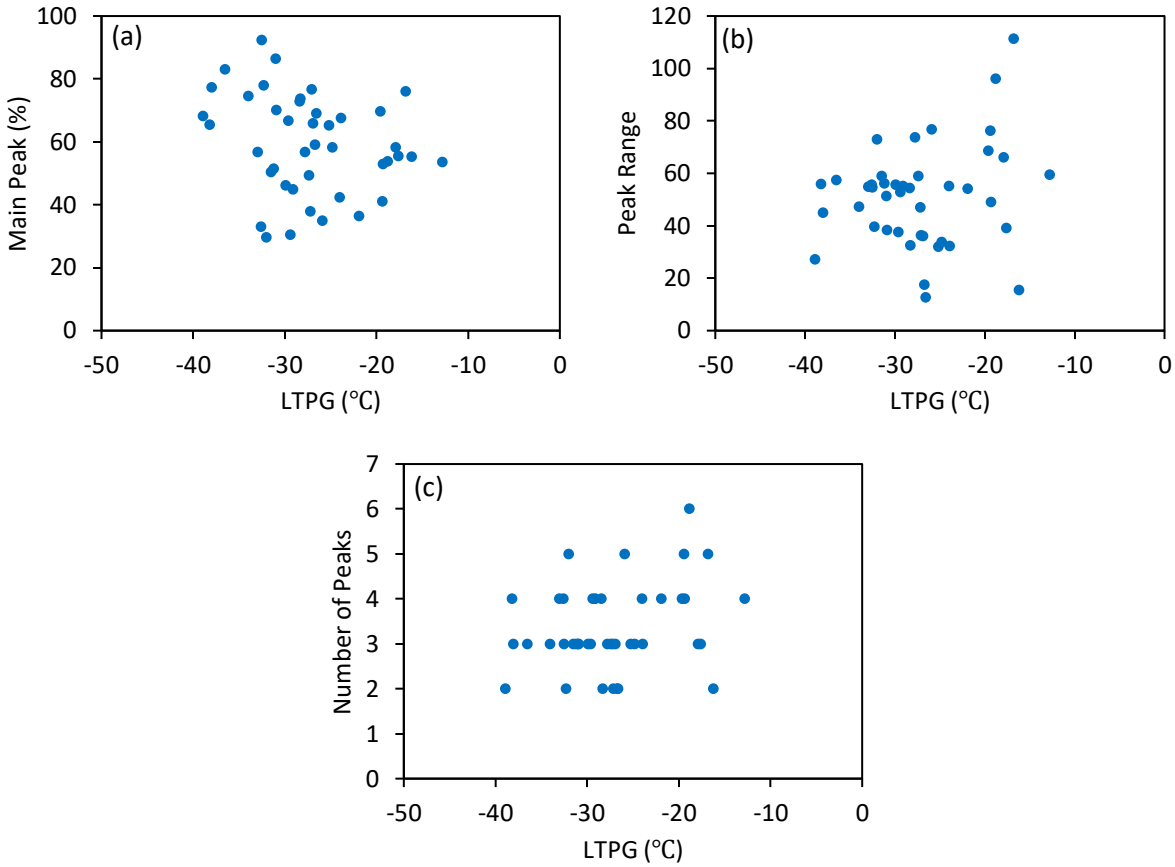

Figure 40. Degree of phase separation vs low temperature performance grade.

The relationship between the degree of phase separation and the thermo-reversible degree, as measured by grade loss, is provided in Figure 41. Interestingly, none of the three indicators for phase separation show a correlation with the grade loss observed in various asphalt binders. These findings call for a reevaluation of the commonly held belief that phase separation is directly related to thermo-reversible aging in asphalt binders. Alternatively, it is possible that an indirect relationship exists between the two factors. Our recent research suggests that the phenomenon of oil exudation could potentially explain these results and shed light on the relationship between phase separation and thermo-reversible aging in asphalt binders. A possible explanation is given in the following section.

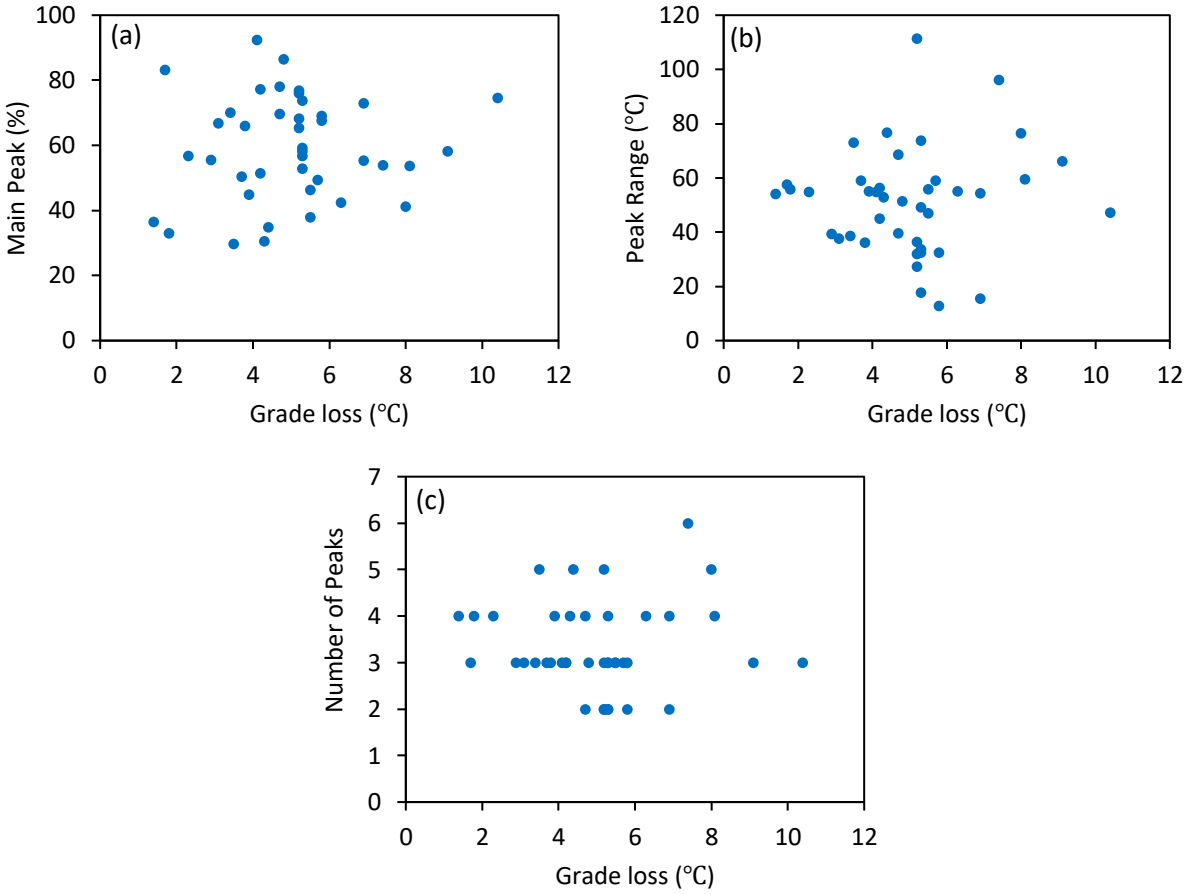

Figure 41. Relation between the degree of phase separation of asphalt binder and grade loss.

4.3.2.2 Exploration of potential mechanisms.

In recent research, we and others discovered that asphalt modified with oil tends to release oil when submerged in ethanol during the EBBR test (Zhang et al., 2024). The release of oil from the asphalt binder likely intensifies the interaction among asphaltenes, leading to an overestimation of the degree of thermo-reversible aging in EBBR tests. Moreover, the rate of oil exudation also increases when the asphalt binder interacts with aggregates. With an ethanol medium, the EBBR tests achieved the same effect of oil exudation as aggregate suction. This may potentially explain why the EBBR test has been highly successful in predicting the field performance of asphalt pavements in Canada. This study reveals that there is no direct correlation between the degree of phase separation and the degree of thermo-reversible aging in asphalt binders, and the primary factor may well be the effect of oil exudation.

Figure 42 outlines the possible relationships among phase separation, oil exudation and the degree of thermo-reversible aging. For an asphalt binder that is phase-unstable, it maintains a homogeneous state at elevated temperatures. However, phase separation occurs when the temperature either drops suddenly or is sustained at a low level for an extended period. The separated phases can be categorized into the associated dispersed phase and the continuous oil phase. This transition is evident in the derivative heat capacity data from the MDSC test, which shows distinct peaks. It is noteworthy that these

separated dispersed phases do not form a macroscopic structure that could contribute to thermo-reversible age hardening. However, oil exudation occurs in phase separated asphalt during the EBBR test and the oil phase is partially released into the ethanol. Following this oil exudation, the dispersed phases combine to form macroscopic structures responsible for thermo-reversible aging. Therefore, it can be speculated that phase separation is merely the initial stage of thermo-reversible aging, and the subsequent step of oil exudation is essential for the final hardening effect to be observed in rheological tests.

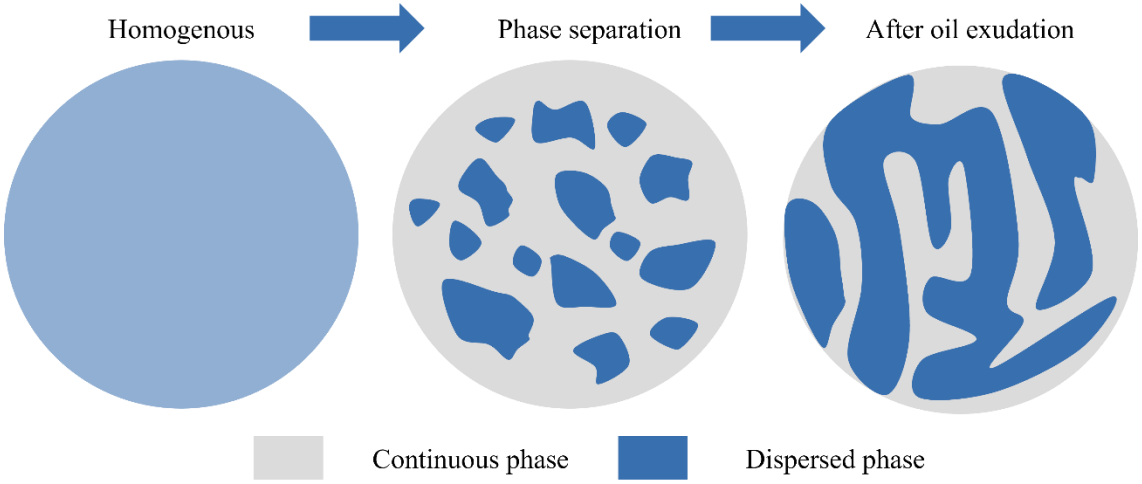

Figure 42. Relationship among phase separation, oil exudation, and thermo-reversible aging.

4.3.3 Summary and Conclusions

This section explored the potential of MDSC as a new approach to grade asphalt binder. Both binders from 2007 Timmins trial sections and contracts were analyzed to investigate aspects such as thermo-reversible aging, glass transition, and phase compatibility. The main conclusions can be summarized as following:

(1) Wax crystallization did not significantly influence the lifespan discrepancies observed across the test sections. Instead, phase separation and the combined rheological and stress relaxation properties, as reported by (Ma et al., 2023), provide a more comprehensive explanation for these variations.

(2) For modified asphalt binders, the presence of multiple Gaussians peaks on the derivative reversible heat capacity curves indicates phase separation, suggesting that a single glass transition temperature does not suffice to describe their glass transition behavior.

(3) Unmodified and unaged binders exhibited high phase compatibility, diminishing with aging and modification. The study identified that modification, especially with REOB, and aging via different mechanisms, contributed to phase incompatibility and adverse effects on pavement performance.

(4) The findings showed that increasing SBS polymer content negatively affected the lifespan of the asphalt, with a notable differentiation in performance and compatibility between sections modified with different amounts and types of SBS and SB polymers. Specifically, SB modification appeared more

favorable in northern climates, offering a longer expected lifespan and higher phase compatibility compared to SBS-modified sections.

(5) The investigation revealed no direct correlation between phase separation and the degree of thermo-reversible aging, challenging the previously held beliefs about their relationship. While phase separation was observable under certain conditions, it did not necessarily lead to structures conducive to thermo-reversible age hardening.

(6) It was noted that the oil exudation during the EBBR test prompted the clustered phases to form structures that induce thermo-reversible aging, highlighting a complex interaction between phase behavior and aging processes.

4.4 Grading Asphalt Binder using DSR

Precise and repeatable test methods for measuring the rheological parameters of asphalt binders are indispensable for grading asphalt binders to be used in asphalt roads. Two such approaches involve the use of EBBR and DENT test methods to measure material properties that are influenced by the flow characteristics of asphalt binders. In Canada, asphalt binders used in paving contracts are evaluated based on their LTPG and grade loss, determined from the EBBR test, as well as CTOD determined by the DENT test. Although the EBBR and DENT tests offer improved specification grading, they require a significant amount of extracted and recovered binder and take longer to complete. Hence, in this section we focused on the development of simplified methods that use less material and take less time to complete while maintaining or improving their precision and accuracy. One potential alternative to the EBBR and DENT test protocols is the DSR, which is currently used by Superpave to determine the high and intermediate temperature properties of binders. The DSR can generate complex modulus and phase angle master curves by fitting the Christensen-Anderson model (CAM) to asphalt binders across various temperatures and frequencies.

The object of this section is to simplify test protocols through the correlation of different rheological parameters of EBBR and DENT tests with DSR parameters such as limiting phase angle temperatures, intermediate temperature performance grade, crossover frequency, crossover modulus, glassy modulus, and rheological index, as shown in Figure 43. In this study, asphalt binders from both Canada and USA were tested, covering a diverse range of binder types and grades. A secondary objective of this section is to study the effect of conditioning time on DSR parameters.

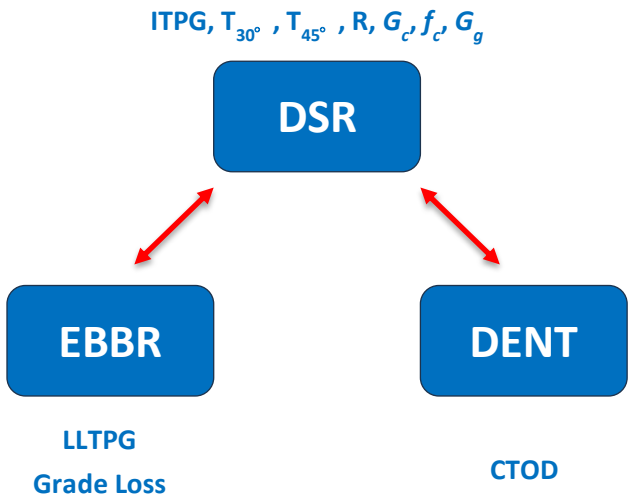

Figure 43. Schematic diagram of correlation analysis of results from different tests.

4.4.1 Correlation Analysis of Contract Samples

4.4.1.1 Correlation analysis of rheological indexes from DSR.

First, the relationship between ITPG and limiting phase angle temperature of recovered and tank samples were analyzed. The correlation results between ITPG and $T_{30°}$ and $T_{45°}$ are shown in Figure 44. It can be found that there is a strong linear correlation between ITPG and $T_{30°}$, with the R^2 above 0.7. In contrast, the correlation between ITPG and $T_{45°}$ is not so obvious since the R^2 varies around 0.5 and 0.6. This means that $T_{30°}$ can be potentially used as a candidate for evaluating the intermediate temperature fatigue resistance of asphalt binder. Moreover, it is interesting to find that long-term conditioning leads to significant improvement in the goodness of fitting between ITPG and limiting phase angle temperature. This means that the limiting phase angle temperature obtained when asphalt binder is in equilibrium state shows better correlation with intermediate temperature performance grade.

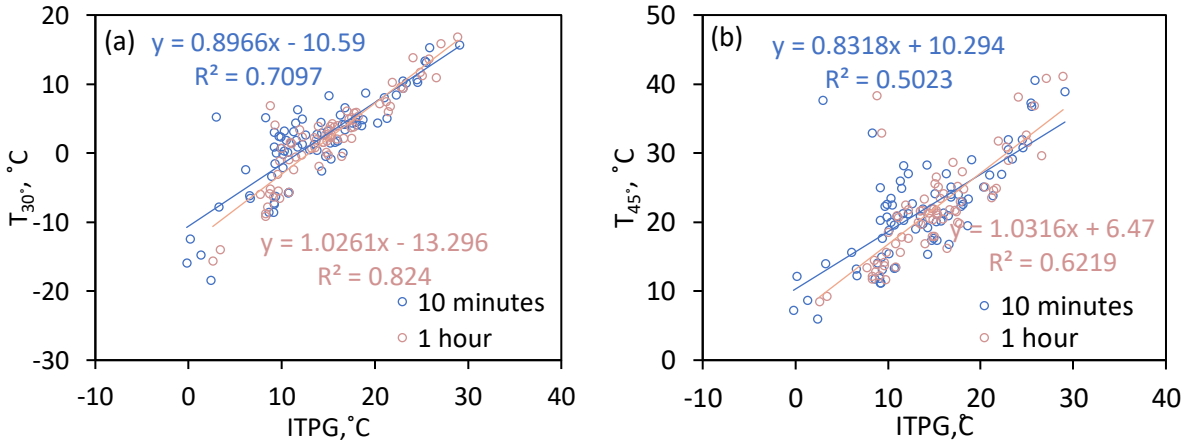

Figure 44. Correlation of ITPG and limiting phase angle temperatures ($T_{30°}$ and $T_{45°}$).

(a) 10 minutes conditioning; (b) 1 hour conditioning.

Second, the rheological results from master curve including glassy modulus G_g, crossover modulus G_c, crossover frequency f_c, and R value were correlated with limiting phase angle temperatures $T_{30°}$ and $T_{45°}$. The results are shown in Figure 45. It can be found the there is no obvious correlation between rheological indexes from master curve (R value, G_g, G_c) and limiting phase angle temperature ($T_{30°}$ and $T_{45°}$) regardless of cooling rate. However, a strong correlation exists between f_c and $T_{45°}$ and a weak correlation exists between f_c and $T_{30°}$. The main reason is that R value, G_g, G_c are all obtained from complex modulus master curve while f_c is derived from phase angle master curve and it refers to frequency where phase angle equals to 45°. f_c is similar to $T_{45°}$ in terms of physical meaning and calculation method. This is the main reason that there is a strong correlation between f_c and $T_{45°}$. Moreover, this results mean that limiting phase angle along may not be sufficient to provide rheological properties of asphalt binder especially complex modulus related properties.

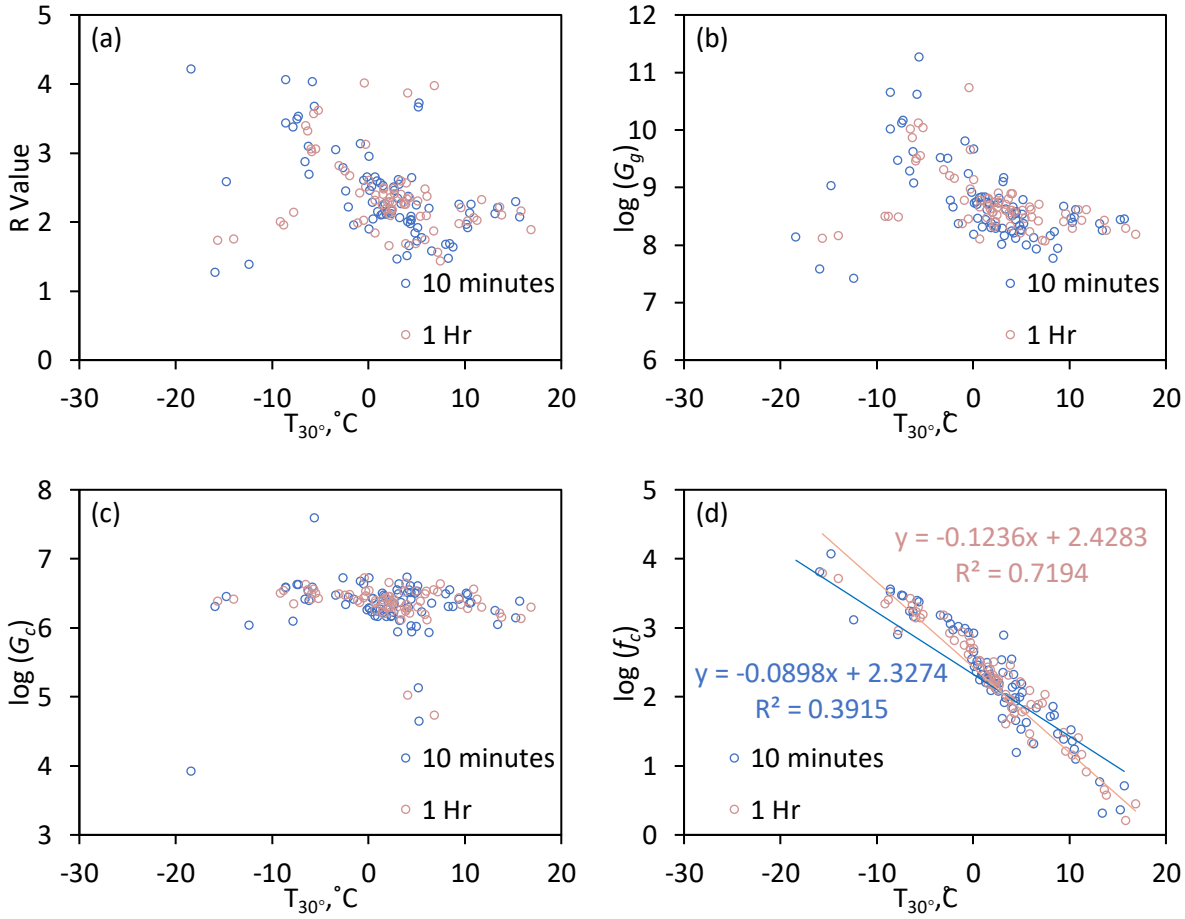

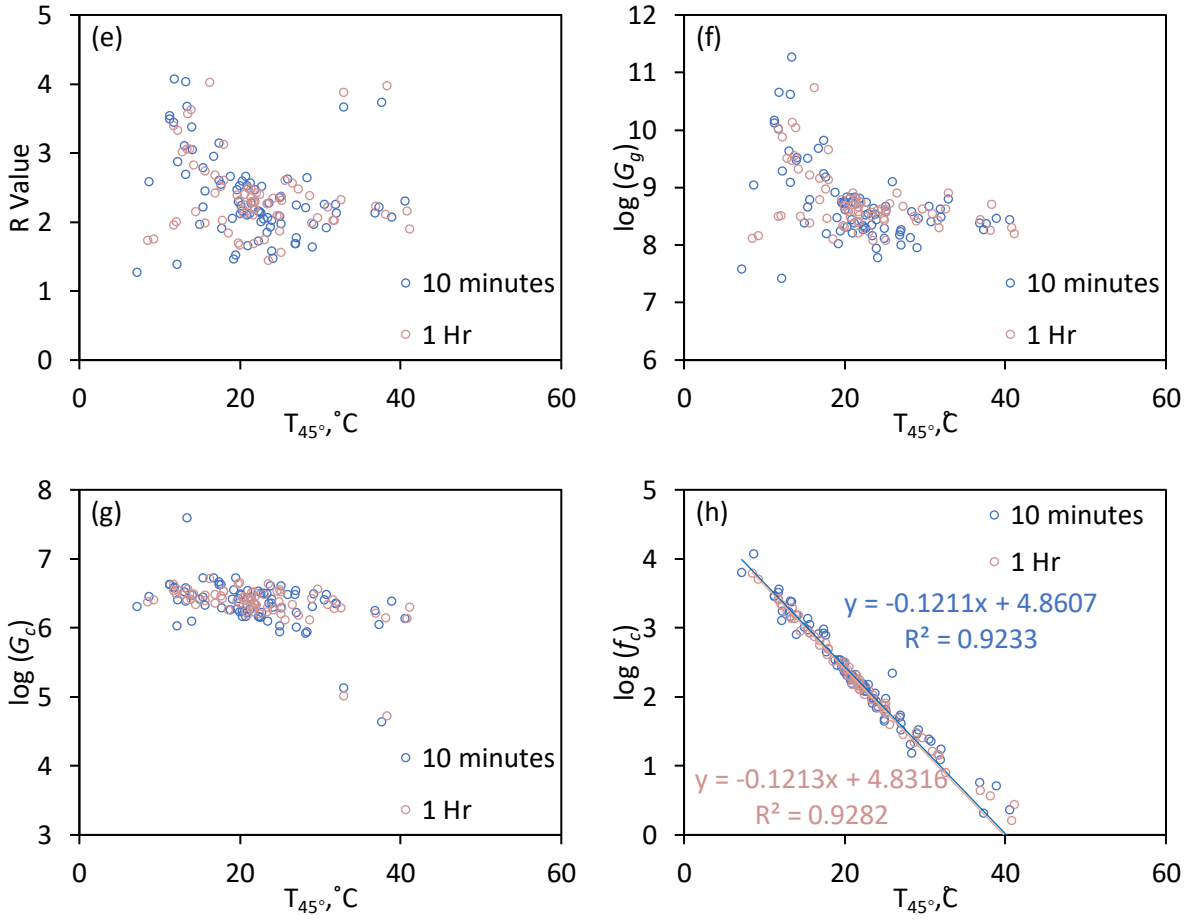

Figure 45. Correlation of limiting phase angle temperature and indicators from master curve.

(a) R value; (b) log (G_g); (c) log (G_c); (d) log (f_c).

4.4.1.2 Correlation analysis of rheological results from DSR and EBBR.

As shown in Figure 46, the LTPG and the grade loss results, as determined by the EBBR test, show a strong correlation with the limiting phase angle temperatures, namely $T_{30°}$ and $T_{45°}$, from DSR test. It can be found that the effect of conditioning time during DSR test on the fitting results is minor, given similar values of the slope of fitting line and the R^2 between the two different conditioning scenarios. It is noteworthy that the correlation between LTPG and $T_{30°}$ is stronger than that between LTPG and $T_{45°}$ since the R2 of linear fitting equation of LLTPG and $T_{30°}$, is higher than that of LLTPG and $T_{45°}$. The main reason for this could be found from studies in our lab and colleagues. Rowe's work demonstrated that an m-value limit of 0.3 in the BBR equates to a phase angle of 26.2° in the DSR, suggesting that a limiting phase angle of approximately 30° may serve as a more accurate and feasible criterion for binder evaluation (Rowe, 2014). Previous research in our lab indicated that the limit temperature for a 30° phase angle offers a more distinct differentiation between binders that perform well and those that do not, especially in terms of resistance to cracking (Ma et al., 2023). From the results above, it can be deduced that $T_{30°}$ can be used as

a viable alternative to conventional BBR testing methods. It should be noticed that grade loss, which serves as an estimate of thermo-reversible aging of asphalt, still needs to be estimated since there is no correlation between low temperature grade loss and limiting phase angle temperature. The corresponding results are provided in Figure 46. It can be observed that the R^2 values in two different conditioning scenarios are all lower than 0.25.

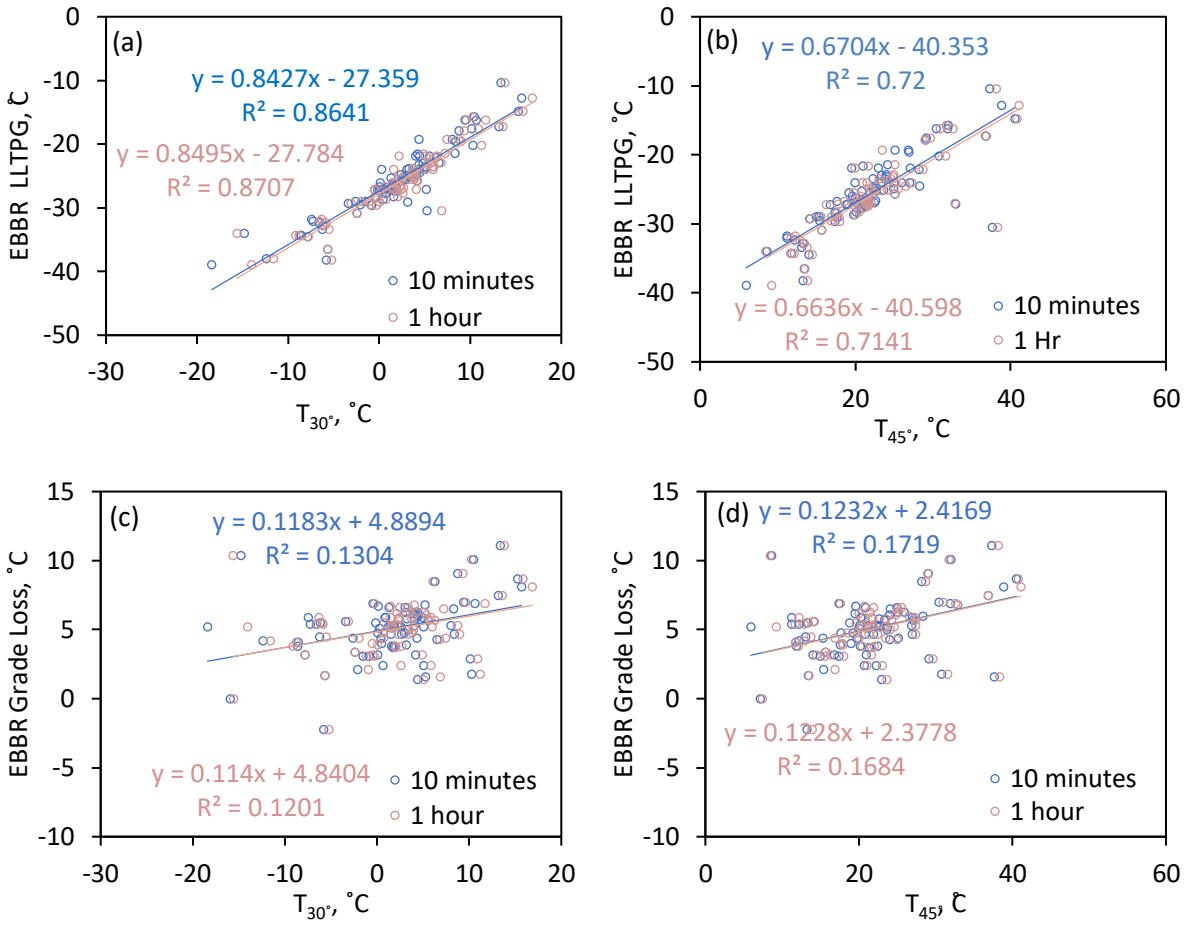

Figure 46. Correlation of LLTPG and grade loss with limiting phase angle temperatures (T_{30° and T_{45°).

(a) 10 minutes conditioning; (b) 1 hour conditioning; (c) 10 minutes conditioning; (d) 1 hour conditioning.

4.4.1.3 Correlation analysis of rheological results from DSR and DENT.

The DENT test was utilized to evaluate the ductile properties of asphalt binders. This method is designed to determine asphalt binder's resilience against fatigue thermal cracking and ductility failure under low-temperature conditions. The CTOD value, derived from the DENT test, is defined as the ratio of the essential work of fracture to the net section stress or yield stress, calculated based on the 5mm ligament length of the DENT mold. The CTOD metric serves as an indicator of the material's strain tolerance in its ductile state under significant confinement conditions, akin to those experienced during ductile fracture

in asphalt binders. Furthermore, the CTOD parameter is rigorously calibrated and utilized to evaluate the capability of asphalt mixtures and binders to withstand fatigue cracking and thermal fatigue cracking at low temperatures. This parameter is instrumental in establishing a correlation between material failure under conditions of high compression amongst coarse aggregate particles, enhancing our understanding of asphalt binder behavior under stress (Hesp et al., 2009).

The correlation between CTOD and various indicators derived from DSR analyses, including limiting phase angle temperatures (T_{30° and T_{45°) and parameters from the complex modulus and phase angle master curves (R Value, G_g, G_c, and f_c), is elucidated and presented in Figure 47. Specifically, Figure 47 (a) and (b) show the relationship between CTOD and the limiting phase angle temperatures, T_{30° and T_{45°, respectively. The correlations observed indicate that increases in T_{30° and T_{45° are associated with the decrease in CTOD values. It is well known that elevated limiting phase angle temperatures reflect an increased gelled fraction which is likely to diminish cracking resistance of asphalt binder. This is further validated by the decrease in CTOD value that indicates the reduced tolerance of cracking. Notably, the functional relationships between CTOD and the temperatures T_{30° and T_{45° exhibit distinct characteristics: CTOD demonstrates a linear negative correlation with T_{30°, whereas its correlation with T_{45°, although also negative, is logarithmic in nature. Subsequently, the CTOD value was correlated with master curve parameters as shown in Figure 47 (c) and (f). Regarding the relationship between the CTOD and the master curve parameters, the analysis reveals no significant correlation between CTOD and parameters such as R Value, G_g, and G_c. Nonetheless, there is a pronounced exponential relationship identified between CTOD and the f_c parameter.

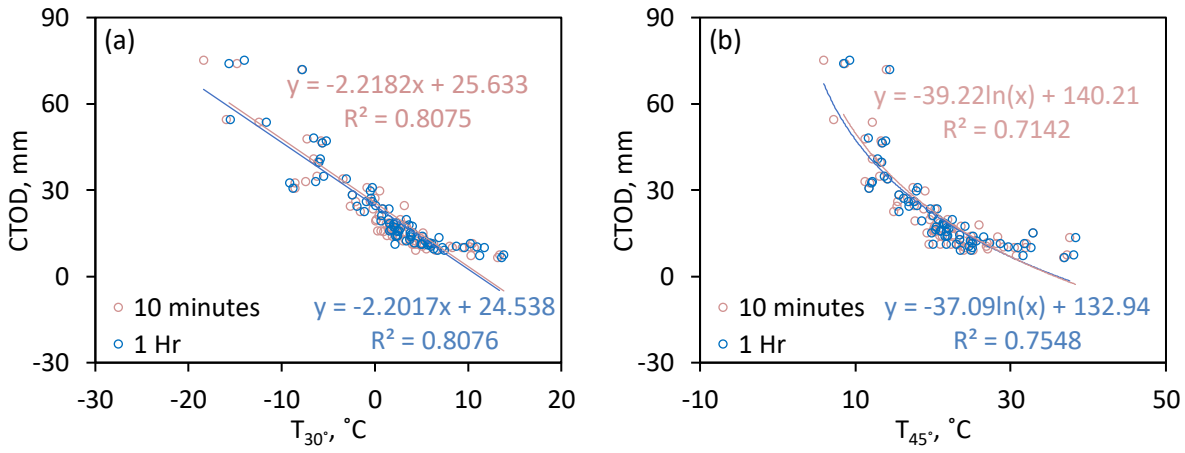

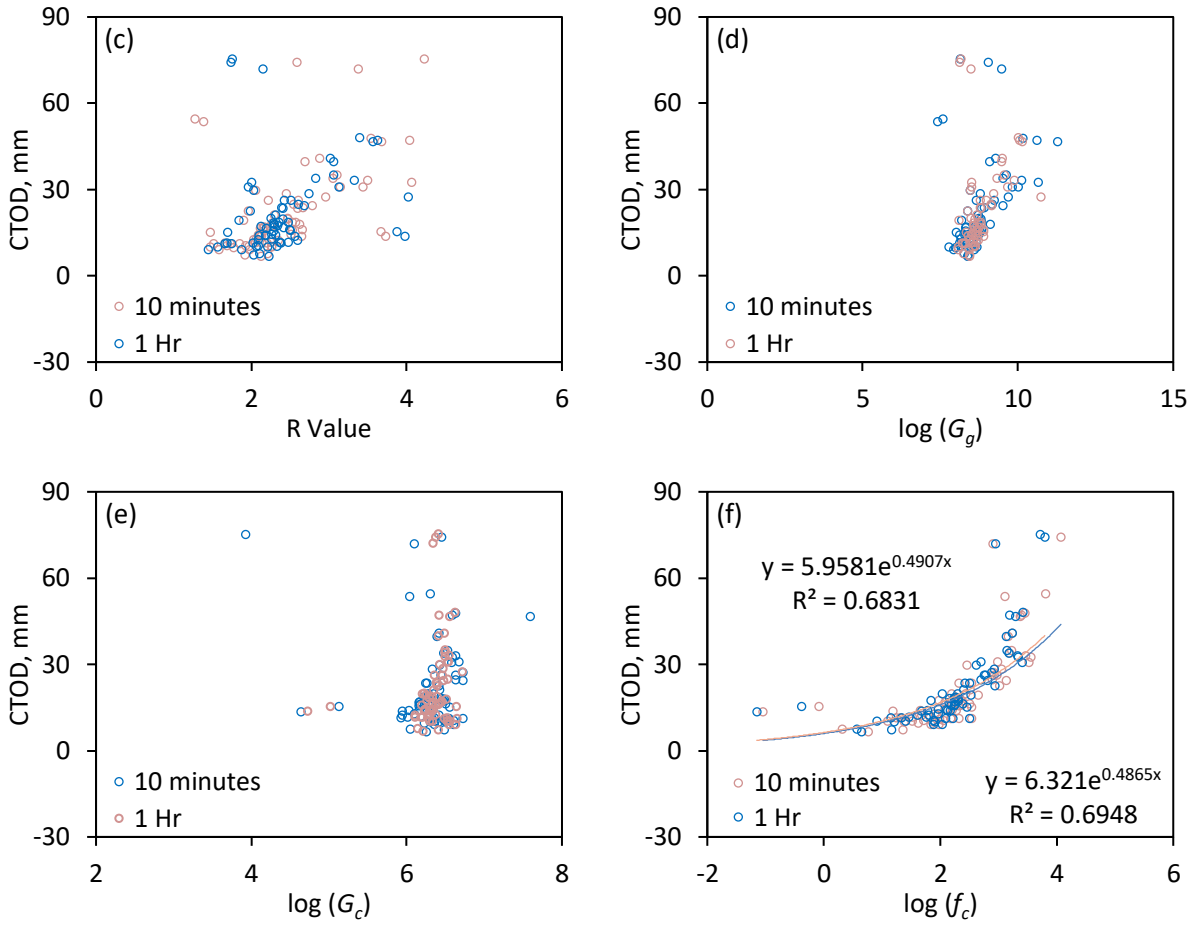

Figure 47. Correlation of CTOD from DENT test with indicators from DSR test.

(a) T_{30°; (b) T_{45°; (c) R Value; (d) log (G_g); (e) log (G_c); (f) log (f_c).

4.4.2 Correlation analysis of pavement trial samples.

The objective of this section was to find reliable and repeatable rheological indicators to rank low temperature performance of different polymer-modified binders including HiMA based on the field performance of a 13-year-old trial near Timmins in northern Ontario, Canada. Also, an optimum aging condition is to be selected to predict performance of polymer-modified asphalt based on laboratory tests. To fulfill these objectives, six modified binders and a straight-run Cold Lake 300/400 penetration grade, used to construct this trial in 2007, were aged using the PAV for various durations (0, 20, 40 and 100 hours at 2.1 MPa and 100 °C). All samples were tested using a dynamic shear rheometer (DSR) to obtain rheological indicators. Finally, the accuracy of each performance indicator for modified asphalt under different aging conditions is documented and discussed.

4.4.2.1 Field performance analysis.

The PCI is a function of the distress manifestation index (DMI) and the international roughness index (IRI). A total of 13 types of distresses are considered in determining the DMI. They are wheel track cracking,

wheel track alligator cracking, raveling, edge cracking, edge alligator cracking, rutting, centerline cracking, centerline alligator cracking, distortions, Midlane cracking, Midlane alligator cracking, flushing and transverse cracking. The detailed calculation process can be found elsewhere (Ma et al., 2021). The PCI value over the years of service for the selected trial sections (655-9 to 655-15) were linearly fitted as shown in Figure 37. The critical value of the PCI for this trial is set as 50, the point at which the pavement is considered to reach the end of its life. The results for the projected life spans determined in this manner are shown in Table 11.

4.4.2.2 Analysis of laboratory test results.

(1) Black space diagram

The Black space diagram provides a plot of complex modulus |G*| on a logarithmic scale versus phase angle δ, without any mathematical shifting based on time-temperature superposition (TTS). It can be used to check the applicability of TTS prior to the construction of rheological master curves. The results in this study show that very limited information can be obtained from the Black space diagram of various modified asphalt binders to explain their field performance. Hence, only the Black space diagrams for a selected few binders are provided in Figure 48 for illustration.

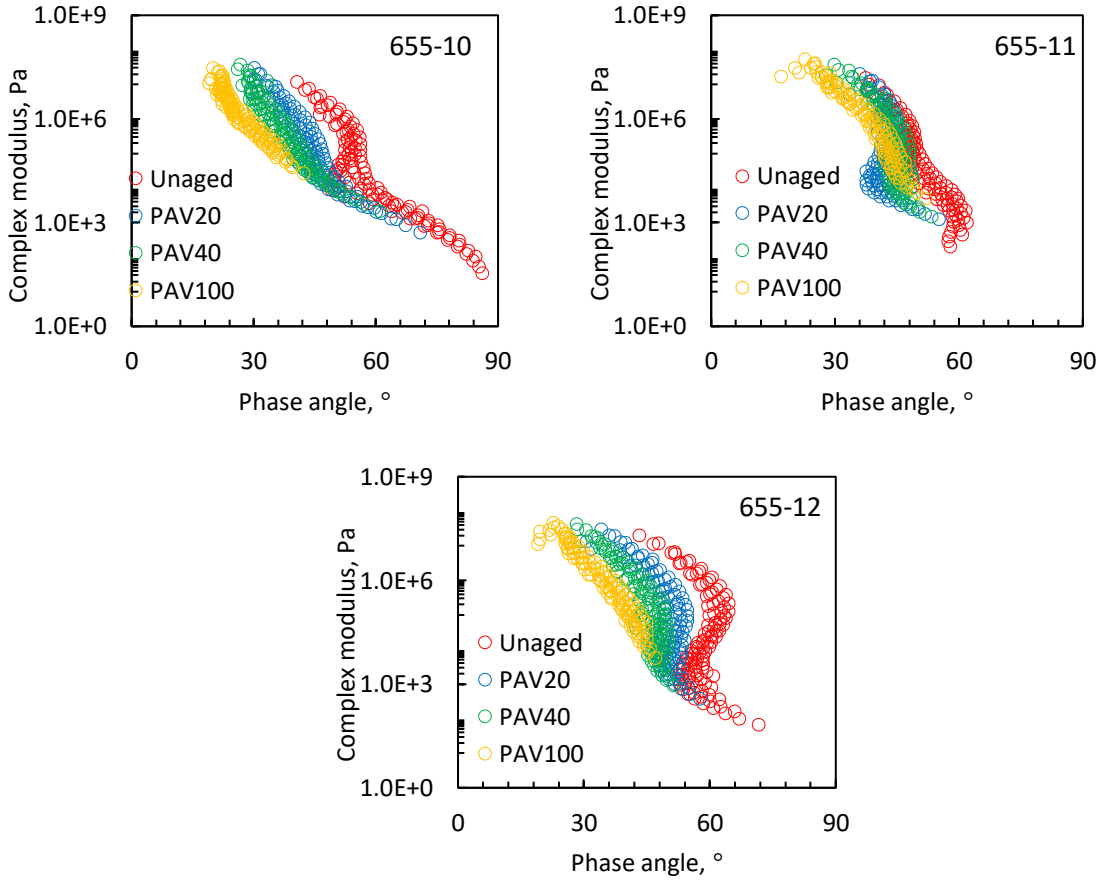

Figure 48. Black space diagrams for 655-10, 655-11 and 655-12 polymer-modified binders.

(2) Phase angle master curves

The phase angle master curves for the complete data sets of all binders are shown in Figure 49. It is noticeable that these curves are not smooth (thermorheologically complex) and hence time-temperature superposition is not applicable. As mentioned, the tangent of the phase angle reflects the ratio of the viscous to elastic component of the complex modulus. Phase angle master curves provide more information over a wider frequency domain than the measurement over a narrower range. For all binders, phase angle in the frequency domain decreased to various extents with aging. Hence, materials become more solid-like during the aging process as the viscous component decreases (Ding et al., 2020). The age hardening in asphalt is also detrimental to its stress relaxation ability which is closely related to transverse cracking distress in field. The residual stress in aged asphalt binder is higher at given relaxation time compared with unaged one. In other words, it takes longer time to relax the stress in asphalt as a result of aging effect (Evans et al., 2011; Jing et al., 2020; Nivitha et al., 2022; Wang et al., 2017). Compared with the master curve for the 655-15 control, the five polymer-modified binders exhibited more complex behavior. The phase angle plateaus appear at low frequencies in 655-13 and 655-14 binders. These plateaus indicate the existence of a crosslinked SBS network within the matrix (i.e., the material behaves like a gel with very high viscosity and low stiffness). However, the plateau gradually disappears with progressive aging in these two binders with different SBS contents (7 % and 3.5 % for 655-13 and 655-14). The main reason for the disappearance of the plateau is that the SBS polymer partially degrades (Lu and Isacsson, 1998). Quantitative evaluation of the percentage of degraded SBS in these two SBS modified asphalts and its dependency on SBS content is still challenging based on phase angle master curve. Experiments with a high vinyl binder in the Highway 655 Phase I trial has shown that it retained its gel structure, even after extensive aging in service (Ding et al., 2020). The phase angle master curves of 655-10, 655-11 and 655-12 exhibit an S-shape over the frequency domain, which gradually becomes flat after aging. The phase angle for the 655-10 binder, containing 1 % PPA and 2 % SBS, decreases continuously with aging in the same way as the control binder. The same trend was observed for the 655-12 binder with 2.5 % RET, and the 655-14 binder containing 3.5 % SBS. This phenomenon can be attributed to the relatively low content of polymer. The aging process for these three binders is therefore mainly controlled by aging of the base asphalt. With respect to 655-11 containing 7 % SB and 655-13 containing 7 % SBS, phase angles remained relatively unchanged after 20 hours of PAV aging. It can be deduced that the degraded polymer segments within the asphalt matrix compensate or hinder further age hardening of the base asphalt, likely due to the formation of a highly viscous or gelled surface layer in the PAV (Erskine et al., 2012). However, it remains challenging to establish the relationship between phase angle master curve and changes in PCI.

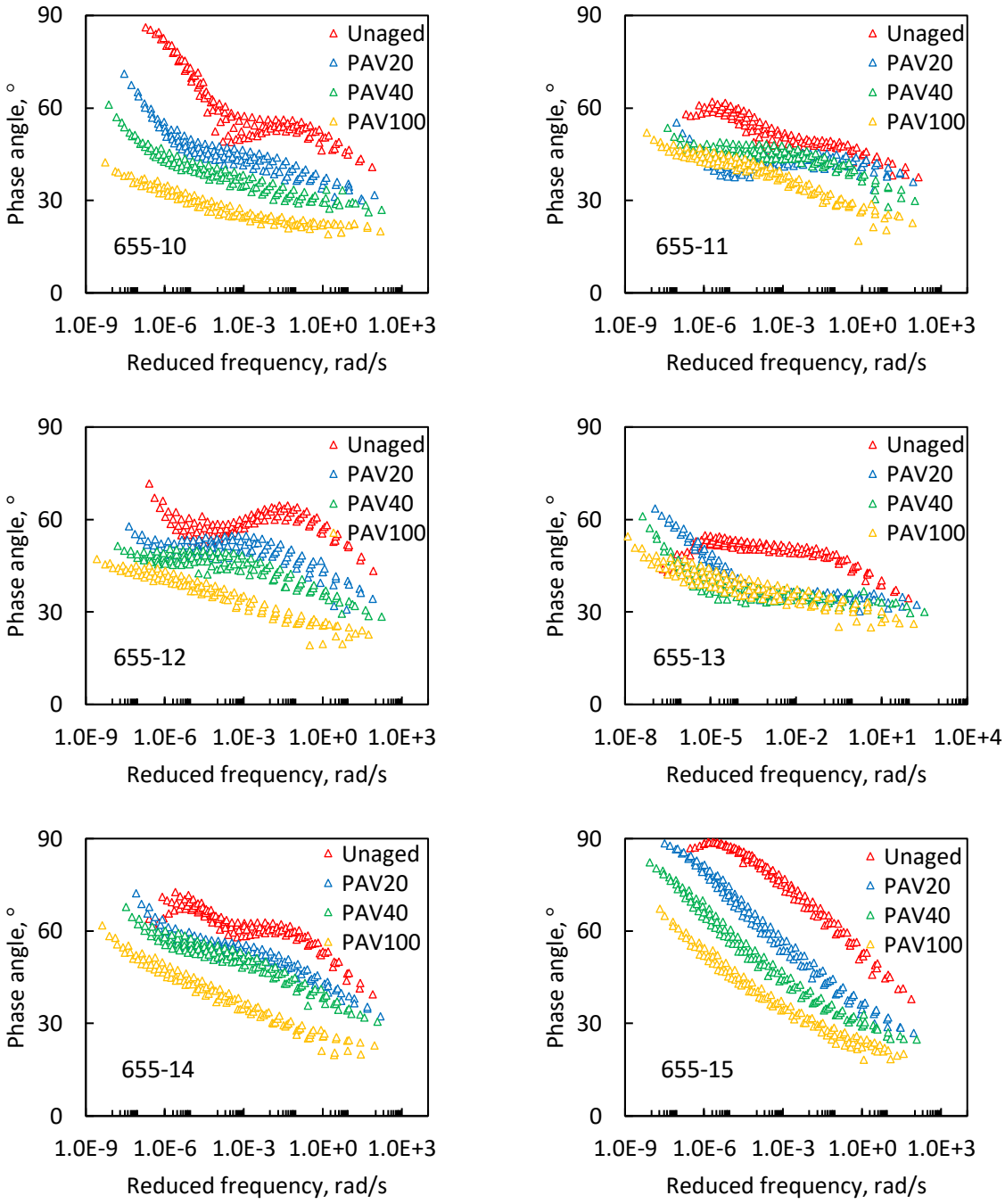

Figure 49. Phase angle master curves in the frequency domain for investigated asphalt binders.

Limiting phase angle temperatures were determined in an attempt to match the performance ranking. The phase angle at 10 rad/s at each temperature was picked from the frequency sweep data that were used in the construction of the rheological master curves. The change of phase angle at 10 rad/s versus temperature is shown in Figure 50. Polynomial fitting was performed for each tested binder and limiting

temperatures where the phase angles reached 30° and 45°, $T_{30°}$ and $T_{45°}$, were determined by interpolation. The results of this exercise are given in

Table *13* and Figure 51.

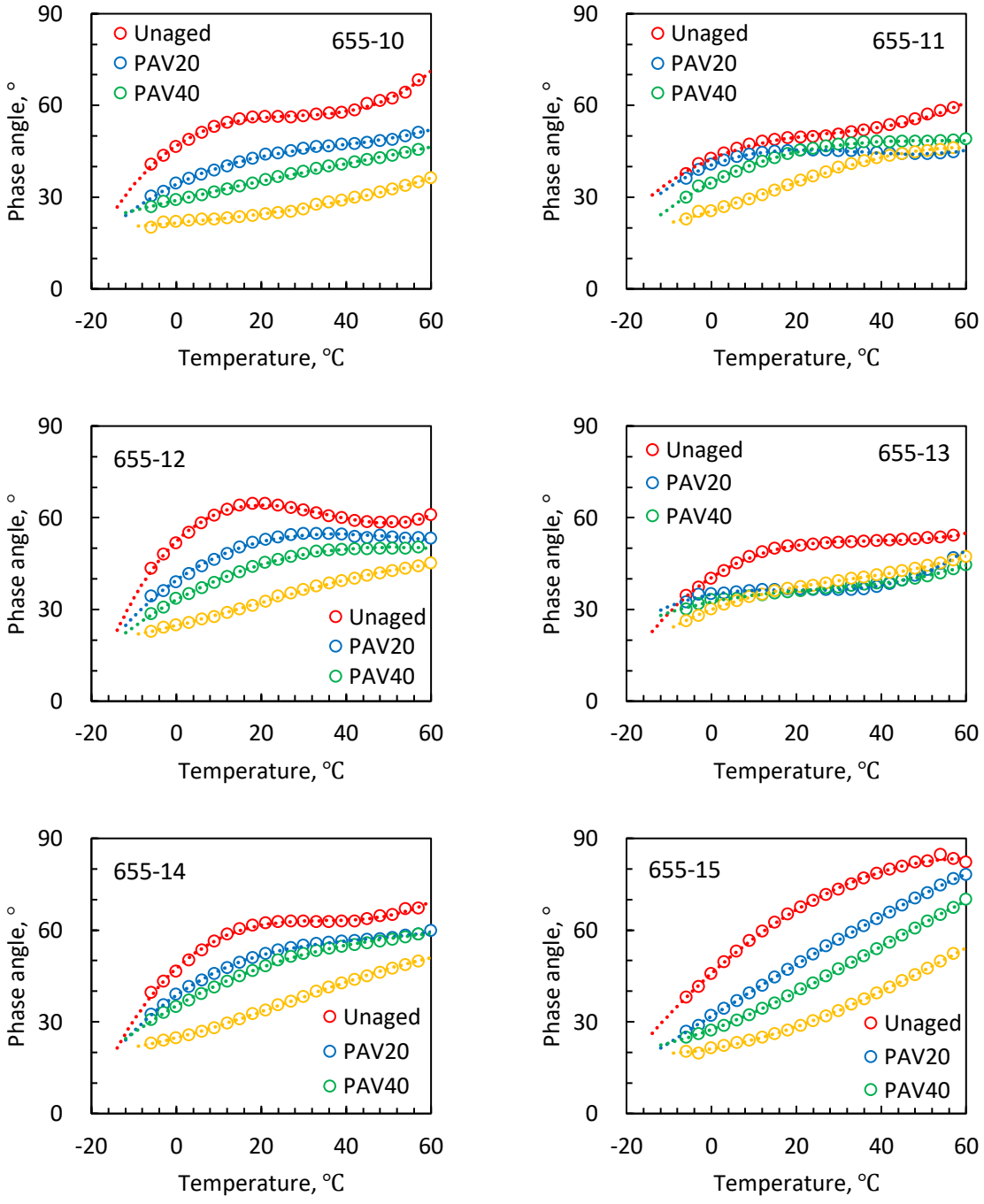

Figure 50. Plot of phase angle value at 10 rad/s vs temperature for investigated asphalt binders.

Table 13. Limiting phase angle temperatures.

Binder	$T_{30°}$, °C	$T_{45°}$, °C	$\Delta T_{c\delta} = T_{45°} - T_{30°}$, °C
655-9 (straight Cold Lake)			
Unaged	-21.0	-7.3	13.7
PAV 20	-8.4	7.4	15.9
PAV 40	-3.4	18.3	21.7
PAV 100	17.7	44.1	26.4
655-10 (1 % PPA + 2 % SBS)			
Unaged	-12.2	-1.8	10.4
PAV 20	-5.6	31.0	36.6
PAV 40	2.9	54.2	51.3
PAV 100	44.7	79.4	34.7
655-11 (7 % SB diblock)			
Unaged	-14.5	4.8	19.3
PAV 20	-13.1	13.9	27.0
PAV 40	-6.0	21.2	27.2
PAV 100	9.8	46.3	36.5
655-12 (2.5 % RET + PPA)			
Unaged	-16.9	-8.8	8.1
PAV 20	-12.8	4.4	17.2
PAV 40	-3.9	20.8	24.7
PAV 100	14.2	62.9	48.7
655-13 (7 % SBS)			
Unaged	-9.2	5.9	15.1
PAV 20	-11.7	57.0	68.7
PAV 40	-7.5	61.3	68.8
PAV 100	0.1	55.6	55.5
655-14 (3.5 % SBS)			
Unaged	-10.3	-1.8	8.5
PAV 20	-7.7	7.5	15.2

PAV 40	-6.2	14.7	20.9
PAV 100	12.9	44.7	31.8
655-15 (Control + REOB)			
Unaged	-11.5	-0.7	10.8
PAV 20	-2.1	15.5	17.6
PAV 40	4.8	27.3	22.5
PAV 100	23.1	46.7	23.6

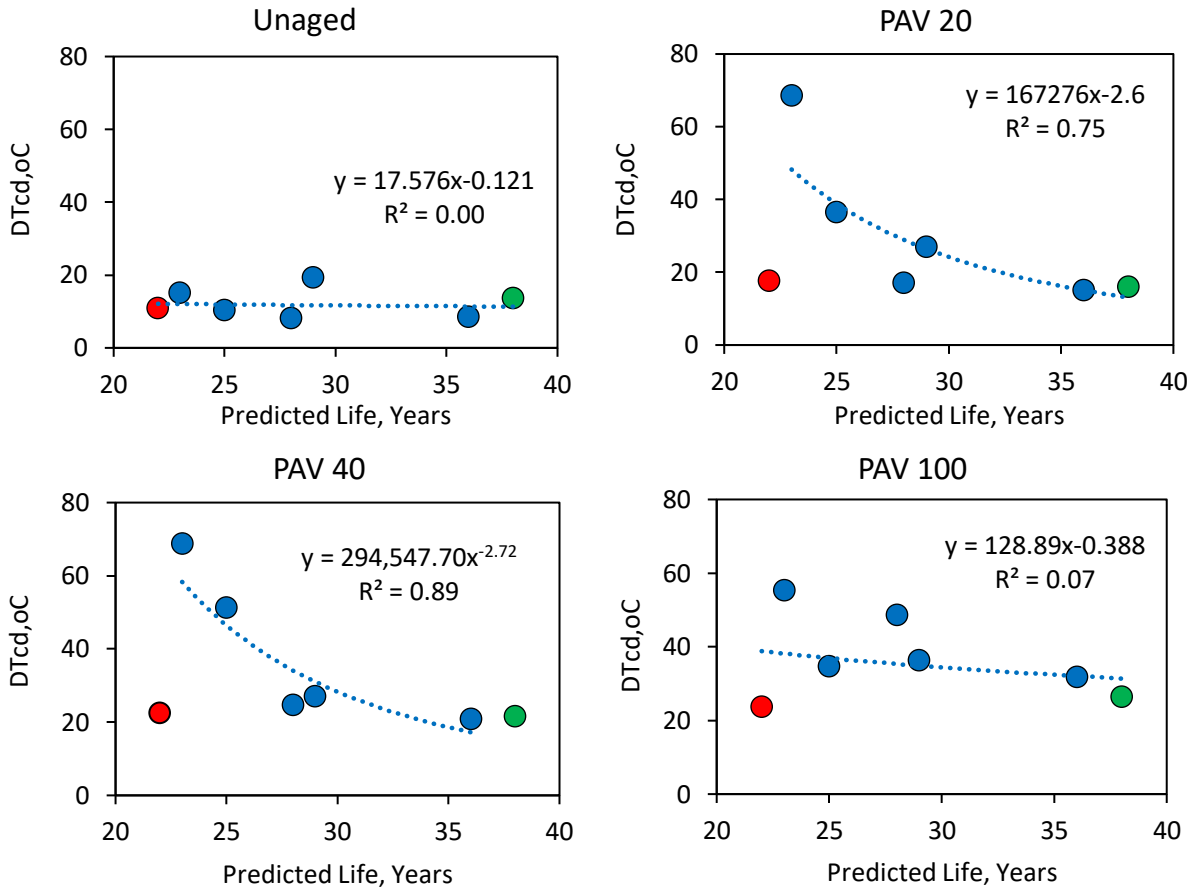

Figure 51. Correlation analysis between $\Delta T_{c\delta}$ and projected life span to PCI of 50.

● 655-9, ● 655-10 to 655-14, ● 655-15

An empirical index $\Delta T_{c\delta}$ can be derived based on the difference in limiting 30° and 45° phase angle temperatures ($\Delta T_{c\delta}=T_{45°}-T_{30°}$). The $\Delta T_{c\delta}$ relates to the slope of the phase angle master curve over a temperature range that is of importance for thermal cracking around the freeze-thaw domain. Baskin (Baskin, 1935) of Imperial Oil in Toronto, Ontario, reported as early as 1935 that "… the fact that most

damage occurs during the period when frost is coming out of the ground would lead one to suspect that the slow and gradual strains caused by the movement of subsoil may well be the most potent cause of cracking. All this would reduce our problem largely to pliability of paving mixtures at 32ºF (0°C)" (Soleimani et al., 2009). The $\Delta T_{c\delta}$ index reflects the degree of solid-like behavior (slope of the phase angle master curve), related to the ability of the binder to relax stress at service temperatures. Given that the main distress type for this trial is thermal stress induced cracking, it is expected that this new empirical indicator can differentiate the field performance of different modified asphalts. It can be seen as a modern day equivalent to the penetration index, first proposed by Pfeiffer and Van Doormaal in 1936 (Pfeiffer and Van Doormaal, 1936).

To verify the assumption made that properties around the freeze-thaw domain are of paramount importance, a correlation analysis was performed between $\Delta T_{c\delta}$ and projected life span from the ARAN PCI data (Table 8). The results shown in Figure 51 provide reassuring findings. It is obvious that for appropriately aged polymer-modified binders, pavement life span is highly correlated with $\Delta T_{c\delta}$. However, when binders were aged excessively after 100 hours of conditioning in the PAV, the parameter fails to properly rank field performance and this is likely because the studied type of thermal fatigue cracking distress is cumulative. The $T_{30°}$ and $T_{45°}$ limits for binders in each section aged for 20 hours and 40 hours are shown in Figure 52. It further shows that $\Delta T_{c\delta}$ can rank the performance of asphalt pavement in service if the asphalt binder is aged to a reasonable degree prior to rheological testing. It should be noted that this conclusion is for polymer-modified asphalts of similar stiffness used in a continental climate where the main distress is cold temperature cracking.

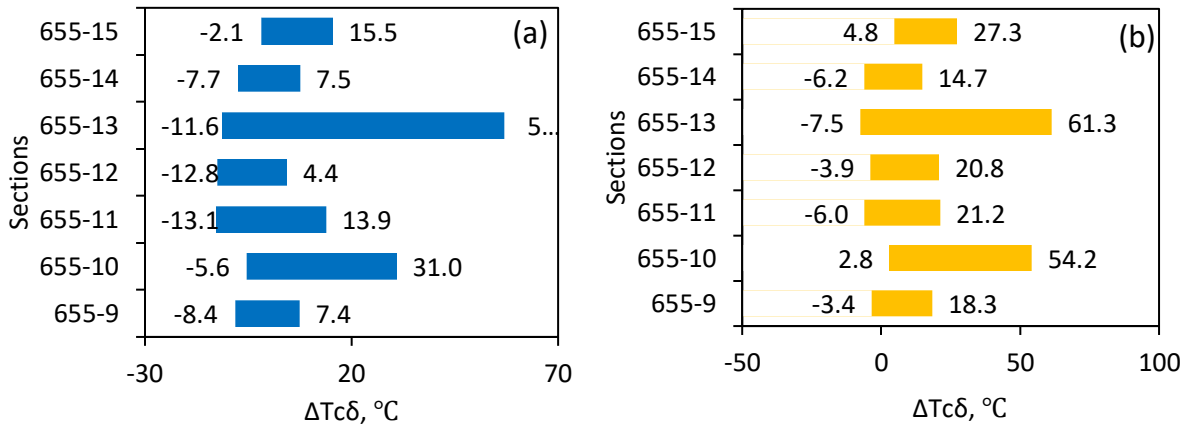

Figure 52.$T_{30°}$ and $T_{45°}$ results for the tested asphalt binders.

(a) PAV aged for 20 hours; (b) PAV aged for 40 hours. The value on the left of each bar is $T_{30°}$ below which crack initiation predominates. The value on the right is $T_{45°}$ below which cracks propagate. Above $T_{45°}$ micro cracks might heal to some degree depending on a number of factors.

Note that the data point for 655-15 was excluded for the correlation in Figure 52 as it was the REOB-tainted control binder, and hence suffered from both premature oxidative, thermo-reversible and likely exudative aging being a spent lubricant full of paraffin, peroxides and degraded polymer additives. It does

relatively well in the DSR frequency sweep protocol for $\Delta T_{c\delta}$ (binder tested after short periods of conditioning in between steel plates) in comparison to the EBBR (binder conditioned for 72 hours in an ethanol bath), as the latter likely penalizes binders through exudative hardening from leaching lighter oils in the ethanol bath (Ding et al., 2021; Rubab et al., 2011). However,

Table *13* shows that 655-15 does have the highest T_{30° after 20 and 40 hours of PAV conditioning, and because of this higher aging tendency has likely suffered more from conventional low temperature cracking damage in comparison to other binders in the trial that suffered from thermal fatigue.

The above discussion indicates that there is a need for limits on both rheological properties that determine the position as well as the shape of the phase angle master curve. Hard pitch-like materials would do well in a $\Delta T_{c\delta}$ ranking with a small R-value, but due to their excessive brittleness would fail prematurely from conventional transverse cold temperature cracking. In contrast, binders such as those used in sections 655-10 to 655-13 are gelled with polymers and acid and might do well in early life but obviously degrade from the effects of long-term thermal cycling (fatigue), owing to their gel-type structure and associated thermal stress retention.

(3) Relaxation spectra

From the above discussion it is understood that the manner in which binder stresses relax has a major effect on the fatigue life of the pavement sections. To further understand the difference among the binders, stress relaxation data was analyzed. Figure 53 shows the stress relaxation data obtained for different binders after 20 hours of PAV aging at 0 °C. It can be seen that the stress relaxation is fastest for the 655-9 binder and slowest for 655-10. If the binders are grouped based on their response, it can be observed that the stress relaxation is relatively fast for 655-9, 655-15 and 655-14 binders. The next group consists of 655-11 and 655-12. The third group that takes the longest time to relax is comprised of binders 655-10 and 655-13. If the thermal fatigue life of these binders is compared, 655-9 and 655-14 have a predicted lifespan of about 36-38 years while 655-10 and 655-13 will last about 23-25 years. The same cannot be said for all binders. For 655-15, the stress relaxation is comparable with 655-9 and 655-14 binders, yet the predicted lifespan is only about 22 years. This is likely due to the high T_{30° for this binder and its relatively high oxidation susceptibility. If the characteristics of the binders are compared for the three groups, as discussed above based on the relaxation behavior, the stress relaxation response of a 3.5 % SBS modified binder is identical to that of the control sample tainted with REOB (655-15) or a 300/400 pen sample with 0.3 % RET (655-9). To probe the stress relaxation in further detail, complete relaxation spectra were determined. The reason for their tendency to suffer from cold temperature cracking to different degrees is in large part due to their variation in relaxation behavior over a wider temperature range.

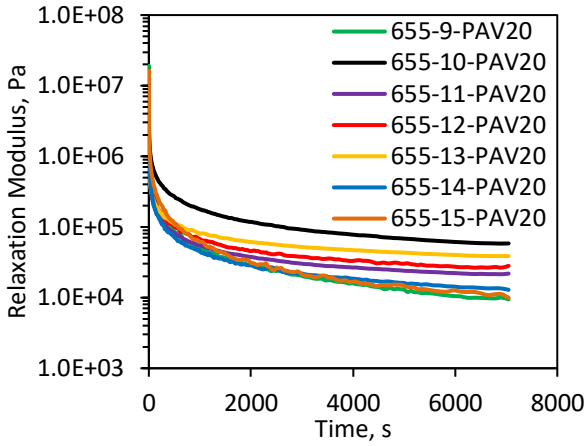

Figure 53. Relaxation modulus for binders after 20 hours of PAV aging.

The relaxation spectrum provides a more complete insight on how the stresses relax. Studies have shown that stress relaxation behavior of a polymer system is highly sensitive to its network structure (Doi and Edwards, 1986). This analysis is expected to provide additional insights into the thermal fatigue cracking response. This technique has been gaining attention due to its ability to correlate with network structure, especially in the case of polymer-modified bitumen (Baumgaertel and Winter, 1989; Bhattacharjee et al., 2012; Huang and Baird, 2002; Liu et al., 2018; Nivitha et al., 2022).

The relaxation spectra for binders aged for 20 hours in the PAV are shown in Figure 54 (a). It can be seen here that for all binders, a prominent peak is seen at about 0.1 s. The exact position of the peak is seen to vary depending on the type of binder. Also, additional peaks corresponding to longer relaxation times are observed on the shoulder of the prominent peak. To compare the relaxation response of different types of binder, the relaxation spectra are normalized in Figure 54 (b). Here, 655-13 exhibits a distinct behavior. It should be noted that it is highly modified with 7 % SBS, and thus exhibits a higher h(τ) corresponding to longer relaxation times. It is also interesting to note that 655-11 also contains 7 % polymer but of the SB type. For this sample, the h(τ) corresponding to longer relaxation times is not as prominent. Such differences in response of SB and SBS modified bitumen have been evaluated by Nivitha et al. (Nivitha et al., 2022). It was shown that SB type modifiers relax stresses faster compared to SBS, as both ends of the polymer are constrained in the case of SBS while one end is free in SB.

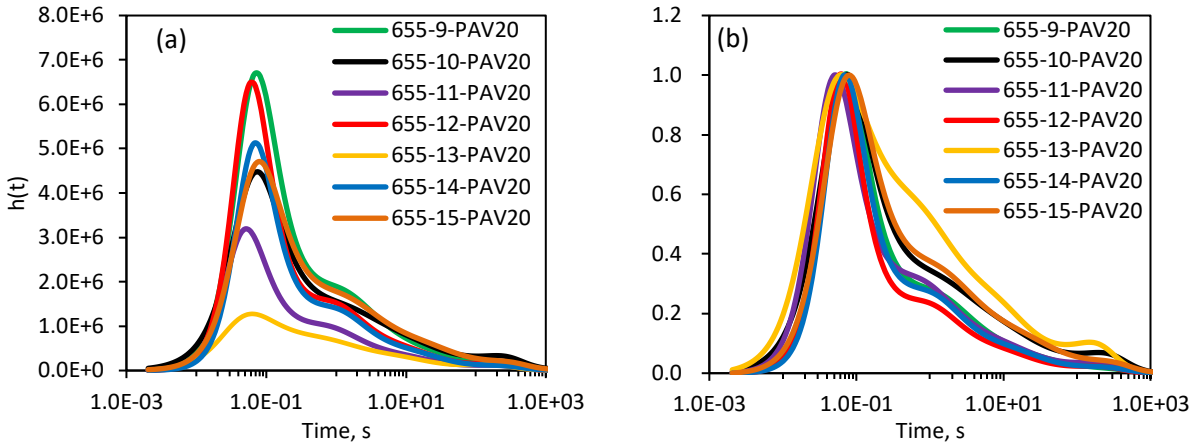

Figure 54. Relaxation spectrum for PAV20 binders

(a) Relaxation spectra; (b) Relaxation spectra normalized to maximum peak height.

To probe the relaxation response in yet more detail and to quantify the characteristics of the individual modes of relaxation, individual peaks were deconvoluted using the Origin software (Origin Lab, 2022). For deconvolution, the number of peaks and their position were identified based on the second derivative of the relaxation curve. The peaks were assumed to be Gaussian shaped. While optimizing the fitting parameters to converge the best fit, peak position and baseline were maintained as constrains. Sample deconvolutions for 655-9 and 655-13 are shown in Figure 55. From the deconvoluted peaks, characteristics such as peak position, height, full width at half maximum (FWHM) and area are computed as shown in Table 14. Full width at half maximum (FWHM) is the difference between the two values of the independent variable at which the dependent variable is equal to half of its maximum value in a normal distribution. In other words, it is the width of a spectrum curve measured between those points on the x-axis which are half the maximum amplitude.

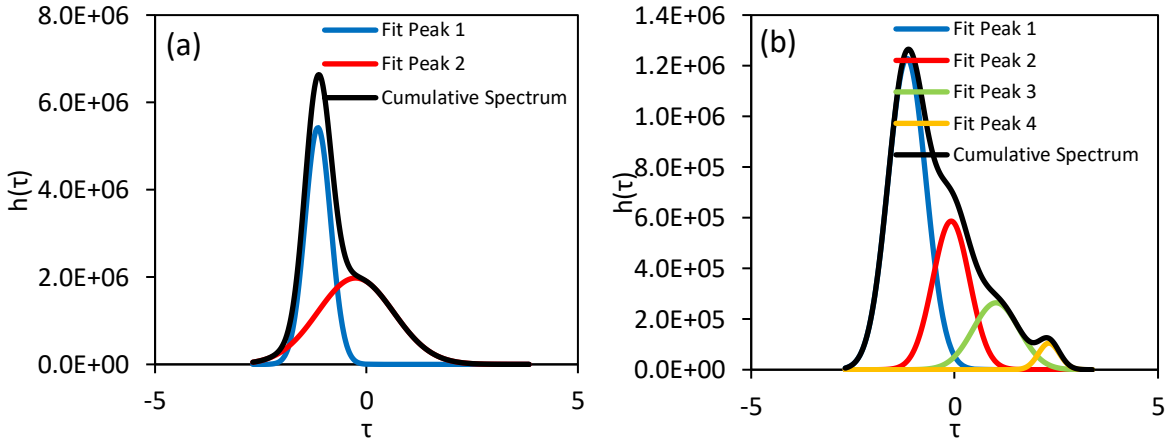

Figure 55. Deconvolution of peaks for selected samples after 20 hours of PAV aging.

(a) Binder 655-9; (b) Binder 655-13.

Table 14. Parameters corresponding to relaxation spectrum (20 hour PAV aged).

Sample	Parameter	655-9	655-10	655-11	655-12	655-13	655-14	655-15
Peak 1	Height	5.42	4.11	2.90	5.93	1.23	4.67	4.21
	Position	0.071	0.079	0.050	0.058	0.068	0.068	0.079
	FWHM	0.72	1.00	0.83	0.73	1.00	0.76	0.93
	Area	4.13	4.36	2.55	4.62	1.44	3.77	4.17
Peak 2	Height	1.98	1.37	1.00	1.48	0.59	1.33	1.58
	Position	0.55	1.72	1.04	1.29	0.82	1.35	1.72
	FWHM	2.11	1.59	1.81	1.81	1.07	1.74	1.81
	Area	4.42	2.32	1.93	2.85	0.67	2.45	3.04
Peak 3	Height					0.26		
	Position					10.46		
	FWHM					1.33		
	Area					0.38		
Peak 4	Height		0.26	0.16		0.11		0.15
	Position		225	243		208		325
	FWHM		1.41	1.17		0.61		1.18
	Area		0.38	0.19		0.07		0.18
Total area		8.58	7.02	4.30	7.39	2.50	6.20	7.34

Note: Height and areas are scaled by a factor of 10^6 in the above table.

Among the different parameters considered, the FWHM of the first peak corresponded well with the projected life span of the binders as given in Table 11. The FWHM of the first peak is in the range of 0.716 to 1.000. Based on the values provided in Table 14, samples can be grouped into three categories: binders 655-9, 655-12 and 655-14 form the first group with FWHM ranging from 0.716 to 0.760; 655-11 forms the second with a FWHM of 0.827; binders 655-10, 655-13 and 655-15 form the third with FWHM in the range of 0.930 to 1.000. This grouping can be seen to closely match with the thermal fatigue lives given in Table 2. Also, it should be noted here that this order is seen to differ from the groups mentioned based on the relaxation modulus shown in Figure 53. Hence, the parameters calculated from the complete relaxation spectrum are seen to explain material behavior somewhat better in comparison with observations on the relaxation modulus variation with time.

4.4.3 Study Limitations

The pavement trial is in northeastern Ontario where temperatures regularly reach below −40 °C. The findings likely also apply to more southerly continental zones that are characterized by hot summers and cold winters. However, poor aggregate designs and higher traffic may confound studies in such regions as PCI is a composite index that includes rutting and cracking. Rutting in the trial sections was not a factor, ranging from a low of around 5 mm (655-11, 655-12 and 655-14) to a high of around 10 mm (655-10). Some of this might have been post-construction compaction rather than rutting but in-place densities were not measured. The PAV aging protocol is inaccurate and provides only a snapshot of the binder at a single age. Hence, as cracking is a cumulative process, the correlation between rheological properties and distress manifestation cannot be expected to be perfect. Aging varies with depth from the surface of the pavement. Hence, it is unclear how the PAV protocol is able to address this, and likely the correlations will vary to some degree with the air voids content in the pavement as constructed. PCI data were extrapolated significantly into the future. While the R2 correlation coefficients were all above 0.95 and most were close to perfect, predicted lifespans are approximate as it is possible PCI may not follow a straight-line trajectory in old age. There were minor differences between northbound and southbound lanes and few obvious PCI outliers were excluded from the regression analysis. Physical and exudative hardening were not included in the above analysis so additional detrimental effects of REOB in that respect were not addressed. Future publications will propose remedies for these issues. It is important to note that both are serious confounders in the current asphalt grading protocols. The correlations were assessed for a single frequency in the DSR but all binders except the straight-run Cold Lake were thermorheologically complex. Figure 49 shows examples of three Black space diagrams, indicating major effects of phase separation and other time-dependent processes that will confound any study of correlating DSR properties with field performance. Most modified and many straight-run binders show similar complexity as is well recognized in the literature (Lesueur, 1999). Hence, it is worthwhile to study the effect of test frequency on the goodness of fit for the various correlations discussed above. It is possible that testing at lower frequencies improves sensitivity, precision and accuracy. The mix design was kept constant for all test sections and there was no variation in asphalt binder content or design air voids. However, it is possible that there were minor variations for in place air void contents. All test sections passed the end result specifications, so this is unlikely a contributing factor to the observed lifespan variation.

4.4.4 Summary and Conclusions

This section delved into the development of simplified, efficient test methods for assessing the rheological properties of asphalt binders, crucial for grading asphalt used in road construction. The focus was on reducing material usage and testing duration while preserving or enhancing the precision and accuracy of traditional tests such as the EBBR and DENT methods. These conventional tests, though effective for specification grading, are material-intensive and time-consuming. An alternative proposed is the DSR, employed by Superpave for evaluating high and intermediate temperature properties of binders, capable of generating complex modulus and phase angle master curves. Moreover, the correlation between

modified asphalts' rheological indicators and their projected lifespan was investigated. The main conclusions were summarized as following:

(1) The DSR emerged as a viable alternative to EBBR and DENT tests for assessing asphalt binders, offering a reduction in material requirements and test duration. By fitting the Christensen-Anderson model (CAM) to various temperatures and frequencies, DSR can accurately determine binder properties with less complexity.

(2) A strong linear correlation was found between ITPG and T_{30°, suggesting T_{30° as a reliable indicator for evaluating intermediate temperature fatigue resistance of asphalt binder. However, the correlation between ITPG and T_{45° was weaker, with variable R^2 values.

(3) The study highlighted that longer conditioning times improve the correlation between ITPG and limiting phase angle temperatures, indicating that equilibrium state measurements provide better insights into binder performance.

(4) There was no significant correlation between CTOD and parameters such as R Value, Gg, and Gc, but a notable exponential relationship exists between CTOD and the fc parameter, underlining the unique insights provided by phase angle master curve analysis.

(5) The findings support the potential to simplify testing protocols by integrating DSR analyses, especially utilizing limiting phase angle temperatures and the f_c parameter for a more efficient and less resource-intensive evaluation of asphalt binder properties.

(6) These streamlined testing methods can enhance the grading of asphalt binders for road construction, ensuring materials meet the required performance standards with greater efficiency and less environmental impact.

(7) Polymer-modified asphalt binders are generally thought to improve pavement lifespans and ride comfort but reliable field data over extended periods have been found lacking.

(8) Careful analysis of the performance data as obtained by a calibrated ARAN vehicle for the Highway 655 Phase II trial has shown the lifespans can vary by significant amounts. Differences of a factor of two to three in benefit/cost ratios have earlier been reported for sections of ostensibly the same design (Lesueur, 1999).

(9) The degree of gel formation within the binder and how well it relaxes stress appears to be critical in determining long-life performance. This finding is in agreement with published reports that go back to the early work on rheological type by Pfeiffer and coworkers (Pfeiffer and Van Doormaal, 1936), McLeod (McLeod, 1972) and others, which ties in directly with the effects of thermal stresses and freeze-thaw cycles.

(10) A limit on an empirical rheological index $\Delta T_{c\delta}$ is proposed to successfully mitigate cold temperature cracking in cold climates. The new index relates to the slope of the phase angle master curve around the freeze-thaw temperature range over which binder properties are thought to be most important.

(11) A significant finding from this study shows that adding too much polymer modifier in asphalt binder could be counterproductive and not lengthen the service life of asphalt pavements in continental climates characterized by hot summers and cold winters. This is contrary to the common belief that highly modified binders extend service life.

(12) The problem of REOB and other more difficult to detect “polymer enhancers” is to be dealt with through the development of enhanced aging techniques that address hardening from exudation, oxidation and volatilization to closely match in situ aging. REOB and other volatile oils readily improve binder performance in specifications that are based on regular PAV, DSR and BBR tests, but run the risk of failing prematurely and excessively in service.

(13) Given the steadily increasing number of publications on improved asphalt binder specifications in recent times, it is likely that this topic will continue to be discussed for years to come. It is up to user agencies to implement the above findings in enhanced specification protocols as the experience with Ontario field trials has shown that potential savings can be substantial.

4.5 Cracking Resistance Evaluation of Asphalt Mixture Based on SCB

Semi-circular bend (SCB) testing has been widely used to evaluate the cracking resistance of asphalt mixtures. However, it remains unresolved which of the various SCB protocols can provide the most sensitive and precise ranking of different asphalt mixtures. This chapter aims to improve the current SCB protocol emphasizing on mixture preparation, testing condition and evaluation indices. Firstly, the effect of mix aging methods in terms of reversible aging and irreversible aging and loading rates on the intermediate and low temperature cracking resistance of asphalt mixtures was analyzed. The response of different cracking evaluation indices was analyzed, and the repeatability of different cracking evaluation indices was discussed. Secondly, the evaluation of thermo-reversible aging phenomena was included to further optimize the SCB protocol especially in cold regions. Finally, core samples collected from a newly paved Newtonville pavement trial in Ontario, Canada were evaluated to further validate the effectiveness of the SCB method in characterizing cracking resistance of asphalt mixture.

4.5.1 Effect of Experimental Conditions on SCB Results

Experimental conditions in terms of mixture preparation, sample conditioning, testing temperature, and loading rate etc., are expected to affect the cracking resistance results of asphalt mixture based on SCB test. In this section. the effect of mix aging methods in terms of reversible aging and irreversible aging and loading rates on the intermediate and low temperature cracking resistance of asphalt mixtures was analyzed firstly. Subsequently, the response of different cracking evaluation indices was analyzed. Finally, the repeatability of different cracking evaluation indices was discussed.

4.5.1.1 Materials.

The asphalt mixtures tested in this section came from 10 different large user agencies in both the USA and Canada. The locations of material providers and the information of mix is summarized in Table 15. Each mix was extracted and recovered following AASHTO method T-164 (AASHTO T-164, 2003). The recovered asphalt binder was aged using the AASHTO R28 pressurized aging vessel (PAV) protocol following standard conditions (100℃, 2.1 MPa) (AASHTO R 28, 2009). Both the recovered asphalt binder and PAV-aged residue were tested using the ASTM D7643 DSR protocol, the AASHTO TP 122 EBBR, and the AASHTO TP 113 DENT test. The performance grade, low temperature grade loss, and CTOD results of each binder are summarized in Table 15.

Table 15. Results of asphalt binders extracted and recovered from asphalt mix.

Label of mix	Origin	LTPG, ℃	Grade loss, ℃	CTOD
A-1	New England State DOT	-20.6	7.5	4.0
A-2		-21.1	6.9	0
B-1	New England State DOT	-28.8	5.0	13.9
B-2		-28.7	5.7	11.1
C-1	Midwest State DOT	-34.9	5.2	23.3

C-2		-33.7	5.4	16.5
D-1	New England State DOT	-31.0	5.0	12.2
D-2		-27.9	4.6	13.6
D-3		-26.9	3.5	9.2
D-4		-35.1	4.4	22.5
E-1	Western State DOT	-23.7	8.7	6.0
F-1	Midwest State DOT	-27.7	4.4	12.3
G-1	Ontario Municipality	-17.3	7.5	6.7
G-2		-27.4	8.0	9.7
G-3		-27.3	5.0	8.9
G-4		-30.6	8.5	11.5
G-5		-33.2	4.4	21.2
G-6		-30.6	4.8	11.4
G-7		-31.5	6.6	12.4
G-8		-26.8	8.7	7.8
G-9		-26.3	6.0	8.9
G-10		-27.3	4.3	9.1

4.5.1.2 Effect of aging.

The asphalt mixtures Typical plots for each aging condition are compared in Figure 56. From the graphs, it can be determined that the peak loads differ. Specimens that were chemically aged at 140°C for 16 hours and subsequently physically aged at −20°C for 72 hours, had the highest peak load at 25°C, followed by the normally aged ones (16 hours at 140°C) and the unaged ones. Moreover, the FI and CII indices show a high sensitivity to reversible aging processes. The CRI index can generally tell apart the different aging treatments. However, both the BCI and FE failed to distinguish unaged results from aged ones. The FI, CRI and CII change due to thermo-reversible aging processes only to minor degrees, while there is no obvious correlation between BCI or FE and the degree of thermo-reversible aging. So, it can be concluded that the maximum load used in the CRI and the slope at the inflection point used in the FI are both sensitive to aging but none of the cracking indices are particularly sensitive as compared to the EBBR data in Table 1. This is likely due to the way in which the SCB mix tests confound stiffening within the binder around the notch and microcracking around the specimen (Togunde and Hesp, 2012).

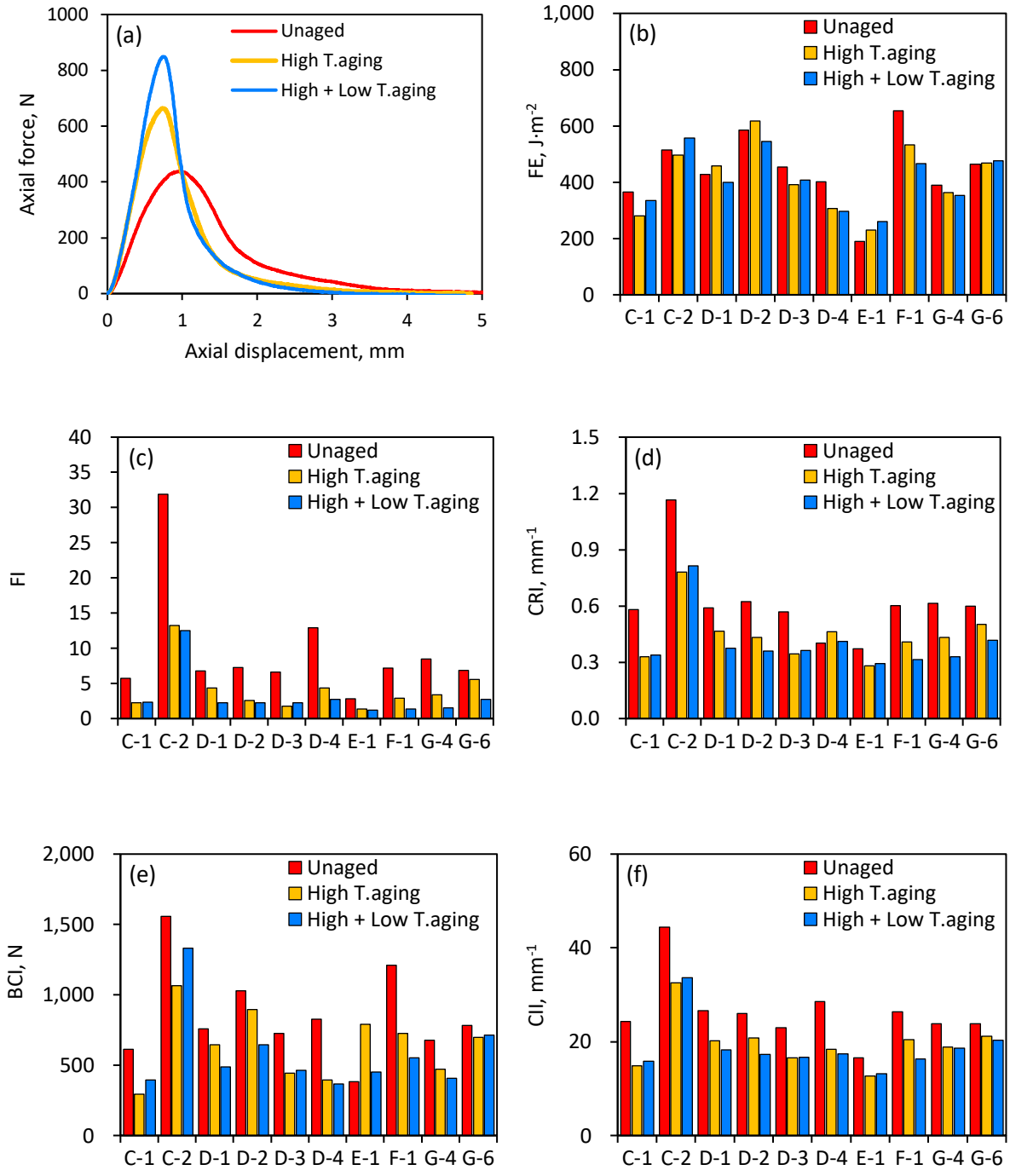

Figure 56. Effect of mixture aging treatment on the cracking resistance of different asphalt mixtures.

(a) effect of aging methods on force-displacement of selected asphalt mix; (b) FE; (c) FI; (d) CRI; (e) BCI; (f) CII.

However, more insights are provided by peak loads at failure and slopes at the inflection points. Figure 57 compares the maximum load and slope at the inflection point of different mixtures under different aging conditions. To maximum load, it turns out that nine out of ten mixtures ranked the three aging conditions successfully, while the number of successful rankings is eight to slope at inflection point. Consequently, thermo-reversible aging process would increase the brittleness of the material. This effect causes residual hardening that can still be observed after conditioning at room temperature for 2.5 hours prior to testing and would be revealed by measuring the crack mouth opening displacement (CMOD) directly with a clip-on gauge (Togunde and Hesp, 2012).

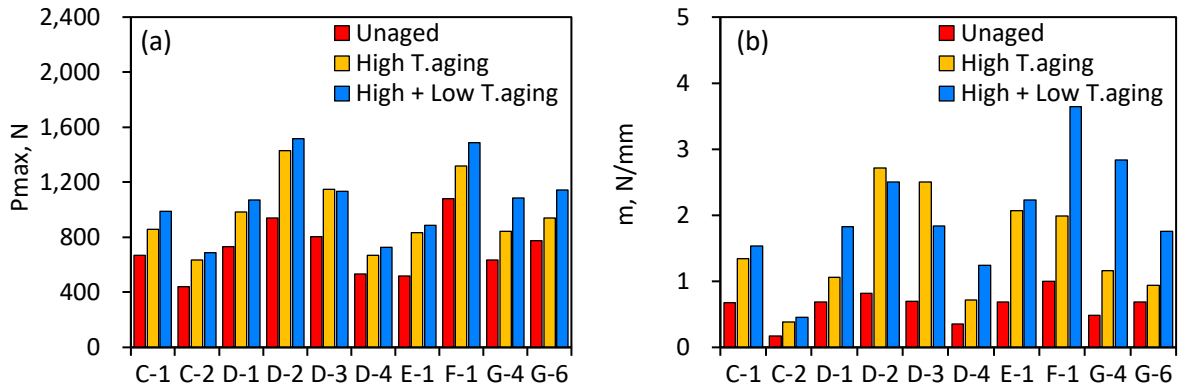

Figure 57. Effect of mixture aging on cracking resistance.

(a) Peak load, Pmax; (b) Slope at inflection point, m.

4.5.1.3 Effect of temperature.

The asphalt mixtures A comparison of typical plots for the two test temperatures employed is depicted in Figure 58. The graph shows that the peak load and total fracture energy for tests at low temperatures were much higher than those at room temperature. This might be explained by the fact that brittle fracture is more likely to happen at low temperatures. The FE, FI, CRI and CII all showed good sensitivity to test temperature. As for BCI, the difference between the two test temperature results was relatively larger than what it was for the other indices or parameters. A possible explanation would be that BCI is equally affected by fracture energy and mixture ductility (Majidifard et al., 2021). As temperature drops, the fracture energy increases while the ductility decreases. The BCI might thus stay unchanged upon temperature change.

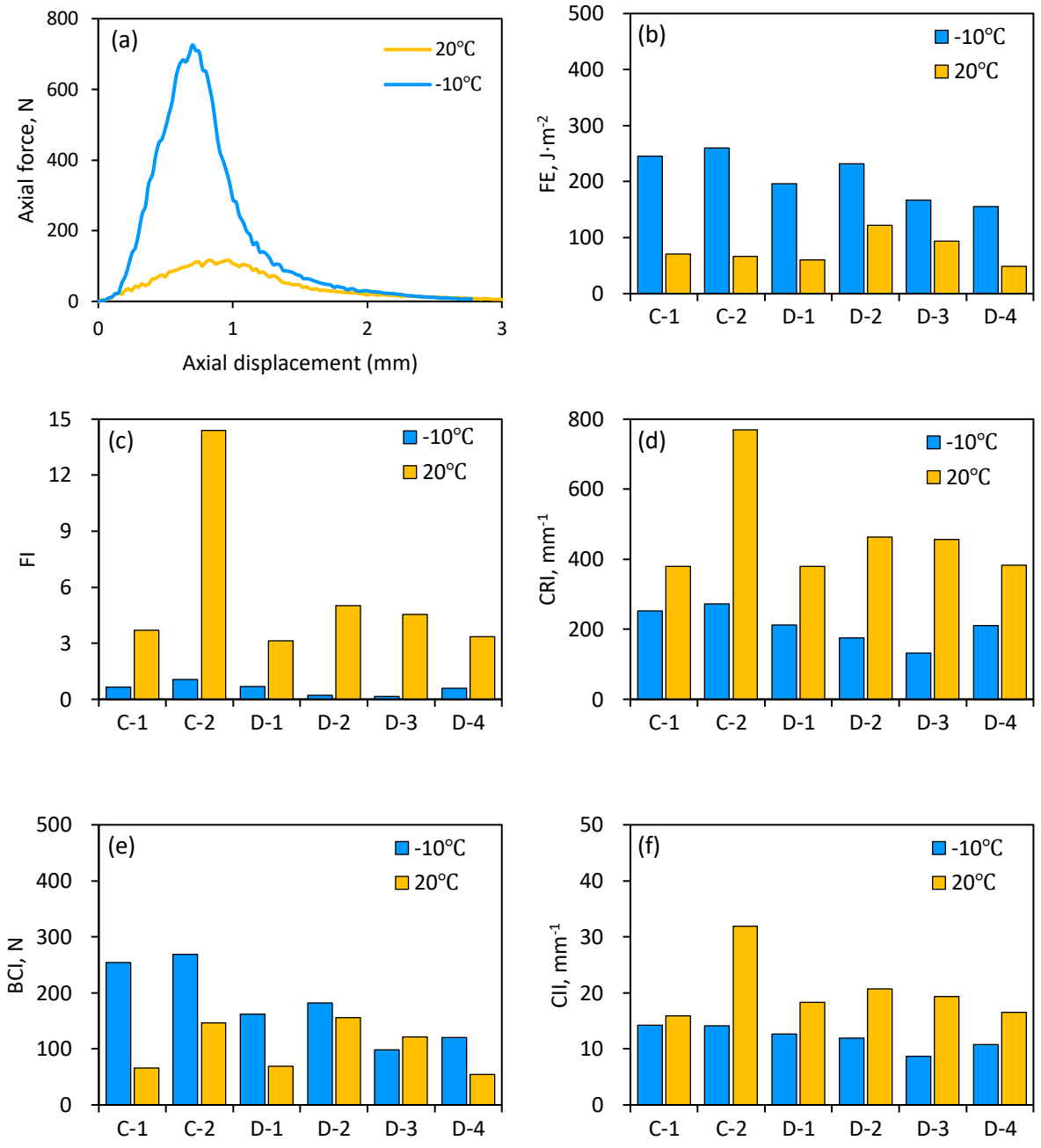

Figure 58. Effect of testing temperature on the cracking resistance of different asphalt mixtures.

(a) Force-displacement; (b) FE; (c) FI; (d) CRI; (e) BCI; (f) CII.

4.5.1.4 Effect of loading rate.

The relationship between indices under different loading rates was explored by performing a correlation analysis. The corresponding results are shown in Figure 59. Under the circumstance of a relatively low loading rate of 0.05 mm/min, a high correlation exists between CRI and FI, CII and FI, and CII and CRI.

Among them, a nearly linear relationship between CII and CRI was observed, which is independent of loading rate. For this reason, CII and CRI can be used interchangeably. With respect to the relationship between BCI and FI, FE and FI, BCI and CRI, FE and CRI, CII and BCI, CII and FE, and FE and BCI, a consistently higher correlation was achieved for the higher loading rate. It is obvious from this analysis that not all indices reward tougher binders to the same degree.

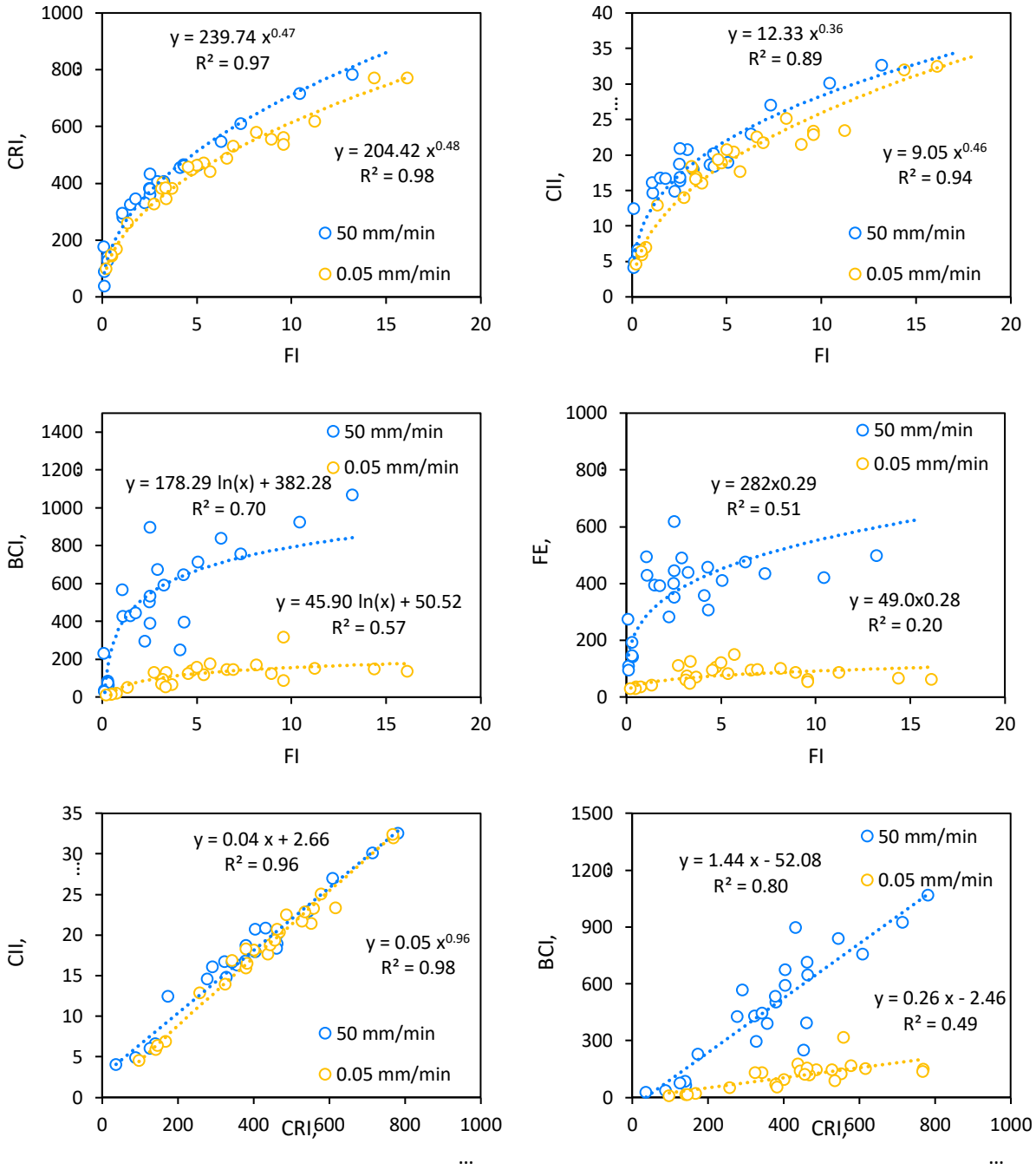

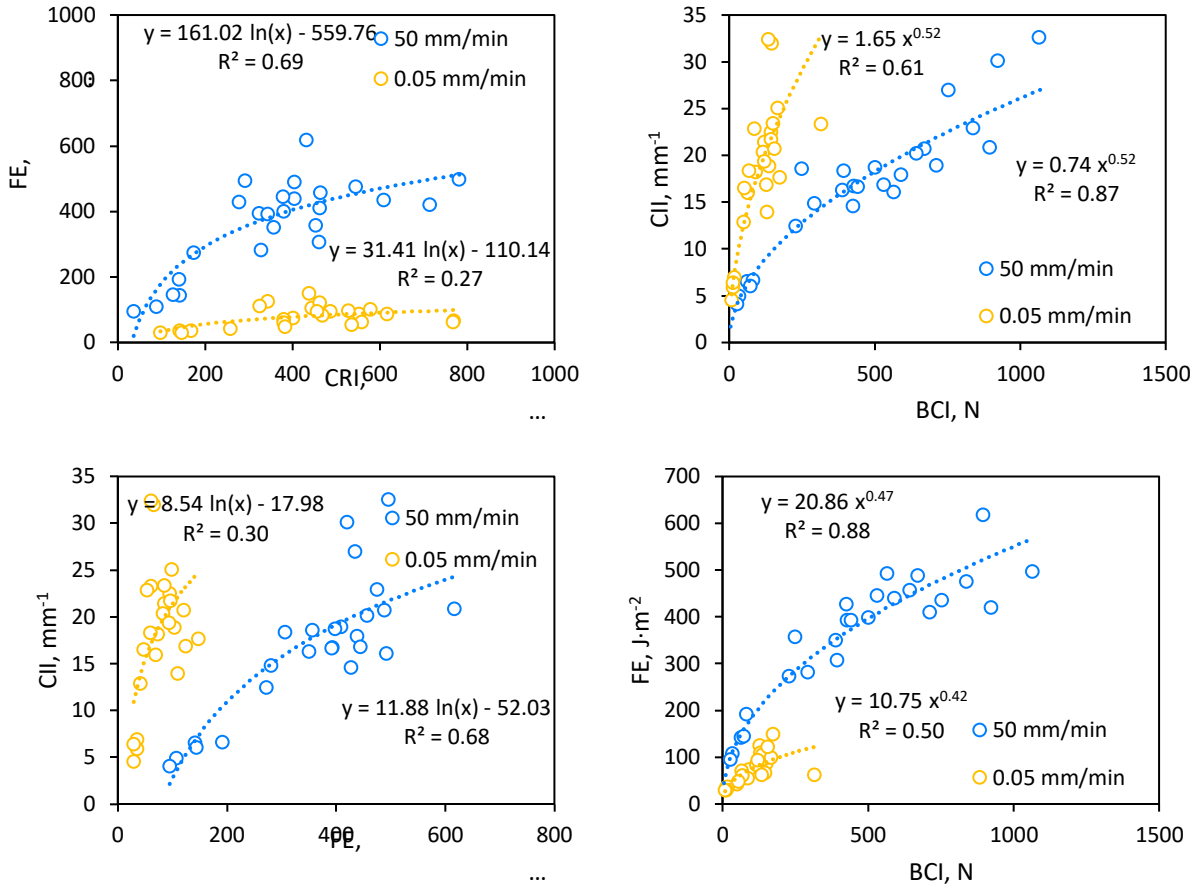

Figure 59. Correlation analysis of different indices at two different loading rates.

4.5.1.5 Statistical analysis.

(1) Dynamic range

The dynamic range is calculated in this study to compare the ability of different indices to distinguish mixtures in terms of their resistance to cracking. In this study, two different methods were used to compare the dynamic range, which are the ratio of the maximum value and the minimum value (R1) and, the ratio of the difference between the highest and lowest over the average value (R2), respectively. The results of R1 and R1 are shown in Figure 60 (a) and (b), respectively. It can be found that a decrease in loading rate leads to a decrease in dynamic range for all but the BCI index, meaning that in general the indices would have a smaller range under a lower loading rate. This observation is important in that loading rates in services are orders of magnitude slower as pavements shrink not only over a 24-hour cycle but also over a yearly cycle from summer to winter. A recent review of pavement trial findings from Ontario has shown that polymers can degrade long-term pavement performance due to reduced stress relaxation and phase separation (Ma et al., 2022a; Sandrasagra et al., 2022). This can lead to exudation of low molecular weight oils (paraffin) (Hesp et al., 2007b) and interfacial failure (Hesp et al., 2000b; Roy and Hesp, 2001c; Roy and Hesp, 2001). The change in dynamic range is not very significant in FE and CII.

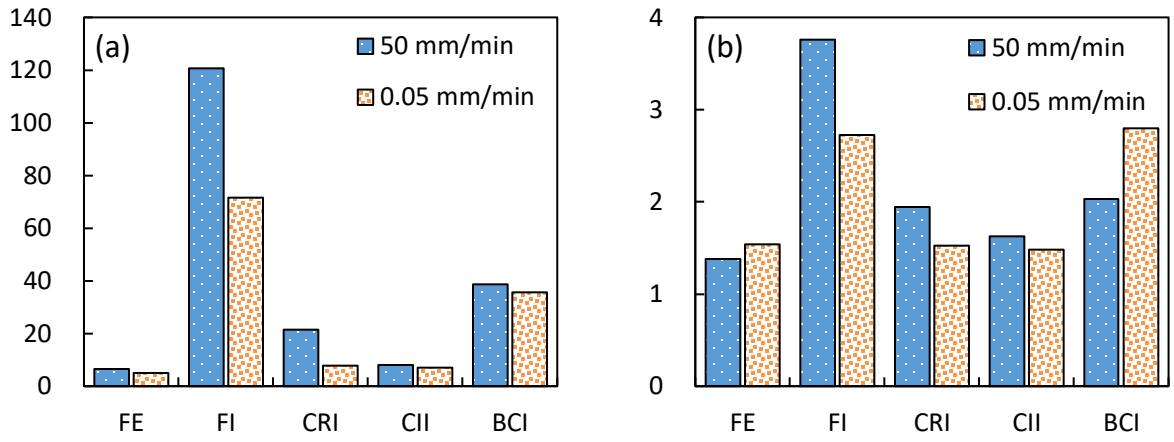

Figure 60. Dynamic range analysis of different indices: (a) R1; (b) R2.

(2) Repeatability

The results of pooled COVs are depicted in the graph below. By comparison, the CRI has a relatively low COV as expected and at 0.05 mm/min loading rate most of the COV values are below 10 %, which is remarkably good for a mixture test. FE also showed good repeatability. As for the FI and BCI, the COVs for them are high. It is noteworthy that under a low loading rate, the improvement in the repeatability is not obvious. For certain mixtures there is an increase in COV instead of an anticipated decrease. Considering the extra time spent on low-rate tests, it might not be worth slowing down to 0.05 mm/min from a repeatability perspective. However, considering the results in Figure 61, it remains an important question to decide what performance index at what loading rate most accurately correlates with field performance.

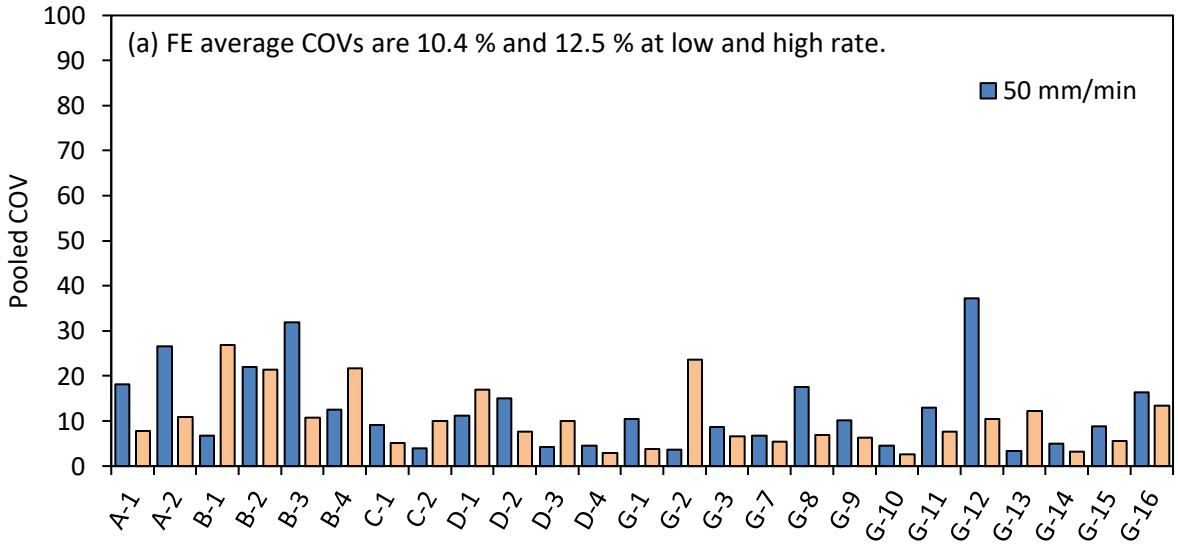

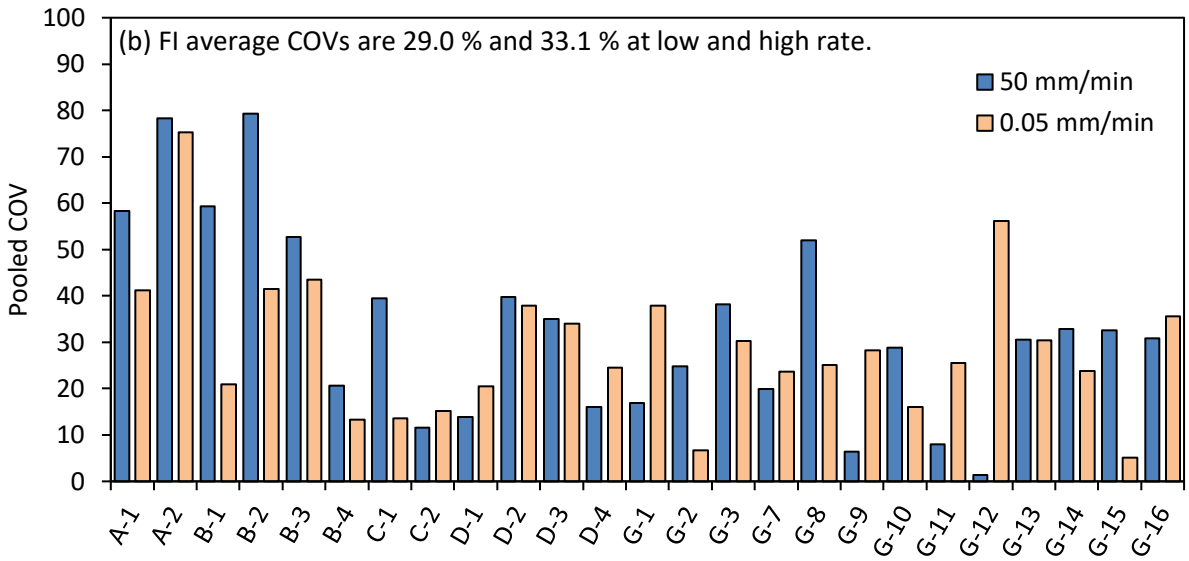

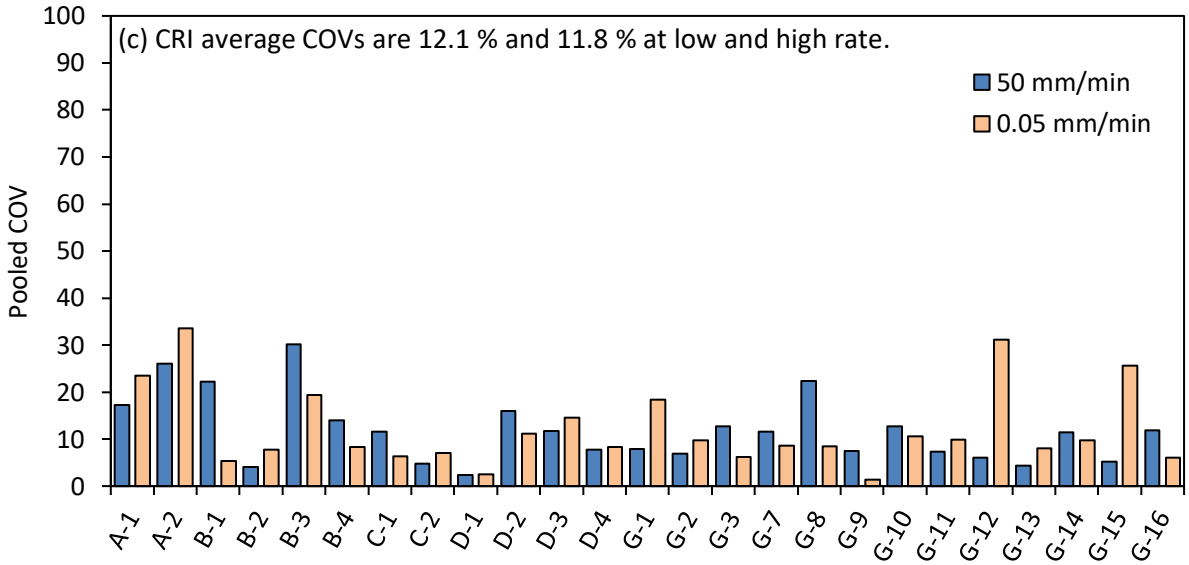

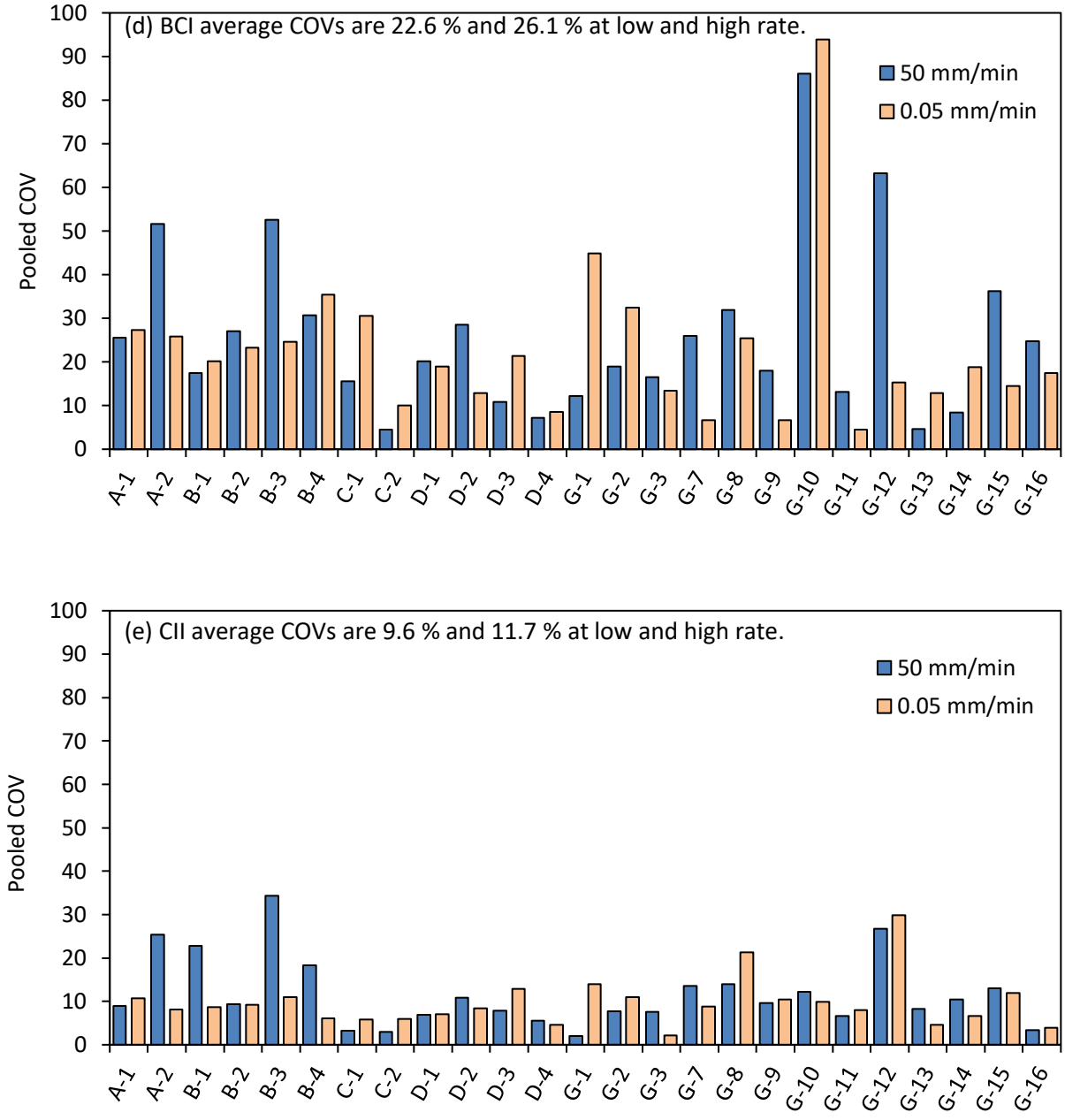

Figure 61. COV of different asphalt mixtures.

(a) FE; (b) FI; (c) CRI; (d) BCI; (e) CII.

The base number for the numerator and denominator is the same because they come from the same data group. To have a larger range covered, the numerator should be larger as well. While a smaller denominator indicates the data group is more stable, meaning it has a higher repeatability. Thus, roughly speaking, a higher R means that the data group has a relatively good repeatability and range. The table below illustrates the R for all indices and parameter involved in this study. It can be concluded that from

a repeatability and dynamic range perspective, both CRI and CII show good performance at both rates while FI shows good performance only at the higher rate.

Finally, it is noteworthy that none of the mix test results at 25°C are consistent with the extracted and recovered asphalt binder test results in terms of ranking as provided in Table 15. This is a serious concern as obviously the observation means that it remains unresolved which approach is more accurate to control pavement cracking distress. It is likely that mixture failure tests at lower temperature, lower rates that measure crack mouth and tip opening displacements directly will show the significant differences due to thermo-reversible aging (Togunde and Hesp, 2012).

Table 16. Results of statistical analysis.

Index/parameter	Loading Rate(mm/min)	Max-Min	Pooled Standard Deviation	R
FE	50.0	522.3	55.3	9.5
	0.05	119.0	11.1	10.7
FI	50.0	13.1	1.0	13.2
	0.05	15.9	1.8	8.6
CRI	50.0	745.4	46.7	16.0
	0.05	671.8	57.9	11.6
CII	50.0	28.5	2.2	13.0
	0.05	27.8	1.8	15.6
BCI	50.0	10.4	1.5	7.0
	0.05	3.1	0.5	6.6

However, such tests are cumbersome and suffer from low reproducibility due to the inherent variability of brittle failure tests on asphalt mixtures. Hence, in the short and medium term it may well be preferrable to conduct asphalt binder tests on appropriately aged binder that is carefully extracted and recovered from samples as placed in the contract.

4.5.1.6 Summary and Conclusions

This section performed a laboratory study on optimizing the cracking resistance evaluation protocol of asphalt mixture based on SCB test. The mixture aging methods and loading rates on the cracking resistance of asphalt mixtures as indicated by various indices were analyzed. On this basis, the optimum indices with lower variability and higher repeatability were recommended. Based on the results and analysis, the following conclusions can be drawn:

(1) Under a low loading rate of 0.05 mm/min, the dynamic range for the indices/parameters investigated tends to get smaller or remained unchanged. Thus, a higher loading rate of 50 mm/min better distinguished different mixtures, which is contrary to what was expected. One possible explanation is that

modifiers like styrene-butadiene-styrene (SBS) and other polymers show better performance at high loading rates. How this relates to field performance remains to be investigated as the SCB tests investigated here might not correlate well with actual in-service performance where stress relaxation appears to be of paramount importance.

(2) It is recommended to use CII and CRI indices to evaluate the cracking resistance of asphalt mixture for their higher repeatability.

(3) Thermo-reversible aging processes can significantly affect cold temperature failure properties of mixtures, which should be considered in evaluating the cracking resistance at intermediate and cold temperatures.

(4) As compared to CII, CRI and FI, BCI is not sensitive to a lowering of the testing temperature. One possible explanation is that ductility is positively correlated to temperature while fracture energy is negatively correlated, leading to a BCI parameter that remains relatively unchanged.

4.5.2 SCB Results of Samples from the Newtonville Pavement Trial

4.5.2.1 Load-displacement curve.

The load-displacement curve offers an intuitive estimate of the impact of recycled plastics and fibers on the cracking resistance of asphalt mixtures. All cracking resistance indicators discussed henceforth are derived from these curves. Figure 62 presents the load-displacement curves for surface lift and binder lift core samples, modified with various recycled plastics and PET fibers, and compares these to control groups. These curves were generated using two distinct displacement measurements for samples under two different low temperature conditioning scenarios. The two displacement measurements used are the LLD, indicating vertical displacement, and the CMOD, representing horizontal displacement at the crack mouth. Both measurements were obtained under a constant vertical load control mode at a loading rate of 0.5 mm/min. In the surface lift, as depicted in Figure 62 (a) to (d), samples conditioned at 0℃ for 2 hours before testing (shown in Figure 62 (a) and (b)) exhibit a rightward shift in the Load-LLD curve with 0.3 % PET fiber, without a notable change in peak force. This suggests an enhancement in the fracture toughness of the surface course due to PET fiber. A similar rightward shift in the Load-CMOD curve is also observed, implying that PET fiber potentially plays a role in delaying crack propagation. For samples undergoing 72 hours of cold conditioning at −20℃, followed by 2 hours at 0℃ before testing (as in Figure 62 (c) and (d)), an increase in peak force is observed in all samples, possibly due to thermal shrinkage induced during low temperature conditioning. The influence of PET fiber on the load-displacement curve shape under these conditions resembles to that observed after the 2-hour 0℃ conditioning. In the case of the binder lift (Figure 62 (e) to (h)), the 2-hour conditioned samples (Figure 62 (e) and (f)) show a decrease in peak force with increasing mixed plastic content in both load-displacement curves. The presence of 0.3 % PET fiber results in a peak force reduction, positioning it between the curves of 0.3 % mixed plastic-modified and 0.6 % mixed plastic-modified samples. A comparable trend is visible in the binder lift samples after conditioning at cold temperatures (Figure 62 (g) and (h)). Similar to the surface lift, conditioning of binder lift samples leads to an increase in peak force. An intriguing observation is that

the effect of PET fiber on enhancing resistance to crack propagation is more pronounced in the load-CMOD curve after conditioning at −20°C.

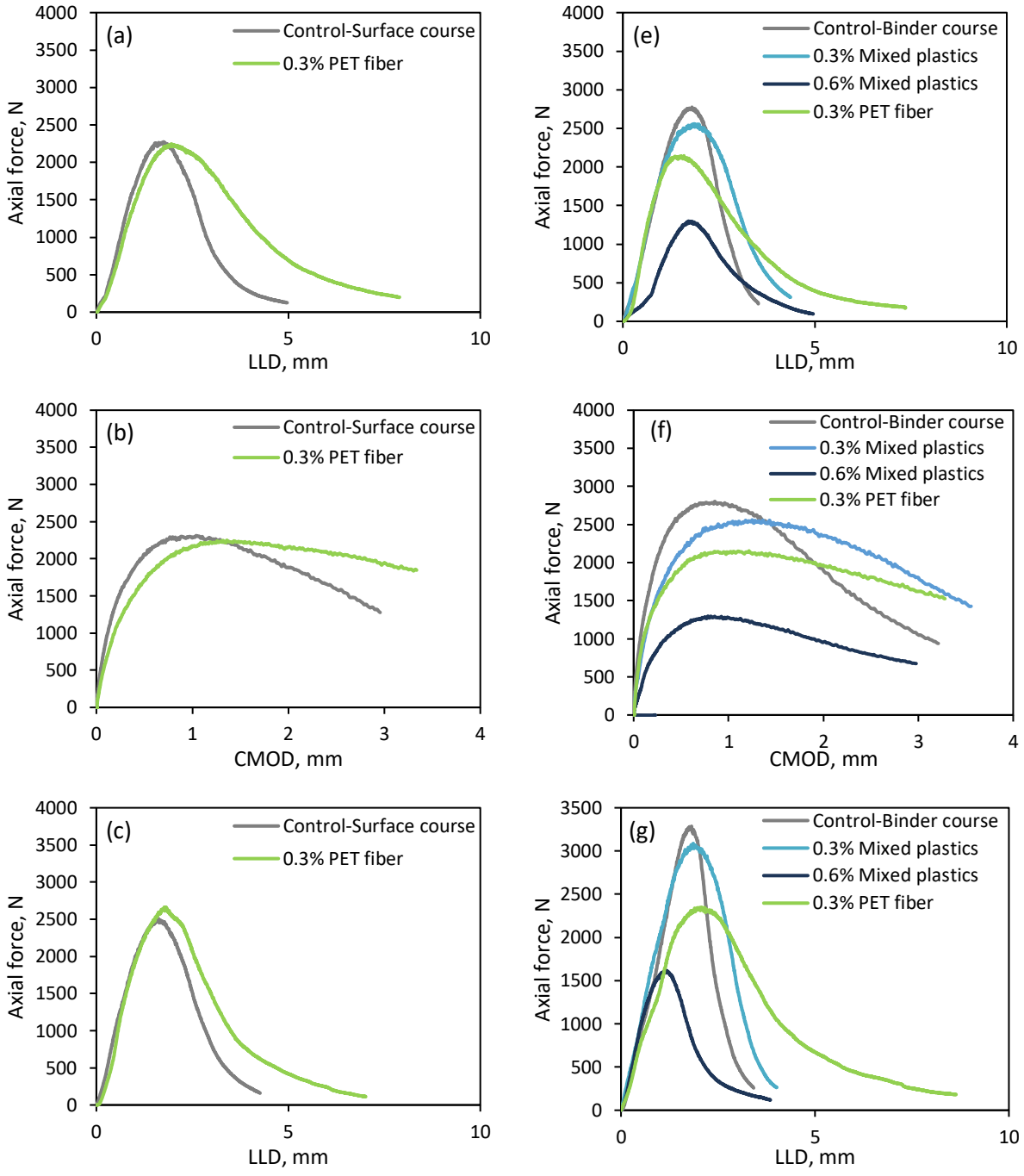

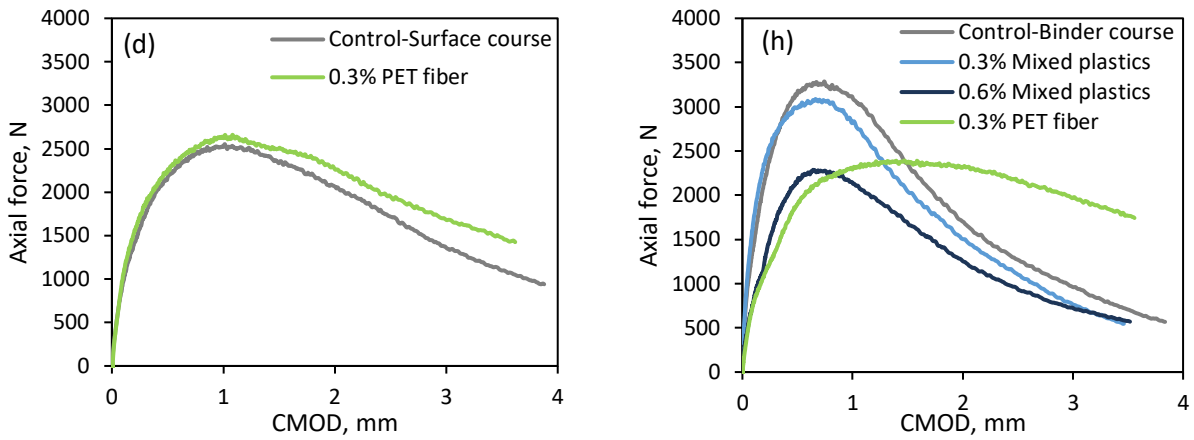

Figure 62. Load-Displacement curve of plastic modified asphalt mixture in surface lift and binder lift.

(a) LLD - 2 h; (b) CMOD - 2 h; (c) LLD - 72 h; (d) CMOD - 72 h; (e) LLD - 2 h; (f) CMOD - 2 h; (g) LLD - 72 h; (h) CMOD - 72 h. Note: (a) ~ (d) represent surface lift, (e) ~ (h) represent binder lift.

4.5.2.2 Cracking resistance and fracture toughness.

Figure 63 presents the results of cracking resistance indicators for core samples taken from the Newtonville trial after construction. Figure 63 (a) to 10(e) depict the results derived from the Load-LLD curve, while Figure 63 (f) to 10(j) correspond to results calculated from the Load-CMOD curve. The notation "2 h" indicates that the SCB sample was conditioned at 0℃ for 2 hours prior to testing at the same temperature. Conversely, "72 h" indicates that the SCB sample underwent conditioning at −20℃ for 72 hours, followed by a 2-hour conditioning period at 0℃ before testing at 0℃. It can be observed from Figure 63 that in the binder lift, the influence of mixed plastics on the cracking resistance of the asphalt mixture varies depending on the chosen cracking resistance index. When FE is employed as an indicator of cracking resistance, the incorporation of 0.3 % mixed plastics appears to enhance cracking resistance of the binder lift, as evidenced by an increase in FE. However, this enhancement becomes marginal when considering the variability in test results. In contrast, increasing the mixed plastic content to 0.6 % diminishes cracking resistance. When comparing the effects of 0.3 % mixed plastic and an equivalent amount of PET fiber, the latter seems to improve the cracking resistance of the binder course more effectively, which can be deduced by the observed increase in FE. FI combines FE and post-peak slope to differentiate cracking resistance of various mixtures, particularly those with high recycled content. As illustrated in Figure 63 (b) and (g), the impact of recycled plastic and fiber on cracking resistance of both surface and binder lifts aligns with FE findings from Figure 63 (a) and (f). A key advantage of FI is its enhanced ability to distinguish between the cracking resistances of different mixture designs. CRI, another novel metric, offers a balanced approach by considering both FE and peak force (Kaseer et al., 2018). It is particularly effective in differentiating asphalt mixtures with identical FE but varying peak forces. Figure 63 (c) and (h) show that the control surface lift has a higher CRI value compared to the control binder lift, indicating superior cracking resistance in dense graded mixtures over coarse graded ones. Notably, the incorporation of mixed plastic up to 0.6 % does not significantly affect CRI, mainly because mixed plastic reduces both peak force and the span of the peak, as seen in Figure 62. In contrast, the addition of 0.3 %

PET fiber significantly increases CRI for the binder course. This increase is attributed to the reduction in peak force by PET fiber, while maintaining or even enhancing FE, as indicated in Figure 62. According to the definition for CRI – the ratio of FE to peak force – the inclusion of PET fiber would eventually lead to a higher CRI. This differing impact between mixed plastic and PET fiber on the cracking resistance of binder lift mixtures is noteworthy. PET fiber plays a reinforcing role, delaying crack propagation, as evidenced in (Andriescu and Hesp, 2009; Lou et al., 2024; Ma et al., 2022b; Ma and Hesp, 2022). Mixed plastic pellets, however, act more like aggregates, offering only a minor hindrance to crack propagation, partly due to their reduced contact surface with the asphalt binder. BCI incorporates a shape parameter, L_{75}, which estimates the span of the peak, aside from fracture energy. BCI has been proposed for its superior repeatability compared to both FE and FI when evaluating the cracking resistance of asphalt mixture (Majidifard et al., 2019). As observed in Figure 63(d), the trends in BCI are like those seen in CRI results from Figure 63 (c). A notable distinction, however, is the decreasing BCI value in the binder lift with increased mixed plastic content. Figure 63 (a) reveals that an increase in mixed plastic content leads to a reduction in peak area, which can be roughly regarded as FE. Meanwhile, L_{75} does not exhibit significant changes. Given that BCI is calculated as the product of FE multiplied by L_{75}, this elucidates why BCI values decrease as the content of mixed plastics increases. The CII shares similarities with the CRI in its formulation, with the primary distinction being that CII calculates FE from the area preceding the peak. Consequently, CII offers an assessment of resistance to crack initiation. This index proves particularly effective in cases of brittle failure, where the post-peak response is represented by a vertical straight line. As illustrated in Figure 63 (e), the CII values for binder lifts, regardless of the inclusion of recycled plastic, consistently remain low. However, the introduction of 0.3 % PET fiber into the binder course leads to a significant increase in CII, elevating it to a level comparable to that of the surface course. This observation suggests that the crack initiation resistance of coarse graded mixtures designs is comparatively lower than that of fine graded ones. Moreover, the influence of recycled plastic pellets on enhancing the crack initiation resistance of coarse graded mixtures is negligible. In contrast, the addition of PET fiber significantly improves the crack initiation resistance of coarse graded mixtures. However, the impact of PET fiber on fine graded mixtures is relatively minor compared to coarse graded ones. A plausible explanation for this is that in fine graded mixtures, PET fibers are predominantly embedded within the asphalt mastic, limiting their interaction with aggregates and consequently, their effectiveness in impeding crack initiation.

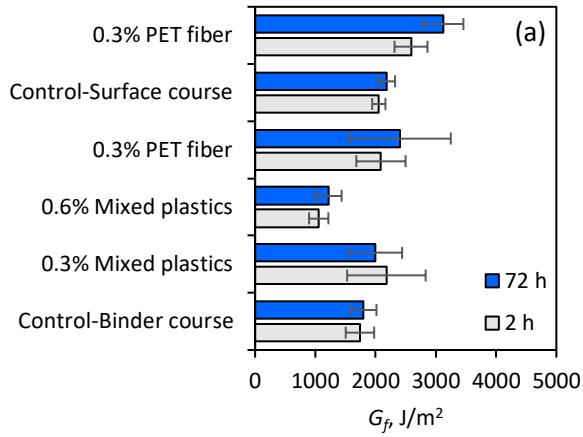

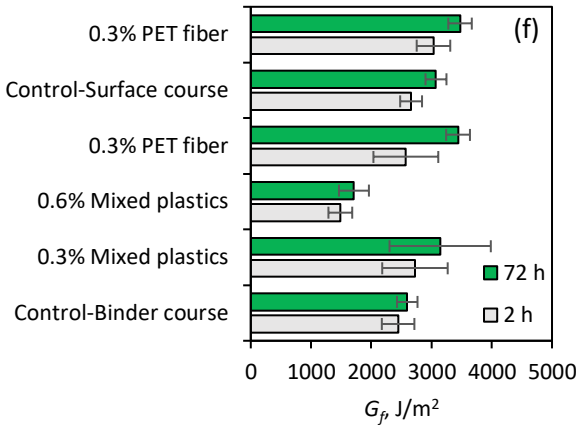

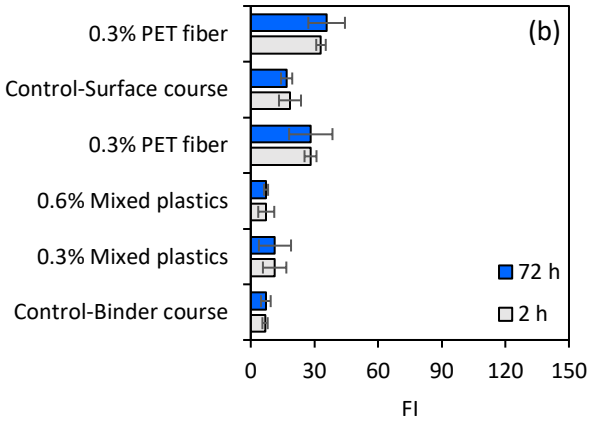

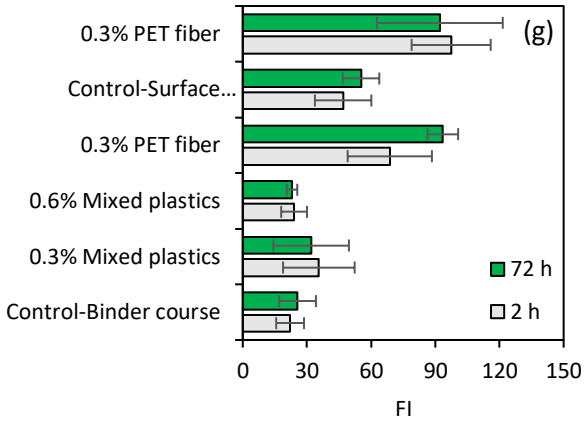

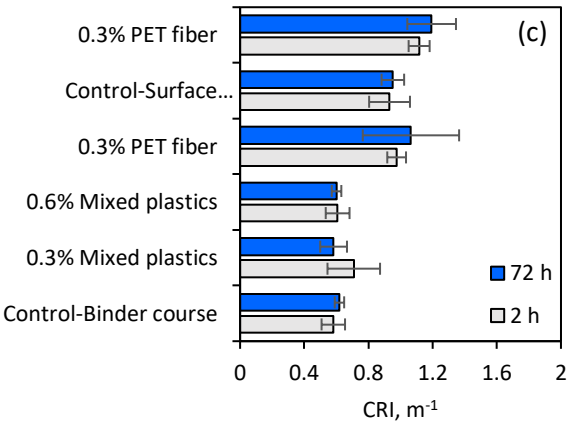

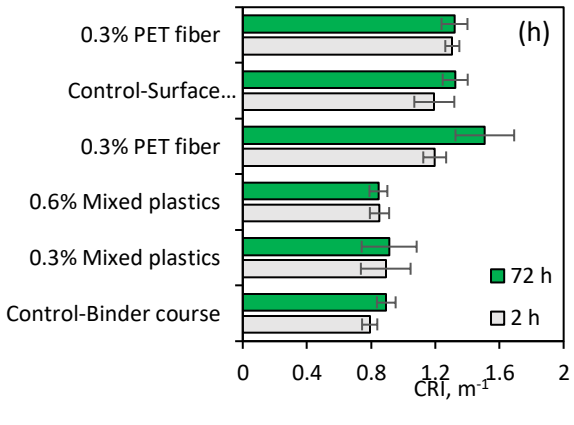

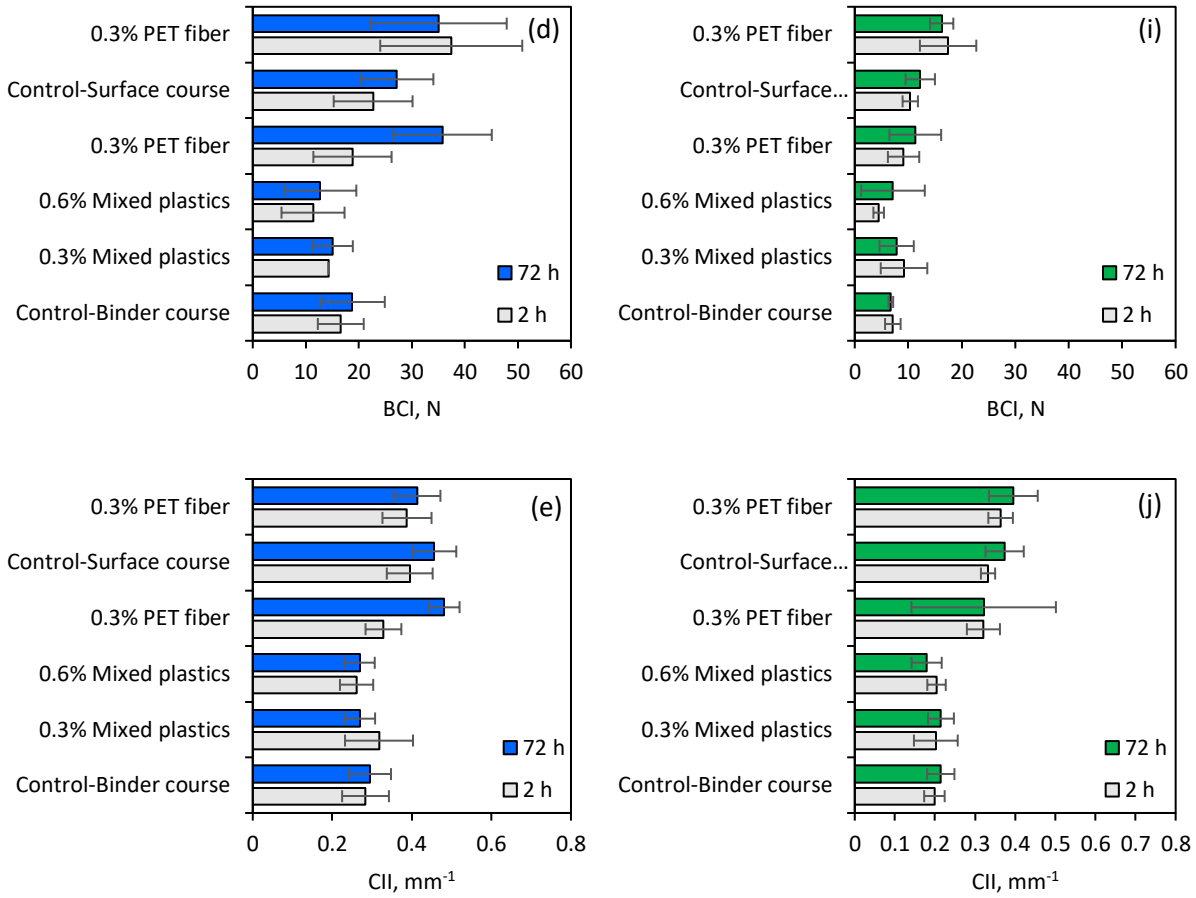

Figure 63. Cracking resistance asphalt mixture.

(a) ~ (e) calculated from Load-LLD curve; (f) ~ (j) calculated from Load-CMOD curve.

Regarding the impact of low temperature conditioning, Figure 63 indicates that conditioning at −20°C for 72 hours results in only minor changes to the cracking resistance of different asphalt mixtures. The cracking resistance indicators, whether derived from the Force-LLD curve or the Force-CMOD curve, show little variance between samples with and without low temperature conditioning. A likely explanation for this is the recent construction of the trial, implying that the asphalt has only experienced short-term aging. Typically, thermal and fatigue cracking intensify over extended periods of field service, during which the asphalt undergoes significant aging and a corresponding decline in cracking resistance. Consequently, it can be inferred that thermal shrinkage induced by low temperature conditioning may rapidly dissipate when the temperature is subsequently raised to 0°C for 2 hours. In terms of differences in cracking resistance as indicated by the Load-LLD and Load-CMOD curves, although there are variations in magnitude and sensitivity, the influence of recycled plastic and PET fiber on the cracking resistance of asphalt mixtures across different pavement layers is largely consistent. Notably, FE values based on the Load-CMOD curve are higher than those from the Load-LLD curve, likely due to the broader peak of the Load-CMOD curve, which results in a larger peak area, as shown in Figure 63. Regarding the FI results, the Load-CMOD curve-based values are higher, attributable to a relatively larger peak area and a lower post-

peak slope. Similarly, CRI values derived from the Load-CMOD curve exceed those from the Load-LLD curve, possibly due to the Load-CMOD curve's larger peak area and lower peak force. BCI results based on the Load-CMOD curve are also relatively higher and more sensitive in differentiating different plastic and fiber-modified asphalt mixtures compared to those based on the Load-LLD curve. However, CII results are consistent between the Load-LLD and Load-CMOD curves.

4.5.2.3 Cracking resistance and fracture toughness results from QA tests.

The results of the cracking resistance of pavement trial asphalt mixtures, post oven-aging, are presented in Figure 64. Following the aging process at 140℃ for 16 hours, it is evident that all asphalt mixtures have undergone extensive aging. As a result, the fracture energy of all mixtures from various test sections decreased. In the meantime, the differences in their fracture energy values diminish and converge to a similar level. Notably, the fracture toughness, as denoted by the FI, declined significantly, suggesting a reduced ability for stress relaxation. The FI data reiterates that PET fiber is more effective than mixed plastic in enhancing the cracking resistance of asphalt mixtures. Comparable trends are observed in CRI results, however FI demonstrates greater sensitivity in distinguishing between different samples. Regarding BCI and CII results, the addition of recycled plastic and PET fiber did not markedly influence cracking resistance of coarse-graded mixtures in the binder lift. In contrast, fine-graded surface courses, with and without PET fiber, exhibited noticeably higher cracking resistance compared to coarse-graded binder courses. This suggests that BCI and CII are more responsive to gradation variations than to modifiers such as plastics and PET fiber.

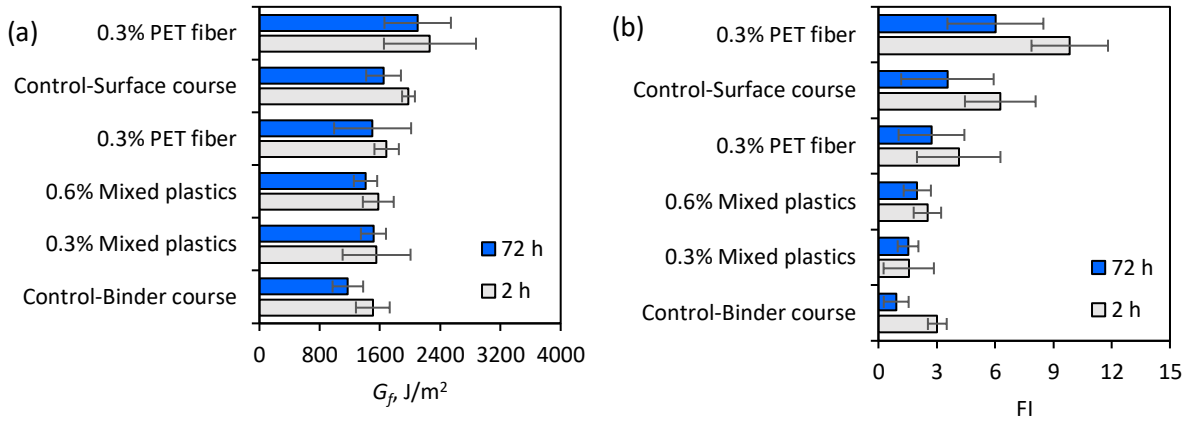

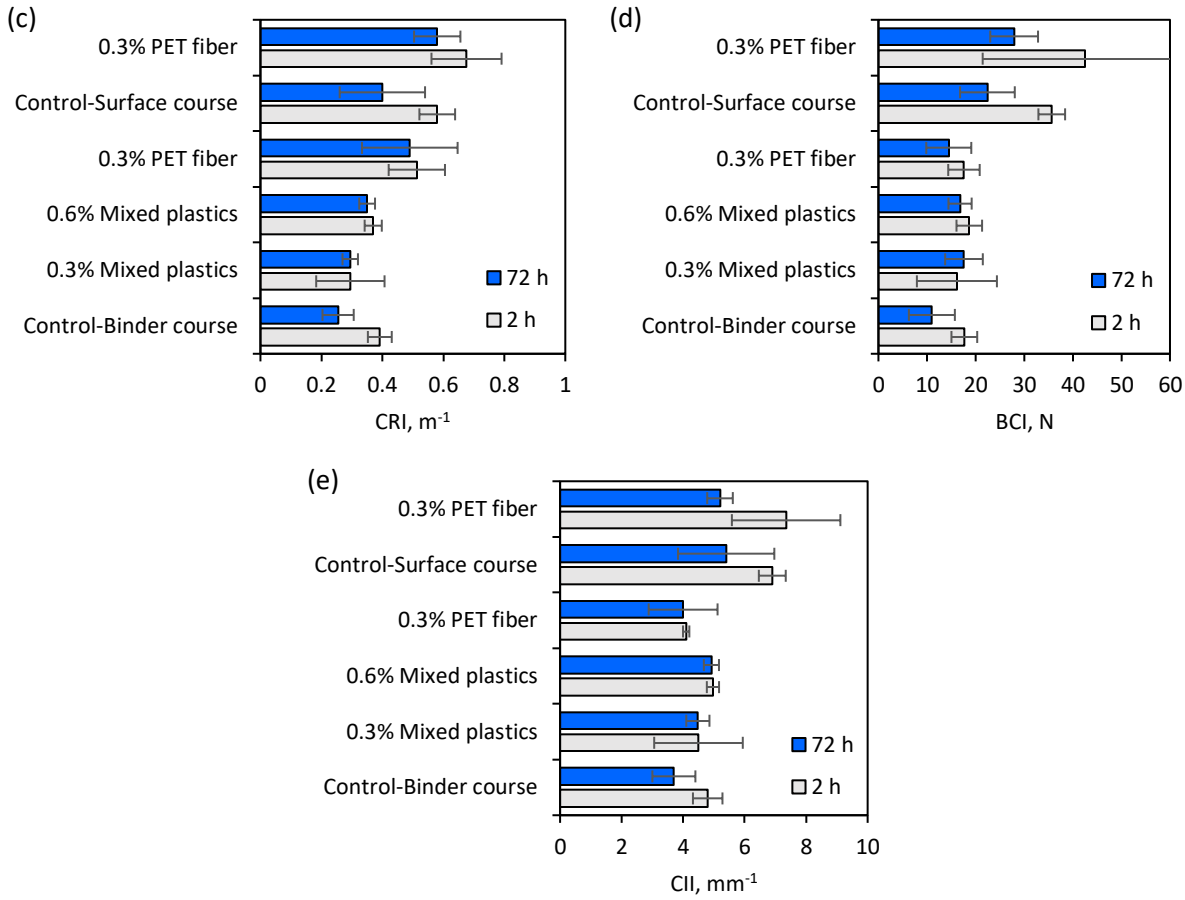

Figure 64. Cracking resistance of mixtures after oven aging.

Note: Results were all obtained from Load-LLD curves.

4.5.3 SCB Results of Samples from Contract Samples

4.5.3.1 Effects of thermo-reversible aging on cracking indicators.

The indicators used all present their own responses to asphalt fracture, hence all can be used to investigate different fracture properties within asphalt. Due to this, long-term conditioning produced different responses within each indicator. In Figure 65, the relation between 2-hour and 72-hour conditioning is shown, with any deviation from a central slope presenting changes caused by long-term conditioning. BCI and FI experienced the most drastic changes in relations, while FE remained the closest to unchanged. It is important to note that CRI, which can be seen as the most stable indicator besides FE, also experienced significant change. This suggests that the impacts of long-term conditioning, which induce thermo-reversible aging, on the cracking resistance of asphalt mixtures are evident. However, the sensitivity of various cracking resistance indicators to thermo-reversible aging varies significantly. All agencies used in this study are labeled, and it should be noted that the Ontario municipality performed the best across the board in fracture testing. This can be explained by the use of enhanced specifications that tend to favor wax-free binder sources from Alberta, Canada. The binder used in this region has a stable low temperature grade due to a very low wax content, preventing both thermo-reversible aging

and associated exudative processes. The primary outlier identified is sample C-10 which has been attributed to an extraordinarily high fracture energy measurement. Upon investigation, we discovered the presence of fibers within the asphalt mixture. The effect of PET fibers is known to enhance the post-peak toughness of the mixture, contributing to a significant increase in overall fracture energy. Distinctly different from pure asphalt mixtures, those modified with PET fibers are believed to increase cracking propagation times and thereby reduce the negative impact of the thermo-reversible aging phenomenon.

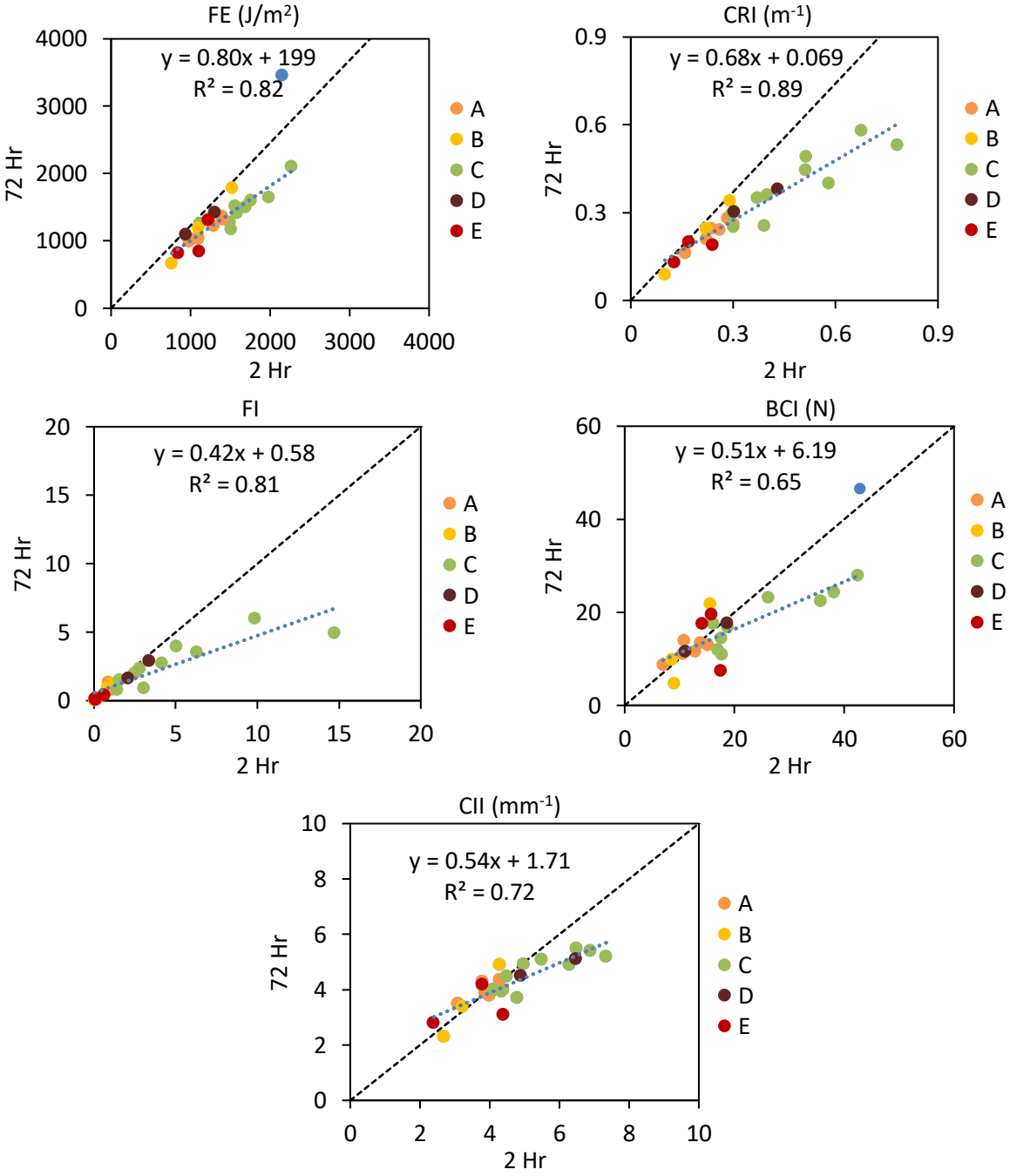

Figure 65. Comparison between short and long conditionings.

Dashed line shows equivalency. Trendline equations added to figures. Outlier: For the single sample highlighted in blue the improvement in performance was potentially attributed to polyethylene terephthalate (PET) fiber modification.

The changes of different cracking performance indicators before and after low temperature conditioning previously outlined are more clearly demonstrated when comparing the ratio of Average and Range (A/R). The A/R is calculated by dividing the average values by the range, which is the difference between the maximum and minimum values. The A/R ratio offers a straightforward estimate of the data dispersion in relation to the mean, providing insight into the variability of the dataset. In this an indicator with a higher average/range can be seen as a potentially more consistent and reliable source of data. This relation is shown over 2-hour and 72-hour conditioning in

Figure 66.

The most drastic impact, in both the above correlations, and the direct comparison below, occurs in FI, which sees a 34.6 % decrease in value on average. Accompanying this is the change in the relative standard deviation of the population shown across all indicators. Demonstrating that while there are some large changes to the relative values of the indicators, the changes in the Coefficient of Variation (COV), are not as significant as the changes in the indicator values after long-term conditioning. This is shown best in BCI, which undergoes a 22.3 % change between 2-hour and 72-hour conditioning, while experiencing little change in COV. Both CRI and CII experience expected levels of change while maintaining relatively low COV; however, CII shows the lowest COV values as well as maintaining the highest values in average/range under both 2-hour and 72-hour conditioning. This helps to establish CII as a slightly more consistent and repeatable indicator than CRI.

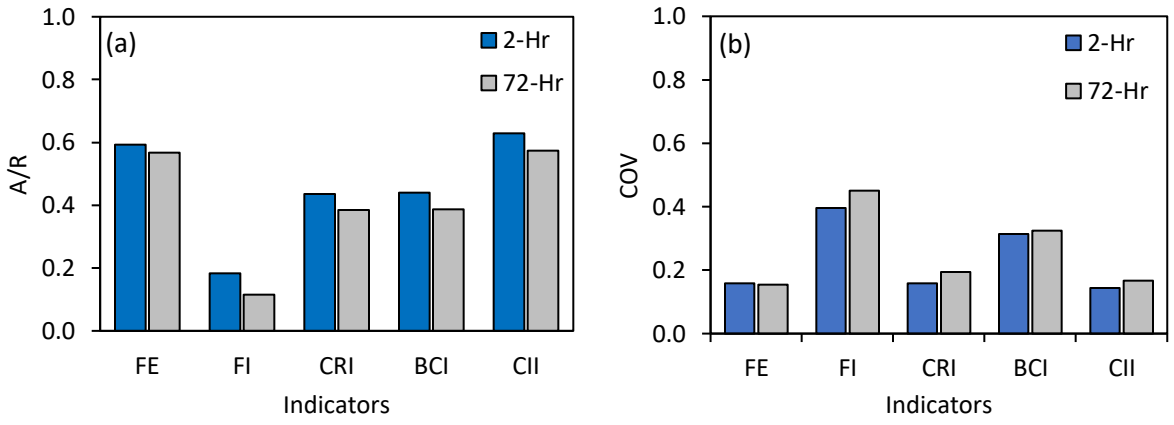

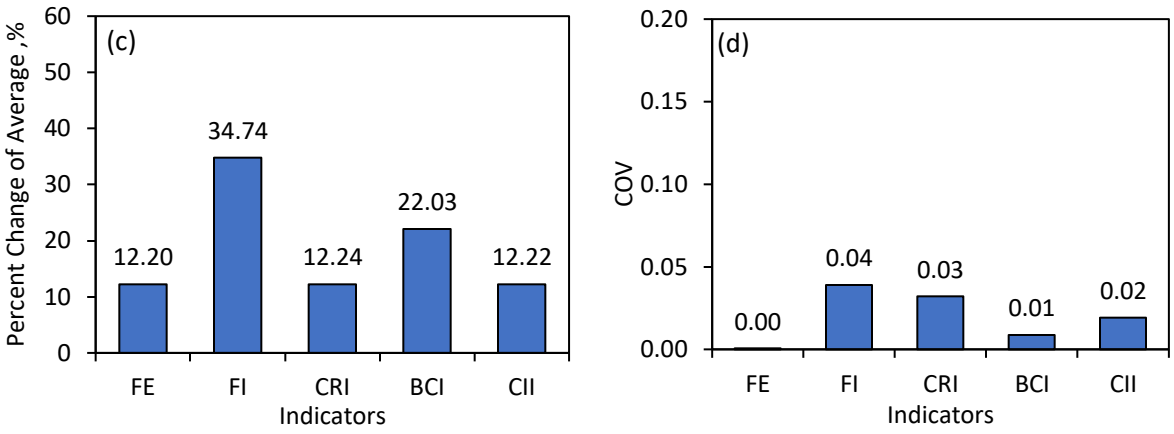

Figure 66. Effect of low-temperature conditioning on the cracking resistance of asphalt mixtures. (a) average/range; (b) COV of A/R; (c) percentage change of average values over conditioning; (d) COV of change over conditioning.

4.5.3.2 Effect of long-term conditioning on HMA performance ranking.

Presented in Table 17 are the performance rankings of the mixes used in this study. Rankings are compared before and after conditioning for both FI and CRI. These indicators were selected because they best show the changes that occur after 72-hour low temperature conditioning, and they independently investigate different parts of the force-displacement curve. The FI reflects an indicator of brittleness utilizing post-peak slope, while the CRI represents cracking resistance using fracture energy and peak load. All ranking changes of two or more are bolded in Table 17. While simple ranking changes of one are not significant, changes of two or more begin to show a trend. Neither of these indicators experienced a significant change in COV value (FI – 0.055, CRI – 0.035). Yet even so, out of the 24 mixtures, 11 experienced a change in performance ranking of at least 2 positions in either FI or CRI, with only 4 mixtures changing at least two positions in both. This demonstrates that there are different aspects of mixtures that are affected by long-term conditioning, with enough of an effect to change rankings. Along with this it is possible to rule out circumstantial change as changes did not occur for all the samples. Another important note is that, for the most part, the mixtures that performed well under mixture testing and binder testing saw the least change in performance ranking and remained consistent. These ranking changes are backed by the binder data presented and help to reveal some potential flaws in the mix design, when designed for low temperature. The binders used in the Ontario municipality region are good quality binders with low and stable LTPG values, along with proper mixture designs. Hence, most of the samples that fall within this region experience little or no change in ranking. Outliers in this can be attributed to testing inconsistencies as well as the variability present in SCB testing. In the case of the Western Federal Agencies region, all samples have quite stable rankings except B-3. This may be due to the high grade loss of the binder at low temperatures as well as poor mixture design. For Midwest State DOT samples, the binders and mixture designs are good. As the ranking changes occur in both indicators for this region, it is likely that these changes can be attributed to inconsistencies within the testing or interfacial failure effects. Regarding Western State DOT samples, the binders used have a significant grade

loss at low temperatures, which may be responsible for the ranking changes present. While these changes in ranking can be explained, it is important to note that without the effects of thermo-reversible aging, it would be more challenging to identify possible flaws in binders and mix design. The use of long-term conditioning as a tool to identify inconsistencies such as those that do not present themselves in initial (short-term conditioning) findings is valuable.

Table 17. Comparison of performance ranks between 2-hour and 72-hour conditioning.

FI 2 h Ranking	FI 2 h Values	FI 72 h Ranking	FI 72 h Values	CRI 2 h Ranking	CRI 2 h Value (m^{-1})	CRI 72 h Ranking	CRI 72 h Value (m^{-1})
C-10	14.72	C-8	6.02	C-10	0.780	C-8	0.580
C-8	9.84	C-10	4.95	C-8	0.676	C-10	0.530
C-7	6.27	C-6	3.95	**C-7**	0.580	C-5	0.490
C-6	5.03	C-7	3.55	C-5	0.513	C-6	0.446
C-5	4.13	D-2	2.89	C-6	0.512	**C-7**	0.400
D-2	3.36	C-5	2.73	D-2	0.430	D-2	0.380
C-1	3.03	C-9	2.36	C-9	0.400	C-9	0.360
C-9	2.80	C-4	2.00	**C-1**	0.392	C-4	0.350
C-4	2.52	D-1	1.63	C-4	0.370	**B-2**	0.340
D-1	2.07	C-2	1.52	D-1	0.303	D-1	0.302
C-2	1.56	**A-3**	1.33	**A-1**	0.300	**C-2**	0.295
C-3	1.39	**B-2**	1.25	**C-3**	0.300	**A-5**	0.280
A-1	1.27	A-5	1.13	**C-2**	0.295	**A-1**	0.260
A-5	1.23	**B-3**	0.95	**B-2**	0.290	**C-1**	0.255
B-2	1.13	**A-1**	0.92	**A-5**	0.284	**C-3**	0.244
A-4	1.07	**C-1**	0.92	**A-4**	0.260	**A-3**	0.244
A-3	0.86	A-4	0.8	E-1	0.240	**B-3**	0.244
B-3	0.83	**C-3**	0.79	**A-3**	0.236	**A-4**	0.240

E-1	0.63	E-1	0.41	**B-3**	0.220	E-2	0.200
A-6	0.22	**E-2**	0.17	E-2	0.170	E-1	0.190
E-3	0.17	A-6	0.16	A-6	0.159	A-6	0.161
E-2	0.07	E-3	0.06	E-3	0.127	E-3	0.130
B-1	0.03	B-1	0.025	B-1	0.100	B-1	0.088

4.5.3.3 Effects of thermo-reversible aging based on post-peak analysis.

The two main forms of graphical analysis, CMOD and LLD, provide similar functions within fracture analysis, but to varying degrees of sensitivity and repeatability. Figure 67 shows relative changes in the average post-peak slope values induced by thermo-reversible aging, accompanied by the changes in the COV values. Post-peak slope is a key parameter in analyzing the force-displacement graph for performance ranking (Al-Qadi et al., 2015a). As shown in Figure 67 (a), there is a notable increase in the post-peak slope of the Force-CMOD curve, amounting to 65.2 %, as a result of extended low-temperature conditioning. Conversely, the post-peak slope of the Force-LLD curve exhibits a minimal change under identical conditions, with only a 0.8 % increase observed. This observation suggests that the post-peak slope of the Force-CMOD curve is more sensitive to the thermo-reversible aging in asphalt mixtures induced by extended low-temperature conditioning compared to the Force-LLD curve (Togunde and Hesp, 2012). Therefore, it can be deduced that the post-peak slope of the Force-CMOD curve provides a more effective means of detecting thermo-reversible aging in asphalt mixtures. Figure 67 (b) shows the COV of the post-peak slope for two distinct force-displacement curves, using asphalt mixture samples subjected to both short- and long-term low-temperature conditioning, which provides an estimate of the consistency of post-peak slope measurements across different scenarios (Togunde and Hesp, 2012). The findings indicate that the COV of the post-peak slope from the Force-LLD curve is notably higher than that from the Force-CMOD curve, especially in samples conditioned at low temperatures for 72 hours. Consequently, this implies that the post-peak slope values obtained from the Force-CMOD curve exhibit more reliable repeatability compared to those from the Force-LLD curve.

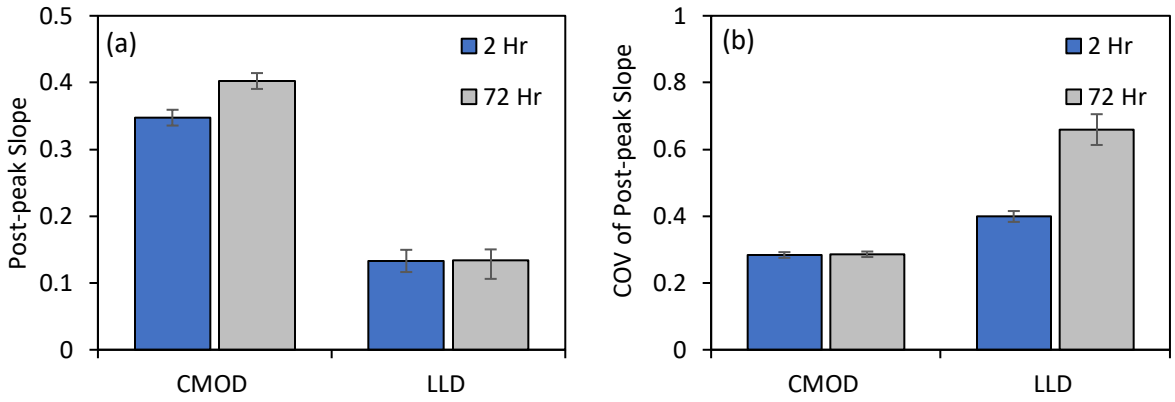

Figure 67. Post-peak slopes at 75 % of the peak force in Force-CMOD and Force-LLD curves.

(a) average post-peak slope; (b) COV of post-peak slope.

4.5.3.4 Correlation analysis of indicators with CMOD and L-D.

A correlation analysis was performed on the indicators used in this study with relation to slope and displacement using Pearson's coefficient. For the Pearson's coefficient, a value of either positive or negative 1 indicates a perfect correlation between data sets. This correlation analysis is shown below in Table 18. The results indicate that the indicator with the most reliable correlation to all displacement and slope values is the CII. Additionally, considering slope and displacement values, it can be noted that CMOD shows the highest average correlation with the indicators present. It also has a very high correlation with the most repeatable indicator, CII, of 0.95 as shown in Table 18. This shows the potential of CMOD to stand on its own as either an indicator for performance ranking or to be used as a key value within a more in-depth protocol (Roy and Hesp, 2001a; Togunde and Hesp, 2012).

Table 18. Pearson's correlation analysis of cracking indicators.

Pearson's correlation indicator	FE	FI	CRI	BCI	CII
LLD Correlation	0.12	0.33	0.32	0.71	0.38
LLD Slope Correlation	0.508	0.37	0.56	0.37	0.56
CMOD Correlation	0.75	0.60	0.89	0.74	0.95
CMOD Slope Correlation	0.60	0.78	0.77	0.55	0.76

Recent results from full scale pavement trials in Ontario have shown that modified asphalt binders can often perform worse in comparison to straight Alberta binders (Ma et al., 2023). Polymer modifiers are known to improve post-peak energy absorption and hence increase BCI, CRI and FI. Hence, it may well be necessary in future specifications to place lower limits on pre-peak fracture energy and upper limits on

post-peak fracture energy. The significance of performance differences between different mixtures indicates that further study on this matter is warranted.

The results from this study show that higher loading rates are slightly more sensitive to mix composition, possibly due to the toughening effect of polymer modifiers. However, whether higher or lower rates are more accurate remains to be investigated with ongoing field studies. Thermo-reversible aging over three days of cold conditioning at −20°C was found to significantly affect binder properties in selected samples. However, none of the corresponding SCB parameters reflected this deterioration after testing appropriately cold conditioned mixture samples at room temperature. Cracking initiation and resistance indices (CII and CRI) were superior from a repeatability and dynamic range perspective in comparison to flexibility and balanced cracking indices (FI and BCI). Finally, BCI was found to be insensitive to lowering the testing temperature, which is contrary to expectation as cracking resistance must deteriorate when temperature falls.

4.6 High Temperature Stability Evaluation of Asphalt Mixtures

4.6.1 Intuitive Analysis of Rutting Performance of Different Asphalt Mixture

Figure 68 presents the rut depth results for five test sections: S_0, S_1, S_2, S_3, and S_4. Detailed descriptions of the asphalt mixtures used in each section are provided in Section 2.1. Core samples from each section comprise two layers: a 50 mm surface lift and a 60 mm binder lift. Figure 68 illustrates the progression of rut depth against the number of passes for each layer in every test section, evaluated at varying temperatures: 30°C, 40°C, and 50°C. It is observed that at 30°C, all core samples demonstrate minimal rutting. This is primarily attributed to the relatively high viscosity of asphalt binder at lower temperatures. As the continuous phase binds both coarse and fine aggregates, its increased viscosity at this temperature reduces aggregate movement under repetitive loading. Consequently, the rutting curves for all samples display two distinct phases: consolidation and permanent deformation. The consolidation phase is marked by a swift increase in rut depth, resulting from further compaction due to repetitive loading. In contrast, a permanent deformation phase is characterized by a steady increase in rut depth, resulting from both repeated loading and shear flow. At a testing temperature of 40°C, there is a marked increase in the rate of rut depth growth. Typically, rut depth curves for most samples can be divided into three phases: consolidation, permanent deformation, and moisture-induced stripping. A notable difference in rutting resistance between the surface and binder courses becomes evident. For example, at 30°C, the rutting curves for both courses almost coincide, while at 40°C, they display significant divergence. Upon increasing the temperature to 50°C, all surface courses in the five test sections show a swift escalation in rutting, characterized by two distinct phases in the curve: consolidation and permanent deformation. However, some binder lifts, like in section S_2, still exhibit the three-phase pattern. Given the rapid progression of rut depth at 50°C, the observations made at 40°C provide a reliable basis for distinguishing variations in rut resistance among different mix designs.

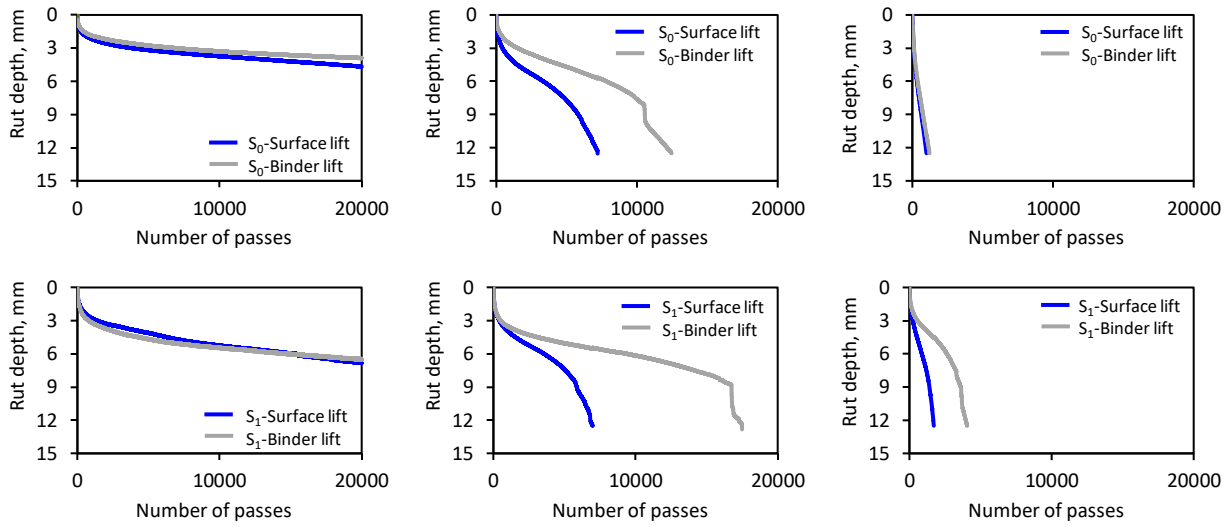

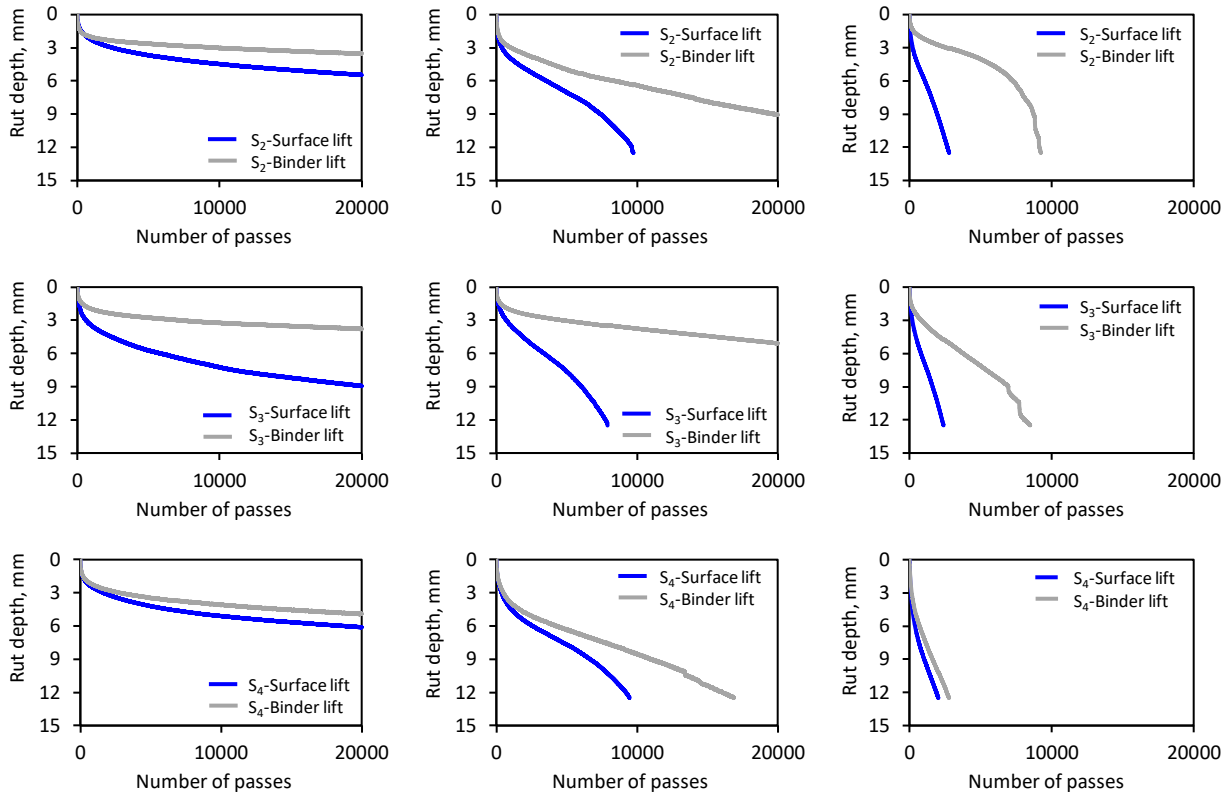

Figure 68. Results of rut depth of different core samples.

To evaluate the rutting resistance of various core samples and to assess the impact of recycled plastic and fibers on the rutting resistance of different asphalt pavement layers, two key indicators were utilized: the rut depth at 20,000 wheel passes and the number of wheel passes required to reach a rut depth of 12.5 mm. Figure 69 presents the outcomes of these indicators for the core samples subjected to distinct testing temperatures (30°C, 40°C, and 50°C). Analysis of Figure 69 reveals that the influence of recycled plastic and fiber on the rutting resistance of asphalt mixtures is contingent on the testing temperature. At 30°C, surface courses in test sections 2 and 4, modified with 0.3 % PET fiber, exhibit similar rut depths at 20,000-wheel passes. However, test sections 0, 1 and 3, which employed the same HL-3 fine-graded asphalt mixture, display inconsistent rut depths at 20,000 passes. Similarly, for the binder course, the inclusion of 0.3 % mixed plastics in test sections 1 and 2 results in disparate rut depths at 20,000 passes. This inconsistency likely arises because the rutting resistance of asphalt mixtures at lower temperatures is predominantly influenced by aggregate gradation rather than by the asphalt binder. At an elevated temperature of 40°C, the addition of 0.3 % PET fiber in surface course in test sections 2 and 4 leads to a noticeable increase in the number of passes to reach a rut depth of 12.5 mm, indicating enhanced rutting resistance due to the PET fiber. In the binder course, the inclusion of 0.3 % mixed plastics marginally increases the passes to 12.5 mm. However, increasing the mixed plastic content to 0.6 % results in fewer passes to reach 12.5 mm, suggesting a reduction in rutting resistance. Conversely, using 0.3 % PET fiber in the binder course leads to more passes to 12.5 mm, implying improved rutting resistance. At a testing temperature of 50°C, the addition of 0.3 % PET fiber in the surface course appears to enhance rutting

resistance, as indicated by the increased number of passes to reach 12.5 mm. For the binder course, adding mixed plastics seems to improve rutting resistance, while the effect of PET fiber on improving rutting resistance is less pronounced.

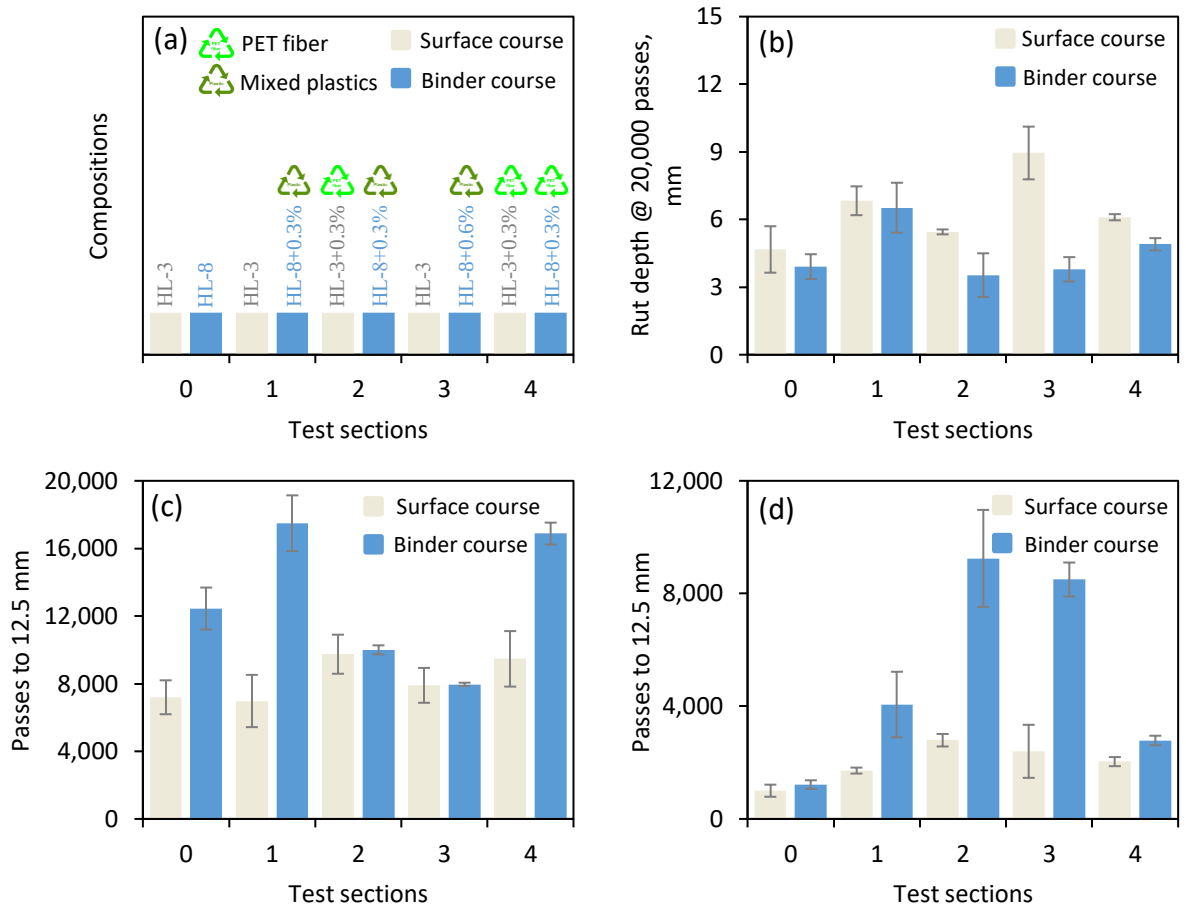

Figure 69. Effect of recycled plastics and fibers on the rutting resistance of asphalt mixture.

(a) Illustration of composition of surface and binder course in each test section; (b) 30°C; (c) 40°C; (d) 50°C.

4.6.2 Area-based Method for Quantifying Rutting Resistance of Different Asphalt Mixtures

In addition to empirically evaluating the rutting resistance of various core samples, our research endeavors to establish an area-based method for quantifying the impact of different recycled plastics and fibers on the rutting resistance of different asphalt mixtures. Illustrated in Figure 70, we compare the change in area under the rutting curve caused by plastic modifiers relative to a control group. A larger shaded area indicates a more pronounced improvement (towards lower rut depth) or degradation (towards higher rut depth) in rutting resistance. As depicted in Figure 70 (a_1) to (a_4), at 30℃, the use of 0.3 % mixed plastic detrimentally affects the rutting resistance of the binder course, as evidenced by an expanded shaded area towards a higher rut depth. However, increasing the mixed plastic content to 0.6 % brings the rutting resistance of the modified asphalt mixture closer to that of the unmodified control

group. For the binder course, incorporating 0.3 % PET fiber significantly enhances rutting resistance, as shown by the enlarged shaded area towards a lower rut depth compared with the control group. In the surface course, 0.3 % PET fiber yields only a marginal improvement in rutting resistance. Examining Figure 70 (b_1) to (b_4) at 40°C reveals interesting observations of how recycled plastic and fiber affect rutting resistance of different layers in asphalt pavement. In the binder course modified with 0.3 % mixed plastic, the initial rutting development is faster than the control group during the consolidation phase. However, this rate significantly decreases during the permanent deformation phase, and the rut depth curve crosses over with that of the control group. Subsequently, a similar pattern in the stripping phase was observed. With an increased dosage of 0.6 % mixed plastic, enhancements in rut resistance are observed across all three phases: reduced rutting rates in both consolidation and permanent deformation phases, and the absence of moisture-induced stripping. The positive impact of 0.3 % PET fiber is noted by the elimination of the moisture-induced stripping phase, although the rut depths during consolidation and permanent deformation are higher than the control group. In surface courses, 0.3 % PET fiber also reduces rut depth in the stripping phase but increases it during the consolidation and permanent deformation phases. At 50°C, as shown in Figure 70 (c_1) to (c_4), both binder lift and surface lift exhibit a significant increase in rut depth with the rutting curve displaying two phases: consolidation and permanent deformation. For binder lifts modified with 0.3 % mixed plastic, there is a decrease in rut depth, with the rutting curve exhibiting the typical three phases mentioned earlier. Doubling the mixed plastic content to 0.6 % further reduces rut depth, with the curve again following a three-phase pattern. The use of 0.3 % PET fiber marginally reduces rut depth, with the rutting curve resembling that of the control. For surface lifts, the efficacy of 0.3 % PET fiber in enhancing rutting resistance resembles that observed in the binder lifts.

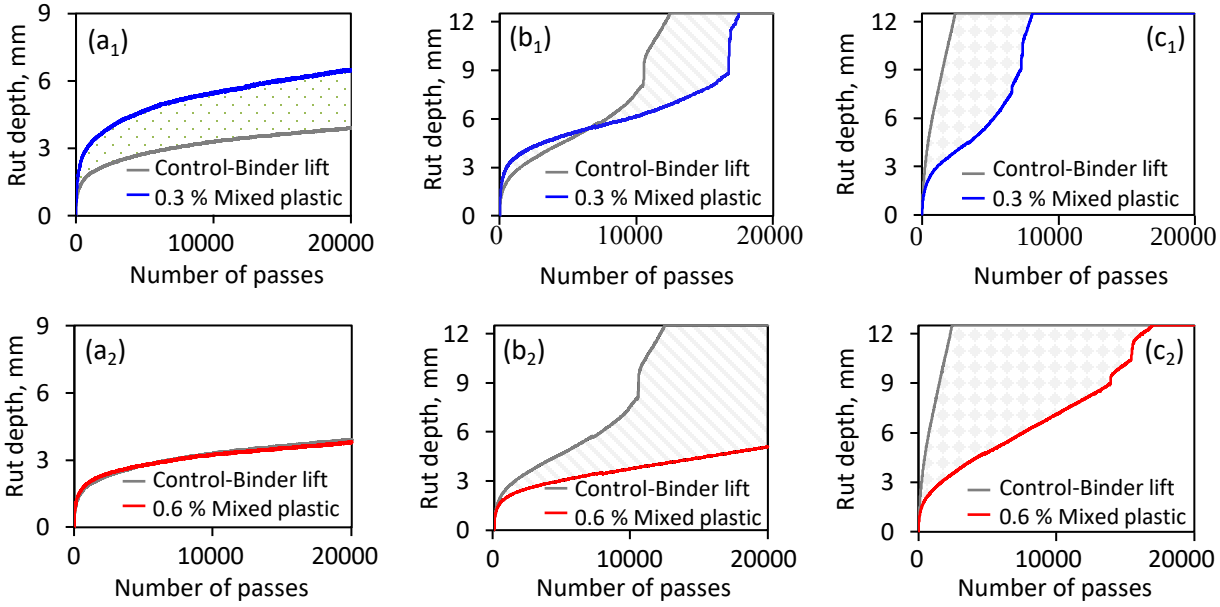

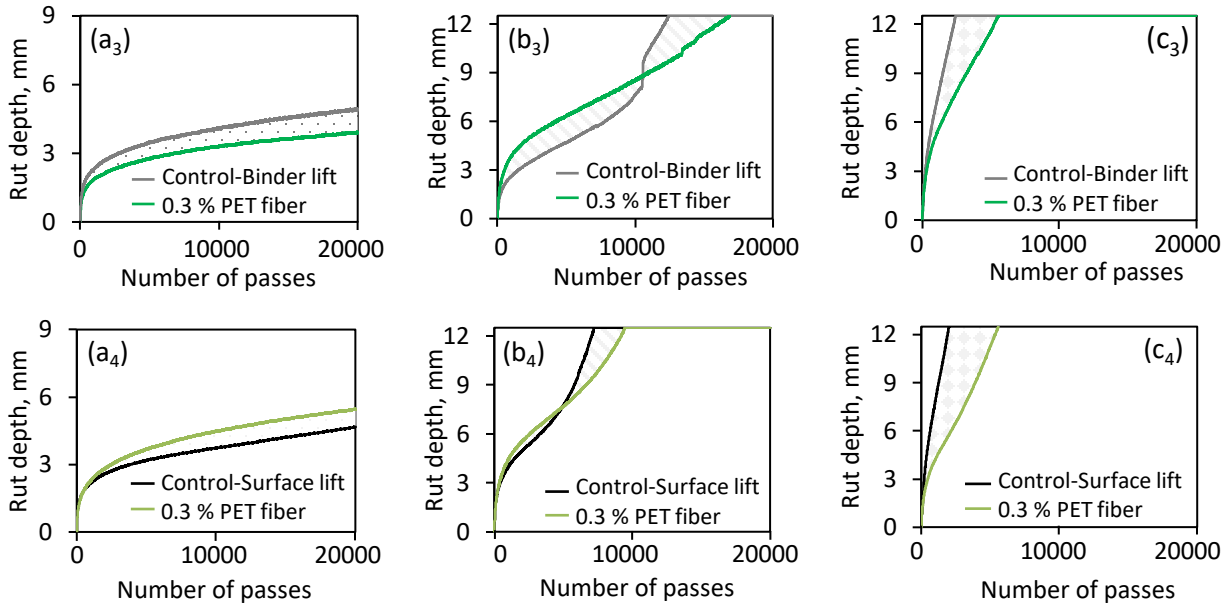

Figure 70. Effect of recycled plastics and fiber on the rutting resistance of asphalt mixture.

Note: Letter (a), (b), and (c) represents 30°C, 40°C and 50°C, respectively. The number in lowercase 1, 2, and 3 represents rut depth of binder lifts modified with 0.3 % mixed plastics, 0.6 % mixed plastics, and 0.3 % PET fiber in comparison to the control binder lift without modification. The number in lowercase 4 represents the surface lift modified with 0.3 % PET fiber in comparison to that without modification.

The influence of recycled plastics and fibers on the rutting resistance of asphalt mixtures was analyzed by examining the change in the area under the rutting curve and the number of passes, as depicted in Figure 70. This analysis, as detailed in Figure 71, involved calculating the percentage increase or decrease in this area. It is important to note that a negative percentage change indicates a detrimental effect of recycled plastics or fibers on rutting resistance, while a positive change indicates an improvement. The magnitude of this percentage change is directly proportional to the extent of the negative or positive impact on rutting resistance. The data from Figure 71 clearly illustrates that the impact of these materials is highly dependent on temperature. At lower temperatures, a 0.3 % addition of mixed plastic significantly reduces the rutting resistance of the binder course. Increasing the mixed plastic content to 0.6 % results in only a marginal improvement in resistance. Conversely, adding 0.3 % PET to the binder course decreases its rutting resistance, though not as drastically as the 0.3 % mixed plastic. In contrast, incorporating 0.3 % PET fiber into the surface course markedly enhances its rutting resistance. As the test temperature rises to 40°C, the effect of mixed plastic becomes more pronounced, improving the rutting resistance of the binder course core sample in correlation with increased plastic content. However, the impact of 0.3 % PET fiber on the rutting resistance remains relatively unchanged for both the binder and surface lifts at this temperature. When the temperature is further increased to 50°C, the addition of recycled plastic and PET fiber generally increases the rutting resistance of both binder and surface course samples. Specifically, the positive impact of mixed plastic on the resistance of binder course samples escalates with higher plastic content. In comparison, at the same concentration, mixed plastic demonstrates a more significant

improvement in the rutting resistance of binder course samples than PET fiber. For surface lifts, a 0.3 % PET fiber content more noticeably enhances rutting resistance compared to its effect on binder lifts.

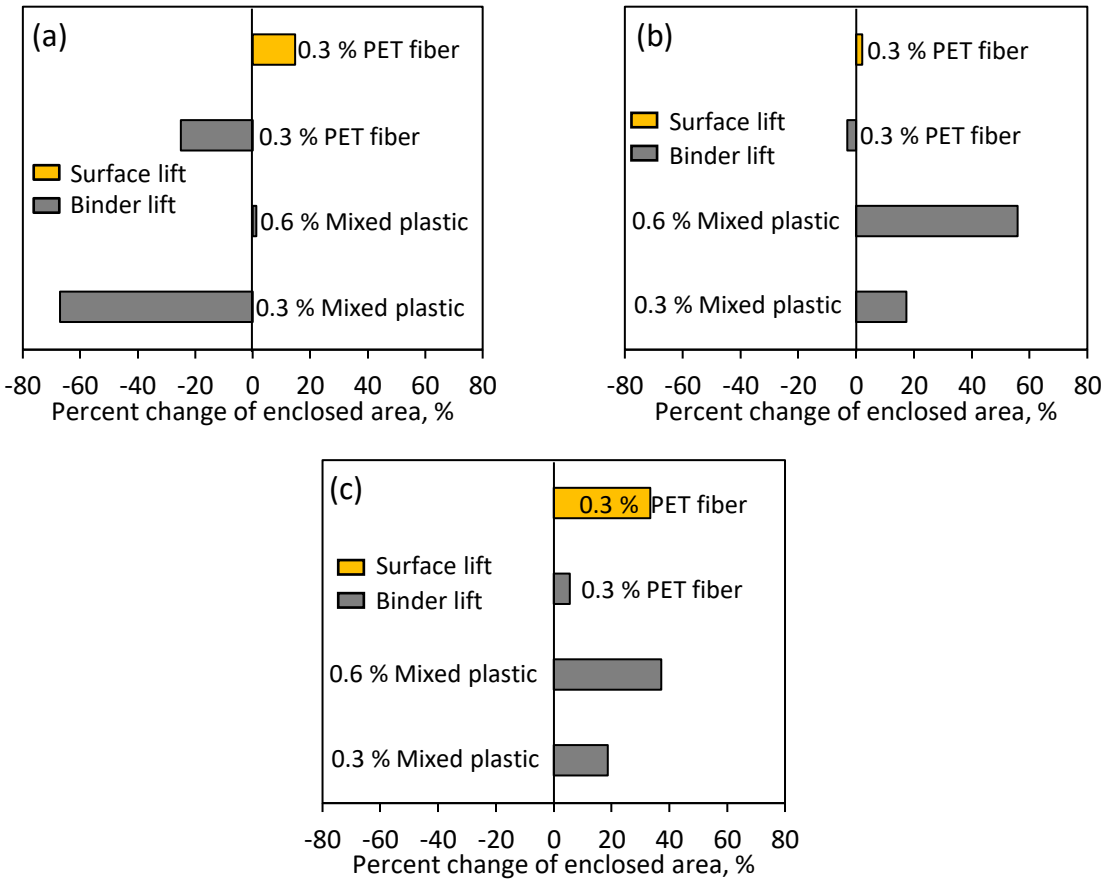

Figure 71. Quantification of the effect of recycled plastics and fiber on the rutting resistance.

(a) 30°C; (b) 40°C; (c) 50°C. Note: negative value indicates negative effect while positive value indicates positive effect.

4.6.3 Summary and Conclusions

This section assessed core samples and loose mixtures from a newly constructed asphalt pavement trial in Ontario, Canada. This trial is the second phase of our ongoing research program on the use of recycled plastics in asphalt pavement construction in cold regions. Rutting resistance was analyzed using the HWT test. The key findings are as follows: At 30°C, both plastic and fiber negatively affect rut resistance of coarse-graded asphalt mixtures in binder lifts, whereas PET fiber has a positive impact on fine graded mixture in surface lifts. At 40°C, mixed plastic significantly enhances the rutting resistance of coarse-graded mixtures, with effectiveness increasing alongside plastic content. However, PET fiber at 0.3 % content shows minimal change in rutting resistance for both coarse and fine-graded mixtures. At 50°C, the influence of mixed plastic on coarse-graded mixture rut resistance increases, while the same PET fiber content proves more effective in fine-graded mixtures.

4.7 Field Performance of Contract Pavements and Its Relation with Binder Properties

The best way to manage the performance lifespan of road surfaces is to test recovered asphalt binder for acceptance during construction. In the late 1990s, acceptance specifications advanced from using empirical methods, such as penetration and viscosity on unaged binder in the Canadian General Standards Board (CGSB) specification of 1990 to Superpave™ rheology-based tests on unaged and laboratory-aged residue. In the early 2000s, Ontario agencies realized that poor-quality binder was responsible for premature and excessive cracking of road surfaces, after which, enhanced aging, rheological and failure tests for unaged and recovered material were developed and implemented. This study correlates pavement service lives in Durham Region with recovered binder properties. Service lives to a PCI of 50 % – which had decreased by about 66 % since 1980 – bounced back immediately after the 2014 implementation of the DENT (AASHTO T 405) and EBBR (AASHTO T 406) protocols for the acceptance of recovered binder. Both protocols favor the use of superior quality Alberta binders. Today, proper designs based on EBBR grade and grade loss in conjunction with DENT critical CTOD have restored pavement service lives from a dismal 11 years in 2014 to their former 35-40 years.

4.7.1 Materials and Methods

In this section, a total of 41 hot mix asphalt (HMA) samples were obtained through Durham Region's quality assurance sampling program during the construction phase of new asphalt pavements between 2015 and 2021. Subsequently, these samples underwent careful extraction and recovery processes and accelerated pressure aging vessel (PAV) aging to produce residue for further testing. All binders were tested according to AASHTO T 405 DENT and AASHTO T 406 EBBR standardized protocols. Additional binders were tested but not included in this study as precise location information was unavailable. Other binders have since been recovered and tested but these are also omitted from this analysis as early pavement condition data cannot be used to project pavement service life with sufficient accuracy.

Pavement condition evaluation is a critical element of all pavement management systems, aimed at ensuring roads remain functional. This evaluation facilitates the timely implementation of necessary rehabilitation measures to extend the service life of roads, thereby delaying the need for reconstruction. The pavement condition index (PCI) is a quantitative index that measures the overall condition of a road surface. It consists of two major components: the ride comfort rating (RCR) and the distress manifestation index (DMI). The RCR represents the functional performance of the road, such as roughness; and is assigned a value between 0 and 10 to indicate the ride quality. In contrast, the DMI reflects the structural integrity; and quantifies the degree of pavement distress.

These two components should be obtained by considering the total length of road section that has a single pavement condition. Given that RCR assesses driving ease, comfort and safety, factors compromising the RCR include excessive or uneven crowning, washboarding, raveling and bumpiness resulting from issues, such as cracking, sealing and uneven patching. These inadequacies are critical when evaluating the overall quality of the driving experience. This assessment can be conducted subjectively or with mechanical devices, such as the portable universal roughness device (PURD) and the Mays ride meter (MRM). In this study, both methods were employed to obtain the PCI. For DMI, distresses were classified into 27 categories, and a detailed guideline was provided to determine the severity of each type of distress (Hajek

et al., 1986; Phang and Chong, 1981). In this study, DMI was calculated as per Eq. (31).

$$DMI = \sum_{i=1}^{n} w_i (s_i + d_i) \tag{31}$$

Where w_i is the weighting value for each distress; s_i and d_i are the severity and the density of distresses, respectively, both on a scale from 0 to 4. The PCI can be calculated through Eq. (11).

$$PCI = \sqrt{100 \cdot (0.1 \cdot RCR)} \cdot \frac{(205 - DMI)}{205} \times c + s \tag{32}$$

where *c* and *s* are calibration constants. If RCR is calculated by PURD, then *c* is 1.077 and *s* is 0. If RCR is determined subjectively, *c* and *s* are 0.924 and 8.856, respectively (Hajek et al., 1986). The primary methodology employed by Durham Region for reporting the PCI involves two key components: structural adequacy and surface condition. The structural adequacy, representing distress manifestations, is scored between 0 and 20, while the surface condition, corresponding to the RCR, ranges from 0 to 10. These components are evaluated periodically by an experienced consultant. The PCI calculation involves multiplying structural adequacy by surface condition, followed by division by 2 to yield a PCI score out of 100. This scoring method has been applied across all road section PCI values discussed.

Ontario municipalities use different evaluation strategies, such as the Inventory Manual, overall condition index, pavement quality index, structural adequacy index, and PCI. However, for paved roads, municipalities are now required to report an average PCI value at regular intervals. While the RCR and structural adequacy can be measured precisely by using automated or mechanical methods, the most common procedure is a visual inspection of the pavement. Video imaging or scan-type methods have been developed to survey distresses but they are not widely accepted as they are prone to pick up artifacts.

In the current study, the results of yearly field surveys for distresses in different road segments were sourced from the Durham Region Infrastructure for Roads Report. This report provides a comprehensive overview of each road section, including the PCI, length, and year of construction or major rehabilitation. The dataset obtained encompasses 968 road sections, cumulatively spanning about 410 kilometers. In addition to the PCI assessments, data on the average annual daily traffic (AADT) was also extracted. The AADT estimates the average daily traffic volume for a particular road segment over the span of one year, and was categorized into four levels, as outlined in Table 19.

Table 19. Number of road segments and length in each AADT category.

AADT	Segments	Total length, km
< 5000	129	85
5000-10000	140	80
10000-20000	171	68
> 20000	136	32

4.7.2 Service Life Changes for Durham Region Pavements

In this study, PCI results for 968 road segments dating as far back as 1976 were included. For pavements constructed in the same year that thus have the same age, the mean PCI was calculated, and the findings shown in Table 20. The lifespan of each road section was determined by either the realized service life (i.e., the point at which PCI reached 20 % and 50 %) or the projected one, using PCI data from 2018 to 2023. The service lives for road segments constructed were obtained by linear fitting of the average PCI versus age data and forcing the lines through 100 % at age zero as shown in Figure 72 (a) for a select number of ages. The findings for all segments are shown in Figure 72 (b).

Table 20. Mean PCI values for all segments constructed or rehabilitated (1976-2021).

Last Construction	Age, years	Segments	Mean Pavement Condition Index (PCI) %				
			2018	2019	2020	2021	2023
1976	48	1	18	18	18	15	15
1979	45	7	32	40	40	29	26
1981	43	1	42	42	39	38	32
1983	41	4	18	18	18	18	19
1984	40	3	29	28	24	25	21
1986	38	4	48	48	45	43	42
1987	37	19	24	23	22	22	22
1988	36	5	42	37	36	33	26
1989	35	9	45	45	38	38	37
1990	34	28	22	21	17	17	16
1991	33	19	31	31	28	28	24
1992	32	10	50	47	46	45	37
1993	31	24	27	28	27	26	25
1994	30	60	37	35	32	31	29
1995	29	11	53	51	50	45	45
1996	28	27	43	42	39	39	35
1997	27	36	45	42	37	36	35
1998	26	19	50	50	45	46	41
1999	25	15	38	35	31	29	27

2000	24	13	53	42	41	36	32
2001	23	28	54	51	45	43	37
2002	22	38	54	49	43	42	36
2003	21	21	63	59	54	47	44
2004	20	15	51	44	40	37	32
2005	19	19	50	45	41	39	34
2006	18	33	56	48	46	40	37
2007	17	14	57	55	47	38	34
2008	16	32	70	65	60	55	50
2009	15	60	68	65	58	55	50
2010	14	53	67	62	57	52	51
2011	13	22	69	68	65	63	58
2013	11	29	69	65	63	58	56
2014	10	9	93	90	85	72	69
2015	9	43	90	90	87	85	80
2016	8	51	88	89	85	84	83
2017	7	22	91	90	86	84	82
2018	6	22	87	91	89	88	84
2019	5	42	---	94	96	92	89
2020	4	36	---	---	97	96	95
2021	3	58	---	---	---	93	92

The average results are shown in Figure 72 (b), which shows an enormous 66 % reduction in average pavement service life over just 28 years, dropping from 33 years in 1986 (average of 4 segments) to just 11 years by 2014 (average of 9 segments). This agrees with the 50-60 % decrease in the average service life for provincial roads in Ontario over 25 years, as reported on by the Office of the Auditor General of Ontario in 2016. With the progressive application of modifiers and recycled asphalt, the Superpave performance acceptance tests, as implemented in the late 1990s, appear to have had no beneficial effect on improving asphalt durability. This contrasts starkly with data after 2015 when the improved specifications were implemented. Asphalt contaminated with harmful modifiers or additives such as REOB, RAP or recycled asphalt shingle can easily pass the Superpave acceptance tests, and this has had devastating consequences for network sustainability.

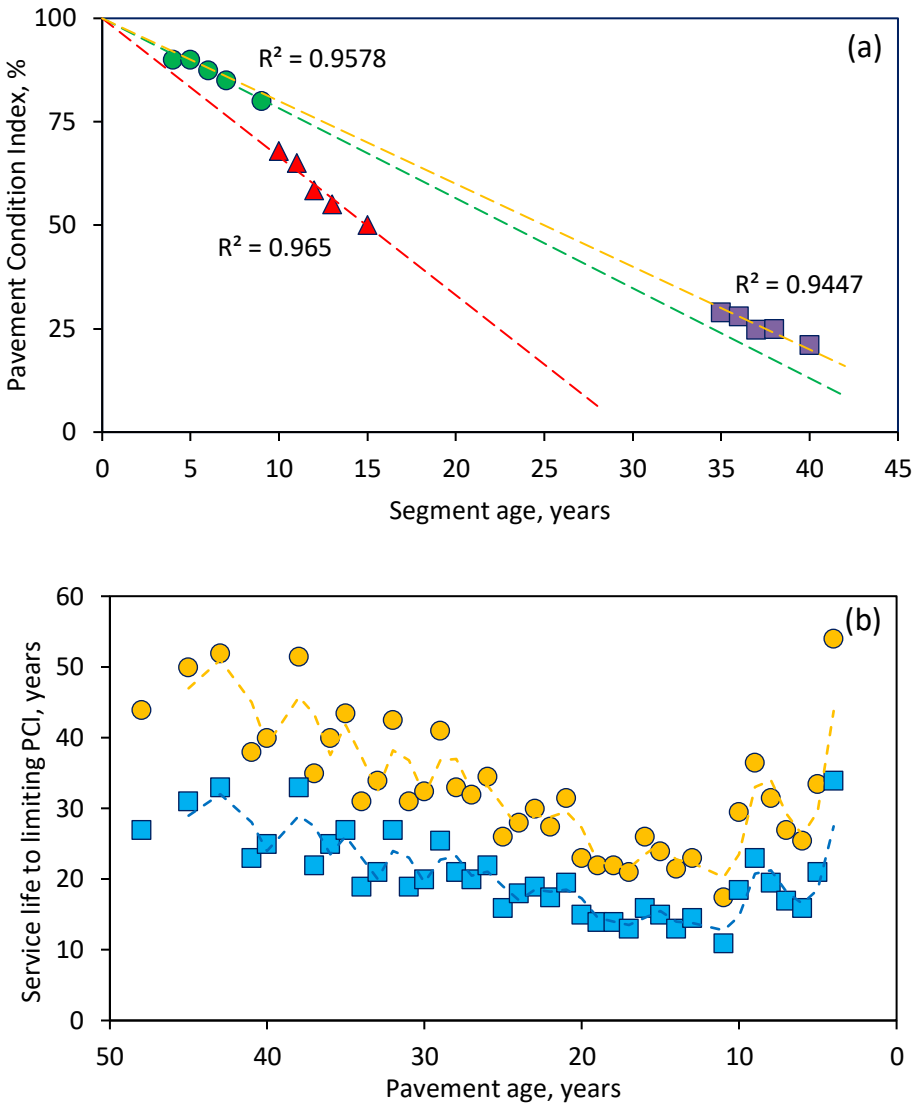

Figure 72. Historical service lives for 968 Durham Region road segments over 50 years.

(a) Extrapolations used to determine realized and projected average service lives (gold squares for 1984 segments (3 locations, 40 years old, realized average service life = 25 years), red triangles for 2009 segments (43 locations, 15 years old, realized average service life = 15 years), green circles for 2015 segments (47 locations, 9 years old, projected average service life = 23 years), (b) Average service lives versus age for 968 road segments (gold circles for 20 % PCI limit, blue squares for 50 % PCI limit, 1984 (25 years), 2014 (11 years) and 2020 (34 years)).

4.7.3 Effect of Traffic on Deterioration Rate

Traffic volume plays a crucial role in influencing the quality of asphalt pavement. With the availability of AADT data for all road segments, the following discussion examines the impact of traffic volume on the PCI deterioration rate. To facilitate this analysis, the AADT ratings were categorized into four groups. PCI

data corresponding to each group are presented in Figure 73. To better understand the effect of the specification changes, the PCI data within each group have been separated into two subgroups: before and after the implementation of the enhanced specifications in 2015. Figure 73 shows the difference in the obvious deterioration rate of pavement condition before and after 2015 for lower traffic volumes (AADT < 20,000). The main reason why there is no significant improvement for high-volume roads might be that the enhanced testing methods only fail binders that are prone to thermal cracking but they are less useful to control rutting distress. In the case of high-traffic volumes, rutting may be the dominant cause of deterioration of the pavement PCI. This issue deserves further investigation as the realized service lives for these roads are not impressive at around 16-17 years.

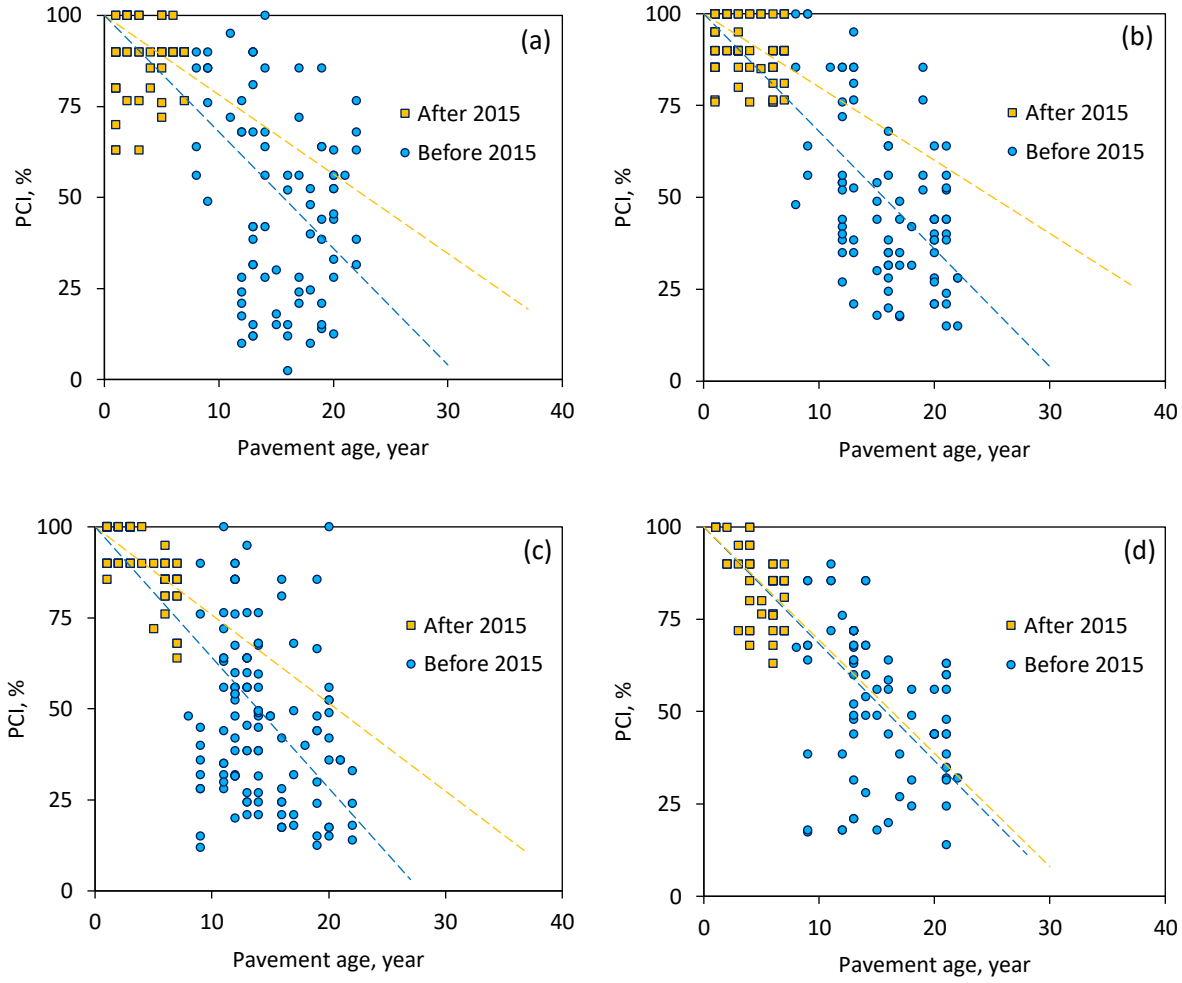

Figure 73. Plot of PCI versus pavement age for different traffic levels.

(a) AADT ≤ 5,000 (87 road segments before 2015 and 42 after 2015); (b) 5,000 < AADT ≤ 10,000 (83 road segments before 2015 and 57 after 2015); (c) 10,000 < AADT ≤ 20,000 (123 road segments before 2015 and 48 after 2015); (d) AADT > 20,000 (78 road segments before 2015 and 58 after 2015).

4.7.4 Effect of Binder Properties on Deterioration Rates

In this section, the latest PCI data obtained from the 2023 Durham Region Infrastructure for Roads Report for segments constructed and rehabilitated from 2015 to 2021, representing pavements constructed under the enhanced specifications, were compared with data from 2000 to 2014, associated with roads built according to Superpave specifications (AASHTO R 320, 2023). To clarify the trends, the mean PCI deterioration rates for asphalt roads constructed in the same year were calculated and are given in Figure 74. Additionally, the standard deviation for each PCI deterioration rate on the graph was provided to illustrate the variability in PCI data among different roads in each year. The change in PCI deterioration rate with pavement age for asphalt pavements constructed before versus after 2015 demonstrated a significant change for the better, with a reduction of around 40 % after 2015. Error bars provide confidence limits of 95 %. The average decay rate for blue is 3.5 %/year while average decay rate for gold is 2.1 %/year, a nearly 40 % improvement.

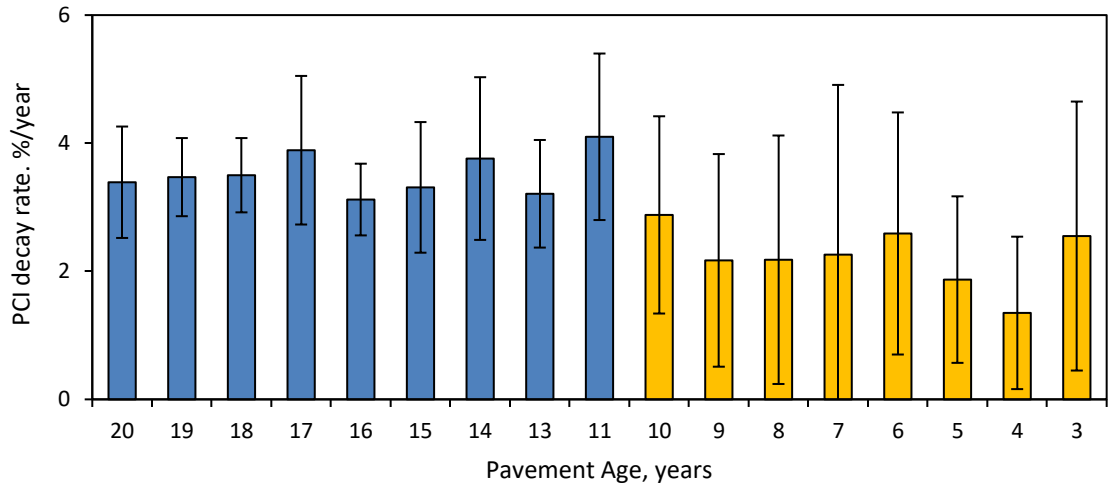

Figure 74. Mean PCI decay rate versus pavement age for pavements before and after 2015.

4.7.5 Effect of Recovered Binder Properties on PCI Deterioration Rates

Based on the above analysis, it can be concluded that the durability of asphalt pavement can be substantially enhanced by adopting enhanced binder testing methods. These improved testing protocols can identify asphalt binders that may detrimentally impact durability – a level of discrimination not attainable with conventional binder testing approaches that are uncoupled from performance. To substantiate this hypothesis, asphalt binders from different pavement sections with known field performance data in Durham Region were evaluated using EBBR and DENT tests. The grade loss as an estimation of thermo-reversible aging was determined through AASHTO T 406 EBBR testing while the CTOD was calculated from the AASHTO T 405 DENT test. Our previous studies on trial sections and prematurely-failed contracts have shown that low-temperature cracking resistance of asphalt binder can be improved by limiting grade loss and increasing the CTOD.

A threshold grade loss of 3°C was established to categorize the road sections into two groups. The 3°C limit was highly discriminating for a series of eastern Ontario paving contracts with extraordinary variability in performance. Linear regression analysis was then applied separately to these two datasets as shown in Figure 75 (a). Additionally, an EBBR LLTPG threshold of −28°C was employed to divide the PCI data into two additional groups, facilitating linear fitting to predict the lifespan of asphalt roads constructed with binders exhibiting diverse low-temperature EBBR grades, as shown in Figure 75 (b). A limit on the DENT CTOD of 14 mm was used to assess the effect of ductile strain tolerance on pavement durability, the results of which are shown in Figure 75 (c).

It can be deduced from Figure 75 that asphalt roads built with binders characterized by better EBBR and DENT performance generally exhibit greatly extended service lives. Decay rates are all reduced by around twofold under stricter acceptance criteria. In contrast, the current asphalt performance standard AASHTO R 320 is unlikely to differentiate asphalt binder with different cracking resistance. The AASHTO R 320 standard employs a fatigue factor to evaluate the fatigue-cracking resistance of asphalt binders. For thermal-cracking resistance, creep stiffness and the stress relaxation rate were used to evaluate different asphalt binder, respectively. It is obvious that the AASHTO R 320 standard overlooks thermo-reversible aging performance and high-strain failure characteristics of asphalt binders. Extensive validation efforts have demonstrated that these two properties are crucial in determining the overall cracking resistance of asphalt pavements. The findings presented in Figure 75 further confirm that the field performance of asphalt pavements can be enhanced significantly by controlling the degree of thermo-reversible aging, gelation and ultimately the failure resistance of the asphalt binder. This conclusion is in broad agreement with the work of McLeod (McLeod, 1978) and our own work on numerous pavement trials and prematurely-cracked regular contracts (Ding et al., 2017; S. A.M. Hesp et al., 2009a, 2009b; Hesp and Shurvell, 2012; S. A. M. Hesp et al., 2009; Rigg et al., 2017).

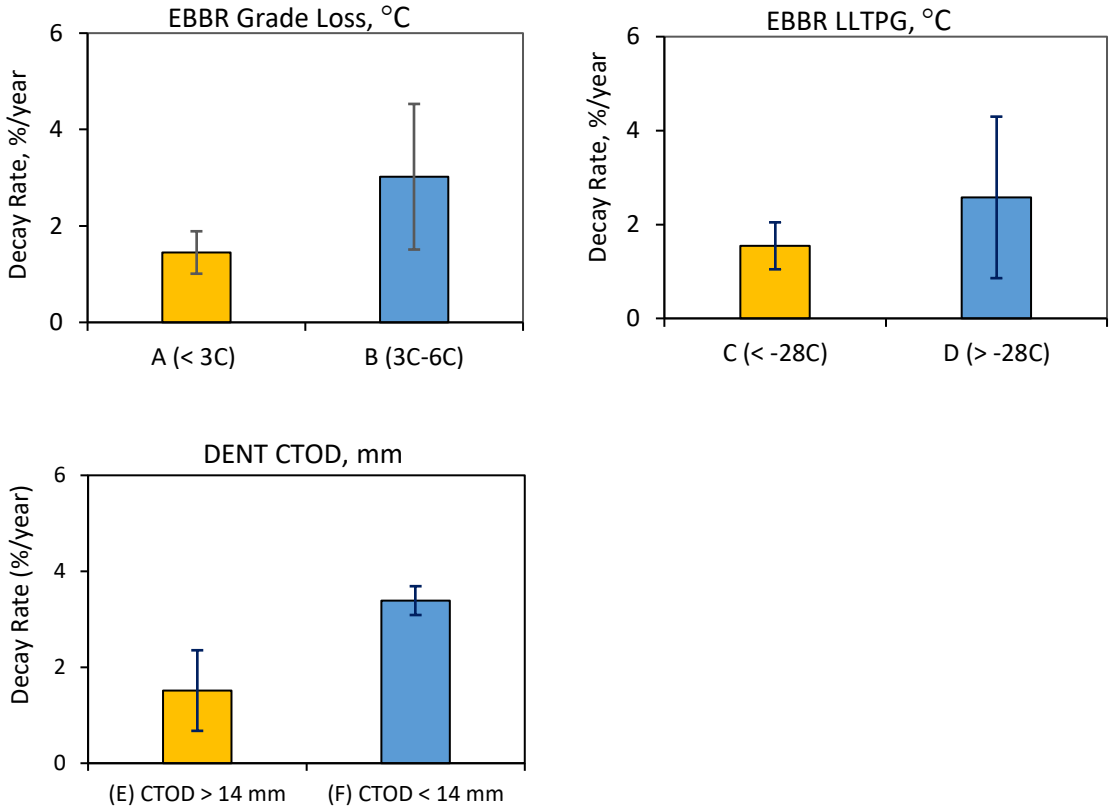

Figure 75. Variation in PCI over the service life of different asphalt roads.

(A) Grade loss < 3°C (32 segments), (B) Grade loss > 3°C and < 6°C (9 segments), (C) LLTPG < −28°C (33 segments), (D) LLTPG > −28°C (9 segments), (E) CTOD > 14 mm (35 segments), and (F) CTOD < 14 mm (6 segments). Decay rates are all reduced by around twofold under the stricter acceptance criteria.

4.7.6 Summary and Conclusions

This study performed a comprehensive analysis of PCI data for 968 asphalt road segments in the Regional Municipality of Durham, Ontario, Canada, dating back to the late 1970s. The average service life for these roads since the 1970s was assessed to show how asphalt binder acceptance criteria affect durability and (in the long run) sustainability. Further, a correlation analysis for service lives with DENT and EBBR results was used to validate the effectiveness of the innovative acceptance testing criteria implemented since ~2010. The main observations and conclusions are:

(1) The average service life of asphalt pavements in Ontario fell dramatically between 1986 and 2014, despite the implementation of Superpave specifications and the use of increased levels of polymer modifiers. This decline can partially be attributed to incomplete and hence inaccurate Superpave binder specifications. Superpave fails to address the well-documented thermo-reversible aging effect in asphalt binders, which has introduced a gradually-increasing bias error in the acceptance specifications. This error always disadvantages user agencies and ultimately the taxpayer. The increased use of RAP and possibly

REOB in the HMA supply chain is likely to explain why pavements are under-designed by ever-increasing amounts.

(2) Traffic volume significantly influences the deterioration rate for ride quality and distress manifestation. Lower traffic-volume roads (AADT < 20,000) have shown noticeable improvements in performance after 2015 due to the implementation of AASHTO T 405 DENT and AASHTO T 406 EBBR acceptance criteria. However, at higher traffic volumes, fatigue cracking due to structural design insufficiencies and rutting might predominate, reducing the effectiveness of the enhanced binder testing methods. This issue deserves further investigation as the 16-17-year service lives currently obtained for major arterial roads in Durham Region is substandard.

(3) The adoption of advanced performance acceptance specifications, specifically EBBR and DENT test methods, after 2015 led to a marked improvement in pavement durability. Analysis shows a 40 % increase in the service life of pavements constructed after 2015 compared to those built between 2000 and 2014, highlighting the critical role of these testing methods in extending pavement life. Service lives have increased by as much as threefold between the construction years of 2014 and 2021.

(4) The intrinsic performance-based properties of asphalt binders, as determined by EBBR and DENT tests, significantly affect field performance. Asphalt binders with lower grade loss and higher CTOD values contribute to extended pavement durability. The findings emphasize the necessity of applying enhanced binder testing protocols to identify and mitigate potential durability issues, suggesting that current standards may be inadequate for differentiating asphalt binder performance effectively.

KEY LEARNINGS

Please provide a narrative that discusses the key learnings from the project.

- Describe the project learnings and importance of those learnings within the project scope. Use milestones as headings, if appropriate.
- Discuss the broader impacts of the learnings to the industry and beyond; this may include changes to regulations, policies, and approval and permitting processes

RESPOND BELOW

The key learnings from the research can be summarized as follows:

(1) Simplified Performance Grading Protocol for Recovered Binder

The development of a practical and accurate performance test method that uses an exceedingly small quantity of asphalt binder extracted and recovered from loose mixture has been completed. It is important to implement such a protocol as it will allow Alberta binder to better compete in the marketplace based on quality and durability attributes. Currently, simple purchase agreements control materials acceptance in road construction, and user agencies are left to trust sellers that a quality product is offered. This leaves superior asphalt from Alberta at a competitive disadvantage, as existing specifications are far from accurate or complete. With the increasing use of recycled asphalt pavement (RAP) in road construction, extraction and recovery of binders from mixtures as placed becomes a critical

aspect of quality assurance testing. However, current extraction and recovery methods are associated with shortcomings, as they are often time consuming, costly, inaccurate and involve toxic solvents. The objective of this part of our research program was to develop a practical and more environmentally friendly protocol for the accurate and precise acceptance testing of recovered binder. The process developed uses a low toxicity solvent for extraction (a mixture of 1,2-trans-dichloroethylene and a fluorinated ether), followed by simple filtration, evaporation and thin film aging. Residual solvent is removed during initial thin film aging and fines are found to have an insignificant effect on rheological properties of importance. More testing at lower cost to the user will mean better performing roads.

The results of this preliminary effort have been published in the Elsevier journal Construction and Building Materials. A second student will present a larger data set in a second paper to be published as part of the 8th International Conference on Bituminous Mixtures and Pavements in Thessaloniki, Greece.

(2) Testing and Evaluation of Model Systems and Commercial Contract Binder Samples

We have learned a great deal about the quality and durability of asphalt used around Canada and the USA by testing a significant number of model binders from prior pavement trials in northern Ontario, the new Durham Region trial on Regional Road 18, samples purposely formulated in the laboratory (wax, asphaltene and polymer modified), and over 300 different contract samples taken from storage tanks in asphalt plants and extracted and recovered from loose mixture as placed in contracts. In a nutshell, it is obvious that most agencies, except Durham and Peel Region in Ontario, under-design their pavements for thermal and fatigue cracking distress. Low temperature grades are on average 1-4°C warmer than the design value. Hence, thermal stresses can be nearly twice as high as critical, sooner or later leading to premature and excessive cracking distress.

We have found that the EBBR protocol, in combination with a simple DSR temperature sweep test, is able to assess binder stability in terms of its tendency to phase separate at low temperatures and exude oils. A significant number of Alberta binders have been tested and none lose oils when stored at low temperatures in alcohol in the EBBR (Figure 5 above). In contrast, commercial binders are found to permanently change – some by as much as a full 5°C – due to the detrimental effects of exudative hardening. The exudative hardening (sweating) causes roads to fail prematurely through weakening of the bond between mastic and coarse aggregate. The binder used for the new pavement trial in Durham Region was over-designed with a large quantity of SBS polymer and tends to sweat because of this. It loses as much as 5°C after conditioning for 72 hours at -24°C.

(3) Testing and Evaluation of Mixture Samples

We have finished the Hamburg and SCB testing of large numbers of asphalt mixtures. Hamburg test results are being compared with extracted and recovered asphalt binder test findings indicating that there is little to no correlation. Hence, future pavement design is best done with acceptance based on Hamburg test results. Another learning from the Hamburg tests is that a reasonable testing temperature is critical in evaluating the rutting performance of different asphalt mixtures. SCB test data are correlated with extracted and recovered binder rheological properties. Findings show that the binder properties are of equal or better precision and more readily obtained. Binder test results are more sensitive to cold

conditioning whereas SCB mixture test results have so far shown little change after cold conditioning although work on this issue is continuing. Binders that are unstable at low temperatures will perform less satisfactorily, hence it is important for the competitiveness of Alberta binder to develop and implement the correct asphalt binder and mixture tests. To improve the current SCB test method to differentiate good asphalt like Alberta binder from those tainted with inferior modifiers/additives, the current SCB testing method was improved by considering the thermo-reversible aging effect. The improved SCB method at a lower loading rate is expected to improve its sensitivity and precision in ranking the cracking resistance of asphalt mixture.

OUTCOMES AND IMPACTS

The following refereed journal articles, conference publications, student theses, and webinar presentation have resulted from the work conducted during the project (corresponding and/or presenting authors are tagged with an asterisk):

Refereed Journal Publications (Published)

1. Zhang, J., Ma, J.*, Hesp, S.A.M.* Development of a simple and quantitative oil exudation test for asphalt binder. Construction and Building Materials, 415 (2024) 135003.
2. Elliott, B., Mohanta, C., Nawarathna, H.M.C., Ma, J.*, Hesp, S.A.M.* Effects of thermo-reversible aging on the cracking resistance of asphalt mixtures in the semi-circular bend test. Transportation Research Record: Journal of the Transportation Research Board, 0(0) (2024) 03611981231225207.
3. Ma, J.*, Dean, G., Nawarathna, H.M., Hesp, S.A.M.* Development and validation of an accurate, precise and safe method for the acceptance testing of recovered asphalt binder. Construction and Building Materials, 409 (2023) 133960.
4. Ren, X., Ma, J.*, Hesp, S.A.M.* Another look at the semi-circular bend test for the performance ranking of hot mix asphalt. Construction and Building Materials, 395 (2023) 132367.
5. Sandrasagra, J., Ma, J.*, Hesp, S.A.M.* Understanding the field performance of asphalt binders in continental climates through modulated differential scanning calorimetry. Construction and Building Materials, 391 (2023) 131857.
6. McCloskey, K., Nivitha, M.R.*, Ma, J.*, Hesp, S.A.M., Krishnan, J.M. Effects of temperature and age on stress relaxation in straight and modified asphalt binders from a northern Ontario pavement trial. Road Materials and Pavement Design, 24(sup1) (2023) 336-351.
7. Ma, J.*, Nivitha, M.R.*, Hesp, S.A.M., Krishnan, J.M. Validation of empirical changes to asphalt specifications based on phase angle and relaxation properties using data from a northern Ontario, Canada pavement trial. Construction and Building Materials, 363 (2023) 129776.

Refereed Journal Publications (Submitted)

1. Ma, J.*, Yuan, H., Nawarathna, H.M.C., Hesp, S.A.M.* On the sustainable use of recycled plastics in pavement construction: Performance analysis of core samples from a trial in Newtonville, Ontario, Canada (2024, Submitted).
2. Yuan, H., Nawarathna, H.M.C., Ma, J.*, Hesp, S.A.M.* Ranking Low Temperature Cracking Performance of Asphalt Binders Based on Limiting Phase Angle Temperatures and Stress Relaxation Properties (2024, Submitted).

Conference Publications (Accepted)

1. Garvin, E., Ma, J.*, Hesp, S.A.M. Comparative analysis of tension-compression and shear oscillatory loading on the rheological response of asphalt binders from a Northern Ontario pavement trial. 20th International Conference on Cold Regions Engineering (ICCRE). Anchorage, Alaska, USA, May 13-16, 2024.
2. Elliott, B., Ma, J.*, Nawarathna, H.M.C., Mohanta, S.C. Hesp, S.A.M. Multiscale characterization of cracking resistance in asphalt: Link between binder and mixture tests. Anchorage, Alaska, USA, May 13-16, 2024.
3. Ma, J.*, Sandrasagra, J., Oriotis, N., Hesp, S.A.M.* Evaluating the phase compatibility of asphalt binders using modulated differential scanning calorimetry. 8th International Conference Bituminous Mixture and Pavements (ICONFBMP), Thessaloniki, Greece, 12-14 June 2024.
4. Zhang, J.*, Ma, J., Nawarathna, H.M.C., Hesp, S.A.M. Development and validation of a greener, safer, cheaper and faster alternative protocol for the quality assurance testing of recovered asphalt binders. 8th International Conference Bituminous Mixture and Pavements (ICONFBMP), Thessaloniki, Greece, 12-14 June 2024.

Masters Theses

1. Pramodya Undugoda. Evaluation of rheological master curve parameters for the practical specification grading of Canadian asphalt binders, April 2024.
2. Prabuddhika Dharmarathna. Exploring the Master Curve Parameters for Efficient Performance Grading of Asphalt Binders from the United States of America, April 2024.
3. Dariush Kokabi. Restoring the Lifespan of Road Pavement in Durham Region in Ontario, Canada, through Innovative Quality Assurance Testing of Recovered Asphalt Binder, September 2024.

Conference Presentations (Lectern or Poster, Completed and Accepted)

1. McCloskey, K., Nivitha, M.R.*, Ma, J.*, Hesp, S.A.M., Krishnan, J.M. Effects of temperature and age on stress relaxation in straight and modified asphalt binders from a Northern Ontario pavement trial. 10th International Conference of the European Asphalt Technology Association (EATA). Gdansk, Poland. June, 2023 (lectern presentation of journal publication 6 listed above).

2. Zhang, J., Ma, J.*, Hesp, S.A.M.* Effects of Thermo-reversible aging of asphalt binder on the stress relaxation spectrum. 60th Petersen Asphalt Research Conference (PARC). Laramie, WY, USA. July, 2023 (poster presentation).
3. Zhang, J., Mohanta, C.S., Nawarathna, H.M.C., Ma, J.*, Hesp, S.A.M.* Low temperature exudation of oils from asphalt. 60th Petersen Asphalt Research Conference (PARC). Laramie, WY, USA. July, 2023 (lectern presentation of refereed journal publication 1 listed above).
4. Elliott, B., Mohanta, C., Nawarathna, H.M.C., Ma, J.*, Hesp, S.A.M.* Effects of thermo-reversible aging on the cracking resistance of asphalt mixtures in the semi-circular bend test. 103rd Transportation Research Board (TRB) Annual Meeting. Washington, DC. USA, January, 2024 (poster presentation of refereed journal publication 2 listed above).
5. Garvin, E., Ma, J.*, Hesp, S.A.M. Comparative analysis of tension-compression and shear oscillatory loading on the rheological response of asphalt binders from a Northern Ontario pavement trial. 20th International Conference on Cold Regions Engineering (ICCRE). Anchorage, Alaska, USA, May 13-16, 2024 (poster presentation).
6. Elliott, B., Ma, J.*, Nawarathna, H.M.C., Mohanta, S.C. Hesp, S.A.M. Multiscale characterization of cracking resistance in asphalt: Link between binder and mixture tests. Anchorage, Alaska, USA, May 13-16, 2024 (poster presentation).
7. Ma, J.*, Sandrasagra, J., Oriotis, N., Hesp, S.A.M.* Evaluating the phase compatibility of asphalt binders using modulated differential scanning calorimetry. 8th International Conference Bituminous Mixture and Pavements (ICONFBMP), Thessaloniki, Greece, 12-14 June 2024 (oral presentation of conference paper 3 listed above).
8. Zhang, J.*, Ma, J., Nawarathna, H.M.C., Hesp, S.A.M. Development and validation of a greener, safer, cheaper and faster alternative protocol for the quality assurance testing of recovered asphalt binders. 8th International Conference Bituminous Mixture and Pavements (ICONFBMP), Thessaloniki, Greece, 12-14 June 2024 (oral presentation of conference paper 4 listed above).

Conference Publications (Submitted)

1. Kokabi, D., Ma, J.*, Nawarathna, H.M.C., Hesp, S.A.M.* Restoring the Lifespan of Road Pavement in Durham Region in Ontario, Canada, through Innovative Quality Assurance Testing of Recovered Asphalt Binder. Transportation Association of Canada (TAC), Vancouver, September 22-24, 2024 (full manuscript submitted).
2. Prabuddhika Dharmarathna, Pramodya Undugoda, Hai Yuan, Jianmin Ma, Chanaka Nawarathna and Simon A.M. Hesp. Roadmap for Returning North America's Asphalt Industry to Sustainability and True Circularity. Canadian Technical Asphalt Association, Edmonton, November 2024 (abstract submitted and full manuscript to be submitted by end of May 2024).

Additional Lectern and Webinar Presentations (No Manuscripts)

1. Simon Hesp*, Development and Implementation of Improved Asphalt Acceptance Specifications for Ontario Municipalities, Lectern Presentation, Annual Meeting, Municipal Engineers Association of Ontario, Toronto, Ontario, November 18, 2022. Approximately 30-40 municipal government attendees from Ontario.
2. Simon Hesp*, Bitumen Beyond Combustion Roundtable, Alberta Innovates, December 12, 2022. Total of 31 attendees of which 24 were senior federal and provincial government officials.
3. Simon A.M. Hesp*, Superior Pavement Performance Through Enhanced Specification of Asphalt Binders, Online Webinar, Southwest Jiaotong University, August 18, 2023. Approximately 35-40 attendees from industry and academic institutions around China.
4. Simon A.M. Hesp*, Asphalt Performance for 26 Canadian and US Agencies, Lectern Presentation, Annual Meeting, Northeastern State Materials Engineers Association (NESMEA), Providence, Rhode Island, October 24, 2023. Approximately 40-50 attendees from northeastern US State Departments of Transportation.
5. Simon A.M. Hesp*, Asphalt Performance for States of Kansas and Nebraska DOT Materials, WebEx Presentation, December 20, 2023.
6. Simon A.M. Hesp*, Asphalt Performance for Illinois Tollway Materials, Teams Presentation, January 22, 2024.
7. Simon A.M. Hesp*, Asphalt Performance for Western Federal Lands Materials, Teams Presentation, January 23, 2024.
8. Simon A.M. Hesp*, Asphalt Specification Harmonization for the Greater Toronto Area, Teams Presentation, February 7, 2023.
9. Simon A.M. Hesp*, Asphalt Performance for Caltrans DOT Materials, WebEx Presentation, February 14, 2024.
10. Simon A.M. Hesp*, Asphalt Performance for New Hampshire DOT Materials, WebEx Presentation, February 14, 2024.
11. Simon A.M. Hesp*, Asphalt Performance for States of Illinois, Michigan, Minnesota, Ohio Materials, WebEx Presentation, March 1, 2024.
12. Simon A.M. Hesp*, Increasing Service Life of Roads for the Regional Municipality of Durham, Teams Presentation, Ontario Public Works Association Webinar, March 27, 2024. Approximately 100 attendees from Ontario stakeholders.

BENEFITS

Please provide a narrative outline the project's benefits. Please use the subheadings of Economic, Environmental, Social and Building Innovation Capacity.

- **Economic:** Describe the project's economic benefits such as job creation, sales, improved efficiencies, development of new commercial opportunities or economic sectors, attraction of new investment, and increased exports.
- **Environmental:** Describe the project's contribution to reducing GHG emissions (direct or indirect) and improving environmental systems (atmospheric, terrestrial, aquatic, biotic, etc.) compared to the industry benchmark. Discuss benefits, impacts and/or trade-offs.
- **Social:** Describe the project's social benefits such as augmentation of recreational value, safeguarded investments, strengthened stakeholder involvement, and entrepreneurship opportunities of value for the province.
- **Building Innovation Capacity:** Describe the project's contribution to the training of highly qualified and skilled personnel (HQSP) in Alberta, their retention, and the attraction of HQSP from outside the province. Discuss the research infrastructure used or developed to complete the project.

RESPOND BELOW

• **Economic**:

The project has stimulated local employment through the involvement of academic researchers, technical staff, and collaborations with various transportation departments. By demonstrating the superior quality of Alberta asphalt, the project has positioned Alberta to capture a larger share of the North American asphalt market. This could lead to the development of new commercial opportunities, especially in the production and supply of high-quality asphalt. The improved asphalt specifications and demonstrable advantages in terms of durability and cost-effectiveness are likely to attract new investment from both domestic and international markets into Alberta's asphalt production sector. By demonstrating the superior performance of Alberta binder and standardize the purchase standard, Alberta asphalt could become a preferred paving material in other regions in the world, leading to increased exports to potential regions like India and China where demand for asphalt binder is still in a high level.

• **Environmental**:

The project's advancements in asphalt specifications are expected to extend the lifespan of asphalt roads, thereby reducing the frequency of rehabilitation and reconstruction, which in turn lowers the carbon footprint associated with road construction and maintenance. Good asphalt road with improved durability paved with Alberta asphalt binder could reduce the carbon dioxide emissions from vehicles since the delay induced by rehabilitation and reconstruction can be significantly reduced.

•**Social**:

Improved asphalt pavement quality enhances the accessibility and safety of roads leading to less cost induced by user delay. The use of high-quality Alberta asphalt ensures that infrastructure investments are long-lasting, safeguarding public and private investments in road infrastructure. The project engaged multiple stakeholders including local governments, transportation agencies, and industry partners, strengthening collaborative ties and fostering a sense of community and shared goals within the province. The advancements in asphalt specifications open up opportunities for local entrepreneurs to innovate in related sectors such as recycling of asphalt materials and development of complementary products like rejuvenators.

• **Building Innovation Capacity**:

The project has contributed significantly to the training of highly qualified and skilled personnel (HQSP) in Alberta by involving postdoctoral researchers, MSc students, and undergraduates in high-level research activities. By providing engaging research opportunities, the project helps students from Alberta at Queen's University. The project utilized advanced research infrastructure including new rheometers and spectrometers, enhancing the research capabilities at Queen's University. This not only supports current research but also lays the groundwork for future innovation in asphalt materials study.

RECOMMENDATIONS AND NEXT STEPS

Please provide a narrative outlining the next steps and recommendations for further development of the technology developed or knowledge generated from this project. If appropriate, include a description of potential follow-up projects. Please consider the following in the narrative:

- Describe the long-term plan for commercialization of the technology developed or implementation of the knowledge generated.
- Based on the project learnings, describe the related actions to be undertaken over the next two years to continue advancing the innovation.
- Describe the potential partnerships being developed to advance the development and learnings from this project.

RESPOND BELOW

Long-term Commercialization Plan

The primary goal is to implement the newly developed asphalt specifications across Alberta and eventually at a national and international level. This includes formal adoption by transportation agencies through policy changes and regulatory updates. Secondly, it is planned to collaborate with asphalt manufacturers and suppliers to produce and market the enhanced Alberta asphalt binder. The focus will be on demonstrating the economic and technical benefits of the new asphalt to the road infrastructure industry to facilitate widespread adoption. Subsequently, it is necessary to develop a branding strategy that

highlights the superior quality and sustainability of Alberta asphalt, positioning it as a premium product in the marketplace.

Actions for the Next Two Years

Continue the 15+ commissioned pavement demonstration projects to include a wider variety of asphalt binders, environmental and traffic conditions. This will provide robust data sets to validate the benefits of the new asphalt specification under diverse environmental conditions. Collect performance data from the demonstration trials. This data will be crucial for refining improved asphalt specifications and for convincing additional stakeholders of Alberta asphalt's enhanced performance characteristics. Host a series of workshops and seminars for potential clients and partners. These events will serve to educate stakeholders about the new specifications and the advantages of the asphalt produced with Alberta oil sands.

Potential Partnerships

Strengthen existing partnerships and forge new ones with key players in the asphalt manufacturing and road construction industries. These partnerships will be crucial for the practical application of research findings and for feedback on the asphalt performance in the field. Continue collaboration with academic institutions for independent verification of the research findings and further studies on the long-term impacts of the adopted asphalt specifications. This may include joint research projects, student engagements, and shared publications. Explore partnerships with international transportation agencies and asphalt producers. This will not only help in validating the asphalt in different climatic conditions but also assist in entering new markets outside Canada.

Please provide a narrative outlining how the knowledge gained from the project was or will be disseminated and the impact it may have on the industry.

RESPOND BELOW

This project focused on promoting the use of Alberta asphalt binder in road construction. It aimed to address the challenges posed by existing specifications which tend to favor inferior asphalt products due to imprecise testing protocols.

Dissemination Strategies

Nine papers have been published or to be published in high-impact journals which have a broad audience. Over twelve presentations were delivered at various conferences and webinars to hundreds of researchers within the industry, helping to disseminate the research findings extensively. As many as 18 pavement trials will be initiated in collaboration with multiple transportation agencies across North America. These projects will serve as practical demonstrations of the advantages of using Alberta asphalt binders. Collaborations with various transport departments and agencies in the U.S. and Canada allowed for extensive testing and validation of the project’s findings.

Industry Impact

The project influenced the adoption of improved specifications for asphalt binders, which could lead to broader industry acceptance of high-quality Alberta asphalt, thereby enhancing asphalt road durability and performance. By demonstrating the superior quality of Alberta asphalt binders, the project positioned Alberta to capture a larger share of the North American asphalt market. This could lead to increased market share and significant economic benefits for Alberta's asphalt producers.

Future Directions

The project has laid the groundwork for ongoing improvements in asphalt specifications and continued advocacy for the use of high-quality Alberta asphalt. The successful implementation of demonstration projects and continued publication and presentation efforts are expected to sustain the momentum gained from this project.

REFERENCES

AASHTO M320, 2016. Standard Method of Test for Performance Graded Asphalt Binder. American Association of State Highway and Transportation Officials, Washington D.C., USA.

AASHTO R 28, 2009. Accelerated Aging of Asphalt Binder Using a Pressurized Aging Vessel (PAV). American Association of State Highway and Transportation Officials, Washington D.C., USA. t American Association of State Highway and Transportation Officials.

AASHTO R29, 2015. Standard Practice for Grading or Verifying the Performance Grade (PG) of an Asphalt Binder. American Association of State Highway and Transportation Officials, Washington D.C., USA. Washington, DC, USA.

AASHTO T 319-15, 2008. Standard Method of Test for Quantitative Extraction and Recovery of Asphalt Binder from Asphalt Mixtures, Washington, D.C, USA.

AASHTO T 405, 2023. Standard Method of Test for Determination of Asphalt Binder Resistance to Ductile Failure Using Double-Edge-Notched Tension (DENT) Test. American Association of State and Highway Transportation Officials, Washington, D.C., USA.

AASHTO T 406, 2023. Standard Method of Test for Determination of Performance Grade of Physically Aged Asphalt Binder Using Extended Bending Beam Rheometer (BBR) Method. American Association of State and Highway Transportation Officials, Washington, D.C., USA.

AASHTO T-164, 2003. Quantitative Extraction of Bitumen from Bituminous Paving Mixtures, American Association of State Highway and Transportation Officials, Washington D.C., USA. 2003.

AASHTO T240-13, 2013. Effect of Heat and Air on a Moving Film of Asphalt Binder (Rolling Thin-Film Oven Test). American Association of State Highway and Transportation Officials, Washington D.C., USA. American Association of State Highway and Transportation Officials.

Al-Qadi, I.L., Ozer, H., Lambros, J., Khatib, A.E., Singhvi, P., Khan, T., Rivera-Perez, J., Doll, B., 2015a. Testing Protocols to Ensure Performance of High Asphalt Binder Replacement Mixes Using RAP and RAS. Illinois Center for Transportation.

Al-Qadi, I., Ozer, H., Lambros, J., Lippert, D., El Khatib, A., Khan, T., Singh, P., Rivera-Perez, J.J., 2015b. Testing Protocols to Ensure Performance of High Asphalt Binder Replacement Mixes Using RAP and RAS. Illinois Center for Transportation.

Andriescu, A., Hesp, S. A.M., 2009. Time-temperature superposition in rheology and ductile failure of asphalt binders. International Journal of Pavement Engineering 10, 229–240. https://doi.org/10.1080/10298430802169440

Bahia, H.U., Zhai, H., Zeng, M., Hu, Y., Turner, P., 2001. Development of binder specification parameters based on characterization of damage behavior (with discussion). Journal of the Association of Asphalt Paving Technologists 70, 442–470.

Baskin, C.M., 1935. American Society for Testing and Materials, Part II 35, 576–579.

Baumgaertel, M., Winter, H.H., 1989. Determination of relaxation and retardation spectra from dynamical mechanical data. Rheol Acta 28, 511–519.

Bhattacharjee, S., Swamy, A. K., Daniel, J. S., 2012. Continuous relaxation and retardation spectrum method for viscoelastic characterization of asphalt concrete. Mech Time Depend Mater 16, 287–305.

Bird, S., Matthews, M., Hesp, S.A.M., 2020. Extended high-temperature oven aging of loose hot mix asphalt and acceptance testing of the extracted and recovered asphalt binders, in: 7th Eurasphalt and Eurobitume Congress.

Branthaver, J.F., Petersen, J.C., Robertson, R.E., Duvall, J.J., Kim, S.S., Harnsberger, P.M., Mill, T., Ensley, E.K., Barbour, F.A., Schabron, J.F., 1993. Binder Characterization and Evaluation: Vol. 2 Chemistry (No. SHRP-A-368). National Research Council, Washington, DC.

Bricker, R. M., Hesp, S. A.M., 2013. Modulated differential scanning calorimetry study of physical hardening rates in asphalt cements, in: Airfield and Highway Pavement Conference. pp. 955–966.

Charlesworth, M., Swinton, F., 2017. Anaesthetic gases, climate change, and sustainable practice. Lancet Planet Health 1, e216–e217.

Claudy, P., Létoffé, J.-M., Chagué, B., Orrit, J., 1988. Crude oils and their distillates: characterization by differential scanning calorimetry. Fuel 67, 58–61.

Ding, H., Fong, S., S.A.M. Hesp, 2020. Laboratory aging and field performance of SBS-modified binders, in: Seventh Eurasphalt & Eurobitume Congress. Madrid, Spain.

Ding, H., Tetteh, N., Hesp, S. A.M., 2017. Preliminary experience with improved asphalt cement specifications in the City of Kingston, Ontario, Canada. Constr Build Mater 157, 467–475. https://doi.org/10.1016/j.conbuildmat.2017.09.118

Ding, H., Zhang, H., Liu, H., Qiu, Y., 2021. Thermo-reversible aging in model asphalt binders. Constr Build Mater 303, 124355.

Doi, M., Edwards, S., 1986. The Theory of Polymer Dynamics. Clarendon, Oxford, U.K.

Edwards, M. A., Hesp, S. A.M., 2006. Compact tension testing of asphalt binders at low temperatures. Transportation Research Record: Journal of Transportation Board 36–43. https://doi.org/10.3141/1962-05

Elliott, B., Mohanta, C., Nawarathna, H.M.C., Ma, J., Hesp, S.A.M., 2024. Effects of Thermo-Reversible Aging on the Cracking Resistance of Asphalt Mixtures in the Semi-Circular Bend Test. Transp Res Rec 0. https://doi.org/10.1177/03611981231225207

Evans, M., Marchildon, R., Hesp, S. A. M., 2011. Effects of Physical Hardening on Stress Relaxation in Asphalt Cements Implications for Pavement Performance. Transportation Research Record: Journal of the Transportation Research Board 2207, 34–42.

Farrar, M., Loveridge, J. L, Rovani, J., 2015. The Limit of Detection (LOD) Method : An FTIR Screening Tool for Evaluating Solvent Remaining after Extraction.Technical White Paper FP03. Western Research Institute, Laramie, WY.

Frolov, I. N., Okhotnikova, E. S., Ziganshin, M. A., Firsin, A. A., 2020. Interpretation of Double-Peak Endotherm on DSC Heating Curves of Bitumen. Energy & Fuels 34, 3960–3968.

Ge, D., You, Z., Chen, S., Liu, C., Gao, J., Lv, S., 2019. The performance of asphalt binder with trichloroethylene: Improving the efficiency of using reclaimed asphalt pavement. J Clean Prod 232, 205–212.

Hajek, J.J., Phang, W.A., Wrong, G.A., Prakash, A., Stott, G.M., 1986. Pavement condition index (PCI) for flexible pavements. Report PAV-86-02. . Downsview, Ontario, Canada.

Hesp, S. A. M., Genin, S.N., Scafe, D., Shurvell, H.F., Subramani, S., 2009. Five Year Performance Review of a Northern Ontario Pavement Trial: Validation of Ontario's Double-Edge-Notched Tension (DENT) and Extended Bending Beam Rheometer (BBR) Test Methods. Proceedings of Canadian Technical Asphalt Association 54, 99–126.

Hesp, S. A.M., Iliuta, S., Shirokoff, J. W., 2007a. Reversible aging in asphalt binders. Energy & Fuels 21, 1112–1121.

Hesp, S.A.M., Iliuta, S., Shirokoff, J.W., 2007b. Reversible aging in asphalt binders. Energy & Fuels 21, 1112–1121.

Hesp, S. A.M., Kodrat, I., Scafe, D., Soleimani, A., Subramani, S., Whitelaw, L., 2009a. Rheological testing of asphalt cements recovered from an Ontario pavement trial, in: 6th International Conference on Maintenance and Rehabilitation of Pavements and Technological Control (MAIREPAV6). Torino, Italy, pp. 1–10.

Hesp, S. A.M., Shurvell, H. G., 2012. Waste Engine Oil Residue in Asphalt Cement, in: Proceedings of Seventh International Conference on Maintenance and Rehabilitation of Pavements and Technological Control. Auckland, New Zealand.

Hesp, S. A.M., Soleimani, A., Subramani, S., Phillips, T., Smith, D., Marks, P., Tam, K. K., 2009b. Asphalt pavement cracking: Analysis of extraordinary life cycle variability in eastern and northeastern Ontario. International Journal of Pavement Engineering 10, 209–227. https://doi.org/10.1080/10298430802343169

Hesp, S. A.M., Terlouw, T., Vonk, W., 2000a. Low temperature performance of SBS-modified asphalt mixes. Asphalt Paving Technology 69, 540–573.

Hesp, S.A.M., Terlouw, T., Vonk, W., 2000b. Low temperature performance of SBS-modified asphalt mixes. Asphalt Paving Technology 69, 540–573.

Huang, J., Baird, D. G., 2002. Ratio of dynamic moduli and estimation of relaxation times. J Rheol (N Y N Y) 46, 777–795.

Erskine, J.A., Hesp, S.A.M., Kaveh, F., 2012. Another look at accelerated aging of asphalt cements in the pressure aging vessel., in: Fifth Eurasphalt & Eurobitumen Congress. Istanbul, Turkey.

Jing, R., Varveri, A., Liu, X., Scarpas, A., Erkens, S., 2020. Rheological, fatigue and relaxation properties of aged bitumen. International Journal of Pavement Engineering 21, 1024–1033. https://doi.org/10.1080/10298436.2019.1654609

Jones, D.R., 1993. SHRP materials reference library: Asphalt cements: A concise data compilation. Washington, DC.

Kaseer, F., Yin, F., Arámbula-Mercado, E., Martin, A.E., Daniel, J. S., Salari, S., 2018. Development of an index to evaluate the cracking potential of asphalt mixtures using the semi-circular bending test. Constr Build Mater 167, 286–298.

Killeen, P.R., 2005. An alternative to null-hypothesis significance tests. Psychol Sci 16, 345–353.

Kriz, P., Stastna, J., Zanzotto, L., 2008. Glass transition and phase stability in asphalt binders. Road Materials and Pavement Design 9, 37–65.

Lesueur, D., 1999. Letter to the Editor: On the thermorheological complexity and relaxation modes of asphalt cements. J Rheol (N Y N Y) 43, 1701–1704.

Liu, S., Peng, A., Wu, J., Zhou, S., 2018. Waste engine oil influences on chemical and rheological properties of different asphalt binders. Constr Build Mater 191, 1210–1220. https://doi.org/10.1016/j.conbuildmat.2018.10.126

López-Montero, T., Miró, R., 2016. Differences in cracking resistance of asphalt mixtures due to ageing and moisture damage. Constr Build Mater 112, 299–306.

Lou, K., Xiao, P., Ong, G., Li, B., Kang, A., Wu, Z., 2024. Micromechanical behavior of single fiber-asphalt mastic interface: Experimental studies by self-designed innovative pullout test. Constr Build Mater 414, 134873. https://doi.org/https://doi.org/10.1016/j.conbuildmat.2024.134873

Lu, X., Isacsson, U., 1998. Chemical and rheological evaluation of ageing properties of SBS polymer modified bitumens. Fuel 77, 961–972. https://doi.org/10.1016/s0016-2361(97)00283-4

Ma, J., Hesp, S. A.M., 2022. Effect of recycled polyethylene terephthalate (PET) fiber on the fracture resistance of asphalt mixtures. Constr Build Mater 342, 127944.

Ma, J., Hesp, S.A.M., Chan, S., Li, J.Z., Lee, S., 2022a. Lessons learned from 60 years of pavement trials in continental climate regions of Canada. Chemical Engineering Journal 444, 136389.

Ma, J., Hesp, S. A.M., Chan, S., Li, J. Z., Lee, S., 2021. Lessons learned from 60 years of pavement trials in continental climate regions of Canada. Chemical Engineering Journal 444, 136389.

Ma, J., Nawarathna, H. M.C., Hesp, S. A.M., 2022b. On the sustainable use of recycled plastics in flexible asphalt pavements. J Clean Prod 359, 132081.

Ma, J., Nivitha, M.R., Hesp, S.A.M., Krishnan, J. M., 2023. Validation of Empirical Changes to Asphalt Specifications Based on Phase Angle and Relaxation Properties Using Data from a Northern Ontario, Canada Pavement Trial. Constr Build Mater 363, 129776.

Majidifard, H., Jahangiri, B., Rath, P., Buttlar, W. G., 2021. Development of a balanced cracking index for asphalt mixtures tested in semi-circular bending with load-LLD measurements. Measurement 173, 108658.

Majidifard, H., Tabatabaee, N., Buttlar, W., 2019. Investigating short-term and long-term binder performance of high-RAP mixtures containing waste cooking oil. Journal of Traffic and Transportation Engineering (English Edition) 6, 396–406. https://doi.org/10.1016/j.jtte.2018.11.002

Masson, J. F., Collins, P., Polomark, G., 2005. Steric hardening and the ordering of asphaltenes in bitumen. Energy and Fuels 19, 120–122.

McLeod, N.W., 1978. Test data from three Ontario test roads after 15 years of service. Proceddings of Canadian Technical Asphalt Association 534–610.

McLeod, N.W., 1972. A 4-year survey of low temperature transverse pavement cracking on the three Ontario test roads. Proceddings of Association of Asphalt Paving Technologists 41, 424–493.

Nivitha, M.R., Devika, R., Murali Krishnan, J., Roy, N., 2022. Influence of bitumen type and polymer dosage on the relaxation spectrum of styrene-butadiene-styrene (SBS)/styrene-butadiene (SB) modified bitumen. Mech Time Depend Mater 27, 79–98.

Ozawa, T., 1971. Kinetics of non-isothermal crystallization. Polymer (Guildf) 12, 150–158.

Ozawa, T, 1971. Kinetics of non-isothermal crystallization. Polymer (Guildf) 12, 150–158.

Pérez-Jiménez, F., Botella, R., Moon, K.-H., Marasteanu, M., 2013. Effect of load application rate and temperature on the fracture energy of asphalt mixtures. Fénix and semi-circular bending tests. Constr Build Mater 48, 1067–1071.

Pfeiffer, J.P., Van Doormaal, P.M., 1936. The rheological properties of asphaltic bitumens. Journal of the Institute of Petroleum Technologists 22, 410–440.

Phang, W.A., Chong, G.J., 1981. Ontario Flexible Pavement Distress Assessment for Use in Pavement Management. Transportation Research Record: Journal of the Transportation Research Board 893, 51–59.

Ren, X., Ma, J., Hesp, S. A M, 2023. Another look at the semi-circular bend test for the performance ranking of hot mix asphalt. Constr Build Mater 395, 132367.

Rigg, A., Duff, A., Nie, Y., Somuah, M., Tetteh, N., Hesp, S. A. M., 2017. Non isothermal kinetic analysis of reversible ageing in asphalt cements. Road Materials and Pavement Design 18, 185–210.

Romberg, J.W., Nesmith, S.D., Traxler, R.N., 1959. Some chemical aspects of the components of asphalt. J Chem Eng Data 4, 159–161.

Rowe, G., 2014. Interrelationships in rheology for asphalt binder specifications, in: 59th Annual Conference of the Canadian Technical Asphalt Association. Winnipeg, Manitoba.

Roy, S.D., Hesp, S.A.M., 2001a. Fracture Energy and Critical Crack Tip Opening Displacement: Fracture Mechanics- Based Failure Criteria for Low-Temperature Grading of Asphalt Binders, in: 46 Th Annual Meeting of Canadian Technical Asphalt Association. Toronto , Ontario.

Roy, S.D., Hesp, S.A.M., 2001b. Low-Temperature Binder Specification Development: Thermal Stress Restrained Specimen Testing of Asphalt Binders and Mixtures. Transportation Research Record: Journal of the Transportation Research Board 1766, 7–14.

Roy, Sushanta D., Hesp, S.A.M., 2001. Low-Temperature Binder Specification Development: Thermal Stress Restrained Specimen Testing of Asphalt Binders and Mixtures. Transportation Research Record: Journal of the Transportation Research Board 1766, 7–14.

Roy, S. D., Hesp, S.A.M., 2001c. Fracture Energy and Critical Crack Tip Opening Displacement: Fracture Mechanics- Based Failure Criteria for Low-Temperature Grading of Asphalt Binders, in: 46 Th Annual Meeting of Canadian Technical Asphalt Association. Toronto , Ontario.

R.T.C. 50-FCM, 1985. Determination of the Fracture Energy of Mortar and Concrete by Means of Three-Point Bend Tests on Notched Beams. Mater Struct 18, 287–290.

Rubab, S., Burke, K., Wright, L., Hesp, S.A.M., Marks, P., Raymond, C., 2011. Effects of engine oil residues on asphalt cement quality, in: Canadian Technical Asphalt Association. pp. 1–12.

Sandrasagra, J., Ma, J., Hesp, S. A. M., 2023. Understanding the field performance of asphalt binders in continental climates through modulated differential scanning calorimetry. Constr Build Mater 391, 131857.

Sandrasagra, J., Ma, J., Hesp, S.A.M., 2022. Understanding the Field Performance of Asphalt Binders in Continental Climates through Modulated Differential Scanning Calorimetry. SSRN 4212683.

Shanbhag, S., 2019. pyReSpect: A Computer Program to Extract Discrete and Continuous Spectra from Stress Relaxation Experiments. Macromol Theory Simul 28. https://doi.org/10.1002/mats.201900005

Soleimani, A., Walsh, S., Hesp, S. A.M., 2009. Asphalt cement loss tangent as surrogate performance indicator for control of thermal cracking. Transportation Research Record Journal of the Transportation Research Board 2126, 39–46. https://doi.org/10.3141/2126-05

Son, S., Said, I. M., Al-Qadi, I. L, 2019. Fracture properties of asphalt concrete under various displacement conditions and temperatures. Constr Build Mater 222, 332–341.

Cser, F., Rasoul, F., Kosior, E., 1997. Modulated Differential Scanning Calorimetry. Journal of Thermal Analysis 50, 727–744.

Togunde, O. P., Hesp, S.A.M., 2012. Physical Hardening in Asphalt Mixtures. International journal of pavement research & technology. 5, 1–8.

Tsai, W. T., 2005. An overview of environmental hazards and exposure risk of hydrofluorocarbons (HFCs). Chemosphere 61, 1539–1547.

Verdonck, E., Schaap, K., Thomas, L.C., 1999. A discussion of the principles and applications of Modulated Temperature DSC (MTDSC). Int J Pharm 192, 3–20.

Wang, Y., Chong, D., Wen, Y., 2017. Quality verification of polymer-modified asphalt binder used in hot-mix asphalt pavement construction. Constr Build Mater 150, 157–166. https://doi.org/10.1016/j.conbuildmat.2017.05.196

Wright, L., Kanabar, A., Moult, E., Rubab, S., Hesp, S.A.M., 2011. Oxidative aging of asphalt cements from an Ontario pavement trial. International Journal of Pavement Research and Technology 4, 259–267.

Zhang, J., Ma, J., Hesp, S.A.M., 2024. Development of an oil exudation test for asphalt binder. Construction and Building Materials 415, 135003–135003. https://doi.org/https://doi.org/10.1016/j.conbuildmat.2024.135003

Zhou, F., Im, S., Sun, L., Scullion, T., 2017. Development of an IDEAL cracking test for asphalt mix design and QC/QA. Road Materials and Pavement Design 86, 549–577.

APPENDIX

A-Tables

Table A-1. AASHTO M 320 grades of asphalt binders.

Sample	HTPG, ˚C	ITPG, ˚C	LTPG, ˚C
1	82.0	18.5	-29.0
2	85.4	19.0	-28.6
3	70.4	23.3	-24.4
4	69.7	21.0	-27.3
5	68.1	20.3	-25.2
6	65.5	19.2	-26.9
7	65.5	20.0	-25.7
8	70.0	25.5	-25.5
9	86.9	19.9	-27.1
10	73.4	19.8	-26.0
11	68.3	21.0	-24.6
12	93.2	29.5	-20.3
13	91.2	29.5	-23.1
14	92.5	25.6	-24.2
15	84.0	25.9	-22.3
16	66.4	20.0	-26.6
17	81.3	27.0	-25.5
18	77.3	27.2	-23.0
19	73.2	26.3	-28.0
20	62.7	13.8	-32.7
21	64.5	13.6	-31.9
22	81.5	17.6	-30.2
23	82.2	12.5	-29.1
24	72.2	15.7	-32.7
25	75.8	14.0	-30.1
26	76.0	11.9	-34.9
27	75.1	16.6	-30.7
28	77.8	19.4	-28.4
29	68.0	20.4	-27.9
30	70.9	16.1	-33.0
31	74.8	16.3	-30.1
32	73.1	16.8	-32.4
33	75.4	16.8	-30.3

34	77.6	20.4	-29.9
35	72.6	16.4	-30.6
36	71.4	24.3	-27.0
37	68.9	22.8	-27.3
38	75.4	16.2	-31.3
39	75.0	17.6	-30.7
40	76.2	19.8	-30.4
41	74.3	16.4	-32.3
42	71.4	15.9	-32.7
43	72.0	18.8	-32.7
44	74.1	17.8	-29.7
45	70.8	17.5	-31.6
46	72.2	15.0	-30.4
47	70.3	19.3	-33.9
48	67.1	13.5	-34.8
49	69.0	14.2	-32.0
50	77.1	18.4	-30.3
51	79.4	16.3	-35.3
52	63.7	16.3	-33.0
53	62.1	15.1	-34.3
54	73.3	15.0	-32.7
55	73.8	9.6	-38.2
56	74.7	10.8	-36.0
57	76.6	12.4	-35.8
58	76.8	13.7	-35.2
59	73.3	11.2	-36.6
60	74.4	14.5	-35.3
61	75.6	14.7	-35.4
62	67.1	13.3	-34.4
63	72.1	18.2	-33.1
64	71.9	11.7	-35.4
65	71.9	13.5	-33.7
66	72.7	15.4	-33.6
67	73.3	13.2	-35.5
68	70.3	14.4	-33.1
69	74.4	13.4	-32.9
70	73.2	12.7	-30.0
71	76.0	14.2	-35.7

72	73.1	10.3	-34.9
73	72.1	11.2	-36.0
74	75.4	11.2	-33.6
75	72.9	15.0	-32.3
76	71.2	12.0	-35.6
77	71.2	16.2	-33.3
78	73.9	12.6	-32.4
79	73.8	10.9	-37.2
80	75.2	14.5	-33.3
81	72.3	13.5	-33.0
82	68.8	14.0	-29.8
83	74.0	10.3	-34.2
84	71.6	14.3	-33.0
85	64.7	10.2	-37.0
86	65.6	13.3	-34.0
87	70.4	15.3	-33.9
88	68.0	14.7	-32.3
89	70.8	11.5	-34.3
90	65.5	10.7	-35.4
91	65.1	10.6	-35.1
92	66.0	10.4	-37.8
93	66.9	8.9	-38.1
94	66.7	10.1	-37.7
95	65.1	9.4	-37.5
96	66.8	8.1	-37.9
97	66.7	11.3	-38.1
98	64.0	10.8	-37.7
99	65.7	10.2	-38.3
100	66.2	10.5	-36.8
101	64.7	12.0	-36.4
102	67.1	12.3	-37.7
103	76.6	18.1	-29.6
104	66.5	18.3	-30.0
105	74.6	8.7	-33.0
106	66.9	17.9	-29.2
107	75.4	17.5	-29.9
108	68.6	14.8	-33.3
109	66.4	13.3	-32.9

110	72.5	15.0	-32.2
111	70.4	13.1	-33.1
112	77.5	8.5	-36.9
113	72.2	12.3	-32.4
114	71.1	14.9	-32.7
115	73.4	18.9	-29.7
116	67.8	12.2	-33.5
117	68.3	13.1	-33.9
118	70.2	13.1	-30.6
119	70.1	13.5	-33.4
120	77.0	15.7	-30.2
121	71.4	14.1	-31.7
122	70.9	17.6	-29.2
123	59.8	22.6	-25.3
124	69.0	10.5	-36.1
125	74.6	19.1	-28.3
126	73.4	27.3	-31.2
127	75.5	7.4	-37.6
128	77.4	7.7	-39.6
129	70.3	7.4	-41.3
130	69.8	14.8	-32.2
131	74.2	7.7	-38.7
132	70.2	16.8	-30.6
133	69.8	12.5	-34.3
134	70.5	10.4	-35.2
135	69.8	10.8	-33.4
136	71.3	12.1	-32.0
137	72.5	18.5	-26.0
138	73.9	13.3	-32.4
139	69.4	9.4	-36.7
140	73.6	12.3	-34.8
141	74.1	13.3	-32.6
142	71.4	15.2	-32.5
143	70.0	11.5	-33.9
144	71.0	13.1	-34.4
145	73.0	13.8	-33.2
146	73.8	18.1	-31.5
147	65.3	12.0	-33.8

148	70.8	10.9	-34.0
149	70.1	12.8	-33.8
150	71.4	20.7	-26.8
151	69.4	12.1	-34.3
152	78.0	27.3	-24.8
153	70.3	20.0	-28.0
154	71.0	23.2	-27.4
155	68.2	21.7	-27.3
156	75.6	17.8	-30.6
157	69.6	14.3	-33.2
158	73.9	19.0	-32.0
159	75.6	17.8	-30.6
160	71.4	15.4	-31.1
161	81.0	19.8	-30.6
162	74.4	15.7	-31.5
163	70.7	12.9	-35.3
164	72.3	21.3	-28.0
165	83.3	22.4	-26.8
166	72.8	17.3	-30.1
167	70.6	22.5	-26.3
168	74.3	21.5	-28.7
169	68.5	21.3	-27.2
170	72.1	31.8	-22.8
171	66.4	22.3	-26.6
172	68.6	11.9	-35.8
173	65.3	9.0	-34.3
174	67.4	12.2	-32.6
175	76.0	7.5	-39.5
176	71.9	20.5	-27.2
177	75.0	23.4	-24.8
178	78.5	14.6	-31.3
179	69.1	15.5	-30.2
180	71.3	19.5	-26.2
181	66.2	17.6	-30.1
182	74.4	12.0	-33.9
183	79.5	12.9	-30.1
184	75.7	21.4	-25.2
185	68.2	18.5	-28.8

186	76.0	16.3	-31.5
187	69.8	19.2	-29.3
188	69.9	21.2	-26.5
189	70.0	12.6	-34.6
190	67.9	20.1	-27.8
191	74.2	18.6	-29.5
192	68.1	19.0	-27.4
193	79.2	17.5	-28.6
194	79.0	17.0	-30.1
195	77.4	15.1	-30.0
196	74.2	12.0	-32.6
197	72.0	8.9	-32.8
198	73.4	8.6	-32.1
199	67.6	24.2	-25.0
200	67.3	15.7	-30.6
201	89.7	23.6	-23.7
202	87.8	25.8	-20.6
203	86.9	30.8	-21.1
204	78.9	24.8	-24.1
205	66.9	21.2	-29.0
206	67.7	20.7	-28.8
207	67.5	19.7	-28.7
208	84.0	18.8	-31.0
209	86.8	20.9	-27.9
210	69.9	21.7	-26.9
211	84.3	12.3	-35.1
212	67.1	10.0	-35.3
213	66.2	12.2	-35.7
214	82.3	24.4	-27.7
215	85.8	16.8	-32.6
216	74.9	17.1	-31.2
217	76.5	14.8	-33.2
218	68.6	12.0	-34.9
219	75.7	15.8	-33.7
220	72.3	19.8	-32.1
221	72.3	24.4	-30.1
222	65.0	18.7	-30.3
223	69.4	23.7	-25.9

224	76.5	18.8	-29.3
225	68.2	22.9	-28.1
226	64.5	20.8	-30.3
227	70.1	13.3	-31.1
228	72.2	26.7	-23.7
229	79.4	18.2	-30.4
230	61.4	17.1	-30.3
231	60.8	16.3	-30.3
232	83.3	16.4	-32.8
233	80.6	28.2	-20.9
234	82.5	24.1	-23.2
235	83.1	24.9	-23.1
236	78.4	24.7	-23.5
237	80.5	25.5	-25.8
238	83.0	23.4	-27.2
239	79.2	27.5	-20.5
240	81.5	27.4	-21.5
241	82.2	23.3	-25.9
242	77.3	28.6	-25.6
243	82.8	26.5	-26.3
244	85.5	27.2	-24.1
245	83.1	29.3	-24.6
246	83.7	28.3	-26.5
247	88.0	25.3	-19.2
248	68.3	19.7	-30.1
249	72.2	22.5	-28.8
250	90.0	19.7	-30.7
251	72.6	10.7	-33.9
252	73.6	20.3	-30.5
253	75.4	18.5	-31.4
254	83.4	12.2	-28.2
255	77.1	25.1	-27.3
256	81.6	20.8	-27.4
257	82.0	21.3	-26.4
258	81.4	27.0	-21.5
259	78.7	7.4	-34.4
260	107.1	30.6	-25.0
261	96.1	19.9	-3.3

262	87.6	26.2	-25.3
263	83.4	19.4	-28.1
264	64.6	10.2	-37.7
265	66.6	12.9	-33.4
266	62.1	4.9	-38.4
267	66.0	12.9	-35.3
268	70.1	11.5	-38.1
269	67.5	18.6	-29.9
270	62.1	12.0	-34.8
271	72.2	15.9	-33.1
272	74.9	16.0	-32.2
273	66.4	14.3	-30.9
274	71.0	17.1	-28.4
275	114.1	5.4	-44.4
276	71.3	5.5	-42.2
277	74.3	23.4	-26.2
278	82.4	28.3	-21.4
279	73.5	23.6	-22.0
280	79.1	23.8	-24.8
281	85.0	24.2	-23.2
282	80.7	21.0	-22.7
283	67.4	24.9	-24.6
284	68.1	26.1	-24.3
285	69.2	20.4	-23.3
286	74.5	20.1	-27.5
287	74.6	20.5	-27.8
288	78.4	26.3	-22.0
289	66.6	8.5	-31.6
290	67.8	16.7	-31.9
291	64.6	14.0	-32.1
292	69.8	19.3	-27.8
293	64.6	17.3	-27.4
294	63.2	20.2	-30.1
295	62.9	14.4	-31.5
296	76.8	25.1	-21.3
297	64.5	13.5	-30.5
298	69.9	21.9	-24.8
299	68.6	16.7	-29.5

300	84.4	17.8	-30.5
301	66.3	15.0	-32.2
302	67.4	15.4	-30.5
303	76.9	20.1	-31.2
304	80.0	20.8	-30.9
305	72.9	20.8	-28.1
306	72.4	18.0	-29.5
307	85.4	23.9	-26.8
308	70.0	18.8	-27.6
309	67.2	19.9	-28.9
310	78.6	23.1	-28.5
311	76.1	20.6	-28.6
312	77.8	17.0	-29.8
313	80.9	18.7	-30.2
314	76.4	16.9	-29.6
315	79.2	18.0	-31.0
316	73.4	16.5	-27.0
317	81.9	23.5	-14.9
318	76.4	16.7	-29.0
319	73.1	15.7	-30.5
320	77.4	20.5	-28.4
321	75.5	19.7	-27.0
322	67.7	12.3	-32.7
323	66.4	11.1	-40.8
324	87.6	24.1	-24.2
325	77.4	11.4	-36.3
326	92.9	20.4	-29.0
327	81.7	18.8	-28.0
328	76.1	13.8	-35.9

Table A-2. DENT and EBBR grades of asphalt binders.

Asphalt	72 h LTPG, ˚C	Grade loss, ˚C	CTOD, mm	Specific essential work, kJ/m^2	Specific plastic work, MJ/m^3
1	-24.1	4.9	25.5	29.8	0.9
2	-22.6	6	25.0	24.3	1.8
3	-21.8	2.6	11.9	17.9	0.8
4	-23.7	3.6	11.3	15.1	0.9
5	-24.8	0.4	-	-	-
6	-22.8	4.1	12.6	13.0	0.5
7	-20.6	5.1	12.6	14.1	0.6
8	-20.7	4.8	-	-	-
9	-20.9	6.2	25.4	22.1	3.3
10	-23.3	2.7	11.3	15.5	0.6
11	-21.2	3.4	12.7	15.5	0.8
12	-16.8	3.5	-	-	-
13	-16.8	6.3	-	-	-
14	-18.7	5.5	8.0	17.2	1.0
15	-16.2	6.1	-	-	-
16	-22.1	4.5	13.0	17.7	0.3
17	-18.1	7.4	-	-	-
18	-17.9	5.1	-	-	-
19	-25.2	2.8	12.8	11.8	0.7
20	-29.5	3.2	16.7	8.8	0.3
21	-28.5	3.4	16.7	11.4	0.1
22	-25.5	4.7	19.8	19.2	0.6
23	-24	5.1	15.8	15.2	0.8
24	-26	6.7	19.9	12.1	0.3
25	-27.7	2.4	16.0	9.2	0.6
26	-29.3	5.6	34.0	13.8	0.8
27	-26.4	4.3	19.1	14.0	0.7
28	-24.8	3.6	13.1	13.5	0.7
29	-21.4	6.5	10.1	14.2	0.7
30	-27.1	5.9	15.7	10.6	0.6
31	-24.8	5.3	17.0	15.7	0.5
32	-26.6	5.8	14.0	11.0	0.8
33	-24	6.3	14.1	14.5	0.6
34	-24	5.9	11.7	12.0	0.7

35	-26.1	4.5	15.5	11.4	0.7
36	-17.9	9.1	-	-	-
37	-18.9	8.4	8.8	11.5	0.8
38	-26.6	4.7	18.7	14.3	0.7
39	-26.9	3.8	16.8	13.9	0.7
40	-25.2	5.2	14.4	13.6	0.8
41	-27.1	5.2	18.5	12.9	0.6
42	-27.2	5.5	23.6	14.2	0.6
43	-26.8	5.9	23.5	15.0	0.6
44	-23.9	5.8	12.8	12.3	0.6
45	-26.3	5.3	16.4	12.0	0.5
46	-23.9	6.5	14.5	12.8	0.4
47	-30.8	3.1	28.5	17.2	1.0
48	-33.2	1.6	42.0	16.1	1.1
49	-26.7	5.3	14.0	9.8	0.5
50	-24	6.3	17.9	17.7	0.5
51	-28.4	6.9	26.2	16.4	0.6
52	-29.1	3.9	24.8	14.6	0.8
53	-30.9	3.4	28.5	12.8	0.2
54	-29.6	3.1	30.9	18.1	1.6
55	-36.5	1.7	46.6	14.8	1.4
56	-38.2	-2.2	47.1	15.4	1.3
57	-31	4.8	36.4	17.2	0.7
58	-31.5	3.7	30.8	12.7	1.3
59	-32.5	4.1	68.4	23.9	1.6
60	-33	2.3	39.6	16.4	1.2
61	-29.9	5.5	48.9	23.6	0.8
62	-32.6	1.8	29.6	12.8	0.6
63	-27.8	5.3	38.8	22.6	1.0
64	-31.2	4.2	34.9	14.3	1.0
65	-29.4	4.3	22.4	13.9	0.8
66	-28.3	5.3	20.1	14.1	1.6
67	-32	3.5	41.2	18.4	0.6
68	-27.4	5.7	27.5	18.7	1.0
69	-29.1	3.8	20.1	12.1	0.3
70	-28.9	1.1	26.1	12.3	0.3
71	-30.8	4.9	16.9	10.4	0.4
72	-33	2	28.8	10.0	0.4

73	-32.4	3.6	23.8	10.5	0.4
74	30.4	3.2	23.4	9.9	0.5
75	-29.1	3.2	21.7	11.2	0.4
76	-33.4	2.2	22.1	9.9	0.4
77	-27.7	5.6	17.3	12.1	0.3
78	-31.1	1.3	28.1	13.2	0.3
79	-31.5	5.7	36.9	14.6	0.3
80	-30.5	2.8	23.9	13.2	0.5
81	-30.3	2.7	23.4	11.5	0.4
82	-28	1.8	17.8	10.4	0.4
83	-34.1	0.1	33.8	11.4	0.4
84	-29.8	3.1	26.8	15.3	0.7
85	-32.3	4.7	31.4	9.9	0.6
86	-29.1	4.9	23.3	12.2	0.3
87	-27.7	6.2	15.2	11.2	0.4
88	-29.9	2.4	23.5	12.8	0.3
89	-33.1	1.3	25.4	10.5	0.4
90	-33.9	1.5	-	-	-
91	-35	0.1	-	-	-
92	-34.4	3.4	49.0	12.5	0.3
93	-32.2	5.9	30.2	10.8	0.4
94	-31.8	5.9	33.1	10.3	0.5
95	-32.1	5.4	47.9	11.4	0.3
96	-33.4	4.5	35.0	10.0	0.4
97	-33.6	4.5	30.7	10.8	0.3
98	-32.3	5.4	40.9	11.5	0.4
99	-32.8	5.5	39.8	12.2	0.3
100	-32.8	4	30.4	11.1	0.4
101	-31.2	5.2	37.1	14.6	0.2
102	-32.8	4.9	32.0	10.6	0.4
103	-24.3	5.3	12.6	13.1	0.5
104	-26.3	3.7	16.1	17.2	0.6
105	-37.8	-4.8	37.9	12.8	0.4
106	-23.9	5.3	11.5	11.9	0.6
107	-26.6	3.3	17.3	18.3	0.4
108	-30.4	2.9	31.7	15.1	0.4
109	-29.7	3.2	31.2	10.4	0.3
110	-28.2	4	24.5	16.1	0.6

111	-28.4	4.7	30.6	13.9	0.7
112	-40.5	-3.6	50.3	16.1	0.2
113	-28.6	3.8	31.6	18.8	0.3
114	-29	3.7	33.7	17.5	0.4
115	-24.2	5.5	14.9	14.0	0.8
116	-29.9	3.6	22.7	9.8	0.6
117	-25.7	8.2	29.7	11.6	0.5
118	-27.7	2.9	17.1	11.7	0.8
119	-28.6	4.8	27.6	12.7	0.9
120	-26.9	3.3	17.7	12.5	0.9
121	-29	2.7	22.9	14.0	0.6
122	-25.1	4.1	18.3	18.5	0.4
123	-20.2	5.1	-	-	-
124	-34.5	1.6	36.2	13.6	0.3
125	-24.1	4.2	10.7	14.5	0.5
126	-26.3	4.9	13.7	11.0	0.7
127	-36	1.6	21.3	6.8	0.4
128	-39.3	0.3	37.3	9.8	0.5
129	-39.4	1.9	58.7	11.7	0.8
130	-28.9	3.3	21.9	13.0	0.6
131	-37.1	1.6	36.7	10.3	0.3
132	-26	4.6	15.4	13.7	0.6
133	-29.4	4.9	20.7	9.9	0.4
134	-33.4	1.8	35.3	11.8	0.6
135	-26.5	6.9	22.6	10.6	0.5
136	-24.8	7.2	18.7	10.6	0.5
137	-15.5	10.5	11.8	12.3	0.6
138	-28.3	4.1	22.6	12.8	0.7
139	-34.3	2.4	35.4	13.5	0.1
140	-32.2	2.6	31.7	15.2	0.4
141	-29.7	2.9	21.9	11.7	0.5
142	-27	5.5	15.1	11.3	0.5
143	-30.4	3.5	23.1	11.1	0.3
144	-31.2	3.2	24.8	11.6	0.4
145	-29.2	4	23.6	12.7	0.5
146	-26.2	5.3	21.4	14.5	0.7
147	-29.9	3.9	27.0	14.5	0.6
148	-30.8	3.2	24.8	12.8	0.6

149	-29.4	4.4	23.4	12.0	0.7
150	-22.1	4.7	9.7	14.8	0.6
151	-30.7	3.6	25.7	12.2	0.4
152	-17.3	7.5	6.7	14.1	0.9
153	-21.5	6.6	9.9	13.4	0.5
154	-19.4	8	9.7	16.3	0.6
155	-22.3	5	8.9	11.9	0.5
156	-22.1	8.5	11.5	11.1	0.5
157	-28.7	4.4	21.2	11.1	0.2
158	-25.7	6.3	11.7	9.9	0.6
159	-26.9	3.6	16.9	15.7	0.3
160	-27.4	3.7	18.3	10.7	0.4
161	-25.8	4.8	11.4	13.0	0.7
162	-24.9	6.6	12.4	7.4	0.4
163	-29.4	5.9	20.1	10.9	0.5
164	-21.3	6.7	17.7	12.3	0.4
165	-18.2	8.7	7.8	11.7	0.4
166	-25.5	4.7	12.6	11.6	0.6
167	-20.3	6	8.9	14.6	0.7
168	-23.5	5.2	10.5	14.9	0.7
169	-22.9	4.3	9.1	13.8	0.6
170	-14	8.7	5.7	13.3	0.7
171	-22.8	3.8	6.4	5.4	1.4
172	-32.7	3.1	35.3	15.5	0.9
173	-30.5	3.7	33.0	17.1	0.4
174	-31.9	0.6	41.5	19.4	0.3
175	-35.8	3.7	52.4	16.7	0.4
176	-22	5.2	11.4	15.2	0.5
177	-19.5	5.3	6.2	11.3	1.1
178	-27	4.3	20.2	13.8	0.6
179	-25.5	4.7	16.7	12.3	0.2
180	-20.8	5.4	9.7	15.0	0.7
181	-25.1	5	13.8	11.9	0.5
182	-30.8	3.1	25.1	11.3	0.4
183	-25	5.1	15.8	13.3	0.8
184	-18.6	6.6	-	-	-
185	-23.4	5.4	12.0	13.4	0.6
186	-26.3	5.2	25.7	15.0	0.7

187	-23.6	5.7	12.1	12.2	0.7
188	-20.5	6	10.2	15.2	0.6
189	-31.5	3.1	35.7	13.7	0.4
190	-23.5	4.3	11.1	12.2	0.7
191	-25.2	4.3	14.1	12.7	0.7
192	-23.7	3.7	7.4	9.2	1.1
193	-21.3	7.3	14.7	15.2	0.9
194	-24.4	5.7	15.4	13.8	0.8
195	-24.8	5.2	17.4	14.3	0.5
196	-30.4	2.2	12.7	7.0	0.3
197	-30.7	2.1	15.4	7.2	0.3
198	-30.5	1.6	13.6	6.2	0.2
199	-22.8	3.8	13.4	23.1	1.1
200	-18.9	6.1	16.3	25.4	0.1
201	-26.4	4.2	12.0	14.1	0.3
202	-15	8.7	6.0	12.1	0.5
203	-13.1	7.5	4.0	10.1	-0.6
204	-14.2	6.9	-	-	-
205	-19.9	4.2	7.1	12.4	0.9
206	-23.1	5.9	10.9	10.0	0.2
207	-23.8	5	13.9	19.0	0.0
208	-23	5.7	11.1	14.4	0.4
209	-26	5	12.2	12.8	0.6
210	-23.3	4.6	13.6	19.4	0.9
211	-23.4	3.5	9.2	13.4	0.4
212	-30.7	4.4	22.5	14.1	0.6
213	-34.3	1	47.2	14.5	0.5
214	-31.2	4.5	37.2	13.4	0.6
215	-23.3	4.4	12.3	20.2	0.9
216	-29.1	3.46	18.9	18.9	0.7
217	-25.5	5.7	35.3	26.1	0.6
218	-30.1	3.1	26.6	18.3	0.6
219	-29.7	5.2	23.3	10.8	0.2
220	-28.3	5.4	16.5	12.6	0.6
221	-28.3	3.8	17.2	12.3	0.4
222	-24.8	5.3	15.4	16.6	0.3
223	-25.9	4.4	14.7	10.6	0.4
224	-23.5	2.4	11.2	14.1	0.6

225	-23.2	6.1	12.5	13.0	0.9
226	-21.9	6.2	11.2	13.7	0.7
227	-25.5	4.8	15.2	12.8	0.5
228	-27.1	4	29.8	15.7	0.9
229	-19.3	4.4	9.1	16.1	1.2
230	-27.2	3.2	27.3	21.1	1.6
231	-25.4	4.9	17.1	12.2	0.1
232	-26	4.3			
233	-27.5	5.3	22.4	18.2	0.5
234	-26.5	5.5	19.1	16.1	0.6
235	-12.8	8.1	-	-	-
236	-16.2	7	10.1	17.5	1.4
237	-16.2	6.9	10.2	28.1	0.6
238	-14.8	8.7	-	-	-
239	-15.7	10.1	11.4	19.3	1.0
240	-21.4	5.8	12.8	22.6	1.2
241	-17.6	2.9	10.3	23.8	1.3
242	-10.4	11.1	7.6	16.2	1.1
243	-18.4	7.5	10.2	16.8	1.6
244	-17.2	8.4	6.9	13.7	0.8
245	-17.4	8.9	10.4	18.8	1.2
246	-15.7	8.4	8.5	19.4	1.3
247	-15.9	8.7	7.3	18.9	1.1
248	-18.6	7.9	3.4	6.4	-0.3
249	-13.3	5.9	-	-	-
250	-25.1	5	17.5	16.5	0.5
251	-21.8	7	9.1	12.8	0.5
252	-23.1	7.6	13.4	10.3	0.5
253	-27.1	6.8	15.3	7.9	0.3
254	-24.5	6	13.7	12.2	0.9
255	-25.2	6.2	14.5	12.6	0.8
256	-22	6.2	9.4	10.6	0.6
257	-17.5	9.8	9.3	15.4	0.9
258	-19.4	8	10.7	14.8	0.7
259	-17.4	9	9.0	13.5	1.1
260	-14.7	6.8	6.8	7.5	-0.5
261	-26.1	8.3	12.8	5.6	0.2
262	-17.3	7.7	19.6	27.4	-0.6

263	23.5	26.8	-	-	-
264	-13	12.3	7.1	15.0	0.8
265	-22.3	5.8	9.3	10.9	0.5
266	-34.5	3.2	72.0	15.5	0.6
267	-29	4.4	24.4	15.1	0.4
268	-34.3	4.1	30.8	9.5	0.3
269	-31.5	3.8	42.3	17.2	0.6
270	-34.3	3.8	32.6	9.5	0.4
271	-27.7	2.2	20.7	19.0	0.6
272	-33.6	1.2	20.8	7.7	0.4
273	-23.3	3.1	-	-	-
274	-29.2	3.9	17.4	9.0	0.3
275	-26.7	5.5	22.6	16.1	0.8
276	-27.8	3.1	16.3	8.7	0.4
277	-24.5	3.9	16.0	14.6	0.6
278	-38.9	5.2	75.3	13.6	0.1
279	-34	10.4	74.2	12.6	0.3
280	*	*	54.6	7.9	0.3
281	-38	4.2	53.6	8.2	0.2
282	-18.8	7.4	11.6	15.4	0.9
283	-16.6	4.8	-	-	-
284	-16.8	5.2	9.3	20.9	1.0
285	-19.1	5.7	9.5	13.6	0.7
286	-19.4	3.8	8.1	17.4	0.9
287	-17	5.7	10.9	15.5	0.6
288	-19.3	5.3	10.6	21.0	0.4
289	-19.6	4.7	-	-	-
290	-21.9	1.4	11.3	13.7	0.8
291	-20.1	7.4	22.4	19.1	0.9
292	-21.6	6.2	14.8	20.0	0.9
293	-20.2	1.8	7.3	15.8	1.0
294	-29.5	2.1	26.2	10.4	0.4
295	-25.3	6.6	14.3	10.3	0.5
296	-29	3.1	22.6	9.1	0.3
297	-19.4	8.4	11.6	15.4	0.5
298	-18	9.4	15.1	12.8	0.3
299	-22.8	7.3	14.6	11.6	0.3
300	-26.7	4.8	19.3	10.6	0.1

301	-13.3	8	8.7	17.7	0.8
302	-26.3	4.2	25.2	13.2	-0.1
303	-21.6	3.2	11.3	12.6	0.5
304	-24.9	4.6	9.0	6.0	0.4
305	-24.7	5.8	20.3	15.1	0.9
306	-29.9	2.3	13.5	9.0	0.3
307	-24.9	5.6	9.7	6.2	0.4
308	-27.2	4	23.1	18.1	1.1
309	-25.6	5.3	21.7	19.8	1.2
310	-20.2	7.9	10.9	12.7	0.8
311	-22.6	6.9	12.4	13.0	0.6
312	-19.1	7.7	5.6	9.3	0.8
313	-21.9	5.7	9.7	10.2	0.5
314	-23.8	5.1	11.8	12.5	0.5
315	-22.5	6	10.8	16.0	1.1
316	-23	5.6	11.8	15.7	0.9
317	-24.5	5.3	21.1	15.2	0.9
318	-24.4	5.8	20.1	17.0	1.3
319	-21	8.6	21.9	15.3	1.0
320	-30.3	0.7	16.6	15.5	0.8
321	-23.3	3.7	7.9	6.9	0.4
322	-11.3	3.6	11.0	15.5	-0.1
323	-24.2	4.8	16.5	12.9	1.1
324	-26.4	4.1	20.3	11.9	1.0
325	-23.7	4.7	23.0	23.7	0.1
326	-24.1	2.9	23.8	18.5	0.6
327	-30.5	2.2	24.4	10.3	0.0
328	-32.6	8.2	25.5	7.5	0.3
329	-21	3.2	10.4	17.7	1.1
330	-30.7	5.6	25.7	9.7	0.8
331	-23.5	5.5	20.9	19.7	0.6
332	-22.9	5.1	16.8	16.8	0.8
333	-29.2	6.7	25.7	13.2	0.3

Note: “-“ Brittle Failure; “*” Outlier;

Table A-3. Glass transition parameters.

Cooling Rate (℃/h)	Aging Degree	655-9	655-10	655-11	655-12	655-13	655-14	655-15
10	Unaged	-22.3	-25.92	-23	-26.84	-28.67	-31.91	-25.4
		-19.5	-29.18	-18.03	-13.17	-23.95	-25.52	-19.6
		2.8	3.26	4.97	13.67	4.72	6.39	5.8
	PAV20	-27.8	-27.89	-27.3	-24.04	-23.83	-29.81	-28
		-19.6	-18.89	-17.77	-15.44	-18.99	-21.77	-11.7
		8.2	9	9.53	8.6	4.84	8.04	16.3
	PAV40	-29.6	-26.19	-27.15	-19.3	-19.3	-26.84	-27.5
		-16.8	-16.07	-17.94	-10.09	-7.59	-18.65	-15.8
		12.8	10.12	9.21	9.21	11.71	8.19	11.7
	PAV100	-29.8	-29.69	-27.39	-27.31	-31.31	-26.57	-33.6
		-18.7	-16.55	-19.57	-7.99	-18.55	-17.66	-20.1
		11.1	13.1	7.82	19.32	12.76	8.91	13.5
30	Unaged	-25.2	-28.45	-26.7	-26.53	-30.61	-26.37	-29.5
		-19.5	-23.86	-17.37	-11.87	-23.11	-21.42	-19.2
		5.8	4.59	9.33	14.66	7.5	4.95	10.3
	PAV20	-27.1	-27.07	-26.13	-27.25	-24.41	-29.1	-27.7
		-19.3	-19.75	-18.64	-13.33	-21.93	-22.53	-13.2
		7.7	7.32	7.49	13.92	2.48	6.57	14.5
	PAV40	-26.8	-25.96	-28.03	-25.86	-25.87	-26.6	-34.8
		-20.2	-16.69	-17.11	-10.42	-9.68	-18.67	-19
		6.7	9.27	10.92	15.44	16.19	7.93	15.9
	PAV100	-27.3	-28.8	-27.69	-26.85	-32.37	-29.83	-36.4
		-12.5	-17.82	-20.03	-10.1	-19.48	-17.51	-18.8
		14.8	11	7.66	16.75	12.89	12.32	17.6
100	Unaged	-26	-29.45	-26.59	-27.31	-24.08	-26.87	-28.8
		-19.9	-23.36	-17.19	-13.62	-12.93	-17.11	-22.4
		6.1	6.09	9.4	13.69	11.15	9.76	6.43
	PAV20	-27.9	-30.22	-29.04	-27.92	-35.34	-30.18	-29.1
		-20.6	-20.37	-22.01	-14.89	-28.68	-22.3	-13.6
		7.3	9.85	7.03	13.03	6.66	7.88	15.4
	PAV40	-28.4	-28.36	-28.65	-26.39	-26.19	-28.74	-32.1
		-18.8	-18.54	-18.08	-9.86	-11.5	-18.62	-19.1
		9.6	9.82	10.57	16.53	14.69	10.12	13
	PAV100	-29.4	-29.95	-29.45	-28.56	-34.03	-29.24	-32.6
		-15.1	-18.12	-22.1	-9.01	-19.73	-20.04	-18.6
		14.3	11.8	7.35	19.55	14.3	9.2	14.1

B-Figures

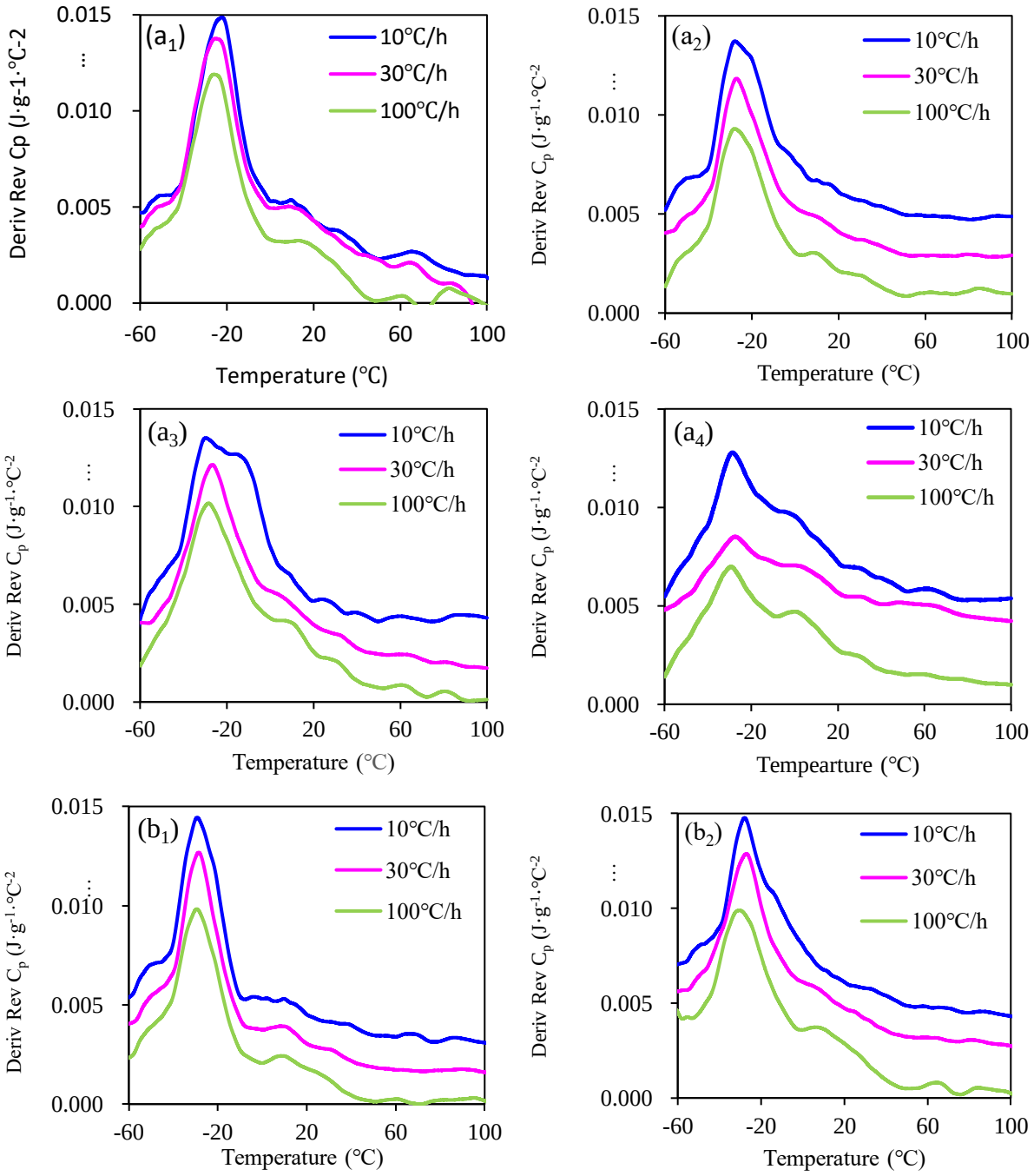

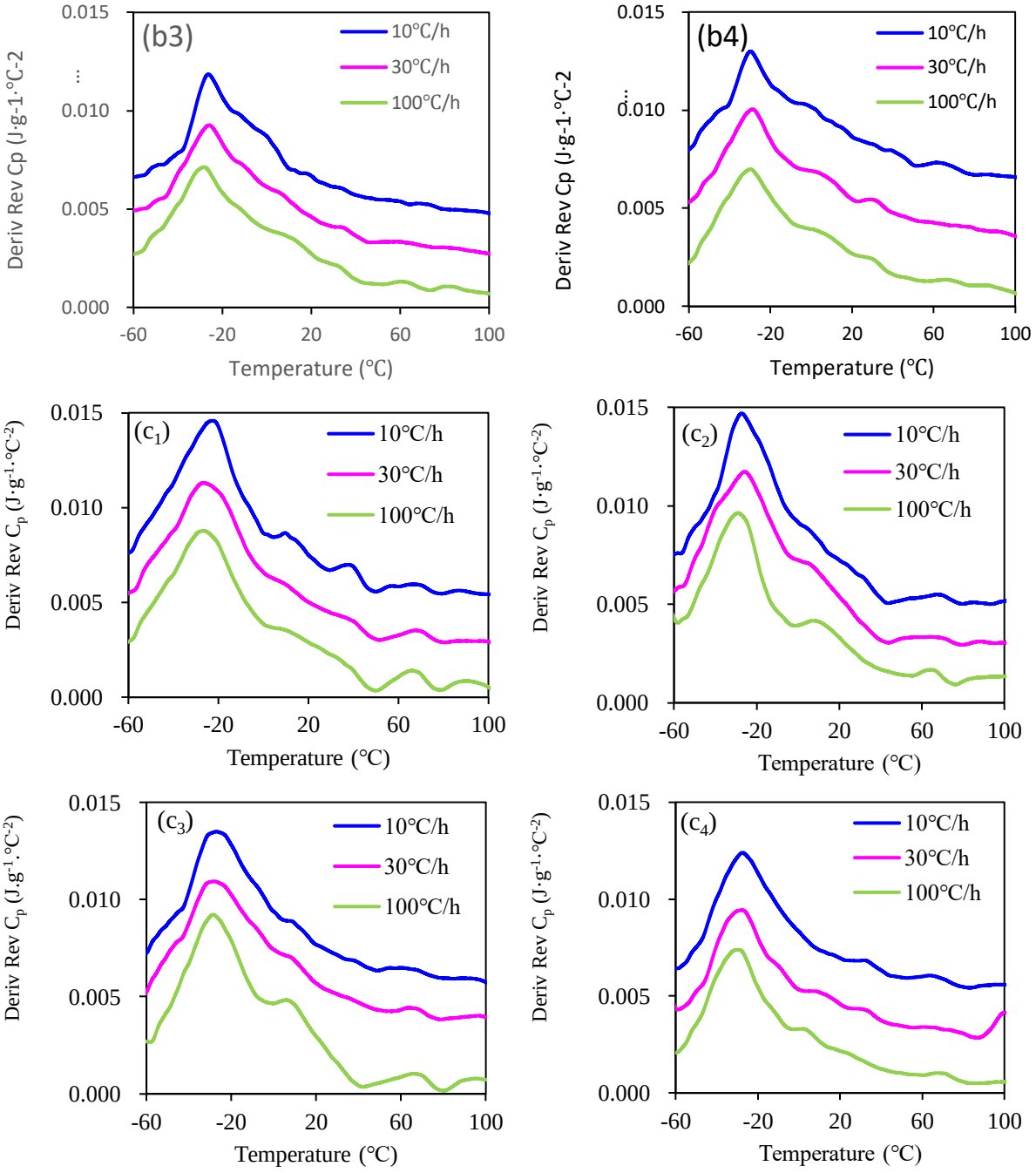

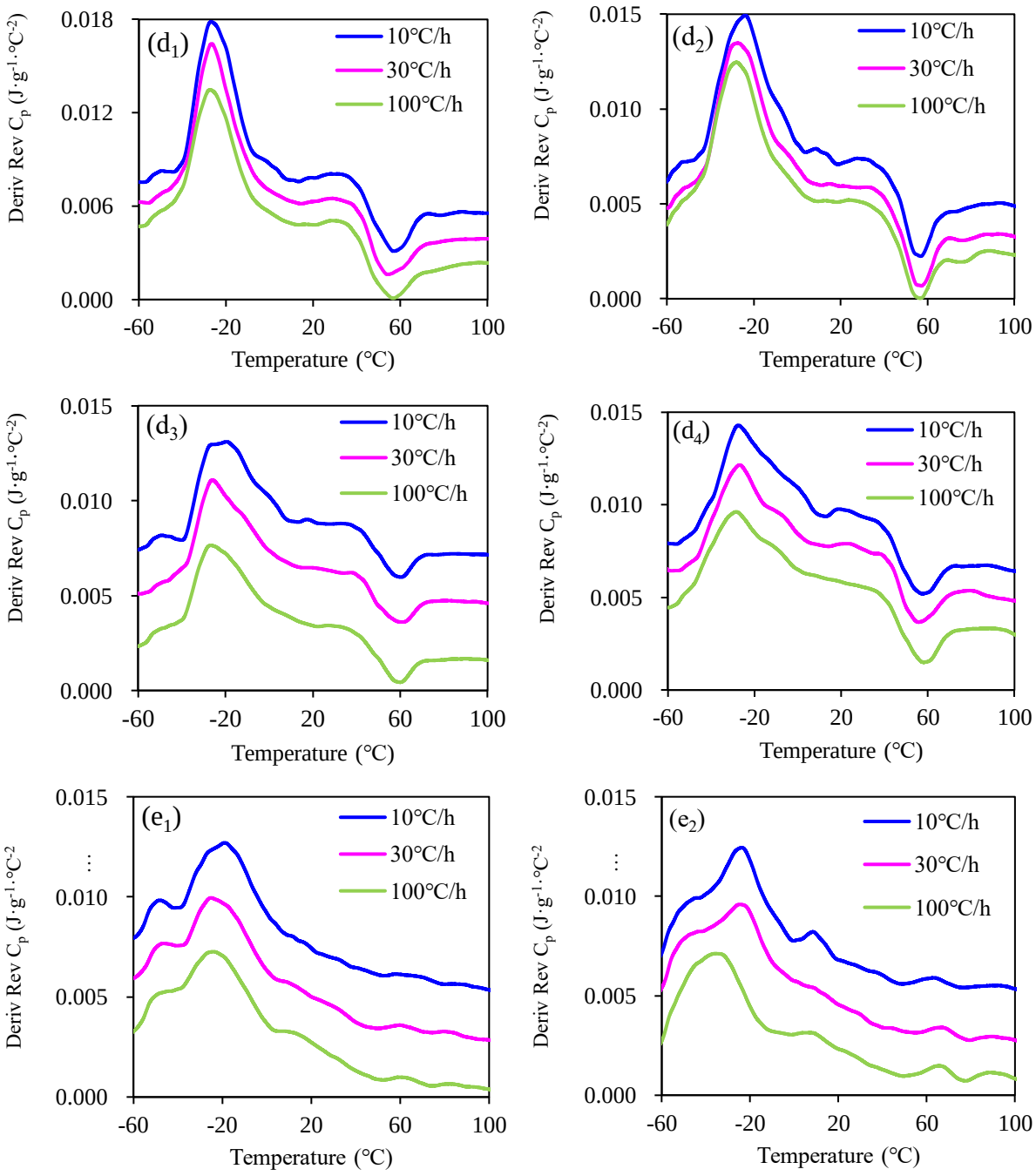

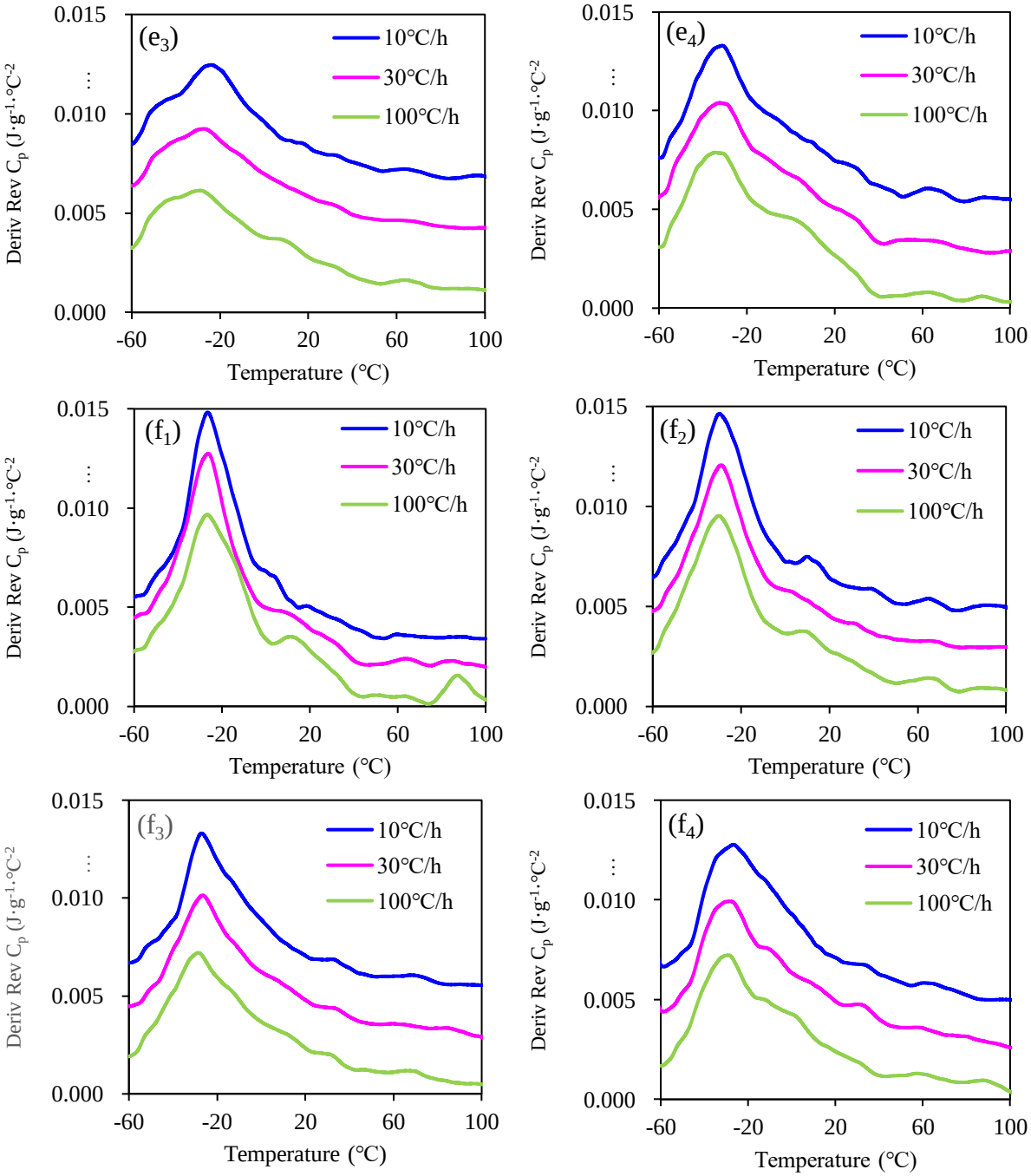

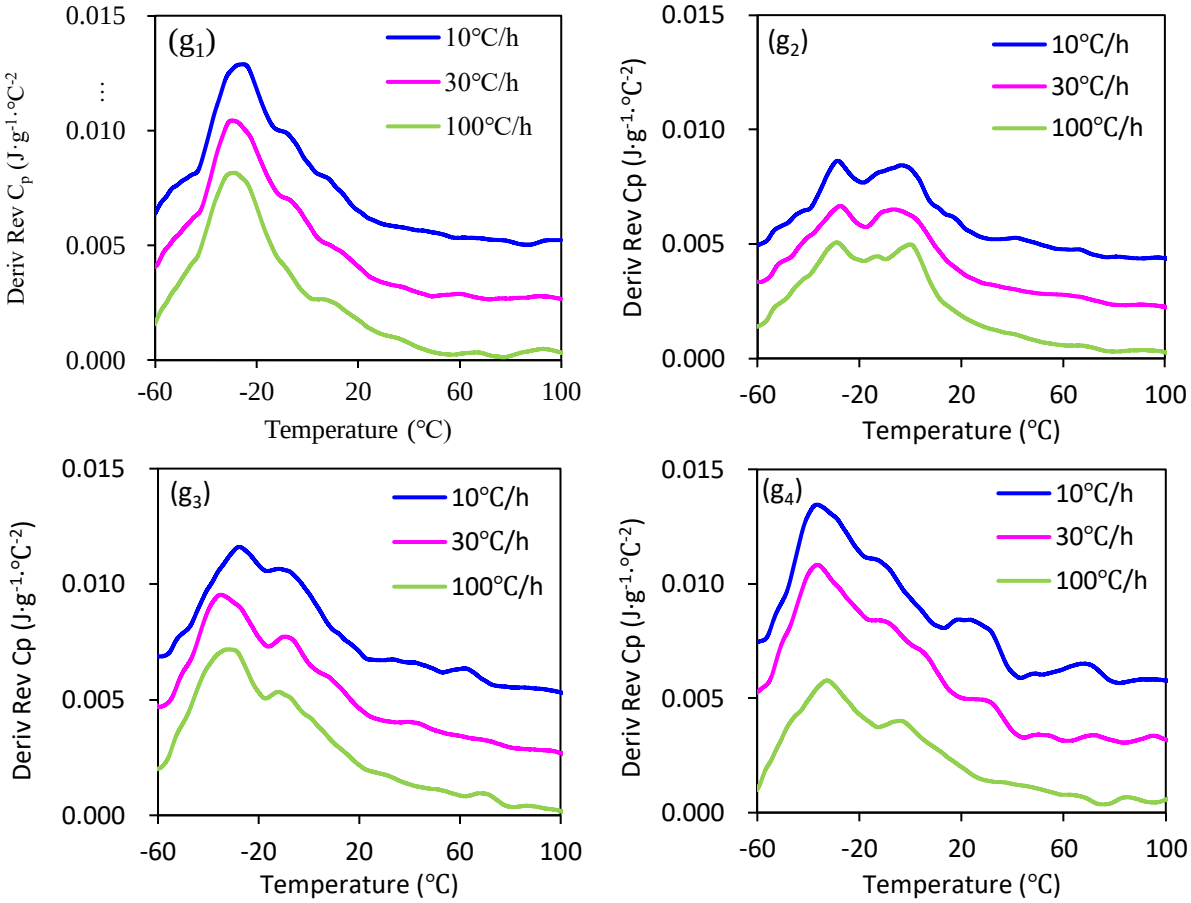

Figure B-1. Derivative of the reversible heat capacity plotted against temperature for pavement trial asphalts under different cooling rates: graphs (a) to (g) represent asphalts 655-9 to 655-15, respectively; Subscript 1 to 4 represent unaged, PAV20, PAV40, PAV100, respectively.